Feynman Integrals for Five-Point Two-Loop One-Mass Amplitudes in QCD

Dissertation

zur Erlangung des Doktorgrades
der Fakultät für Mathematik und Physik der

Albert-Ludwigs-Universität Freiburg

vorgelegt von

Wladimir Tschernow

Dezember 2021

Abstract

The energy reach and anticipated data of the Large Hadron Collider (LHC) at CERN will allow precision tests of the Standard Model and New Physics searches. In this thesis we contribute to crucial theory predictions for these quests. We obtain the two-loop five-point Feynman integrals with one massive external leg, and massless virtual particles. These play an important role for the theory predictions of Z- and W-boson production in association with two jets in Quantum Chromodynamics (QCD), as well as the production of a Higgs-boson in association with two jets in the large top-mass approximation.

The main result of this thesis is the computation of the full set of planar five-point integrals as well as three distinct non-planar hexa-box topologies.

The computation was done by setting up first-order differential equations for the Feynman integrals, which are solved in a second step. We find the canonical basis of 'pure' Feynman integrals, which simplifies their dependence on the dimensional regulator and allows for efficient solution of the differential equation. We identify the algebraic kinematic dependence of the differential equation, given by the so-called symbol alphabet which determines the function's analytic properties. Ansatz techniques, based on universal properties of Feynman integrals, are applied to allow for the construction of the analytic differential equation from a small number of numerical evaluations. This technique circumvents the main bottleneck in Feynman integral computation originating in large linear systems in six parameters. Such systems appear in the integration-by-parts identities relating generic Feynman integrals to the basis. We integrate the canonical differential equation numerically using the generalized power-series approach and provide high-precision numerical values for all integrals in all kinematic regions. Moreover, for the planar integrals we performed a dedicated study of the computation-time requirements and confirmed the efficiency of the numerical integration.

Zusammenfassung

Sehr hohe Schwerpunktsenergie sowie die riesige Menge an Daten, die am Großen Hadronenspeicherring am CERN bereits gesammelt sowie in Zukunft erwartet werden, ermöglichen sowohl die Durchführung von Präzisionstests des Standardmodells der Teilchenphysik als auch die Suche nach Neuer Physik. In dieser Arbeit liefern wir einen Beitrag zu wichtigen theoretischen Vorhersagen, die zur Bewältigung der genannten Herausforderungen notwendig sind. Wir berechnen die Zwei-Schleifen Fünf-Punkt Feynman Integrale mit einem massiven externen Bein und masselosen virtuellen Teilchen. Diese spielen eine wichtige Rolle für die theoretische Vorhersage sowohl für die Produktion von W- und Z-Bosonen zusammen mit zwei Jets im Rahmen der Quantenchromodynamik (QCD) als auch für die Produktion von Higgs-Bosonen mit zwei Jets im Limes der großen Top-Masse.
Das zentrale Ergebnis dieser Arbeit ist die Berechnung des vollständigen Satzes an planaren Fünf-Punkt Integralen sowie drei unabhängiger nicht-planarer "Hexabox"-Topologien.
Wir konstruieren ein System gewöhnlicher linearer Differentialgleichungen, denen die Integrale genügen müssen und lösen diese Gleichungen anschließend. Für jede der berechneten Integraltopologien fanden wir eine "kanonische" Basis, wodurch die funktionelle Abhängigkeit der Differentialgleichung vom Regularisierungsparameter deutlich vereinfacht werden konnte. Wir bestimmten die kinematische Struktur der Differentialgleichungen, gegeben durch das sogenannte "Symbolalphabet". Ansatz-basierte Methoden wurden angewandt, um die analytische Form der Differentialgleichung aus einer vergleichsweise kleinen Anzahl numerischer Auswertungen zu bestimmen. Dadurch vermieden wir, mit sehr großen analytischen linearen Gleichungssystemen in sechs Variablen arbeiten zu müssen, was derzeit eine der größten Hürden bei der Berechnung von Feynman Integralen ist. Wir lösten die kanonischen Differentialgleichungen numerisch, indem wir einen verallgemeinerten Potenzreihenansatz benutzten, und lieferten hoch-präzise numerische Werte in jedem der kinematischen Phasenraumgebiete. Außerdem führten wir eine Untersuchung der Berechnungsdauer für die planaren Integrale durch und bestätigten die Effizienz der numerischen Integration.

Dekan: Prof. Dr. Michael Thoss
Referent: Prof. Dr. Harald Ita
Koreferent: Prof. Dr. Stefan Dittmaier
Tag der mündlichen Prüfung: 14.03.2022

List of publications

[1] S. Abreu, H. Ita, B. Page, and W. Tschernow, "Two-loop hexa-box integrals for non-planar five-point one-mass processes," *JHEP*, vol. 03, p. 182, 2022.

[2] S. Abreu, H. Ita, F. Moriello, B. Page, W. Tschernow, and M. Zeng, "Two-Loop Integrals for Planar Five-Point One-Mass Processes," *JHEP*, vol. 11, p. 117, 2020.

Contents

Chapter 1

Introduction

In the 20th century physics was revolutionized by two radically new theories which not only greatly increased our understanding of Nature but also changed some of the most fundamental concepts of reality we have had before. The *Special* (SR) and *General* (GR) theory of *Relativity* demonstrated that both space and time are intrinsically combined to a dynamical *space-time* unlike just being the static background of the physical processes. Furthermore, GR explained *Gravity* as geometrical curvature of space-time caused by presence of the energy and momentum of matter and fields. For weak gravitational fields and curvature, the theories gave us also a new fundamental symmetry of Nature, the *Lorentzian* symmetry which replaced the previous concept of *Galilean* symmetry. The second great achievement of the last century is *Quantum Mechanics* (QM) developed in order to explain the structure of microscopic systems like molecules and atoms and also e.g. the phenomenon of *black-body radiation*. Probably, the most significant difference of Quantum Mechanics compared to the classical physics is its *non-deterministic* description of reality which states that we are not able to predict the exact outcome of a measurement but only the *possible* outcomes and their *probabilities* to occur.
During the second half of the century SR and QM have been unified into the *Standard Model* (SM) of particle physics, aided by the development of high-energy experiments. While all known elementary particles and forces, except Gravity, are incorporated into the SM it does not include many important observable phenomena like e.g. *Dark Matter*, sufficient *CP violation* or *neutrino oscillations*. Moreover, it contains 19 (including *strong CP* parameter θ) numerical constants whose values have to be determined experimentally. On the other hand, all particles which had been predicted by the SM have been experimentally observed by now. This was completed with the discovery of the Higgs boson at the Large Hadron Collider (LHC) in 2012 [1, 2].
In the energy range of modern particle colliders the SM is a perturbative theory where predictions are computed as formal series expansions in coupling constants of fundamental interactions. Due to an enormous increase of the experimental precision over the last decades, achieving nowadays a typical level of few percent, increasing accuracy of theoretical predictions is needed which requires computing higher orders in the perturbation theory. The Feynman rules give a clear prescription how to obtain precision predictions, from drawing diagrams, which, in a second step, imply quantitative mathematical expressions. Theoretical high-precision calculations include both dealing with multiple loops (two and more) and also multiple final-state particles (two and more). The evaluation of multi-loop and multi-leg Feynman amplitudes is a challenging task. A crucial obstacle is the analytic complexity and the number of contributions which both grow very rapidly with increasing number of loops and/or external legs. For instance, in terms of the traditional Feynman diagram approach, the number of diagrams contributing to the *tree level* $2 \to n$ gluon amplitude grows approximately factorially with n [3]. On the other hand, the final result for any

value of n, expressed in terms of appropriate variables, is given by a remarkably simple *Parke-Taylor* formula, first conjectured in [4] and later rigorously proven by a recursive argument [5]. To benefit from this hidden structure new methods were developed which explicitly make use of gauge invariance of the amplitude and work with on-shell states only. At tree-level this approach led to the *Britto-Cachazo-Feng-Witten recursion* (BCFW) [6].

At one-loop level the *generalized unitarity* [7] approach was developed [8–11] which makes an efficient computation of *master integral coefficients* of one-loop amplitudes with generic number of external particles possible by relating cuts of one-loop amplitudes to products of tree-level amplitudes. Together with the fact that at one-loop the basis of master integrals for *all* processes is finite and known [12, 13], this allowed for an efficient automated calculation of one-loop amplitudes [14, 15] which led to the "*next-to-leading-order* (NLO) revolution".

However, for many important processes the amount of collected experimental data at the LHC during Run 1 and 2 reduces the statistical uncertainty so far that *next-to-next-to-leading order* (NNLO) calculations are needed to match the experimental precision (see e.g. [16, 17]). On the other hand, for some processes NLO predictions differ notably from experimental measurements. A prominent example is here the cross section of W-pair production [18] where significantly better agreement with experiment was achieved after NNLO QCD corrections had been added [19–21]. A further important application of NNLO corrections are standard *background* processes at the LHC which have to be known to very high accuracy to enable complex experimental analyses. A more theoretical reason for higher-order calculations is that they can be used to estimate the quality of the perturbative convergence, for example, by analyzing the dependence on the renormalization scale.

Recently, first steps towards extension of the generalized unitarity approach to the two-loop level were done [22–29]. In contrast to the one-loop case, at two loops no universal master integral basis exists. That means a complete set of master integrals has to be computed separately for each family of two-loop processes sharing the same kinematics. Feynman integral calculus has developed significantly in the recent years establishing new techniques for computing multi-loop integrals. One of the most successful is the *differential equation* approach [30–34] augmented by the notion of the *canonical basis* [35]. This progress in understanding both master integrals and coefficients enabled some great advances in computing amplitudes for two-loop five-point processes with massless external and loop particles [23, 36–43, 43–46]. The corresponding master integrals were obtained by the canonical differential equation method [36, 47–49] and the *simplified differential equation* approach [50]. Later, the massless five-point integrals have been expressed in terms of special *pentagon functions* [51, 52] which are more suited for multiple numerical evaluations.

In contrast to the massless case, only little was known about five-point amplitudes and integrals with one off-shell leg. Partial results were obtained in [50, 53]. Furthermore, the amplitude for W-boson production associated with four partons was computed numerically [54].

In this thesis, we contribute to the understanding of NNLO corrections for production of a massive boson associated with four massless particles by computing for the first time the complete set of planar five-point master integrals [55] as well as three non-planar hexa-box integral topologies [56] with one off-shell leg. Two further non-planar *double-pentagon* topologies remain the only unknown part of five-point integrals with one off-shell leg. The planar integrals allow, for instance, for the computation of *leading color* W-boson production associated with two jets. This process is particularly important for both precise measurements of SM parameters and constraining models beyond SM. So, for instance, $pp \to Wb\bar{b}$ is an important background for Higgs boson production associated with a vector boson. Many observables for the $W + 2$ jets production are, by now,

known to 10% relative uncertainty [57, 58] and further progress is expected during Run 3 and high-luminosity phase of the LHC. An important feature of this process is that all production channels are already contributing at Born level with comparably small NLO QCD corrections and small sensitivity to higher-order corrections [59–63]. An NNLO QCD calculation can help to assess the quality of higher-order corrections [64–66].
Further important applications of the five-point integrals with one off-shell leg are the Higgs- and Z/γ^*-boson production associated with two jets. Here, some of the non-planar integral topologies contribute even at the level of the leading-color result so that the complete set of integrals is needed for the full calculation. The $H + 2$ jets production is interesting both on its own (for example in the $Hb\bar{b}$ channel) and as background for HH-production. Furthermore, five-point integrals with one off-shell leg can be used for computing amplitudes in the *Higgs Effective Theory* (HEFT) where the loop-induced top-quark effects are approximated by an effective Higgs-gluon coupling (see e.g. [67]). This allows, at least approximately, to include top-induced Higgs production without computing master integrals with massive propagators.
Let us give a brief overview of the main steps of the integral calculation. One of the most crucial obstacles by evaluating multi-loop multi-scale integrals is the tremendous algebraic complexity of the integral reduction which is necessary for computing the differential equation. To avoid this problem, we worked with numerical *integration-by-parts* (IBP) tables computed on rational kinematic points and, consequently, with numerical differential equations [48]. An important ingredient is the construction of the canonical basis for each of the computed integral topologies. We applied a combination of heuristic and (semi)-algorithmic approaches to solve this problem. Construction of the pure bases was the author's main contribution to this project. In this work, we also provide first partial results on the pure bases for the two remaining double-pentagon topologies. Another important result is the *symbol alphabet* [68–70] for the planar and the hexa-box integral topologies. Unlike in the traditional differential equation approach, the numerical method requires the knowledge of the alphabet in advance. Finally, we integrated the canonical differential equations numerically using the *generalized power-series* approach [71, 72] which has already been used for computing NNLO QCD corrections for Higgs+jet production [73, 74].
Our results have been used for computing a polylogarithmic [75] and, very recently, a pentagon-function [76] representation of the planar five-point integrals with one off-shell leg. The planar integrals enabled the computation of several amplitudes [77–79] for a massive boson production as well as a new two-loop form-factor in planar $\mathcal{N} = 4$ *Super-Yang-Mills* (SYM) theory [80].
The thesis is organized as follows. In Chapter 2 we introduce the basic concepts and notions needed for this work. In section 2.1 we give a brief overview of the SM while section 2.2 deals with perturbative calculations and introduces the notion of *scattering amplitudes*. In section 2.3 *Feynman integrals* are defined and their basic properties are discussed while in section 2.4 we present the *differential equation approach* together with the notion of the *canonical basis* and give an overview over special functions used in Feynman integral calculations.
In Chapter 3 we discuss in detail the main steps of our calculation and present special techniques which have been used in these steps. In section 3.1 we introduce our notation and discuss the five-point phase space while section 3.2 deals with the computation of the *pre-canonical* differential equation. The next section 3.3 contains an extended discussion of various strategies for obtaining a pure basis. Finally, in sections 3.4 and 3.5 we present the numerical reconstruction procedure of the analytic canonical differential equation and the generalized power-series approach of numerical integration.

In Chapter 4 we present our results: section 4.1 deals with the planar topologies while the results for the non-planar hexa-box topologies are presented in section 4.2. The first insights on the double-pentagon topologies are given in 4.3.
In Chapter 5 we summarize the main parts of this thesis and give an outlook on possible extensions of the work.
Finally, in the appendices A, B and C we provide more detailed discussions on a selection of special topics like *momentum-twistor* variables or *functional reconstruction*.

Chapter 2

Theoretical Preliminaries

In the first chapter of the thesis we are going to give a brief introduction to the state-of-the-art perturbative calculations in high-energy physics.
Currently, quantum-field theories (QFTs) are our best framework for understanding physical processes at short distances with negligible effects of Gravity, such as e.g. scattering processes at modern colliders. All known particles and the three fundamental interactions which are relevant at the considered energy scale: the *strong* and the *weak* nuclear forces as well as the *electromagnetic* force are described as either matter or gauge fields. Modern theories of strong and electromagnetic interactions are called *quantum chromodynamics* (QCD) and *quantum electrodynamics* (QED). The weak interaction is best described together with the electromagnetic force in terms of a unified *electroweak* (EW) theory [81–85]. The mass spectrum of the electroweak theory is explained by the *Higgs mechanism* [86–88] which also provides an explanation for the matter particles' masses. Together, QCD and EW theory build the so-called *Standard Model* (SM) of Particle Physics. The gauge group of the SM is

$$SU(3)_C \times SU(2)_F \times U(1)_Y, \tag{2.1}$$

where the first factor encodes the color gauge group of the QCD with eight color-charged gluons and the second factor $SU(2)_F \times U(1)_Y$ contains four vector bosons which are related to the three experimentally observable massive vector bosons $W^{\pm}, Z$ of the weak force and the massless photon of the electromagnetic interaction via the Higgs mechanism. This part of the SM is usually called the *Weinberg-Glashow-Salam Theory*. It is an open question whether the SM can be understood as a part of a bigger unified theory with a gauge group which would include the gauge group of the SM as a subgoup. Candidates for such a theory are usually referred to as *Great Unified Theories* (GUTs) [89–91]
Measurable quantities such as cross sections, decay widths or anomalous magnetic moments can be computed perturbatively within the QFT as formal power-series expansions in the coupling constants of the corresponding forces which mediate the underlying interaction. Some of these observables are among both the most accurately predicted and precisely measured physical quantities [92–96].
This chapter is structured as follows: In the sections 2.1 and 2.2 we give a brief introduction to both the general structure of QFT and its calculational framework which relates abstract objects of the theory to measurable observables via *scattering amplitudes*. We will find that quantum corrections require the knowledge of complicated multi-dimensional integrals taken over momentum variables. These integrals are called *Feynman* or *loop* integrals. Since Feynman integrals are the central objects of this work we will define them and discuss their basic properties in 2.3.

2.1 Structure of QFT

2.1.1 Standard-Model Lagrangian

The basic object of a QFT which encodes both the particle spectrum and the interaction structure of the theory is the *Lagrangian density* (most simply called *Lagrangian*) $\mathcal{L}$. The Lagrangian is a function of underlying fields and their derivatives and has to be a Lorentz scalar in order to provide a valid relativistic theory. The Lagrangian of the SM is given by

$$\mathcal{L}_{SM} = \mathcal{L}_{YM} + \mathcal{L}_{Matter} + \mathcal{L}_{Higgs} + \mathcal{L}_{Yukawa}. \tag{2.2}$$

Let us consider the four constituents of the SM Lagrangian in more detail:
The *Yang-Mills* Lagrangian $\mathcal{L}_{YM}$ contains the gauge part

$$\mathcal{L}_{YM} = -\frac{1}{4} G^a_{\mu\nu} G^{a,\mu\nu} - \frac{1}{4} W^i_{\mu\nu} W^{i,\mu\nu} - \frac{1}{4} B_{\mu\nu} B^{\mu\nu}, \tag{2.3}$$

where $G^{a,\mu\nu}, W^{i,\mu\nu}$ and $B^{\mu\nu}$ are the *field-strength* tensors of the strong, the weak and the electromagnetic interactions. They can be written in terms of spin-1 massless gauge fields $G^{a,\mu}, W^{i,\mu}$ and B^μ as follows

$$\begin{aligned} G^{a,\mu\nu} &= \partial^\mu G^{a,\nu} - \partial^\nu G^{a,\mu} - g_S f^{abc} G^{b,\mu} G^{c,\nu}, \quad a,b,c = 1,\dots,8\,, \\ W^{i,\mu\nu} &= \partial^\mu W^{i,\nu} - \partial^\nu W^{i,\mu} - g \epsilon^{ijk} W^{j,\mu} W^{k,\nu}, \quad i,j,k = 1,2,3\,, \\ B^{\mu\nu} &= \partial^\mu B^\nu - \partial^\nu B^\mu, \end{aligned} \tag{2.4}$$

with g_S and g being the coupling constants, and f^{abc} and ϵ^{ijk} the *structure constants* of $SU(3)_C$ and $SU(2)_F$ gauge groups. While the $G^{a,\mu}$ are associated to the physical gluon fields, the three $SU(2)_F$-and the $U(1)_Y$-gauge fields are related to the physical $W^\pm, Z$ bosons and the physical photon. The relation between them will be shown later in this section. We denote the here absent $U(1)_Y$ coupling constant with g'. The structure constants f and ϵ are a manifestation of the non-abelian nature of the both gauge groups and encode the self-interaction between gluons and vector bosons of the weak force, respectively.
The term $\mathcal{L}_{Matter}$ contains all matter particles of the SM which are given by spin-$\frac{1}{2}$ fermions grouped into 6 types of color-charged quarks and 6 types of colorless leptons. All electrically charged leptons are described by *Dirac* fields which transform as $\left(\frac{1}{2},0\right) \oplus \left(0,\frac{1}{2}\right)$ representations of the Lorentz group, minimally coupled to the gauge fields. Note that for neutrinos it is still unknown whether they are described by *Dirac* or *Majorana* states. In the latter case, neutrinos would be their own antiparticles. There is an additional subtelty due to the chiral structure of the weak interaction which distinguishes between the $\left(\frac{1}{2},0\right)$ and the $\left(0,\frac{1}{2}\right)$ representations. While the *left-handed* $\left(\frac{1}{2},0\right)$ fields transform as doublets under the $SU(2)_F$ the *right-handed* $\left(0,\frac{1}{2}\right)$ fields correspond to singlets. In physical terms this means that there are two types of fermions which behave identically under the strong and the electromagnetic forces but only the first type is affected by the weak force. Both quarks and leptons appear in three so-called *generations* which differ only by the particles' masses but have identical charges with respect to the gauge groups. The mass range of the matter particles reaches from 511 keV for the electron up to ca. 173 GeV for the top-quark.[1]. The explicit form of the matter part Lagrangian is

$$\mathcal{L}_{Matter} = i\bar{\Psi}^r_{L,l} \not{D} \Psi^r_{L,l} + i\bar{\psi}^r_{R,l} \not{D} \psi^r_{R,l} + i\bar{\Psi}^r_{L,q} \not{D} \Psi^r_{L,q} + i\bar{\psi}^r_{R,q_d} \not{D} \psi^r_{R,q_d} + \bar{\psi}^r_{R,q_u} \not{D} \psi^r_{R,q_u}, \quad r = 1,2,3, \tag{2.5}$$

[1] Neutrinos are considered as exactly massless in the SM which is a very good approximation for all high-energy applications. In fact, neutrino oscillation experiments [97–101] show that at least two neutrino generations have very small but non-vanishing masses [102, 103]. This can be, in principle, incorporated into the SM via e.g. the *seesaw mechanism* [104].

with $\bar{\psi} \equiv \psi^\dagger \gamma^0$. Here $\Psi^r_{L,l} = \binom{e^r_L}{\nu^r_L}$ and $\Psi^r_{L,q} = \binom{u^r_L}{d^r_L}$ denote the left-handed lepton and quark doublets while $\psi^r_{R,l} = e^r_R$, $\psi^r_{R,q_u} = u^r_R$ and $\psi^r_{R,q_d} = d^r_R$ are the right-handed charged leptons and the right-handed up- and down-type quarks which are singlets under the weak force, respectively. The index r labels the three fermion generations. Right-handed neutrinos are not included in the SM. If incorporated, they would be singlets under all three gauge groups and so completely *sterile* with respect to all SM interactions. The gauge-matter interaction in the SM is encoded in the $\mathcal{L}_{Matter}$ through the *covariant derivative* $\not{D} \equiv D_\mu \gamma^\mu$, with

$$D_\mu = \partial_\mu - \frac{ig_S}{2}\lambda^a G^a_\mu - \frac{ig}{2}\tau^i W^i_\mu - \frac{ig'}{2} Y B_\mu. \tag{2.6}$$

Here λ^a are the Gell-Mann matrices and τ^i the Pauli-matrices which are the generators of the $\mathfrak{su}(3)$ and $\mathfrak{su}(2)$ algebras, respectively. Y is called the *hypercharge* which is given in terms of the *weak isospin* by

$$Q = T_3 + \frac{1}{2}Y, \tag{2.7}$$

where Q is the electric charge in units of the elementary charge e and T_3 is the third component of the weak isospin which takes the values $\pm\frac{1}{2}$ for left-handed and 0 for right-handed fermions. The strong interaction part of the covariant derivative does not contribute in the leptonic terms in $\mathcal{L}_{Matter}$.

Beyond the matter and gauge fields, the SM contains a further scalar field, the so-called *Higgs*-field, through which both the matter fermions (excluding the neutrinos) and the three massive gauge bosons acquire mass through the mechanism of *spontaneous symmetry breaking*. The Higgs-field contributes to the SM Lagrangian with a kinetic term and a quartic potential given by

$$\mathcal{L}_{Higgs} = (D_\mu \Phi)^\dagger (D^\mu \Phi) - V(\Phi), \tag{2.8}$$

with

$$V(\Phi) = -\mu^2 \left(\Phi^\dagger \Phi\right) + \frac{1}{2}\lambda \left(\Phi^\dagger \Phi\right)^2, \tag{2.9}$$

where $\mu^2 > 0, \lambda > 0$. The *complex* Higgs-field Φ is a $SU(2)_F$-doublet and can be brought into the following form

$$\Phi = \frac{1}{\sqrt{2}} \begin{pmatrix} 0 \\ v + h \end{pmatrix} \tag{2.10}$$

by a $SU(2)_F$ gauge transformation. Here $v = \frac{\mu}{\sqrt{\lambda}}$ is the vacuum expectation value of the Higgs-field and h is the *real* scalar Higgs-field which describes fluctuations around the minimum of the Higgs-potential. The physical Higgs-particle is a manifestation of the h-field. By inserting the Higgs-field (2.10) into the kinetic part of (2.8), expanding the result and performing a suitable rotation in the space of the $\mathfrak{su}(2)_F \times \mathfrak{u}(1)_Y$ generators, we obtain the mass eigenbasis of the physical $W^\pm$ and Z bosons. The obtained gauge-boson masses can be expressed in terms of the Higgs-field vacuum expectation value v and the coupling constants g and g' by

$$m_W = \frac{vg}{2}, \qquad m_Z = \frac{v\sqrt{g^2 + g'^2}}{2}. \tag{2.11}$$

The massive gauge-boson fields are given by

$$W^\pm_\mu = \frac{1}{\sqrt{2}} \left(W^1_\mu \mp W^2_\mu\right), \quad Z_\mu = \frac{1}{\sqrt{g^2 + g'^2}} \left(g W^3_\mu - g' B_\mu\right). \tag{2.12}$$

The fourth field which is massless and orthogonal to Z_μ represents the *physical photon* field A_μ with

$$A_\mu = \frac{1}{\sqrt{g^2 + g'^2}} \left(g' W_\mu^3 + g B_\mu \right). \tag{2.13}$$

Finally, the SM Lagrangian contains the interaction terms between the Higgs-field and the matter fields. The *Yukawa* part [85] of the Lagrangian

$$\mathcal{L}_{Yukawa} = -\lambda_l^{rs} \bar{\Psi}_{L,l}^r \cdot \Phi \psi_{R,l}^s - \lambda_{q_d}^{rs} \bar{\Psi}_{L,q}^r \cdot \Phi \psi_{R,q_d}^s - \lambda_{q_u}^{rs} \epsilon^{ab} \bar{\Psi}_{L,q}^{r,a} \Phi^b \psi_{R,q_u}^s + \text{h.c.}, \quad r,s = 1,2,3, \tag{2.14}$$

where λ_f with $f = l, q_u, q_d$ are generic complex-valued matrices. The mass terms can be diagonalized by inserting the gauge-fixed form (2.10) into (2.14) and rotating the fermion fields via

$$\begin{aligned} u_L^r &\to U_u^{rs} u_L^s, \quad d_L^r \to U_d^{rs} d_L^s, \\ u_R^r &\to W_u^{rs} u_R^s, \quad d_R^r \to W_d^{rs} d_R^s, \\ e_L^r &\to U_l^{rs} e_L^s, \quad \nu_L^r \to U_l^{rs} \nu_L^s, \quad e_R^r \to W_l^{rs} e_R^s, \end{aligned} \tag{2.15}$$

such that $\lambda_f \lambda_f^\dagger = U_f D_f^2 U_f^\dagger$ and $\lambda_f^\dagger \lambda_f = W_f D_f^2 W_f^\dagger$ for diagonal matrices D_f^2 with positive eigenvalues and unitary matrices U_f, W_f. The new fermion fields diagonalize the fermion-Higgs coupling such that the Yukawa part becomes

$$\mathcal{L}_{Yukawa} = -\left[m_e^r \bar{e}_L^r e_R^r + m_u^r \bar{u}_L^r u_R^r + m_d^r \bar{d}_L^r d_R^r \right] \left(1 + \frac{h}{v} \right), \quad r = 1,2,3, \tag{2.16}$$

with $m_f^r = \frac{v}{\sqrt{2}} D_f^{rr}$. It can be shown that the transformation (2.15) does not affect any couplings containing either leptons or the right-handed quarks but it changes the coupling of the left-handed quarks to the W-boson such that mixing of the quark generations by the weak interaction becomes possible. This mixing is provided by the off-diagonal terms of the *Cabibbo-Kobayashi-Maskawa* (CKM) matrix V [105, 106] given by

$$V = U_u^\dagger U_d. \tag{2.17}$$

2.2 Scattering amplitudes

2.2.1 The S-matrix and cross section

In the section 2.1.1, the SM Lagrangian was introduced which is the basic abstract object of the modern theory of Particle Physics. Here, we are going to sketch the method which allows to extract information about experimentally measurable observables from the Lagrangian. As will be seen, the notion of *scattering amplitudes* will play a central role in this considerations.
The central observable in high-energy Particle Physics is the *cross section* σ. For a particle collider the cross section of a particular process is defined as the number of times N this process occurs divided by the collider's *integrated luminosity* $\int \mathrm{d}t\, L$

$$\sigma = \frac{N}{\int \mathrm{d}t\, L}. \tag{2.18}$$

The luminosity L gives the total number of collisions per beam area and time unit. So the cross section has the physical dimension of an area. The theoretical task is to relate the physically measurable quantity σ to the microscopic description of the scattering process. The latter is

encoded in the *S-matrix* which quantifies the quantum mechanical overlap between the initial and the final states. In this picture, particles in the initial and final states are considered to be in the far past ($t \to -\infty$), respectively the far future ($t \to +\infty$) relative to the time range of the interaction ($t \sim 0$) such that they can be treated as *free states*. The free theory can be obtained from the SM by setting all couplings to zero and solved exactly. So the initial and final states are given by exact solutions of the free theory. In the following, we consider a generic $2 \to n$ scattering process which is the most suitable setup for physics at particle colliders. Here, the S-matrix is defined as

$$ {}_{\text{out}}\langle \mathbf{p_1 p_2} \dots \mathbf{p}_n | \mathbf{p}_\mathcal{A} \mathbf{p}_\mathcal{B} \rangle_{\text{in}} \equiv \langle \mathbf{p_1 p_2} \dots \mathbf{p}_n | S | \mathbf{p}_\mathcal{A} \mathbf{p}_\mathcal{B} \rangle. \tag{2.19} $$

The states at the right-hand-side of eq.(2.19) are defined at a common reference time. So, informally, the scattering matrix S provides the time-evolution from the initial state to the final state. Here, $\mathbf{p}_1, \dots, \mathbf{p}_n$ are the 3-momenta of the final-state particles while $\mathbf{p}_\mathcal{A}, \mathbf{p}_\mathcal{B}$ denote the 3-momenta of the initial-state particles. The principle of probability conservation requires the unitarity of the S-matrix, e.g. $SS^\dagger = S^\dagger S = \mathbb{1}$. To isolate the non-trivial part of the scattering process we split up the unity operator from the S-matrix such that

$$ S = \mathbb{1} + iT, \tag{2.20} $$

where the *transition matrix* T contains now the actual interaction part of the scattering. The *scattering amplitude* $\mathcal{M}$ of the process is defined by

$$ \langle \mathbf{p_1 p_2} \dots \mathbf{p}_n | iT | \mathbf{p}_\mathcal{A} \mathbf{p}_\mathcal{B} \rangle = (2\pi)^4 \delta^{(4)} \left(p_\mathcal{A} + p_\mathcal{B} - \sum_{i=1}^{n} p_i \right) i\mathcal{M}(p_\mathcal{A}, p_\mathcal{B} \to p_1, \dots, p_n), \tag{2.21} $$

where we factored out the overall 4-momentum conservation.
From non-relativistic quantum mechanics we know that the cross section is proportional to the absolute square of the scattering amplitude. Simultaneously, it is proportional to the infinitesimal final-state phase-space element. The exact master formula for a $2 \to n$ scattering process in the relativistic case is (see e.g. [107])

$$ \mathrm{d}\sigma = \frac{1}{2E_\mathcal{A} 2E_\mathcal{B} |v_\mathcal{A} - v_\mathcal{B}|} \left(\prod_{i=1}^{n} \frac{\mathrm{d}^3 p_i}{(2\pi)^3} \frac{1}{2E_i} \right) |\mathcal{M}(p_\mathcal{A}, p_\mathcal{B} \to p_1, \dots, p_n)|^2 \, (2\pi)^4 \delta^{(4)} \left(p_\mathcal{A} + p_\mathcal{B} - \sum_{i=1}^{n} p_i \right). \tag{2.22} $$

Here $|v_\mathcal{A} - v_\mathcal{B}|$ indicates the relative velocity of the colliding beams in the laboratory frame in units of the speed of light. To obtain the full cross section we have to integrate over the complete n-particle final-state phase space. For some special cases of low multiplicity n this integral can be performed analytically for a generic amplitude but, in general, only numerical integration is possible.

2.2.2 Amplitudes and Feynman diagrams

Eq. (2.22) allows to relate the observable cross section to the quantum-mechanical amplitude which contains the microscopic information about the scattering process. So our task now is to compute the scattering amplitude. In general, it is not feasible to calculate exact amplitudes. Instead, we proceed *perturbatively* and expand the amplitude and, subsequently, the cross section into a series in powers of the relevant coupling constants. In order for such an expansion to make

sense, all expansion parameters have to be significantly smaller than 1[2].
Since all three coupling constants of the SM are *running*, e.g. they depend on the energy scale at which they are measured, we need to ensure that the couplings at the experiment's energy scale are small such that the perturbation theory is still valid. At typical energy scales of particle colliders (at least for sufficiently hard interactions) all (appropriately normalized) couplings have values clearly lower than 1. This energy range is called the *perturbative regime*. Note that the strong coupling grows at low energies so that the theory becomes non-perturbative at energies around $\Lambda_{\mathrm{QCD}} \sim 200\,\mathrm{MeV}$. At these energies, strongly-coupled bound states such as hadrons and mesons start to occur. At hadron colliders like the LHC, the non-perturbative physics has to be taken into account in two different ways. First, the initial-state particles at the LHC are protons which are strongly-coupled bound states whose internal structure is governed by non-perturbative effects parametrized by the *parton distribution functions* (PDF's). Second, the quarks and gluons in the final state do not remain isolated particles till they are measured but form *jets* consisting of collimated bundles of hadrons and mesons which then can be measured inside the detectors. This process is called *hadronization*. In the following, we will completely focus on the *hard part* of the scattering process which can be described in terms of the perturbative QFT.
In the 40s and 50s [109–116] an algorithmic procedure for computing scattering amplitudes order-by-order in the expansion parameter was established. Feynman found a way to express the scattering amplitude at each order in the perturbative expansion as a sum of objects which can be written down in a purely combinatorial way for any physical process. Furthermore, these objects can be systematically represented by special diagrams which are called *Feynman graphs*.

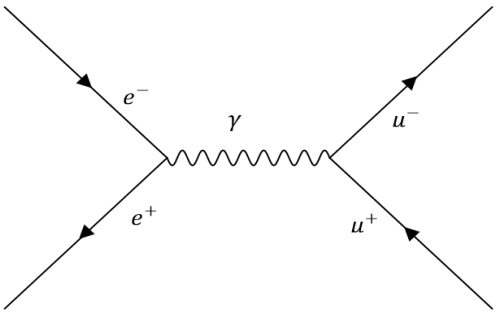

Figure 2.1: LO contribution to $e^+e^- \to \mu^+\mu^-$.

[2]This is of course necessary but not sufficient to ensure convergence of the perturbative series. Indeed, it was argued [108] that the coefficients of the series grow too fast such that the convergence radius of the perturbative series is 0! Nevertheless, for the first $\mathcal{O}(\frac{1}{g})$ orders, where $g < 1$ is the corresponding coupling constant, the series is expected to behave like it would converge.

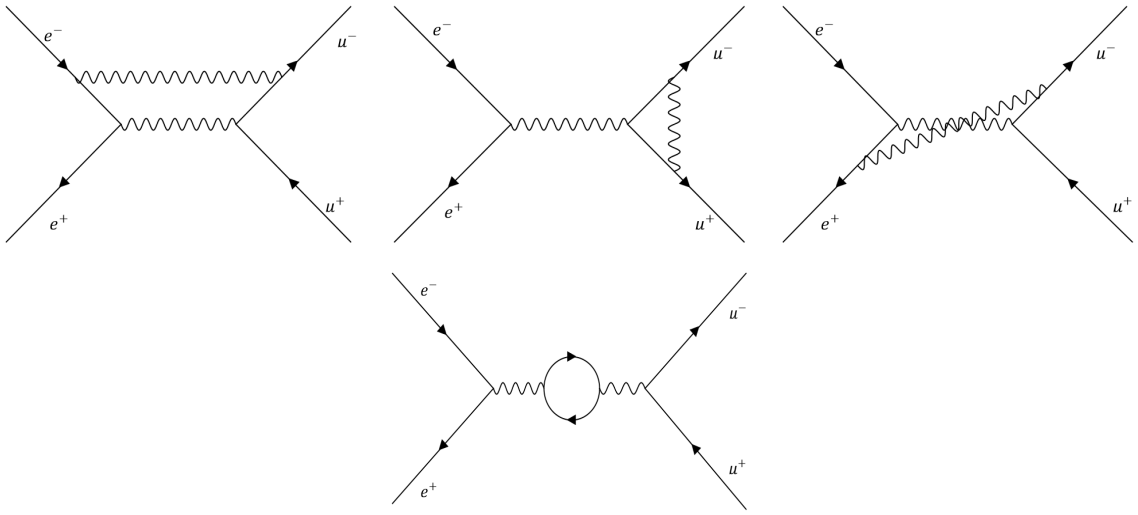

Figure 2.2: Some of the diagrams contributing at NLO to $e^+e^- \to \mu^+\mu^-$.

Figures 2.1 and 2.2 show examples for Feynman diagrams contributing to $e^+e^- \to \mu^+\mu^-$ at the first two orders in the *fine-structure constant* α. Feynman diagrams are drawn according to *Feynman rules* which can be derived from the Lagrangian of the considered theory and contain information about the fields and the propagators of the free theory as well as couplings between fields. Feynman rules give an exact mathematical expression for each Feynman diagram. According to these rules, a power of the coupling constant is assigned to each vertex in the diagram such that the number of vertices determines the order of the perturbative expansion this diagram contributes to. Diagrams with the lowest possible number of vertices sum up to the *leading order* (LO) contribution. Adding extra vertices leads to *next-to-leading order* (NLO), *next-next-to-leading order* (NNLO) contributions and so on as shown in 2.1 and 2.2. The algorithmic procedure of computing scattering amplitudes can be summarized as follows: Draw all Feynman diagrams which contribute to the process up to a fixed perturbative order and replace external lines, internal lines and vertices by the corresponding mathematical expressions accor-ding to the Feynman rules. Then, we need to integrate over all momenta flowing through internal lines of every diagram. Here, we have to distinguish between diagrams which do not contain closed internal lines (see fig. 2.1) and ones which do (see fig. 2.2). The first type of Feynman graphs is called *tree-level*-diagrams or simply *trees* while the second type is called *loop*-diagrams. Since we have to impose momentum conservation at every vertex due to the Feynman rules, all internal momenta of tree-level diagrams are fixed. For every loop, however, we have an undetermined internal momentum which has to be integrated over. Second, each loop adds two vertices, and so two powers of the coupling constant to the diagram which means that loop diagrams always contribute at higher order compared to the corresponding tree-level diagrams. Symbolically, a scattering amplitude can be written as follows

$$i\mathcal{M} = \sum_k \sum_A \mathcal{D}_k^A = i \sum_{k=0}^{\infty} \mathcal{M}^{(k)}, \tag{2.23}$$

where $\mathcal{D}_k^A$ denote Feynman diagrams at order k.
Let us now analyze which contributions need to be computed at the cross-section level in order to obtain a fixed-order phenomenological prediction. Apart from loop corrections which were discussed previously there is a second class of corrections due to production of additional gluons

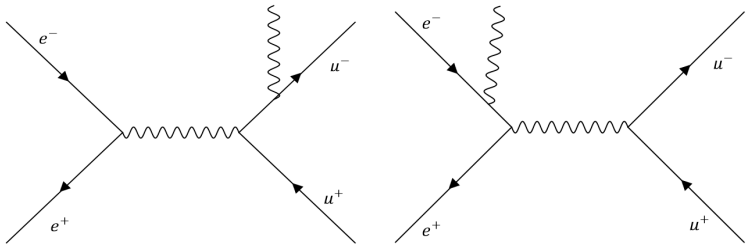

Figure 2.3: Two examples of real NLO corrections to $e^+e^- \to \mu^+\mu^-$. External photons are either soft or collinear.

or photons which contribute at the same order. These corrections are referred to as *real radiation* while the loop-type corrections are called *virtual* since loop particles only exist as intermediate states. Real corrections need to be added due to finite energy sensitivity and spatial resolution of any physical detector. Therefore, there is no possibility to distinguish between a $2 \to n$ process and a $2 \to n+1$ process with an additional arbitrary *soft* or *collinear* massless gauge boson radiated from one of the *hard* particles. Figure 2.3 shows two diagrams contributing to NLO real corrections to $e^+e^- \to \mu^+\mu^-$.

Let us now write down all terms which contribute to the cross-section at LO, NLO and NNLO level for an arbitrary $2 \to n$ process.

$$\begin{aligned}
\sigma_{\mathrm{LO}} &= \int \mathrm{d}\Phi_n |\mathcal{M}_n^{(0)}|^2, \\
\sigma_{\mathrm{NLO}} &= \int \mathrm{d}\Phi_n \left(\mathcal{M}_n^{(0)^\dagger} \mathcal{M}_n^{(1)} + \mathcal{M}_n^{(0)} \mathcal{M}_n^{(1)^\dagger} \right) + \int \mathrm{d}\Phi_{n+1} |\mathcal{M}_{n+1}^{(0)}|^2 + \sigma_{\mathrm{LO}}, \\
\sigma_{\mathrm{NNLO}} &= \int \mathrm{d}\Phi_n \left(\mathcal{M}_n^{(0)^\dagger} \mathcal{M}_n^{(2)} + \mathcal{M}_n^{(0)} \mathcal{M}_n^{(2)^\dagger} + |\mathcal{M}_n^{(1)}|^2 \right) + \int \mathrm{d}\Phi_{n+1} \left(\mathcal{M}_{n+1}^{(0)^\dagger} \mathcal{M}_{n+1}^{(1)} + \mathcal{M}_{n+1}^{(0)} \mathcal{M}_{n+1}^{(1)^\dagger} \right) \\
&\quad + \int \mathrm{d}\Phi_{n+2} |\mathcal{M}_{n+2}^{(0)}|^2 + \sigma_{\mathrm{NLO}}.
\end{aligned} \tag{2.24}$$

Since in this thesis we are interested in NNLO corrections for a selection of five-particle processes we have to compute three types of contributions:

- *Double-virtual*: Five-point diagrams with one and two loops,
- *Double-real*: Seven-point tree-level diagrams with two additional, particles
- *Mixed real-virtual*: Six-point diagrams with one loop and one additional particle.

Some of the diagrams contribute in multiple places, e.g. trees appear in interference terms in all contributions, similarly one-loop diagrams contribute to both double-virtual and mixed real-virtual corrections. Figure 2.4 shows some generic diagrams contributing to each of three classes. All three types of corrections are in general *infrared* (IR) divergent but the full cross-section (including PDF's) can be shown to be always infrared finite (*Kinoshita-Lee-Nauenberg-theorem* (KLN) [117, 118]). In the following, we will focus on the double-virtual part since the other two types of corrections can be, by now, computed by automated methods. Note, however, that the numeric integration over the soft and collinear phase-space is, in practice, very challenging, in particular for final states with many massless particles.

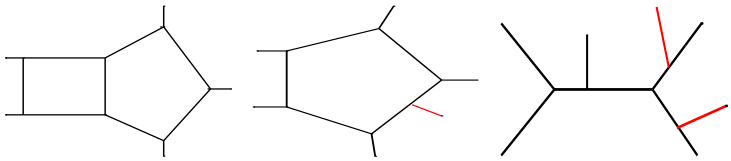

Figure 2.4: Generic examples for double-virtual, mixed real-virtual and double-real corrections. Red lines denote soft particles.

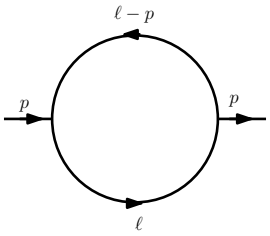

Figure 2.5: One-loop bubble integral with massless propagators.

Since the momenta of virtual particles in loops are not constrained by momentum conservation, they can take arbitrary values and we have to integrate over all loop momenta in order to obtain the correct result. This type of integrals which remain after applying momentum conservation constraints is called *loop* or *Feynman integrals*. In terms of Feynman diagrams, the double-virtual part of the amplitude can be seen as a sum of many two-loop integrals[3] whose integrands can be written down by Feynman rules. However, it can be shown (see 2.3.3 for details) that a very large set of linear relations among different Feynman integrals exists such that only a small subset of Feynman integrals (typically few dozens up to few hunderts) is independent and has to be computed in the first place. In terms of these so-called *master integrals* I_i, the double-virtual amplitude can be written as

$$\mathcal{M}^{(2)}_{\text{double-virtual}} = \sum_i \alpha_i I_i, \tag{2.25}$$

where α_i are functions of the kinematics.

The modern *unitarity-based* techniques [8, 11, 25, 119–123] which were upgraded to the two-loop level in the last decade [22–24] allow to compute the coefficients α_i without generating Feynman diagrams by comparing the *cuts* (see section 2.3.4) of the amplitude which are given by products of tree-level diagrams to the cuts of the master integrands and *surface terms* [22]. This reduces the problem of computing the amplitude to a linear algebra computation if the master integrals are known. A very important extension of this approach is the *numerical unitary method* which combines the unitarity approach with efficient numerical methods followed by a *functional reconstruction* of the final result [39, 124, 125].

Before we continue with a more formal discussion of Feynman integrals, let us briefly review a further very important ingredient of higher-order calculations, namely the concept of *renormalization*. It is a well-known fact that many of the Feynman integrals are divergent in four space-time dimensions. As a simple example, consider the so-called *bubble* integral 2.5 with massless internal particles which contributes e.g. to the gluon propagator-type corrections. The analytic expression is given by

$$I_{bubble} \sim \int \mathrm{d}^4\ell \, \frac{1}{\ell^2(\ell+p)^2}, \tag{2.26}$$

[3] Products of two one-loop integrals can be considered as two-loop integrals as well.

with the loop momentum ℓ and the external momentum p. In the *hard region* of the loop-momentum space ($\ell^2 \to \infty$), the leading part of the integral becomes

$$I_{bubble}^{hard} \sim \int_0^\infty \frac{\mathrm{d}R}{R}, \tag{2.27}$$

where we integrated out the angular variables. This integral is logarithmically divergent. This type of divergencies is called *UV-divergencies*. To deal with this class of infinitities, a *regularization* procedure is used in order to formulate the divergent behaviour of the Feynman integrals in an exact analytic way. Nowadays, the standard regularization method is the *dimensional regularization* [126]. The idea is to use the space-time dimension as a dynamical parameter and work with integrals which are defined in an arbitrary space-time dimension D instead of working in a space with a fixed number of space-time dimensions. Typically, we parametrize D as $D = 4 - 2\epsilon$ for some arbitrary $\epsilon \in \mathbb{C}$ and assume ϵ to be small so that we can expand the integrals around $\epsilon = 0$. In this framework, both UV and IR divergencies manifest themselves as poles in ϵ. In 2.3.1 we will provide a formal definition of dimensionally-regularized Feynman integrals. Here we just want to mention that many of the modern techniques which deal with Feynman integrals rely on dimensional regularization and are not applicable in other regularization schemes.
After we regularized all Feynman integrals, the basic ingredients of the field theory such as fields, masses and couplings are redefined in such a way that they absorb all UV-type infinities. The *renormalized* masses and couplings are then matched to the experimentally measured values. Though this cannot be done for every possible QFT, the *renormalizability* of the SM is proven to all orders in perturbation theory [127].

2.3 Feynman integrals

At the end of section 2.2.2, we saw that higher-order corrections in the perturbative QFT require computation of integrals over the loop-momentum space. We have also shown that these integrals are often divergent in $D = 4$ space-time dimensions and a regularization procedure is needed in order to deal with these divergencies. In this thesis, we work in the framework of the dimensional regularization and set $D = 4 - 2\epsilon$.
Although the focus of the present work clearly lies on practical computation of some particular two-loop integral families, it needs to be said that Feynman integrals are highly interesting objects by themselves and have been studied from a purely theoretical point of view for many years. A short overview can be found in [128–134]. The underlying mathematical structure reaches from the theory of special functions over multi-dimensional complex analysis up to modern methods of algebraic and differential geometry. Since a detailed discussion of these very different aspects is far beyond the scope of this work we will mainly concentrate on computational aspects and only briefly touch on mathematical questions if they are of direct relevance for our goals.
In the present section, we will give a general definition of dimensionally-regularized multi-loop Feynman integrals, introduce both *parameter* and *Baikov* representations as well as the notion of the *master integrals* which we declare via *integration-by-parts relations*. After that, we define the *cut* Feynman integrals and discuss the *differential equation* method which is, nowadays, the most powerfull tool for computing master integrals. In this section we keep our discussion general. A detailed treatment of the massive five-point integrals and more special methods will follow in Chapter 3.

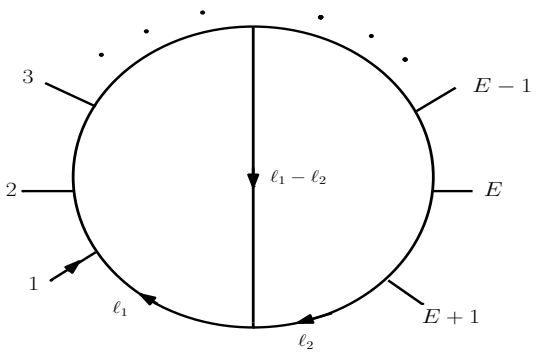

Figure 2.6: Generic two-loop planar integral. All external momenta are ingoing.

2.3.1 Formal definition of Feynman integrals

We begin with the definition of Feynman integrals in dimensional regularization. A L-loop integral with $E+1$ external legs is defined as

$$I\left[\vec{D},\vec{s},\vec{\nu},L,E,\mathcal{N}\right] := e^{L\gamma_E\epsilon}\int\prod_{k=1}^{L}\left(\frac{\mathrm{d}^D\ell_k}{i\pi^{D/2}}\right)\frac{\mathcal{N}(\ell)}{\prod_{j=1}^{n}D_j^{\nu_j}}. \tag{2.28}$$

Let us explain our notation. The internal or *loop* momenta are denoted with $\ell_k, \quad k=1,\ldots,L$. They are elements of a D-dimensional vector space and can be parametrized as

$$\ell_k = \hat{\ell}_k + \tilde{\ell}_k, \tag{2.29}$$

where $\hat{\ell}_k$ are the four-dimensional and $\tilde{\ell}_k$ the extra-dimensional parts of the loop momenta. The denominator factors D_j are called *inverse propagators* if their powers ν_j are positive and *irreducible scalar products* (ISP's) if their powers are negative. The inverse propagators are derived from the Feynman rules of the underlying theory and define the kinematic dependence of a Feynman diagram. In general, they are given by

$$D_j = q_j^2 - m_j^2 + i\varepsilon, \qquad j=1,\ldots n, \tag{2.30}$$

with

$$q_j = \sum_{k=1}^{L} a_{jk}\ell_k + \sum_{r=1}^{E} b_{jr}p_r, \tag{2.31}$$

where $a_{jk}, b_{jr} \in \{+1,0,-1\}$, m_j^2 are the internal masses and $i\varepsilon$ arises from the Feynman's $i\varepsilon$ prescription which encodes the causality condition. The explicit form of the propagators depends on the way in which loop momenta are associated to the Feynman graph. At one loop one usually works with a cyclic association such that $q_i = \ell + \sum_{j=0}^{i-1} p_j$ with $p_0 := 0$. At multi-loop level no canonical way to define propagators exists. In diagram 2.6 we show a generic planar two-loop graph where ℓ_1 flows in the left part of the diagram (*left rung*) and ℓ_2 in the right part (*right rung*). Only the central edge (*central rung*) contains both loop momenta. Since in this work we are interested only in processes with massless internal particles we can set $m_j^2 = 0$ and we will omit the Feynman's $i\varepsilon$-prescription for the sake of simplicity for most of the time. A set of Feynman integrals which share the same set of propagators is called an *integral topology*. A particular member of a given topology is specified by the list of *indices* $\vec{\nu} \in \mathbb{Z}^n$.

A subset of integrals is called a *subtopology* if every integral of this subset also appears in the bigger topology. At the level of indices, that means that an index of a sub-integral can only be positive if the corresponding index of the parent topology is positive. Subtopologies correspond to sub-graphs and setting an index to zero is equivalent to pinching an edge of the corresponding diagram. Let us discuss the role of the ISP's. At one-loop level every scalar product of a loop and an external momentum can be written as linear combination of the inverse propagators via

$$\ell \cdot p_i = \frac{1}{2}\left[D_{i+1} - D_i - 2p_i \cdot \sum_{j=0}^{i-1} p_j - p_i^2\right], \quad i = 1, \ldots, E. \tag{2.32}$$

However, for $L \geq 2$ inverse propagators might not be enough to span the vector space of loop-dependent scalar products. So ISP's need to be added. In the present work, ISP's are chosen to have the form of eq. (2.30) and can be treated just like inverse propagators. The dimension $n = n(L, E)$ of the ISP vector space is given by

$$n = \frac{1}{2}L(L+1) + LE. \tag{2.33}$$

For $L = 1$ eq. (2.33) indeed produces $n = E + 1$ as already shown in (2.32) .
The vector $\vec{s}$ contains all external kinematic quantities I depends on. Since Feynman integrals are Lorentz-invariant objects they can only be functions of scalar products of external momenta $p_1, \ldots, p_{E+1}$ which respect the total momentum conservation, expessed in the form $\sum_{i=1}^{E+1} p_i = 0$. External momenta are considered as strictly four-dimensional with $p_i \cdot \tilde{\ell}_j := 0$. The number N_{kin} of independent kinematic quantities is given by the total number of momentum components $4(E+1)$ minus the number of on-shell constraints and the dimension of the space-time symmetry group which is here the Poincare group of the four-dimensional Minkowski space. Let E' be the number of massless external legs so

$$N_{kin} = 4(E+1) - E' - 10, \tag{2.34}$$

where 10 is the dimension of the Poincare group. External kinematics is usually parametrized in form of the momentum squares of the external legs p_i^2 and the so-called *Mandelstam* invariants $s_{ij} := (p_i + p_j)^2$ with $i \neq j$. In dimensional regularization all *scaleless* integrals (that means $N_{\text{kin}} \leq 0$) vanish [12]. If $N_{\text{kin}} = 1$, the integral is a homogenous function of a single kinematic scale s and followingly takes the form

$$I = s^{a(\epsilon)} b(\epsilon), \tag{2.35}$$

where a is given by the half of the integral's mass dimension and b is an arbitrary constant.
Before we continue with the discussion of integrals, it has to be mentioned that for most of the time we are not interested in the full dependence of the Feynman integral on the dimensional regulator ϵ but only in its behaviour near four dimensions $\epsilon \to 0$. So, often, we will replace the full integral by its Laurent expansion

$$I = \sum_{n=-2L}^{\infty} I^{(n)} \epsilon^n \tag{2.36}$$

and drop the $\mathcal{O}(\epsilon)$ part. The degree of the highest pole can be derived from the analytic structure of generic L-loop Feynman amplitude [135]. Finally, γ_E in the exponential prefactor of eq. (2.28) denotes the *Euler-Mascheroni constant* and can be defined as $\gamma_E = -\Gamma'(1)$. The normalisation ensures that no factors of γ_E appear in the ϵ-expansion of I.

2.3.2 Parameter and Baikov representations

For some applications the momentum-space representation of the Feynman integral eq. (2.28) is not the most convenient one. In the following, we present two alternatives: the *Feynman parameter* and the *Baikov* representation.
The Feynman parameter form is based on the observation [107] that the product of two inverse factors can be replaced by one inverse factor at the cost of introducing an integration over an auxiliary variable. Concretely,

$$\frac{1}{A_1 A_2} = \int_0^1 \mathrm{d}x \, \frac{1}{\left[xA_1 + (1-x)A_2\right]^2} = \int_0^1 \mathrm{d}x \int_0^1 \mathrm{d}y \, \frac{\delta(1-x-y)}{\left[xA_1 + yA_2\right]^2}. \tag{2.37}$$

The second integration is introduced in order to make the integrand symmetric with respect to A_1 and A_2. By induction, eq. (2.37) can be generalized to an arbitrary number of inverse factors with arbitrary powers

$$\frac{1}{\prod_{i=1}^n A_i^{\nu_i}} = \frac{\Gamma(\nu)}{\prod_{i=1}^n \Gamma(\nu_i)} \int_0^1 \frac{\prod_{i=1}^n \mathrm{d}x_i \, x_i^{\nu_i - 1} \delta\left(1 - \sum_{j=1}^n x_j\right)}{\left[\sum_{j=1}^n x_j A_j\right]^\nu}, \tag{2.38}$$

where $\nu := \sum_{i=1}^n \nu_i$. Obviously, eq. (2.38) can be used to put all propagators of a Feynman integral to a single "propagator"-like factor whose power is given by the sum of all indices. By completing the squares and linear shifts of the right-most loop momentum ℓ_L, the new denominator can be brought into the form

$$\sum_{i=1}^n x_i D_i = \ell_L^2 + \Delta(\ell_1, \ldots, \ell_{L-1}, p_1, \ldots, p_E). \tag{2.39}$$

The integral with respect to ℓ_L has now the form of a simple tadpole integral with no angular dependence on ℓ_L and can be evaluated in terms of Γ-functions to

$$\int \frac{\mathrm{d}^D \ell_L}{i\pi^{D/2}} \frac{1}{\left[\ell_L^2 + \Delta\right]^\nu} = (-1)^\nu \frac{\Gamma(\nu + \epsilon - 2)}{\Gamma(\nu)} \frac{1}{(-\Delta)^{\nu+\epsilon-2}}. \tag{2.40}$$

Now we can proceed by induction and perform all loop-momenta integrations. We trade the momentum-space integration for a n-dimensional parameter integral where n is the number of propagators. It has the form [136]

$$I[\vec{D}, \vec{\nu}] = e^{L\gamma_E \epsilon} \frac{\Gamma(\nu - LD/2)}{\prod_{i=1}^n \Gamma(\nu_i)} \int_0^1 \prod_{i=1}^n \left(\mathrm{d}x_i \, x_i^{\nu_i - 1}\right) \delta\left(1 - \sum_{i=1}^n x_i\right) \frac{U^{\nu - (L+1)D/2}}{F^{\nu - LD/2}}. \tag{2.41}$$

U and F are polynomials in the Feynman parameters which encode the kinematic structure of the integral (see e.g. [137] for a review). In the literature, they are usually called the *first and second Symanzik polynomials*. Both polynomials can be directly constructed from the denominator of eq.(2.38) which can be written as

$$\sum_{i=1}^n x_i D_i = \sum_{i=1}^n x_i q_i^2 = \sum_{r=1}^L \sum_{s=1}^L M_{rs} \ell_r \cdot \ell_s - 2 \sum_{r=1}^L \ell_r \cdot Q_r - J, \tag{2.42}$$

with a $L \times L$-dimensional matrix M, a L-dimensional set of four-vectors Q and a scalar quantity J depending on Feynman parameters and external kinematics. The Symanzik polynomials are

given by

$$\begin{aligned} U &= \det M, \\ F &= \det M \left(J + Q^\top M^{-1} Q \right). \end{aligned} \tag{2.43}$$

Let us emphasize some properties of the Symanzik polynomials:

- U and F are homogenous polynomials in Feynman parameters of degree L and $L+1$, respectively.
- U is linear in each variable while F is also linear in case of massless propagators.
- Each monomial of U has coefficient $+1$. So, at one loop $U = \sum_{i=1}^{n} x_i$.

Alternatively, U and F can be computed directly from underlying Feynman graph using graph-theoretical methods [137]. In this language,

$$\begin{aligned} U &= \sum_{T \in \tau_1} \prod_{e_i \notin T} x_i, \\ F &= \sum_{(T_1,T_2) \in \tau_2} \prod_{e_i \notin (T_1,T_2)} x_i (-s_{(T_1,T_2)}) \end{aligned} \tag{2.44}$$

in case of massless internal propagators. Here τ_k denote the *spanning k-forests* of the Feynman graph G and $(T_1, \ldots, T_k) \in \tau_k$ are *connected components*. Finally, $\{e_1, \ldots, e_n\}$ are the edges of G. The kinematic quantity $s_{(T_1,T_2)}$ denotes the square of the sum of the external momenta attached to the connected components T_1 and T_2 which are equal by momentum conservation. The kinematic region where all $s_{(T_1,T_2)} < 0$ and so $F > 0$ is called *Euclidean*. According to eq. (2.41), a Feynman integral is manifestly real inside the Euclidean region. If G is a planar graph then all $s_{(T_1,T_2)}$ are given by cyclic Mandelstam invariants $s_{i(i+1)} = (p_i + p_{i+1})^2$ and momentum squares p_i^2 where the index addition is understood to be modulo n. In this case, the Euclidean region is simply the region of the phase space with all cyclic Mandelstam invariants and external momentum squares being negative.

We close the discussion of the Feynman parameter representation with the *Cheng-Wu theorem* [138] which states that the δ-function in eq. (2.41) can always be replaced by $\delta(1 - H(\vec{x}))$ where H is an arbitrary hyperplane $H(\vec{x}) = \sum_{i=1}^{n} H_i x_i$ with $H_i \geq 0$ [133].

Another very useful integral representation which will be used very often throughout this thesis is the *Baikov coordinate* representation [139–142]. It is based on the idea of using inverse propagators and ISP's as integration variables. This approach makes use of the specific structure of the Feynman integrals and also makes the number of integral variables manifest which is given in eq. (2.33). We perform the variable change

$$(\ell_1^\mu, \ldots, \ell_L^\mu) \to (\rho_1, \ldots, \rho_n), \tag{2.45}$$

with $\rho_i = D_i$. After this variable change, the generic Feynman integral becomes [143]

$$\begin{aligned} I\left[\vec{D}, \vec{\nu}, \mathcal{N}, \right] =& C_n^L (G(p_1, \ldots, p_E))^{(-D+E+1)/2} \int \left(\prod_{i=1}^{n} \frac{\mathrm{d}\rho_i}{\rho_i^{\nu_i}} \right) \mathcal{N}(\vec{\rho}) \\ & \times (P(\ell_1, \ldots, \ell_L, p_1, \ldots, p_E))^{(D-L-E-1)/2}, \end{aligned} \tag{2.46}$$

where $P = G(\ell_1, \ldots, \ell_L, p_1, \ldots, p_E)$ is usually called the *Baikov polynomial*. G denotes the *Gram* determinant defined by $G(v_1, \ldots, v_n) = \det (v_i \cdot v_j)_{i,j=1}^{n}$ and $\mathcal{N}$ is an arbitrary numerator insertion

polynomial in the ρ's. We refer to [141, 142] for a detailed derivation of this result. Note that P is a quadratic polynomial in the ρ_i and

$$C_n^L = e^{L\gamma_E\epsilon}\frac{\pi^{-L(L-1)/4-LE/2}}{\prod_{i=1}^{L}\Gamma(\frac{D-L-E+i}{2})}\det A^{-1} \tag{2.47}$$

is a numerical constant with a $n \times n$ matrix A whose entries are given by

$$D_a = \sum_{i=1}^{L}\sum_{j=i}^{L} A_{a,ij}\ell_i\cdot\ell_j + \sum_{i=1}^{L}\sum_{j=L+1}^{L+E} A_{a,ij}\ell_i\cdot p_{j-L} + f_a, \quad a = 1,\ldots,n. \tag{2.48}$$

We consider $a = 1,\ldots,n$ to be the row index and the n pairs (ij) with $j \geq i$ are the column indices. The entries $A_{a,ij}$ are integers from the set $\{-2,-1,0,1,2\}$. The scalar quantities f_a contain the dependence on the external kinematics. Both the matrix A and the f_a can be related to the matrices $(a_{ak})_{a=1,k=1}^{n,L}$ and $(b_{ar})_{a=1,r=1}^{n,E}$ from eq. (2.31). The Baikov representation makes the pole structure of the Feynman integrals manifest and is well-suited for residue computation, as will be shown in 2.3.4. Another advantage of this representation is the manifest dependence of P on the external kinematic quantities $\vec{s}$. This fact will allow us to use Baikov representation for computing derivatives of the Feynman integrals with respect to $\vec{s}$, as will be shown in 3.2.

2.3.3 Integration-by-parts and Lorentz-invariance identities

Since the indices in eq. (2.28) can take any integer value there are formally infinitely many integrals in each topology. The number of loop integrals which appear in an amplitude computation eq. (2.23) is finite but can become large for a two-loop calculation. However, linear relations exist among the integrals such that only a comparably small number of integrals $\mathcal{O}(100)$ in a family is linear independent. These integrals provide a basis of the linear space of all Feynman integrals in a given topology and are usually referred to as *master integrals* (MI). It was proven [144] that the number of master integrals for a single topology is indeed always finite.
The most important type of the linear relations satisfied by Feynman integrals are *integration-by-parts* (IBP) identities [145, 146]. They arise from the fact that integrals of total derivatives vanish identically in dimensional regularization

$$\int\left(\prod_{j=1}^{L}\frac{\mathrm{d}^D\ell_j}{i\pi^{D/2}}\right)\frac{\partial}{\partial\ell_k^\mu}\left(\xi^\mu\frac{\mathcal{N}}{\prod_{i=1}^{n}D_i^{\nu_i}}\right) = 0, \quad k = 1,\ldots,L, \tag{2.49}$$

where ξ^μ is an arbitrary four-vector depending on loop or external momenta. By expanding the integrand in eq. (2.49) by the Leibnitz rule we obtain a vanishing linear combination of Feynman integrals of the same topology.

$$\sum_i C_i(\vec{s},D)I_i = 0, \tag{2.50}$$

where C_i are rational functions of the kinematics and the space-time dimension. Using different ξ^μ and different loop momenta in eq. (2.49) we can generate multiple independent IBP relations for a single Feynman integral. We can repeat this for a sufficiently large number of different integrals of the same topology until we get no new IBP relations. Integrals which remain unreduced at the end are by definition master integrals. Note that the number of MI's can be obtained independently by different methods [147, 148].

A widely used strategy of Feynman integral reduction is the *Laporta algorithm* [149] which is by now implemented in several public codes like `AIR` [150], `REDUZE` [151,152], `FIRE` [153–155] and `KIRA` [156,157] as well as numerous private programs. Laporta's algorithm is based on a systematic ordering of integrals inside an integral topology which allows to reduce more complicated integrals to linear combinations of simpler ones. Roughly speaking, this ranking compares absolute values of indices such that integrals with higher powers are ranked higher as integrals with lower powers.[4]

First of all, we split a given topology into subtopologies and reduce all integrals inside a subtopology to integrals with propagator powers smaller than a previously chosen constant. Let N be the number of propagators in the given topology and fix $L \leq n \leq N$. Then, we define a n-propagator subtopology τ_n^a via its set of inverse propagators and ISP's $\tau_n^a := \{D_{i_1}, \ldots, D_{i_n}\} \subset \{D_1, \ldots, D_N\}$, with $a = 1, \ldots, \binom{N}{n}$. Here, we assume that the first $r_n \leq n$ elements are inverse propagators and the last $s_n = n - r_n$ elements are ISP's. Once all subtopologies with n propagators are reduced, the algorithm proceeds with the $(n+1)$-subtopologies. For L loops and N propagators there are

$$S = \sum_{n=L}^{N} \binom{N}{n} < 2^N \tag{2.51}$$

different subtopologies. For each subtopology we choose positive integers a_n^a, b_n^a as upper boundaries for powers of inverse propagators and ISP's in the subtopology. More precisely,

$$\begin{aligned} \sum_{j=1}^{r_n} \nu_{i_j} &\leq a_n, \\ -\sum_{j=r_n+1}^{n} \nu_{i_j} &\leq b_n. \end{aligned} \tag{2.52}$$

Now we can start with generating IBP relations for the integrals with the lowest sum of absolute values for both positive and negative indices. We generate all IBP identities for these integrals and eliminate all integrals which are already reduced. Then, we solve the relations for the integral with the highest rank and obtain

$$I_{\text{h.r.}} = \sum_i C_i I_i, \tag{2.53}$$

where all integrals on the right-hand-side have lower rank than the integral on the left-hand-side and C_i are rational functions of D and the kinematics. We add eq. (2.53) to the list of known identities and proceed with the next-to-lowest ranked integral until the boundaries a_n and b_n are reached. Integrals which remain unreduced at this point will be added to the list of MI's. After that, the algorithm proceeds with the next subtopology. Note that we might get too many master integrals if the boundaries are set too low. The complete reduction can also be performed at a single phase-space point $\vec{s}_0$ and for a single value of the space-time dimension D_0 which is, in general, much faster than the fully analytic computation and also requires far less memory. For many two-loop problems only a numerical IBP reduction is possible in practice.

We close this section with a short discussion of a further type of linear relations among Feynman integrals. As already emphasized, Feynman integrals are Lorentz-invariant objects. This means in particular that

$$I(p_i^\mu + \delta p_i^\mu) = I(p_i^\mu) \tag{2.54}$$

[4] See [149] for details.

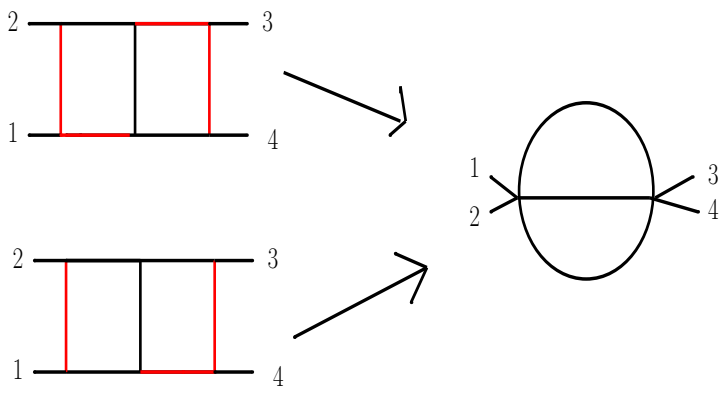

Figure 2.7: Two different pinches of the double-box topology lead to the same sunrise topology.

for any infinitesimal Lorentz transformation of any external momentum p_i^μ. Let us parametrize the transformation as

$$\delta p_i^\mu = \omega^{\mu\nu} p_{i,\nu} \tag{2.55}$$

for an infinitesimal totally anti-symmetric tensor $\omega^{\mu\nu}$. The general transformation behaviour of I can then be expressed as

$$I(p+\delta p) = I(p) + \omega^{\mu\nu} \sum_{i=1}^{E} p_{i,\mu} \frac{\partial I(p)}{\partial p_i^\nu}. \tag{2.56}$$

Using the anti-symmetry of ω, the Lorentz invariance of I can be cast into the form

$$(p_n^\mu p_m^\nu - p_m^\mu p_n^\nu) \sum_{i=1}^{E} \left(p_{i,\mu} \frac{\partial I}{\partial p_i^\nu} - p_{i,\nu} \frac{\partial I}{\partial p_i^\mu} \right) = 0, \quad n,m = 1,\ldots,E. \tag{2.57}$$

It is not difficult to see that $\binom{E}{2}$ independent identities can be built out of eq. (2.57). It can be shown [158] that Lorentz identities are not independent from IBP identities and, therefore, they do not provide additional information. So, in future, we will not distinguish between these two types of relations and call them both IBP identities, independently of how exactly they were generated.
Finally, we should mention that there can be symmetry relations between different subtopologies which are not captured by IBP identities. At the level of Feynman graphs that means that a particular sub-graph can be obtained by more than one sequence of pinches (see fig. 2.7 where red lines are pinched) and so it corresponds to two different subtopologies. In practice, these symmetries either have to be provided by hand or are detected automatically by some of the IBP-reduction programs.

2.3.4 Cut Feynman integrals, multivariate residues and leading singularities

Cut Feynman integrals have been studied since the early days of the perturbative QFT [139, 159]. By the *optical theorem* they are naturally related to discontinuities and branch cuts of Feynman integrals and are also the main ingredient of the unitarity-based approaches of the amplitude

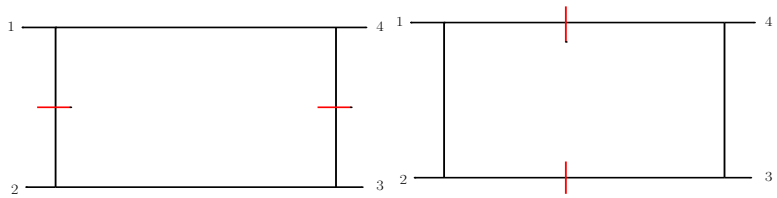

Figure 2.8: S-channel cut (*left*) and t-channel cut (*right*) of a massless box topology.

calculations. Typically, cut integrals are understood as ordinary Feynman integrals with a set of propagators $\left\{\frac{1}{D_{i_1}}, \cdots, \frac{1}{D_{i_m}}\right\}$ replaced by corresponding δ-functions

$$\frac{1}{D_{i_j}} \to \delta(D_{i_j}),\ j = 1, \cdots, m \leq n. \tag{2.58}$$

A *unitary cut* [160] selects a particular kinematic channel and an *iterated unitary cut* [161, 162] selects multiple channels. Fig. 2.8 represents s- and t-channel cuts of a box diagram. But also *non-unitary* cuts can be important, e.g. in the context of *generalized unitarity*. In this thesis, especially *maximal* cuts are of interest where all propagators of a topology are cut simultaneously. Here a weakness of the informal definition of cut integrals (2.58) becomes problematic. It is, for example, a well-known fact that there is no real solution for the maximal cut equations of the massless box integral at one-loop [11, 163]. Therefore, it is useful to define generalized cuts via multivariate residue calculation [163–165]. The idea behind this is to deform the integral contour of a Feynman integral to a closed contour that encircles all poles of the integrand and apply the residue theorem. Let us briefly review the multivariate residue calculus by Leray [166]. Here, we closely follow [167]. Note that the close link between cuts and discontinuities will be not important for the present discussion.
Let X be a finite-dimensional vector space and S an irreducible algebraic variety defined by $s(z) = 0, \forall z \in S$ for a polynomial s. Let ω be a differential form defined on $X \setminus S$. ω is said to have a pole of degree n on S if there exist a regular form ψ and a form θ which has a pole of degree maximally $n-1$ on S such that

$$\omega = \frac{\mathrm{d}s}{s^n} \wedge \psi + \theta. \tag{2.59}$$

For $n = 1$, both ψ and θ have to be regular on entire X and we can directly define the *residue* of ω on S to be the restriction of ψ on S.

$$\mathrm{Res}_S[\omega] \equiv \psi|_S. \tag{2.60}$$

This definition can be iteratively extended to poles of higher degree via the Leibnitz rule. If ω_n has a pole of degree n on S, then

$$\omega_n = \frac{\mathrm{d}s}{s^n} \wedge \psi + \theta = \mathrm{d}\left(-\frac{\psi}{(n-1)s^{n-1}}\right) + \frac{\mathrm{d}\psi}{(n-1)s^{n-1}} + \theta. \tag{2.61}$$

So, up to an exact form, ω_n can be replaced by a new form ω_{n-1} with

$$\omega_{n-1} \equiv \frac{\mathrm{d}\psi}{(n-1)s^{n-1}} + \theta, \tag{2.62}$$

which has a pole of degree at most $n-1$ on S. We conclude by induction that ω_n can be related to another differential form ω_1 with at most a simple pole on S up to an exact form. So, we define the residue of ω_n on S to be equal to the residue of ω_1

$$\text{Res}_S[\omega_n] \equiv \text{Res}_S[\omega_1]. \tag{2.63}$$

So, strictly speaking, the residue acts not on forms themselves but on the cohomology classes of forms and defines a map on the *De Rham cohomology group* of $X \setminus S$. It is easy to verify that for $X = \mathbb{C}$ this residue definition agrees with the standard residue definition of the complex calculus. After the multivariate residue is defined, we need a generalized version of the *residue theorem*. First of all, a generalization of a contour is needed which encloses the singular surface S if S is not a collection of isolated points. We assume that S is maximal in the sense that it has complex codimension 1. Let $\sigma \subset S$ be a *k-cycle* on S. For each point $P \in S$ we can define a small circle in the plane which is transverse to S. This is possible since the real codimension of S is 2. The collection of all such circles for all points in σ defines a $(k+1)$-cycle $\delta\sigma$ which is called the *tubular neighborhood*. The linear operator δ which assigns to a k-cycle its tubular neighborhood is called *Leray coboundary*. We can now state the generalized residue theorem. Let ω be a $(k+1)$ form on $X \setminus S$ and σ a k-cycle in S, then [166]

$$\int_{\delta\sigma} \omega = 2\pi i \int_{\sigma} \text{Res}_S[\omega]. \tag{2.64}$$

If we apply the Leray calculus to the special case of Feynman integrals the right-hand-side of eq. (2.64) can be considered as a definition for a *cut* Feynman integral. For one-loop integrals this was strictly formulated in [167]. In particular, we will be interested in the special case of a cut integral where no integration on the right-hand-side of eq. (2.64) is needed. Geometrically, this corresponds to the situation where S consists of isolated points. The residues on such points are often called *leading singularities* of the integral. While in the one-loop case the leading singularity is unique up to a sign and equals the so-called *global pole* of the integral (see [164]), at the two-loop level the situation is more difficult and only partial results are known. Cutting propagators leads to loop-momenta dependent Jacobian factors which might give rise to additional poles which have to be cut as well in order to compute the leading singularities. For instance, the leading singularities of the double-box integral with up to six external legs have been studied in reference [168].

We close this section with a concrete example of computing the two-loop leading singularities of the scalar massless double-box integral from eq. (2.102) and fig. 2.9. We change to Baikov representation since it makes the zeros of the denominator manifest. According to eq. (2.46), the double-box integral becomes

$$I_{db} \sim G(p_1,p_2,p_3)^{(4-D)/2} \int \frac{\mathrm{d}\rho_1 \ldots \mathrm{d}\rho_9}{\rho_1 \ldots \rho_7} P(\ell_1,\ell_2,p_1,p_2,p_3)^{(D-6)/2}, \tag{2.65}$$

where G is the Gram determinant and P is the Baikov polynomial, as defined in 2.3.2. Since, in general, we are only interested in the kinematic dependence of the leading singularities we omit here all global constant prefactors from eq. (2.46). We use now eq. (2.64) to compute iteratively the residue of the loop-integrand differential form which will be denoted by $\mathcal{I}_{db}$ in following. First, we compute the residue at $S = \{\vec{\rho} | \rho_1 = \ldots = \rho_7 = 0\}$ surface. We obtain

$$\text{Res}_S[\mathcal{I}_{db}] = \frac{G^{\epsilon}\, \mathrm{d}\rho_8\, \mathrm{d}\rho_9}{(P|_S)^{-1-\epsilon}}. \tag{2.66}$$

We take the $\epsilon \to 0$ limit and obtain explicitly

$$\mathrm{Res}_S[\mathcal{I}_{db}^{(D=4)}] = \frac{16\,\mathrm{d}\rho_8\,\mathrm{d}\rho_9}{s\rho_8\rho_9(\rho_8\rho_9 + s(-t+\rho_8+\rho_9))}, \tag{2.67}$$

with $s = (p_1+p_2)^2$ and $t = (p_2+p_3)^2$. While computing residues we will work in the $\epsilon \to 0$ limit. The residue computation often avoids UV and IR singularities, so that this procedure is well defined.
We proceed with localizing the expression (2.67) until the zero surface S becomes a set of isolated points. We find 7 solutions for the vanishing denominator. We summarize the corresponding residues in table 2.1.

Singular point	Leading singularity
$(\rho_8^0 = 0,\ \rho_9^0 = 0)$	$-\frac{16}{s^2t}$
$(\rho_8^0 = 0,\ \rho_9^0 = t)$	$\frac{16}{s^2t}$
$\left(\rho_8^0 = 0,\ \rho_9^0 = \frac{s(t-\rho_8)}{s+\rho_8}\right)$	0
$\left(\rho_8^0 = \frac{s(t-\rho_9)}{s+\rho_9},\ \rho_9^0 = 0\right)$	$\frac{16}{s^2t}$
$\left(\rho_8^0 = \frac{s(t-\rho_9)}{s+\rho_9},\ \rho_9^0 = t\right)$	$-\frac{16}{s^2t}$
$(\rho_8^0 = t,\ \rho_9^0 = 0)$	0
$\left(\rho_8^0 = t,\ \rho_9^0 = \frac{s(t-\rho_8)}{s+\rho_8}\right)$	0

Table 2.1: Leading singularities of the scalar massless double-box integral.

We see that only four leading singularities are non-zero and they all are given by $\pm\frac{16}{s^2t}$. Note that e.g. the second and the fifth rows of table 2.1 only differ in the order of taking residues which leads to different signs of the corresponding leading singularities. If we normalize I_{db} by s^2t, we get an integral with all leading singularities being constant. That explains the basis choice in eq. (2.106).

2.4 Differential equation method

In the sections 2.3.1–2.3.4 we introduced Feynman integrals and discussed some of their important properties like IBP identities and behaviour on cuts. We also showed that we can use different integral representations to investigate different aspects of loop integrals. Here we concentrate on actually solving integrals. By now, there exists a large toolkit of various approaches which often use very different mathematical frameworks. Since, in this thesis we exclusively use the *differential equation* (DE) method, we want to summarize just briefly some of the other methods before we continue with DE. We also point to some of the existing public implementations of these methods.
These approaches are:

- Direct integration in Feynman or Schwinger parameters. A modern extension of this idea is implemented in `HyperInt` [169].
- *Mellin-Barnes representation* technique [170].

- Purely numerical approaches based on *sector decomposition* and *Monte-Carlo integration* [171,172].
- *Dimensional recurrence* relations [173–175].
- Differential equation methood [136].

An extended pedagogical introduction to these methods can be found e.g. in [138].

2.4.1 Construction of DE and canonical basis

Let us now concentrate on the DE approach. The idea is to take derivatives of master integrals with respect to the kinematic invariants and/or internal masses they depend on and to use then IBP relations in order to reduce the right-hand-side back to a linear combination of MI's. Let $\mathbf{I}$ be a set of m MI's, then

$$\frac{\partial \mathbf{I}}{\partial s_i} = A_i(\vec{s}, D)\mathbf{I}, \quad i = 1, \ldots, N_{kin}, \tag{2.68}$$

where A_i are $m \times m$-matrices whose entries are at most algebraic functions of $\vec{s}$ and D and N_{kin} is the number of independent kinematic variables. So now the problem of integrating $\mathbf{I}$ is shifted to the problem of solving a system of linear first-order matrix-valued differential equations (2.68). Historically, this idea was first introduced by A.V. Kotikov in 1991 [30, 31] and then extended by T.Gehrmann and E.Remiddi [33, 34]. In the first publication, only derivatives with respect to internal masses were considered. Later, the method was extended to external kinematic quantities. Since we only deal with massless internal propagators in this thesis we will exclude internal masses from our discussion.
To obtain A_i we, first of all, need to express the differential operator $\frac{\partial}{\partial s_i}$ in terms of the partial derivatives with respect to the external momenta. By the chain rule, we have

$$\frac{\partial}{\partial p_i^\mu} = \sum_{k=1}^{N_{kin}} \frac{\partial s_k}{\partial p_k^\mu} \frac{\partial}{\partial s_k}, \quad i = 1, \ldots, E. \tag{2.69}$$

By contracting eq. (2.69) with external momenta, we obtain E^2 relations of the form

$$p_j^\mu \frac{\partial}{\partial p_i^\mu} = p_j^\mu \sum_{k=1}^{N_{kin}} \frac{\partial s_k}{\partial p_i^\mu} \frac{\partial}{\partial s_k}, \quad i, j = 1, \ldots, E. \tag{2.70}$$

Since we only have N_{kin} independent kinematic invariants we need $E^2 - N_{kin}$ additional constraints to find a unique solution of eq. (2.70). These constraints are provided by Lorentz-invariance identities and on-shell conditions for massless external momenta. In section 3.2 we will give an alternative derivation of DE based on Baikov representation.
Note that the coefficient matrices A_i in eq. (2.68) have to obey two further consistency conditions. The first is the *integrability* condition [176]

$$\partial_i A_j - \partial_j A_i + [A_i, A_j] = 0, \tag{2.71}$$

where $[A, B] := AB - BA$. The second relation comes from the fact that Feynman integrals are homogenous functions in $\vec{s}$, so they fulfill the Euler relation

$$\sum_{k=1}^{N_{kin}} s_k \frac{\partial \mathbf{I}}{\partial s_k} = \mathrm{diag}(a_1(D), \ldots, a_m(D))\mathbf{I}, \tag{2.72}$$

where $2a_i(D)$ is the mass dimension of the i-th master integral. Eq. (2.72) shows that only $N_{kin}-1$ differential equations are independent. So we can always reduce the number of kinematic invariants by setting one of them to 1 and restore the dependence on it at the end by dimensional analysis. Therefore, DE's do not provide any non-trivial information for one-scale integrals beyond their scaling behaviour.
From basic linear algebra we know that choosing a basis is never unique. On the other side, the form of the coefficient matrices A_i in eq. (2.68) strongly depends on the explicit choice of the basis $\mathbf{I}$. So we can ask whether a particular choice of basis exists such that eq. (2.68) takes a simpler form. In 2013 J.Henn [35] introduced the so-called *canonical basis* $\mathbf{G}$ which fulfills a set of differential equations of the form

$$\frac{\partial \mathbf{G}}{\partial s_i} = \epsilon B_i(\vec{s})\mathbf{G}, \quad i = 1, \cdots, N_{kin}, \tag{2.73}$$

where the coefficient matrices B_i do not depend on ϵ and can be derived from a *potential* M

$$\mathrm{d}\mathbf{G} = \epsilon\, \mathrm{d}M\mathbf{G}, \tag{2.74}$$

where

$$\mathrm{d}M = \sum_{k=1}^{N_{kin}} B_k \mathrm{d}s_k. \tag{2.75}$$

In the case of the canonical DE, the integrability conditions (2.71) simplify to

$$\partial_i B_j - \partial_j B_i = 0, \qquad [B_i, B_j] = 0. \tag{2.76}$$

If the new basis $\mathbf{G}$ can be obtained from the old basis $\mathbf{I}$ via $\mathbf{I} = T\mathbf{G}$ for an invertible matrix $T = T(\vec{s}, D)$, then the new coefficient matrices are related to the old ones by

$$B_i = T^{-1}A_iT - T^{-1}\partial_i T, \quad i = 1, \ldots, N_{kin}. \tag{2.77}$$

In the general case, constructing canonical basis may require loop-momenta dependent numerator insertions such that it cannot be related to the old basis by kinematic terms alone. In any case, every two integral bases can be transformed into each other by IBP identities.
Moreover, we assume that the *connection* $\mathrm{d}M$ is a logarithmic one-form [35] such that

$$\mathrm{d}M = \sum_{i=1}^{N} M_i\, \mathrm{d}\log(W_i), \tag{2.78}$$

where M_i are constant $m \times m$ matrices with rational entries and the set $\mathbb{A} = \{W_1, \ldots, W_N\}$ is called the *symbol alphabet* of the integral topology. The *letters* $W_1, \ldots, W_N$ are at most algebraic functions of external kinematics. The logarithmic differential forms $\mathrm{dlog}(W_i)$ are given by

$$\mathrm{d}\log(W_i) = \sum_{j=1}^{N_{sc}} \frac{\partial_j W_i}{W_i} \mathrm{d}s_j. \tag{2.79}$$

Forms of the type (2.79) are usually referred to as *dlog-forms* in the literature.
The *canonical* DE has the form

$$\mathrm{d}\mathbf{G} = \epsilon \sum_{i=1}^{N} M_i \mathrm{d}\log(W_i)\mathbf{G}. \tag{2.80}$$

Once the DE is brought into the canonical form (2.80) it can be solved in terms of *Chen's iterated integrals* [177]

$$\mathbf{G}(\vec{s},\epsilon) = \mathbb{P}\exp\left[\epsilon\int_\gamma \mathrm{d}M\right]\mathbf{G}(\vec{s}_0,\epsilon), \tag{2.81}$$

where $\mathbb{P}$ denotes the path-ordering operator, $\mathbf{G}(\vec{s}_0,\epsilon)$ encodes the boundary conditions and γ is the integration path from $\vec{s}_0$ to $\vec{s}$. Since, for practical purposes, it is mostly sufficient to know a finite number of coefficients in the ϵ-expansion of $\mathbf{G}$ we can consider eq. (2.80) as an order-by-order equation. If

$$\mathbf{G} = \sum_{n=n_0}^{\infty}\mathbf{G}^{(n)}\epsilon^n, \quad n_0\in\mathbb{Z}, \tag{2.82}$$

then

$$\mathrm{d}\mathbf{G}^{(n)} = \sum_{i=1}^{N} M_i \mathrm{d}\log(W_i)\mathbf{G}^{(n-1)}, \tag{2.83}$$

with

$$\mathbf{G}^{(n)} \equiv 0 \quad \text{for} \quad n < n_0. \tag{2.84}$$

For each n only the derivatives of $\mathbf{G}^{(n)}$ appear in eq. (2.83). So the canonical differential equation reduces to a set of *purely inhomogenous* equations which can be solved by integrating order-by-order in ϵ, beginning with the lowest order $\mathcal{O}(\epsilon^{n_0})$ where $\mathbf{G}^{(n_0)}$ has to be constant and is, therefore, fully determined by the lowest-order boundary conditions. The solution of eq. (2.83) is automatically given by iterated integrals of a linear combination of dlog forms.

2.4.2 Solving the canonical DE and pure functions

Section 2.4.1 shows how the task of computing MI's can be replaced by integrating a recursive system of purely inhomogenous differential equations over dlog-forms. The non-trivial part of the calculation is now shifted to the problem of constructing the canonical basis $\mathbf{G}$. For all topologies we discuss in this thesis canonical form can be achieved. However, this is a challenging task and, by now, no algorithmic solution of this problem exists. We will discuss our approach in detail in section 3.3.

Let us for now assume that we have a canonical basis and discuss some properties of the soluton of eq. (2.83). As already mentioned, the solutions are iterated integrals of dlog-forms. In this context, the notion of *trancendental weight* $\tau(f)$ [178,179] of a function f is helpful. Trancendental weight is defined as the minimal number of integrations needed to obtain f from an algebraic integration kernel. So e.g. $\tau(\log(x)) = 1$. Algebraic functions have by definition weight 0. Analogously, trancendental weight can be assigned to real or complex numbers which can be written as integrals over an algebraic function. Such numbers are called *periods* [180]. Simple examples for periods are π and $\log(2)$ since

$$\pi = 2\int_{-1}^{1}\mathrm{d}x\,\sqrt{1-x^2}, \qquad \log(2) = \int_1^2\frac{\mathrm{d}x}{x}. \tag{2.85}$$

We have $\tau(\pi) = \tau(\log(2)) = 1$. For the trancendental weight of a product holds $\tau(f_1 f_2) = \tau(f_1)+\tau(f_2)$. If a function f is given by a linear combination of terms of weight n with coefficients given by algebraic functions we say that f is a *uniform* function of weight n. If, moreover, all coefficients are constant such that $\tau(f') = n-1$, f is called a *pure function* of weight n. Since the integration kernel in (2.81) is manifestly algebraic the $\mathcal{O}(\epsilon^n)$-term in the power series expansion

of the path-ordered exponential is by definition a pure function of weight n. If we set $\tau(\epsilon) \equiv -1$ the path-ordered exponential becomes a pure function of weight 0. If now the boundary vector $\mathbf{G}(\vec{s}_0, \epsilon)$ is a pure function, then the full solution $\mathbf{G}$ is a pure function as well.
It has been conjectured [181] that differential forms with *constant leading singularities* (see section 2.3.4) can be expressed in terms of dlog-forms and so give rise to pure functions which fulfill canonical differential equations. Despite being an unproven conjecture, this observation has been experimentally validated for many multi-loop examples [182–185]. It has led to a powerfull strategy of constructing candidates for a pure basis: We try to find a set of numerator insertions such that all MI's of the given topology have constant leading singularities. Then, we can verify the purity of this basis by checking whether it fulfills the canonical differential equation. Note that no explicit construction of a dlog-form *integrand* is needed for this approach.

2.4.3 Fuchsian form and generalized polylogarithms

Let us consider a special case of iterated integrals where the integration kernel of (2.79) can be brought into *Fuchsian form* [186, 187]

$$\mathrm{d}M = \sum_{k=1}^{\tilde{N}} \frac{\tilde{M}_k}{x - x_k} \mathrm{d}x. \tag{2.86}$$

For the sake of simplicity, we will only discuss the univariate DE depending on x.[5] The special feature of the Fuchsian form is the manifest linearity of the alphabet $\tilde{\mathbb{A}} = \{x - x_1, \ldots, x - x_{\tilde{N}}\}$. In this case, the ϵ-expanded solution can trivially be expressed in terms of the so-called *Goncharov polylogarithms* (GPL's) [178, 188]. They are defined recursively for a set of complex numbers $\{a_1, \ldots, a_n\} \subset \mathbb{C}$ via

$$G(a_1, \ldots, a_n; x) := \int_0^x \frac{\mathrm{d}t}{t - a_1} G(a_2, \ldots, a_n; t), \tag{2.87}$$

if $a_i \neq 0$ for one i and

$$G(\vec{0}_n; x) := \frac{1}{n!} \log^n(x), \tag{2.88}$$

with

$$G(; x) := 1 \tag{2.89}$$

as the starting point of the recursion.
For $a_i \in \{-1, 0, 1\}$ a sub-class of GPL's exists which is usually called *harmonic polylogarithms* (HPL's) [189]. The *classical polylogarithms* which are known since the 19th century [190] build a subset of GPL's as well and can be defined by the following recursion

$$\mathrm{Li}_{n+1}(z) := \int_0^z \mathrm{d}t \, \frac{\mathrm{Li}_n(t)}{t} \quad \forall z \in \mathbb{C} \setminus (1, \infty) \tag{2.90}$$

and

$$\mathrm{Li}_1(z) := -\log(1 - z). \tag{2.91}$$

There is an alternative representation via series expansion

$$\mathrm{Li}_n(z) = \sum_{k=1}^{\infty} \frac{z^k}{k^n} \quad \text{for} \quad |z| < 1. \tag{2.92}$$

[5] In the multivariate case we can think of x as a path parameter along a univariate slice.

For $z = 1$ and $n \geq 2$ the series is still konvergent and we have

$$\mathrm{Li}_n(1) = \zeta(n) =: \zeta_n, \tag{2.93}$$

where ζ denotes the Riemann's ζ-function

$$\zeta(s) := \sum_{k=1}^{\infty} \frac{1}{k^s} \quad \text{for} \quad \mathrm{Re}s > 1. \tag{2.94}$$

Both GPL's and classical polylogarithms have a well-defined trancendental weight

$$\tau(G(a_1, \ldots, a_n; x)) = \tau(\mathrm{Li}_n(x)) = n. \tag{2.95}$$

According to eq. (2.93), we have also $\tau(\zeta_n) = n$. It should be mentioned that the functions $\log(x)$, $\log^2(x)$ and $\mathrm{Li}_2(x)$ are sufficient in order to express all integral contributions which are needed for one-loop amplitudes.
Despite the existence of the formal solution (2.81) in terms of iterated integrals, solving canonical DE might still be very challenging in practice especially if the Fuchsian form (2.86) cannot be achieved. For instance, this can happen in presence of non-rationalizable letters. Another potentially very hard problem which can appear while integrating is the analytic continuation of the multi-valued iterated integrals to all kinematic regions of the phase space. In such cases an efficient numerical approach might be the better choice. We implemented a numerical algorithm which will be discussed in 3.5. In order to have still access to some analytic properties of the integrals without having an analytic solution, the notion of the so-called *symbol* has been introduced [68, 69].
Roughly speaking, a symbol is a linear combination of tensor products of equal length built from dlog-forms of letters [69]. More precisely, the symbol of a trancendental function $F_w(x_1, \ldots, x_n)$ of weight w is defined from its total derivative expressed in terms of dlog-forms

$$\mathrm{d}F_w = \sum_i F_{i,w-1} \mathrm{dlog} W_i, \tag{2.96}$$

where $F_{i,w-1}$ are trancendental functions of weight $w-1$ and W_i are rational functions of $\vec{x}$ [70]. Now, the symbol can be computed recursively via

$$S(F_w) = \sum_i S(F_{i,w-1}) \otimes W_i. \tag{2.97}$$

From the definition (2.97) a close relation between symbols and differential equations can be derived. If $\mathbf{G}$ fulfills a canonical differential equation in the form

$$\mathrm{d}\mathbf{G}^{(n)} = \sum_k M_k \mathrm{dlog} W_k \mathbf{G}^{(n-1)} \tag{2.98}$$

order-by-order in ϵ, then the symbol of $\mathbf{G}^{(n)}$ is given by

$$S(\mathbf{G}^{(n)}) = \sum_{i_1,\ldots,i_n} c_{i_1,\ldots,i_n} W_{i_1} \otimes \ldots \otimes W_{i_n}, \tag{2.99}$$

where $c_{i_1,\ldots,i_n}$ are rational numbers which can be computed from n-fold products of the coefficient matrices M_k. The symbol of a Feynman integral has some very useful properties. The so-called

first-entry condition controls which letters can appear in the leftmost factor of the tensor product in eq. (2.99). It is well-known that branch points of Feynman integrals with massless propagators can appear only if a Mandelstam invariant built from an adjacent pair of external momenta (external masses can be considered as pairs of massless legs as well) is going to zero or infinity. It was shown in [191] that this constraint can be translated to the requirement $c_{i_1,\ldots,i_n} = 0$, if W_{i_1} is not an adjacent Mandelstam invariant. In the planar case, the only possible first-entry letters are the cyclic Mandelstams and external masses. In terms of the coefficient matrices, the first-entry condition can be reformulated as a requirement on the constant weight-zero part of the MI's $\mathbf{G}^{(n_0)}$

$$M_k \mathbf{G}^{(n_0)} = 0, \quad \text{if} \quad W_k \notin \mathbb{A}_{\text{first-entry}}. \tag{2.100}$$

The first-entry condition can provide information about boundary values of Feynman integrals.
Moreover, the notion of the symbol can be used to derive identities between different trancendental functions [70]. For instance, multiple polylogarithms are known to fulfill a large number of highly non-trivial relations among themselves. A simple example which is known for a very long time relates $\mathrm{Li}_2(x)$ and $\mathrm{Li}_2\left(\frac{1}{x}\right)$ via

$$\mathrm{Li}_2\left(\frac{1}{x}\right) = -\mathrm{Li}_2(x) - \zeta_2 - \frac{1}{2}\log^2(-x), \quad \text{for} \quad x \in \mathbb{C} \setminus [1, \infty)\,. \tag{2.101}$$

All types of polylogarithms fulfill relations of the type (2.101) which can be very helpful for handling complicated expressions appearing in multi-loop calculations. However, for GPL's much lesser identities are known explicitly than for classical polylogarithms. In practice, we still can often circumvent these problems by considering the symbol of the expression instead of the full polylogarithmic term.
It should be mentioned that the symbol definition (2.97) is blind to constant terms with positive weight like π, ζ_n or $\log(2)$. By induction, also the symbol of products of functions and constants with positive weight like $\pi \log(x)$ vanishes. So, the symbol alone is not sufficient to fully fix the function-level solution of the canonical differential equation.
Finally, it should be mentioned that the notion of *pure function* has been at least partially extended beyond Feynman integrals which evaluate to GPL's. So, it was shown [192] that the notion of uniform weight can be assigned to a particular type of *elliptic integrals* called *elliptic multiple polylogarithms* (eMPL's) [193]. Moreover, elliptic integrals of uniform trancendental weight satisfy ϵ-factorized differential equation [192] (see also [194] for some very recent results).

2.4.4 A pedagogical example of DE approach

In this section, we want to illustrate the application of the DE method combined with the notion of the canonical basis to a simple pedagogical example where the basic features of the approach become clear.
We will consider one of the standard examples for two-loop Feynman integrals: the planar massless four-point function. In the following, we will refer to this integral as the *massless double-box*.
According to the conventions of 2.3.1, it takes the form

$$I_{db}[\vec{\nu}] = e^{2\epsilon\gamma_E} \int \frac{d^D\ell_1}{i\pi^{D/2}} \frac{d^D\ell_2}{i\pi^{D/2}} \frac{1}{\prod_{j=1}^{9} \rho_j^{\nu_j}}. \tag{2.102}$$

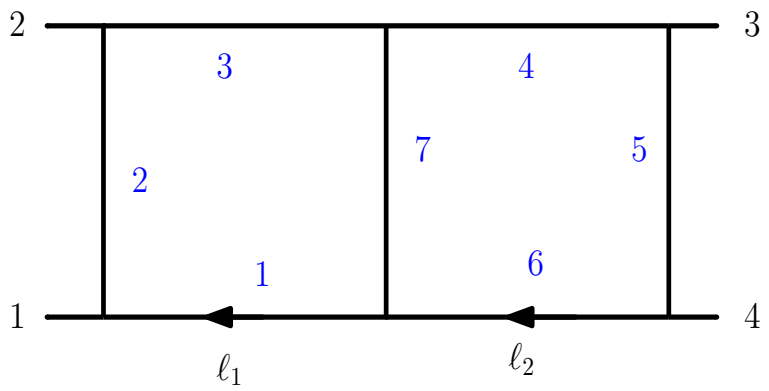

Figure 2.9: Massless double-box topology. All external momenta are incoming. Propagators are labeled by blue numbers.

The Feynman graph of the double-box topology is depicted in fig. 2.9. The inverse propagators are given by

$$\rho_1 = \ell_1^2,\ \rho_2 = (\ell_1 + p_1)^2,\ \rho_3 = (\ell_1 + p_1 + p_2)^2,\ \rho_4 = (\ell_2 + p_1 + p_2)^2,\ \rho_5 = (\ell_2 - p_4)^2,\ \rho_6 = \ell_2^2,\ \rho_7 = (\ell_1 - \ell_2)^2. \tag{2.103}$$

Additionally, we need to choose two ISP's to complete the basis of loop-momenta dependent scalar products. We define $\rho_8 = (\ell_2 + p_1)^2$, $\rho_9 = (\ell_1 - p_4)^2$. The integral depends on two Mandelstam invariants $s = (p_1 + p_2)^2$ and $t = (p_2 + p_3)^2$. The third Mandelstam invariant $u = (p_2 + p_4)^2$ is related to the first two by momentum conservation

$$s + t + u = 0. \tag{2.104}$$

The double-box topology supports 8 master integrals. We pick a set of independent integrals

$$\mathbf{I} = \{I_{1111111-10}, I_{111111100}, I_{011011100}, I_{111010200}, I_{201102000}, I_{010101200}, I_{002001200}, I_{020010200}\}\,. \tag{2.105}$$

Following the procedure discussed in 2.4, we change to a canonical basis $\mathbf{G}$ which is given by

$$\begin{aligned}
\mathbf{G}_1 &= \epsilon^2(-s)^{2\epsilon} t I_{020010200},\\
\mathbf{G}_2 &= \epsilon^2(-s)^{2\epsilon} s I_{002001200},\\
\mathbf{G}_3 &= \epsilon^3(-s)^{2\epsilon} s I_{010101200},\\
\mathbf{G}_4 &= -\epsilon^2(-s)^{2\epsilon} s^2 I_{201102000},\\
\mathbf{G}_5 &= -\epsilon^3(-s)^{2\epsilon} st I_{111010200},\\
\mathbf{G}_6 &= \epsilon^4(-s)^{2\epsilon}(s+t) I_{011011100},\\
\mathbf{G}_7 &= \epsilon^4(-s)^{2\epsilon} s^2 t I_{111111100},\\
\mathbf{G}_8 &= -\epsilon^4(-s)^{2\epsilon} s^2 I_{1111111-10}.
\end{aligned} \tag{2.106}$$

Here, the basis is taken from [35]. The ideas used to construct the pure basis will be discussed in details in 3.3. Let us for now just assume that the pure basis is known. However, two comments on the basis are in order. First, note that the choice of lower sector integrals (like sunrises and bubble-triangles) differs here from our choice in the five-point bases where we prefer integrals with

lowest possible number of doubled propagators. Note that the particular choice which is made here is more common in the literature. The second point is the overall normalization $\epsilon^4(-s)^{2\epsilon}$ making pure integrals dimensionless and finite in the $\epsilon \to 0$ limit. Now, the Laurent expansion of $\mathbf{G}$ has to start at $\mathcal{O}(\epsilon^0)$.
We proceed with taking derivatives of $\mathbf{G}$ with respect to s and t. We compute the derivatives with our own tool which uses Baikov representation and is described in section 3.2 and perform IBP reduction with `KIRA` [156]. Expressions for differential operators $\frac{\partial}{\partial s}$ and $\frac{\partial}{\partial t}$ in terms of the derivatives with respect to external momenta, as introduced in 2.4, can be found e.g. in [136].
We obtain the DE in the form of a total derivative

$$\mathrm{d}\mathbf{G} = \epsilon \left[B_s \mathrm{d}s + B_t \mathrm{d}t\right] \mathbf{G}, \tag{2.107}$$

with

$$B_s = \begin{pmatrix}
\frac{2}{s} & 0 & 0 & 0 & 0 & 0 & 0 & 0 \\
0 & 0 & 0 & 0 & 0 & 0 & 0 & 0 \\
0 & 0 & 0 & 0 & 0 & 0 & 0 & 0 \\
0 & 0 & 0 & 0 & 0 & 0 & 0 & 0 \\
-\frac{3}{2(s+t)} & 0 & -\frac{3t}{s(s+t)} & 0 & \frac{2}{s} - \frac{t}{s(s+t)} & 0 & 0 & 0 \\
\frac{1}{2s} & -\frac{1}{2s} & 0 & 0 & 0 & \frac{2}{s} - \frac{2t}{s(s+t)} & 0 & 0 \\
\frac{3}{s+t} & \frac{3(s-t)}{s(s+t)} & -\frac{6t}{s(s+t)} & -\frac{2t}{s(s+t)} & -\frac{4}{s+t} & -\frac{12}{s+t} & \frac{2}{s} - \frac{2t}{s(s+t)} & -\frac{2t}{s(s+t)} \\
-\frac{9}{2(s+t)} & -\frac{3}{s+t} & \frac{3}{s+t} & \frac{s+2t}{s^2+st} & \frac{4}{s+t} & \frac{18}{s+t} & -\frac{1}{s+t} & \frac{2}{s} - \frac{3s+2t}{s^2+st}
\end{pmatrix} \tag{2.108}$$

and

$$B_t = \begin{pmatrix}
-\frac{2}{t} & 0 & 0 & 0 & 0 & 0 & 0 & 0 \\
0 & 0 & 0 & 0 & 0 & 0 & 0 & 0 \\
0 & 0 & 0 & 0 & 0 & 0 & 0 & 0 \\
0 & 0 & 0 & 0 & 0 & 0 & 0 & 0 \\
\frac{3s}{2t(s+t)} & 0 & \frac{3}{s+t} & 0 & -\frac{2s+t}{st+t^2} & 0 & 0 & 0 \\
-\frac{1}{2t} & \frac{1}{2t} & 0 & 0 & 0 & -\frac{2s}{t(s+t)} & 0 & 0 \\
-\frac{3s}{t(s+t)} & -\frac{3(s-t)}{t(s+t)} & \frac{6}{s+t} & \frac{2}{s+t} & \frac{4s}{t(s+t)} & \frac{12s}{t(s+t)} & -\frac{2s}{t(s+t)} & \frac{2}{s+t} \\
\frac{9s}{2t(s+t)} & \frac{3s}{t(s+t)} & -\frac{3s}{t(s+t)} & -\frac{s+2t}{st+t^2} & -\frac{4s}{t(s+t)} & -\frac{18s}{t(s+t)} & \frac{s}{t(s+t)} & \frac{s}{t(s+t)}
\end{pmatrix}. \tag{2.109}$$

Since our master integrals are dimensionless the matrices B_s and B_t have to fulfill

$$sB_s + tB_t = 0, \tag{2.110}$$

which they indeed do. We also check the integrability constraints

$$\begin{aligned} [B_t, B_s] &= 0, \\ \partial_s B_t - \partial_t B_s &= 0, \end{aligned} \tag{2.111}$$

which are also fulfilled. Since the normalized integrals only depend on the ratio of kinematic scales we introduce the new parameter $x := \frac{t}{s}$ and cast the differential equation into the manifestly Fuchsian form

$$\mathrm{d}\mathbf{G} = \epsilon \left[B_0 \frac{1}{x} + B_1 \frac{1}{1+x}\right] \mathrm{d}x\, \mathbf{G}, \tag{2.112}$$

with

$$B_0 = \begin{pmatrix} -2 & 0 & 0 & 0 & 0 & 0 & 0 & 0 \\ 0 & 0 & 0 & 0 & 0 & 0 & 0 & 0 \\ 0 & 0 & 0 & 0 & 0 & 0 & 0 & 0 \\ 0 & 0 & 0 & 0 & 0 & 0 & 0 & 0 \\ \frac{3}{2} & 0 & 0 & 0 & -2 & 0 & 0 & 0 \\ -\frac{1}{2} & \frac{1}{2} & 0 & 0 & 0 & -2 & 0 & 0 \\ -3 & -3 & 0 & 0 & 4 & 12 & -2 & 0 \\ \frac{9}{2} & 3 & -3 & -1 & -4 & -18 & 1 & 1 \end{pmatrix} \tag{2.113}$$

and

$$B_1 = \begin{pmatrix} 0 & 0 & 0 & 0 & 0 & 0 & 0 & 0 \\ 0 & 0 & 0 & 0 & 0 & 0 & 0 & 0 \\ 0 & 0 & 0 & 0 & 0 & 0 & 0 & 0 \\ 0 & 0 & 0 & 0 & 0 & 0 & 0 & 0 \\ -\frac{3}{2} & 0 & 3 & 0 & 1 & 0 & 0 & 0 \\ 0 & 0 & 0 & 0 & 0 & 2 & 0 & 0 \\ 3 & 6 & 6 & 2 & -4 & -12 & 2 & 2 \\ -\frac{9}{2} & -3 & 3 & -1 & 4 & 18 & -1 & -1 \end{pmatrix}. \tag{2.114}$$

The matrices B_0 and B_1 agree with [35]. The alphabet of the massless two-point function can be read off the differential equation

$$\mathbb{A} = \{x, 1+x\}. \tag{2.115}$$

The alphabet encodes the positions of the two singular points $x = 0$ and $x = -1$. The latter corresponds to the kinematic point $s = -t$ or, equivalently, $u = 0$. Since the double-box topology is planar the first-entry condition tells us that all integrals have to be regular at this point. A second important condition is that all integrals have to be real in the Euclidean region which is given by $s < 0, t < 0$ or $x > 0$.
We insert the Laurent expansion of the integral basis

$$\mathbf{G}(x) = \sum_{i=0}^{\infty} \epsilon^i \mathbf{G}^{(i)}(x) \tag{2.116}$$

into eq.(2.112) and obtain a purely inhomogenous set of equations

$$\frac{\partial \mathbf{G}^{(i)}(x)}{\partial x} = \left[\frac{B_0}{x} + \frac{B_1}{1+x}\right] \mathbf{G}^{(i-1)}(x), \quad \text{for } i \geq 0, \tag{2.117}$$

with $\mathbf{G}^{(-1)} \equiv 0$ by definition. Note that here the summation index i directly labels the trancendental weight of the i-th order solution. We can compute $\mathbf{G}(x)$ to any order in ϵ by iterative integration of eq. (2.117) and inserting the boundary condition. The regularity condition at $x = -1$ together with vanishing of all imaginary parts in the Euclidean region is indeed sufficient in order to fix all integration constants at every weight up to two free parameters. The latter can be determined from the two single-scale integrals G_2 and G_4 which do not depend on x and can easily be computed in closed form via Feynman parametrization. They are given by

$$\begin{aligned} G_2 =& \frac{e^{2\gamma_E \epsilon}\Gamma^3(1-\epsilon)\Gamma(2\epsilon+1)}{\Gamma(1-3\epsilon)} = 1 - \zeta_2\epsilon^2 - \frac{32}{3}\zeta_3\epsilon^3 - \frac{57}{4}\zeta_4\epsilon^4 + \mathcal{O}(\epsilon^5), \\ G_4 =& -\left[\frac{e^{\gamma_E \epsilon}(1-2\epsilon)\epsilon\Gamma^2(1-\epsilon)\Gamma(\epsilon)}{\Gamma(2-2\epsilon)}\right]^2 = -1 + \zeta_2\epsilon^2 + \frac{14}{3}\zeta_3\epsilon^3 + \frac{21}{4}\zeta_4\epsilon^4 + \mathcal{O}(\epsilon^5). \end{aligned} \tag{2.118}$$

Chapter 3

Techniques used in the five-point calculation

In the following, we discuss different aspects of computing the two-loop five-point integral topologies with one external massive leg. We use the canonical DE approach introduced in 2.4. However, due to the complexity of the present problem, many standard techniques cannot be applied directly which requires more case-tailored and sometimes heuristic treatment of many practical problems. Although, the results for planar and non-planar topologies will be presented in two separate sections 4.1 and 4.2 of Chapter 4 most of the points here are equally valid for both types of integrals. One of the biggest obstacles which required many modifications to the standard DE approach was the absence of analytic IBP tables which are normally needed at multiple steps while constructing the differential equation. Computing these tables, especially for non-planar topologies, is out of reach at the moment.
We divide the whole computational problem into four parts.
The first part is the construction of the canonical basis which is crucial for all following steps. We obtained the canonical bases mainly in a heuristic way employing various ideas and approaches based on both choosing integrands with constant leading singularities and making use of the numerical structure of the pre-canonical differential equation. Construction of the pure basis is discussed in detail in 3.3.
The second crucial step is the construction of the symbol alphabet. While in the traditional DE approach the symbol alphabet is a by-product of the canonical DE, here it has to be found in advance. We showed that the alphabet can be extracted from (semi-)analytic[1] one-loop and *cut* two-loop differential equations which require only a small fraction of the full analytic IBP tables. Since the construction of the alphabet is case-dependent we will discuss it and present both the planar alphabet and its non-planar extension in Chapter 4 in sections 4.1.3 and 4.2.3.
Part three is the computation of the analytic form of the canonical differential equation. Here, we employ the idea of [48] where the canonical differential equation of the massless hexa-box topology was reconstructed from a sufficiently large set of numerical samples. We present this approach in 3.4.
Finally, section 3.5 deals with the integration of the canonical DE including determing boundary conditions and analytic continuation. We decided not to aim for a formal solution in terms of GPL's mainly because of the complicated structure of the symbol alphabet and related complexity of the analytic continuation but chose a purely numerical approach based on a generalized power-series expansion on a univariate slice [71, 72] which allows high-precision numerical evalu-

[1] Sometimes we worked with univariate on-shell DE.

ations in arbitrary phase-space regions.
Additionally, in sections 3.1 and 3.2 we discuss the analytic structure of the five-point kinematic space and introduce a method of computing differential equations based on the Baikov representation [143].

3.1 Scattering kinematics

We begin with introducing our notation and discussing the kinematics of five-point scattering processes. We also introduce some quantities which will be used throughout this thesis. After that, we briefly describe the structure of the five-point massive phase space.
Each of the considered topologies has five external momenta which we denote by $p_1, \ldots, p_5$, where p_1 is massive $p_1^2 = q^2$ and four others are massless, so $p_i^2 = 0,\ i = 2, 3, 4, 5$. All momenta are considered to be incoming so that the momentum conservation takes the form $\sum_{i=1}^{5} p_i = 0$. According to eq. (2.34) there are six linear independent kinematic invariants. We choose them to be the cyclic Mandelstam variables and the off-shell scale

$$\vec{s} = \left\{q^2, s_{12}, s_{23}, s_{34}, s_{45}, s_{15}\right\}, \tag{3.1}$$

with $s_{ij} = (p_i + p_j)^2$. The remaining five non-cyclic Mandelstam variables are important both for non-planar integrals and at the amplitude level so we give them also explicitly in terms of the cyclic invariants

$$\begin{aligned} &s_{13} = -s_{12} - s_{23} + s_{45} + q^2,\ s_{14} = -s_{15} + s_{23} - s_{45} + q^2,\ s_{24} = s_{15} - s_{23} - s_{34}, \\ &s_{25} = -s_{12} - s_{15} + s_{34} + q^2,\ s_{35} = s_{12} - s_{34} - s_{45}. \end{aligned} \tag{3.2}$$

However, Mandelstam variables alone are not sufficient to fully characterize the scattering kinematics. We need an additional quantity which captures the information about the orientation of the external momenta and has so to be odd under the parity operator

$$\mathcal{P}: \quad (p^0, \vec{p}) \mapsto (p^0, -\vec{p}). \tag{3.3}$$

This is realized by an odd Levi-Civita contraction

$$\mathrm{tr}_5 := 4i\epsilon_{\mu\nu\rho\sigma} p^\mu p^\nu p^\rho p^\sigma = 4i \,\mathrm{det} V(p_1, p_2, p_3, p_4), \tag{3.4}$$

where $V(p_1, \ldots, p_n)$ is a $4 \times n$ matrix with columns given by $p_1, \ldots, p_n$. This object is indeed parity-odd since every term in the sum (eq. (3.4)) has exactly three spatial components. The variable tr_5 is closely related to the Gram determinant of the external momenta

$$\Delta_5 := 16G(p_1, p_2, p_3, p_4) = \det\left\{2p_i \cdot p_j\right\}_{i,j=1}^{4} \tag{3.5}$$

by

$$\Delta_5 = \det\left[2V(p_1, \ldots, p_4)^\top g V(p_1, \ldots, p_4)\right] = \mathrm{tr}_5^2, \tag{3.6}$$

where $g = \mathrm{diag}(1, -1, -1, -1)$ is the space-time metric which we extend with further minus signs when working with extra-dimensional quantities. Note that eq. (3.6) cannot be used to determine the sign of tr_5 but only its absolute value. The sign has to be derived from the momenta. For completeness, we give an explicit expression of Δ_5 in terms of the Mandelstam variables

$$\Delta_5 = (s_{12}s_{15} - s_{12}s_{23} - q^2 s_{34} - s_{15}s_{45} + s_{34}s_{45} + s_{23}s_{34})^2 - 4s_{23}s_{34}s_{45}(q^2 - s_{12} - s_{15} + s_{34}). \tag{3.7}$$

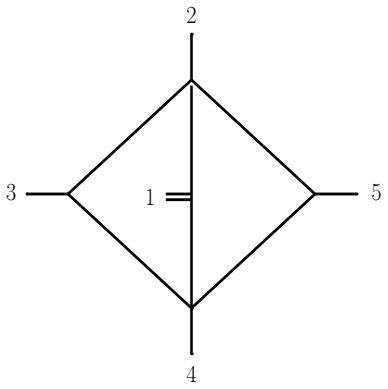

Figure 3.1: Five-point non-planar double-box with the massive leg at the central rung.

Apart from Δ_5, there are two more types of kinematic quantities which give rise to irreducible square-roots for the given kinematics. This is a three-point Gram determinant associated to a triangle diagram with three external masses on the one hand and a new Gram determinant which is associated to a particular five-point non-planar double-box diagram (see fig. 3.1) on the other hand. Let us first look at the three-point Gram determinants. They appear in three permutations

$$\begin{aligned}\Delta_3^{(1)} &= -4G(p_1, p_2+p_3) = \lambda(q^2, s_{23}, s_{45}),\\ \Delta_3^{(2)} &= -4G(p_1, p_2+p_4) = \lambda(q^2, s_{24}, s_{35}),\\ \Delta_3^{(3)} &= -4G(p_1, p_3+p_4) = \lambda(q^2, s_{25}, s_{34}),\end{aligned} \tag{3.8}$$

where

$$\lambda(a,b,c) := a^2+b^2+c^2-2ab-2ac-2bc \tag{3.9}$$

is the so-called Källén function [195]. The second object is the square of the leading singularity of the scalar integral depicted in 3.1 and is given by

$$\Sigma_5^{(1)} = (s_{12}s_{15}-s_{12}s_{23}-s_{15}s_{45}+s_{34}s_{45}+s_{23}s_{34})^2 - 4s_{23}s_{34}s_{45}(s_{34}-s_{12}-s_{15}). \tag{3.10}$$

The origin and the derivation of Σ_5 will be discussed in more detail in 3.3.6. Permutations of the massless external momenta give five further versions of $\Sigma_5^{(1)}$ which we denote by

$$\Sigma_5^{(k)} = \Sigma_5^{(\sigma_k(1))}, \quad \sigma_k \in S_4/(S_2[3,4]\times S_2[2,5]). \tag{3.11}$$

Note that the σ_k denote here, strictly speaking, *equivalence classes* of permutations and not the permutations themselves since permuting of p_3, p_4 and p_2, p_5 among each other lets $\Sigma_5^{(1)}$ invariant. So, two permutations can be distinguished by acting on $\Sigma_5^{(1)}$ only up to elements of $(S_2[3,4]\times S_2[2,5])$. We observe that

$$\Sigma_5^{(k)} \to \Delta_5^0, \quad \text{for} \;\; q^2\to 0, \;\; \forall k, \tag{3.12}$$

where Δ_5^0 is the Gram determinant of the massless five-point kinematics.
All together, we have 10 irreducible square-roots in the one-mass case which differs clearly from the massless case where tr_5 is the only algebraic quantity. Not all of the square-roots appear simultaneously in every topology. tr_5 and $\sqrt{\Delta_3^{(1)}}$ are already present at the one-loop level. For

the planar two-loop topologies we have to add $\sqrt{\Delta_3^{(3)}}$. The remaining 7 square-roots are genuinely non-planar quantities. Four out of the six new square-roots $\sqrt{\Sigma_5^{(k)}}$ appear only at the amplitude level where all permutations of independent topologies contribute and are so, in principle, irrelevant for the present work. So the number of relevant square-roots is 6.
Next, we want to discuss some properties of the loop-momentum space. Since we have four independent external momenta the loop momenta can be written as

$$\ell_i = \sum_{j=1}^{4} \alpha_{ij} p_j + \tilde{\ell}_i, \quad \alpha_{ij} \in \mathbb{C}, \quad i = 1, 2, \tag{3.13}$$

where $\tilde{\ell}_i$ denote the $(D-4)$-dimensional part of the loop momenta. We define the extra-dimensional scalar products

$$\mu_{ij} := \tilde{\ell}_i \cdot \tilde{\ell}_j, \quad i, j = 1, 2. \tag{3.14}$$

Eq. (eq. (3.13)) together with $\tilde{\ell}_i \cdot p_j = 0$ can be used to simplify the Baikov polynomials of both one- and two-loop five-point topologies and write them in terms of the μ_{ij}'s. Let $P^{(1)}$ and $P^{(2)}$ denote the one-loop and the two-loop Baikov polynomials, then the following identities hold

$$\begin{aligned} P^{(1)} &= G\left(\ell, p_1, p_2, p_3, p_4\right) = G\left(\sum_{j=1}^{4} \alpha_j p_j + \tilde{\ell}, p_1, p_2, p_3, p_4\right) = G(\tilde{\ell}, p_1, p_2, p_3, p_4) = \frac{1}{16}\mu \mathrm{tr}_5^2, \\ P^{(2)} &= G(\ell_1, \ell_2, p_1, p_2, p_3, p_4) = G\left(\sum_{j=1}^{4} \alpha_{1j} p_j + \tilde{\ell}_1, \sum_{j=1}^{4} \alpha_{2j} p_j + \tilde{\ell}_2, p_1, p_2, p_3, p_4\right) \\ &= G(\tilde{\ell}_1, \tilde{\ell}_2, p_1, p_2, p_3, p_4) = \frac{1}{16}\left(\mu_{11}\mu_{22} - \mu_{12}^2\right) \mathrm{tr}_5^2, \end{aligned} \tag{3.15}$$

with $\mu := \tilde{\ell}^2$. Eq. (3.15) can be used to express μ in terms of ISP's and Mandelstam invariants. The analogous relations at two loop are

$$\mu_{11} = 16\frac{G_{11}}{\mathrm{tr}_5^2}, \quad \mu_{22} = 16\frac{G_{22}}{\mathrm{tr}_5^2}, \quad \mu_{12} = 16\frac{G_{12}}{\mathrm{tr}_5^2} \qquad i, j = 1, 2, \tag{3.16}$$

where G_{ij} are obtained from the Gram matrix by deleting the i-th row and the j-th column.
Finally, we discuss the analytic structure of the five-point phase space with one massive leg. The phase space consists of multiple regions which are specified by different signs of the Mandelstam variables. The boundaries of the regions are given by hypersurfaces on which some Mandelstam invariants vanish. We expect the integrals to have physical branch cuts on surfaces where first-entry letters (see 2.4.3) vanish. In the planar case, these are exactly the cyclic Mandelstam variables and the off-shell scale q^2 while in the non-planar case some of the non-cyclic Mandelstam invariants are first-entry letters, too. First of all, we should specify the Euclidean regions for all topologies where all integrals are either manifestly real or manifestly imaginary.[2] In the planar case the Euclidean region is characterized by all cyclic Mandelstams being negative $s_i < 0, \quad i = 1, \ldots, 6$. For the three non-planar hexa-box topologies, the Euclidean regions have to be determined case-by-case and are given in eq. (4.79). A further interesting kinematic region which is particularly important for phenomenological studies corresponds to the production of

[2]Some of the pure integrals are normalized by square-roots like $\sqrt{\Delta_3^{(1)}}$ which might become imaginary in the Euclidean region.

Initial State	> 0	< 0
$2,3$	$s_{23}, s_{45}, s_{15}, q^2$	s_{12}, s_{34}
$2,4$	s_{15}, q^2	$s_{12}, s_{23}, s_{34}, s_{45}$
$2,5$	s_{34}, q^2	$s_{12}, s_{23}, s_{45}, s_{15}$
$3,4$	$s_{12}, s_{34}, s_{15}, q^2$	s_{23}, s_{45}
$3,5$	s_{12}, q^2	$s_{23}, s_{34}, s_{45}, s_{15}$
$4,5$	$s_{12}, s_{23}, s_{45}, q^2$	s_{34}, s_{15}

Table 3.1: Signs of cyclic Mandelstam invariants in the physical phase-space.

a heavy particle in association with two massless jets. Without loss of generality, we assign p_1 to the massive particle and assume that it decays into a pair of light particles (e.g. leptons) which implies $p_1^2 > 0$. The four remaining massless momenta can be assigned either to the two initial-state particles or the two final-state jets. So, the process can be characterized by

$$p_i + p_j \to p_1 + p_k + p_l, \tag{3.17}$$

with $i \neq j \neq k \neq l \in \{2,3,4,5\}$. There are six different choices of i,j,k,l. Every particular choice is specified by the signs of the Mandelstams. Concretely, all s-channel variables have to be chosen positive and all t-channel variables have to be negative. In table 3.1 we summarize the signs of the Mandelstam invariants corresponding to all six combinations. In the following, we will refer to these six phase-space regions as the *physical regions*. Eq. (3.6) implies that $\Delta_5 < 0$ for all physical regions since $\det g = -1$ and all momenta are real inside the physically relevant part of the phase space.

3.2 Construction of the pre-canonical differential equation

In this section, we discuss the computation of the *pre-canonical* differential equation for an arbitrary chosen integral basis. As shown in section 2.4, the differential equation is obtained first by computing the derivatives of the master integrals and a subsequent IBP-reduction of the result to a linear combination of MI's. This means that analytic IBP-tables are required for an analytic differential equation. Computing analytic IBP-tables for five-point two-loop integrals with one external mass is an extremely challenging task (this is already true for massless five-point integrals), especially for non-planar topologies. The way we circumvent this obstacle is by focusing on numerical differential equations on the one hand and using analytic and semi-analytic *on-shell* differential equations on the other hand. The pre-canonical differential equation is the starting point of our computation so we need to be able to extract the maximally possible amount of information from it and also be able to evaluate it efficiently multiple times.
We decided not to use the explicit differential operator which relates derivatives with respect to kinematic invariants to derivatives with respect to external momenta, but to perform the calculation in the Baikov representation instead where derivatives with respect to the s_{ij}'s can be taken directly. This approach is based on [143]. According to eq. (2.46), the i-th master integral I_i in the pre-canonical basis can be written as

$$I_i = I[\vec{\rho}, \vec{\nu}_i, \vec{s}, E, L, \mathcal{N}] = C_N^L (G(p_1, \ldots, p_E))^{(-D+E+1)/2} \int \frac{\mathrm{d}\rho_1 \ldots \mathrm{d}\rho_N \, \mathcal{N}(\ell_1, \ldots, \ell_L, p_1, \ldots, p_E)}{\rho_1^{\nu_1} \ldots \rho_N^{\nu_N}} \\ (P(\ell_1, \ldots, \ell_L, p_1, \ldots, p_E))^{(D-L-E-1)/2}. \tag{3.18}$$

An explanation of the notation used in eq. (3.18) can be found in eq. (2.46).
$\mathcal{N}(\ell_1, \ldots, \ell_L, p_1, \ldots, p_E)$ represents a generic numerator insertion which is a function of both loop and external momenta. In the following, we will assume that $\nu_i \in \{0, 1\}$, $i = 1, \ldots, N$. Any additional factors of ρ_i can be included in the numerator insertion. Since the Baikov representation makes the $\vec{s}$-dependence of the loop integral manifest we can simply take the derivative with respect to a kinematic variable

$$\frac{\partial I_i}{\partial s_j} = I_i \left[\frac{\partial \mathcal{N}}{\partial s_j} + \frac{-D + E + 1}{2G} \frac{\partial G}{\partial s_j} + \frac{D - L - E - 1}{2P} \frac{\partial P}{\partial s_j} \right]. \tag{3.19}$$

The goal is now to rewrite the right-hand-side of eq. (3.19) such that it can be expressed as a linear combination of standard Feynman integrals. This can be achieved by getting rid of the Baikov polynomial in the denominator by dimension shifting. In the Baikov representation, the dimension shift $D - 2 \to D$ can be implemented by multiplying the insertion with $\frac{P}{G}$ and some numerical constant. Concretely, we have

$$I^{(D)}[\mathcal{N}] = \frac{C_N^L(D)}{C_N^L(D-2)} I^{(D-2)} \left[\mathcal{N} \frac{P}{G} \right]. \tag{3.20}$$

Applying the dimension shift on both sides of eq.(3.19) we obtain

$$\frac{\partial I_i^{(D-2)}}{\partial s_j} \left[\mathcal{N} \frac{P}{G} \right] = I_i^{(D-2)} \left[\frac{P}{G} \frac{\partial \mathcal{N}}{\partial s_j} + P \frac{-D + E + 1}{2G^2} \frac{\partial G}{\partial s_j} + \frac{D - L - E - 1}{2G} \frac{\partial P}{\partial s_j} \right]. \tag{3.21}$$

Since eq. (3.21) is valid for any D, we can simply redefine $D \to D + 2$ at the end. As already mentioned above, we cannot perform the analytic IBP reduction for integrals considered in this thesis. So, we replace the kinematic invariants $\vec{s}$ and the space-time dimension D in eq. (3.21) by numerical values

$$\vec{s} \to \vec{s}_0 \in \mathbb{Q}^6, \quad D \to D_0 \in \mathbb{Q}. \tag{3.22}$$

We work with rational numbers to be able to use exact arithmetics. Alternatively, we could also work within modular arithmetics. We discuss some possible strategies of choosing suitable phase-space points in appendix A. Of course, we can also compute semi-analytic differential equation where some of the external parameters are kept generic. Finally, we need to prepare eq. (3.21) for an IBP reduction program. Since P is a polynomial in terms of inverse propagators and ISP's both the master integrals and their derivatives can be expressed as linear combinations of standard Feynman integrals $I[\vec{\nu}, \vec{s}]$. Concretely,

$$\left. \frac{\partial I}{\partial s_i} \right|_{\vec{s}=\vec{s}_0, D=D_0} = \sum_j c_j(\vec{s}_0, D_0) I[\vec{\nu}_j], \tag{3.23}$$

where the coefficients c_j are at most algebraic numbers and $\vec{\nu}_j \in \mathbb{Z}^N$. Now the right-hand-side of eq. (3.23) can be reduced to master integrals. The output of the calculation is the total derivative of the integral basis

$$\mathrm{d}\mathbf{I}(\vec{s}_0, D_0) = \sum_{i=1}^{6} A_i(\vec{s}_0, D_0) \mathrm{d}s_i \mathbf{I} = \mathbf{A}(\vec{s}_0, D_0)\mathbf{I}, \tag{3.24}$$

where $\mathbf{A}(\vec{s}_0, D_0)$ will be referred to the as numerical connection. In our implementation the one-forms $\mathrm{d}s_i$ are represented by placeholders and can at any time be replaced by an arbitrary chosen numerical vector $\vec{c}$ which determines the direction of the derivative in the space of kinematic

invariants. We define $A(\vec{s}_0, D_0) = \vec{A} \cdot \vec{c}$.
As well-known in the literature (see e.g. [136]), the cut operation commutes wih taking derivatives with respect to external kinematics. Since this is also true for the IBP reduction procedure we can compute the differential equation for any cut integral in exactly the same manner as for uncut integrals. In the following, differential equations for *cut* Feynman integrals will be referred to as *on-shell* DE's. On-shell DE's can trivially be implemented in the Baikov representation by just setting all relevant inverse propagators to zero at the integrand level on both sides of eq. (3.21). On-shell IBP reduction is implemented in `KIRA` [156]. Working with on-shell DE's simplifies the pure basis construction significantly since it allows to proceed topology-by-topology without having to recompute the full differential equation each time the basis gets changed. Especially for non-planar topologies this becomes really crucial since the off-shell IBP reduction can easily take many hours while the on-shell reduction typically requires only munites. Furthermore, pure-integral construction strategies mostly require only the maximal and next-to-maximal cut DE's such that results obtained from cut DE's are in most cases already pure off-shell.
Finally, we want to discuss how numerical differential equations can be used for checking whether a given integral basis is pure. For this purpose, we compute the differential equation at the same numerical point $\vec{s}_0$ and for the same direction $\vec{c}$ for two different values of the dimensional regulator ϵ_1 and ϵ_2 and check whether $A(\vec{s}_0, \epsilon)$ is indeed linear in ϵ. Explicitly, we ask if

$$\Delta A(\vec{s}_0) := \frac{1}{\epsilon_1} A(\vec{s}_0, \epsilon_1) - \frac{1}{\epsilon_2} A(\vec{s}_0, \epsilon_2) = 0. \tag{3.25}$$

It is clear that this is not a strict proof of purity but vanishing of ΔA at several points and for several values of ϵ provides an arbitrary strong check. The actual proof of purity will be given by the success of the reconstruction procedure of section 3.4. If $\Delta A(\vec{s}_0)$ does not vanish both the distribution of non-vanishing entries and their numerical complexity can be used as a kind of a qualitative "measure" for the "quality" of a pure candidate. Furthermore, in some cases we reconsructed ΔA as function of kinematic invariants and used it as a starting point for a semi-algorithmic approach described in section 3.3.5. See appendix C for details on the functional reconstruction.
We implemented the described algorithm of computing numerical differential equations in a `Mathematica` program which includes interfaces to both `FIRE6` and `KIRA` and verified our implementation on several known two-loop examples including the planar massless five-point penta-box topology.

3.3 Strategies for constructing pure basis

3.3.1 Introduction

In section 2.4 we reviewed the general method for computing Feynman integrals by using the differential equation approach and highlighted how crucial the knowledge of pure basis is.
A remarkable progress in developing strategies for constructing a canonical basis for a given integral topology was made in recent years [43, 47, 48, 182, 196–202], including both case-by-case constructions and algorithmic approaches. Especially the univariate case is quite well understood by now [196–199, 203]. However, in the multivariate case, the construction of a pure basis remains an open problem. In 2.4.2 we also briefly reviewed the definition of d-log forms, UT integrals and sketched the close relation of these objects to the concept of the pure basis. It is a widely accepted conjecture (see e.g. [181]) that only if all leading singularities of a given differential form

are constant (kinematicly independent), it can be written as a dlog form and gives rise to an integral of uniform trancendental weight. This connection was first observed in planar $\mathcal{N} = 4$ SYM [181,204,205]. This observation can be used in practice as a guiding principle for constructing pure integral candidates. We investigate the leading singularities of a given topology and construct integrals with all leading singularities being simultaneously constant. In this thesis, we work with the definition of the leading singularity given in 2.3.4. Note that we typically only check some of the leading singularities. Since the connection between the ϵ-factorized DE and integrals with constant leading singularities is a conjecture anyway we have to check explicitly for any candidate whether it fulfills the canonical DE. So working with only few leading singularities is not a real problem in practice.
In the remaining part of this section we will see how these mathematical concepts and ideas can be applied in the special case of the five-point integrals with one massive external leg. We will focus on the planar and the hexa-box topologies. The more challenging case of both double-pentagon topologies will be discussed separately in section 4.3.2 at the end of chapter 4. The pure basis for one of the double-pentagon topologies still needs to be completed. An interesting observation which first arose for five-point topologies is that a four-dimensional analysis of leading singularities is not sufficient to obtain all pure integrals [43, 47, 48]. In some cases, we will need to deal with higher-dimensional objects which vanish in exactly four dimensions.
The structure of the discussion is following: In sections 3.3.2 and 3.3.3 we discuss the computation of multivariate residues of five-point two-loop integrals based on combining residues of one-loop sub-graphs. Section 3.3.4 deals with the extra-dimensional extensions of the approach and shows how many pure five-point integrals can be constructed without an explicit calculation of the corresponding residues. In section 3.3.5 we sketch a semi-algorithmic procedure for completing a *near-to-pure* insertion based on functional reconstruction of the differential equation and integrating out the $\mathcal{O}(\epsilon^0)$ part. In section 3.3.6 we complete the general discussion with a detailed analysis of two special integral topologies which required some case-tailored strategies.

3.3.2 Loop-by-loop residue computation

We begin our discussion of the pure-basis construction with a loop-by-loop approach of computing maximal cuts of two-loop integrals by using known one-loop results. In the first part we will consider the simplest situation where the two-loop leading singularity is given by the product of two one-loop constituents. At first, we are going to deal with integrals with box- and triangle-subloops and set $D = 4$ exactly.
We begin with collecting some well-known results (see e.g. [206]) for maximal cuts of some scalar one-loop integrals in table 3.2 which will be relevant in the following. Here we set $s = (p_1 + p_2)^2$ and $t = (p_2 + p_3)^2$. Double lines denote massive external momenta, λ is the Källén function and all maximal cuts are understood to be strictly four-dimensional. Box integrals with two massive lines on the same side of the box will be referred to as *hard-boxes* while integrals with two massive lines opposite to each other are called *easy-boxes*.

Topology	Leading singularity
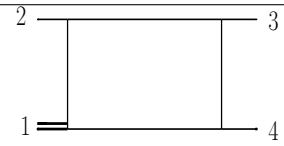	$\frac{1}{st}$
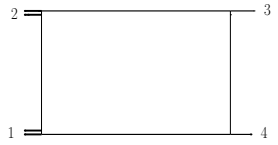	$\frac{1}{st}$
	$\frac{1}{st-p_1^2p_3^2}$
	$\frac{1}{st-p_1^2p_3^2}$
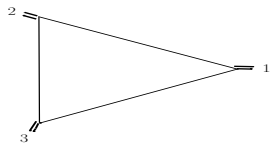	$\frac{1}{\sqrt{\lambda(p_1^2,p_2^2,p_3^2)}}$
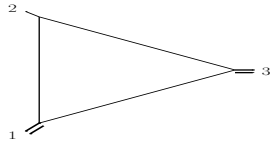	$\frac{1}{p_1^2-p_3^2}$
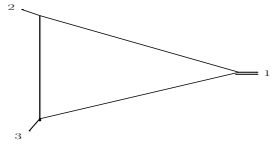	$\frac{1}{p_1^2}$

Table 3.2: Maximal cuts of one-loop box and triangle integrals with massless propagators.

Let us now consider a series of planar two-loop topologies with $N+2$ external legs which are built up of a box subloop with two massless external legs and a N-gon subloop with N external legs (see fig. 3.2) which can be either massive or massless. Note that for some integral topologies p_1 and/or p_N have to be set to 0. In the following, we will refer to topologies with both $p_1 \neq 0$ and $p_N \neq 0$ as *generic* while topologies with either $p_1 = 0$ or $p_N = 0$ are called *semi-generic* and topologies with $p_1 = 0$ and $p_N = 0$ will be referred to as *simple*.
The loop-momentum representation of the series is given by

$$I_{N,pl} = e^{2\gamma_E \epsilon} \int \frac{d^D\ell_1}{i\pi^{D/2}} \frac{d^D\ell_2}{i\pi^{D/2}} \frac{1}{\ell_2^2(\ell_2 - p_{N+2})^2(\ell_2 - p_{N+1} - p_{N+2})^2(\ell_1 - \ell_2)^2} \frac{1}{\prod_{i=1}^{N-1}(\ell_1 + q_i)^2}, \quad (3.26)$$

where $q_i = \sum_{j=1}^{i} p_j$ and we assume $p_{N+1}^2 = p_{N+2}^2 = 0$.

For integrals in this thesis we can assume $N \in \{3, 4, 5\}$. [3]

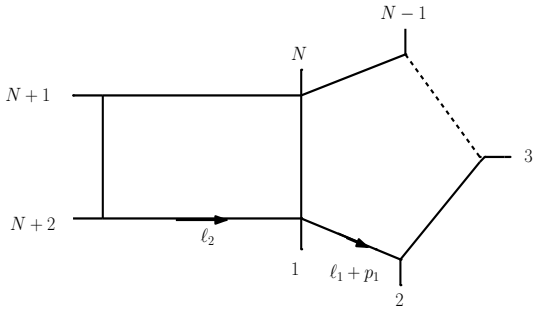

Figure 3.2: The planar N-gon-box diagram with $N+2$ external momenta.

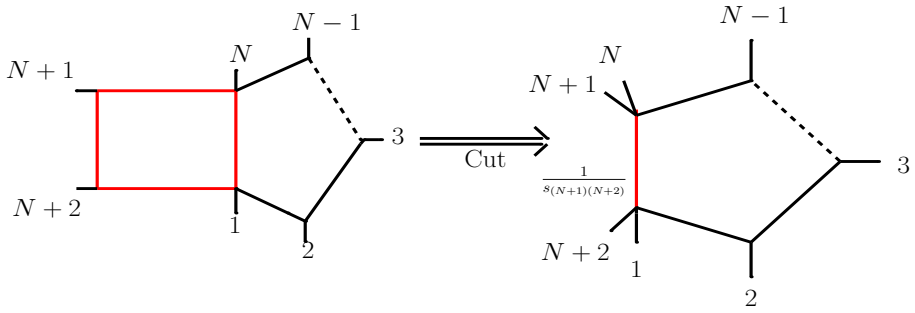

(a) Cutting the left-side box (in red) gives a one-loop N-point integral.

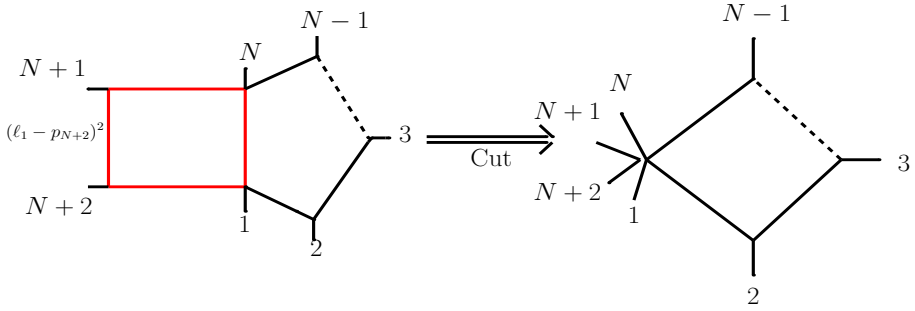

(b) The numerator factor $(\ell_1 - p_{N+2})^2$ cancels the Jacobian factor coming from cutting the left-side box.

Figure 3.3: Application of loop-by-loop approach to the planar N-gon-box integral family.

We want to calculate a maximal cut of $I_{N,pl}$ by using the loop-by-loop approach. First, we compute the residue of the left-side box which is equivalent to cutting the following four propagators $\left\{\frac{1}{\ell_2^2}, \frac{1}{(\ell_2-p_{N+2})^2}, \frac{1}{(\ell_2-p_{N+2}-p_{N+1})^2}, \frac{1}{(\ell_1-\ell_2)^2}\right\}$. This subloop can be viewed as a two-mass hard-box integral over ℓ_2 with external momenta $\{p_{N+2}, p_{N+1}, -\ell_1, (\ell_1 - p_{N+2} - p_{N+1})\}$. Note that ℓ_1 has to be considered as an off-shell momentum since it can take any value before integration. According to the table 3.2, the leading singularity of this subbox is given by

$$\mathcal{R}_{box} = \frac{1}{s_{(N+1)(N+2)}(\ell_1 - p_{N+2})^2}. \tag{3.27}$$

So, up to a rational prefactor, we obtain an additional propagator which can be combined with the $N-1$ propagators from the right subloop to a one-loop N-point integral $I_{N,1-loop}$. Followingly,

[3] The case $N = 2$ will be considered separately.

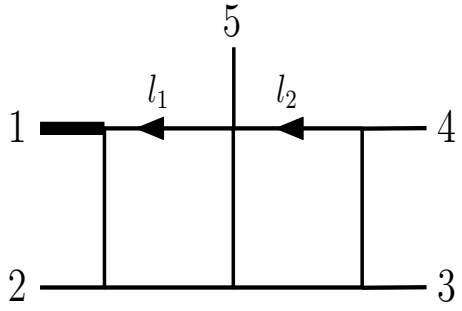

Figure 3.4: Planar five-point double-box integral. The thick line denotes the massive leg.

the maximal cut of $I_{N,pl}$ is obtained in the loop-by-loop approach by

$$\mathcal{R}_{N,pl} = \frac{1}{s_{(N+1)(N+2)}} \mathcal{R}_{N,1L}, \tag{3.28}$$

where the second factor denotes the maximal cut of the corresponding one-loop N-point integral. This computation can be represented graphically by replacing the left sub-loop box in 3.2 by a single edge connecting the p_1-vertex with the p_N-vertex (see fig. 3.3a). This computation shows that the problem of constructing a pure insertion for $I_{N,pl}$ can be traded for the problem of finding a pure insertion for the *one-loop integral* $I_{N,1L}$ which is a much simpler task. For $N = 3, 4$ the required one-loop insertion is given by a kinematic prefactor which can be read off table 3.2. In this case

$$\mathcal{N}^{(1)}_{N,pl} = \frac{s_{(N+1)(N+2)}}{\mathcal{R}_{N,1L}} \tag{3.29}$$

is a valid candidate for a pure numerator insertion. In this analysis, we are not confined to scalar integrals. We can assume having a numerator factor $\mathcal{N}(\ell_1)$ such that $I_{N,1L}[\mathcal{N}(\ell_1)]$ is a pure integral. Then, we can expect that also $s_{(N+1)(N+2)}\mathcal{N}(\ell_1)$ is a pure candidate insertion. We will exploit this idea in more detail in section 3.3.4 where we discuss the more subtle case of a pentagon subloop with $N = 5$.
For $N = 4, 5$ the presented approach can be used to construct a further pure tensor insertion independent of the previously obtained pure scalar one. Since cutting the left-side box generates a new propagator it is a natural idea to cancel this additional factor by inserting it in the numerator. Then, after computing the box-side cut, we are left with a scalar one-loop $(N-1)$-gon integral. The corresponding leading singularity $\mathcal{R}_{N-1,1L}$ can be again read off table 3.2. We conclude that

$$\mathcal{N}^{(2)}_{N,pl} = \frac{s_{(N+1)(N+2)}(\ell_1 - p_{N+2})^2}{\mathcal{R}_{N-1,1L}} \tag{3.30}$$

is a valid candidate for a pure insertion. This calculation can be represented in a pictorial way by shrinking the left-side box to a single point (see fig. 3.3b).
In order to illustrate the loop-by-loop procedure, we will explicitly construct two independent pure integrals for the planar five-point double-box topology with a massive external leg attached to one of the two subboxes. The propagator structure of this topology can be extracted from figure 3.4. Since the topology has a sub-box part with two massless external momenta attached to it we can apply the previously discussed algorithm. According to our analysis, the cutting of the ℓ_2-subbox generates the Jacobian factor $\frac{1}{s_{34}(\ell_1 - p_4 - p_5)^2}$ leaving a two-mass hard-box integral with external momenta $\{p_1, p_4 + p_5, p_3, p_4\}$. Its leading singularity is given by $\frac{1}{s_{12}s_{23}}$. So, our first pure candidate is given by

$$\mathcal{N}^{(1)}_{pl,db} = s_{34}s_{12}s_{23}. \tag{3.31}$$

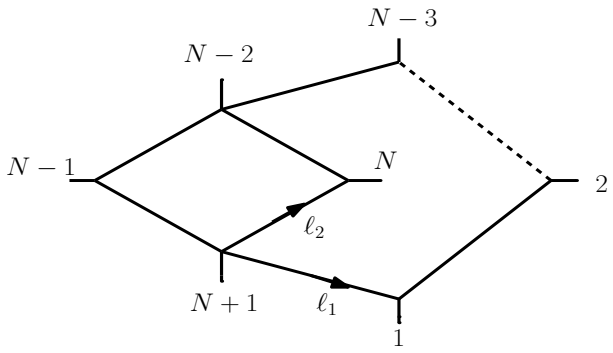

(a) Non-planar N-gon-box diagram with $N+1$ external momenta.

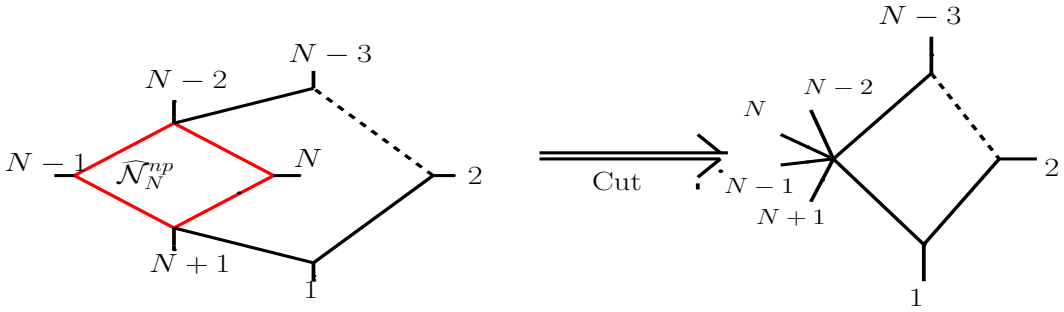

(b) Cutting the left box sub-loop (in red) gives a one-loop $(N-1)$-point integral. $\widehat{\mathcal{N}}_N^{(np)}$ denotes the numerator insertion defined in eq. (3.34).

Figure 3.5: Application of loop-by-loop approach to the non-planar N-gon-box integral family.

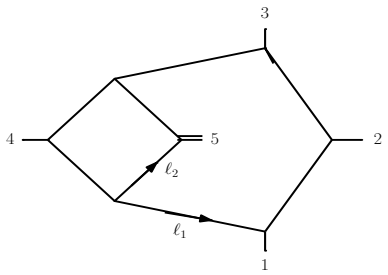

Figure 3.6: Hexa-box diagram with the massive leg on the box sub-loop.

The second pure integrand is obtained by inserting $(\ell_1 - p_4 - p_5)^2$ in the numerator which leads to a two-mass triangle integral spanned by $\{p_1, p_3 + p_4 + p_5, p_2\}$ after cutting the ℓ_2-subloop. The leading singularity of this triangle is given by $\frac{1}{s_{12}-q^2} = \frac{1}{2p_1\cdot p_2}$. So, the second candidate insertion reads

$$\mathcal{N}^{(2)}_{pl,db} = (\ell_1 - p_4 - p_5)^2 s_{34}(s_{12} - q^2). \tag{3.32}$$

A second integral family relevant for five-point scattering where the loop-by-loop approach can be applied directly is the non-planar N-gon-box family (fig. 3.5a) consisting of an *internal* box-subloop and an *external* N-gon part. The integral family is defined by

$$I_N^{(np)} = e^{2\gamma_E\epsilon}\int \frac{d^D\ell_1}{i\pi^{D/2}}\frac{d^D\ell_2}{i\pi^{D/2}}\frac{1}{\ell_2^2(\ell_2+p_N)^2(\ell_1+\ell_2-p_{N-1}-p_{N+1})^2(\ell_1+\ell_2-p_{N+1})^2} \times \frac{1}{\prod_{i=0}^{N-3}(\ell_1+q_i)^2}, \tag{3.33}$$

with $q_i = \sum_{j=1}^{i} p_j$, $q_0 = 0$, $p_{N-1}^2 = 0$ and generic p_N. As before, p_{N-2} and p_{N+1} will be set to 0

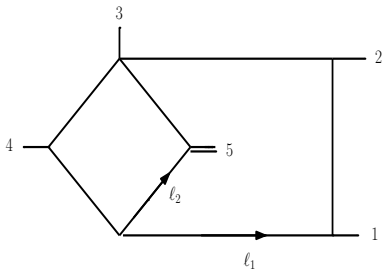

Figure 3.7: Non-planar penta-box diagram with the massive leg on the box sub-loop.

for simple and semi-simple momentum configurations. Let us compute the maximal cut of the ℓ_2-subloop with external momenta $\{-(\ell_1 - p_{N+1}), p_{N-1}, (\ell_1 - p_{N-1} - p_N - p_{N+1}), p_N\}$. Depending on, whether p_N is massive, the subloop corresponds to either a two-mass-easy box or a three-mass box integral. According to the table 3.2, they both have the same maximal cut given by

$$\mathcal{R}_{box,np} = \frac{1}{(\ell_1 - p_{N+1} - p_{N-1})^2(\ell_1 - p_{N+1} - p_N)^2 - (\ell_1 - p_{N+1})^2(\ell_1 - p_{N-1} - p_N - p_{N+1})^2}. \quad (3.34)$$

We insert the inverse of $\mathcal{R}_{box,np}$ into the numerator. After cutting the box subloop and cancelling the corresponding leading singularity we are left with a one-loop $(N-2)$-point integral with external momenta $\{p_1, \cdots, p_{N-3}, (p_{N-2} + p_{N-1} + p_N + p_{N+1})\}$. Graphically, this can be represented by shrinking the ℓ_2-subloop to a single point (see fig. 3.5b). Consequently, we obtain

$$\mathcal{N}_{np} = \frac{(\ell_1 - p_{N+1} - p_{N-1})^2(\ell_1 - p_{N+1} - p_N)^2 - (\ell_1 - p_{N+1})^2(\ell_1 - p_{N-1} - p_N - p_{N+1})^2}{\mathcal{R}_{N-2,1L}} \quad (3.35)$$

as pure candidate insertion where $\mathcal{R}_{N-2,1L}$ is the leading singularity of the residual one-loop integral of figure 3.5b.
Let us consider a concrete example of a simple hexa-box integral with $N = 6$ with the massive leg sitting on the ℓ_2-sub-box (fig. 3.6). The leading singularity of this sub-loop is gven by

$$\mathcal{R}_{box,np} = \frac{1}{(\ell_1 - p_4)^2(\ell_1 - p_5)^2 - \ell_1^2(\ell_1 + p_1 + p_2 + p_3)^2}. \quad (3.36)$$

Following the loop-by-loop algorithm, we obtain a pure candidate insertion

$$\mathcal{N}_{np,hb} = s_{12}s_{23}\left[(\ell_1 - p_4)^2(\ell_1 - p_5)^2 - \ell_1^2(\ell_1 + p_1 + p_2 + p_3)^2\right]. \quad (3.37)$$

The kinematic prefactor cancels the leading singularity left over after cutting the ℓ_2 sub-loop.
For the special cases of simple and semi-simple topologies in the $I_N^{(np)}$ family, we can extract even more information from the loop-by-loop approach. Let us again investigate the maximal cut of the ℓ_2 sub-loop given by eq. (3.34). For $p_{N+1} = 0$, the second term in the denominator becomes proportional to an inverse propagator and, consequently, vanishes on the maximal cut of $I_N^{(np)}$. So, the sub-loop leading singularity factorizes into a product of two quadratic expressions in ℓ_1. We can cancel one of these factors by inserting it in the numerator and calculate the maximal cut of the residual one-loop integral with $N-1$ external legs. However, it is important to remember that an integral constructed in such a way is expected to be pure only on the maximal cut since we explicitly replaced the ℓ_2-leading singularity by its maximal-cut expression. So we might need additional terms proportional to the corresponding inverse propagator to complete the pure integrand. We will discuss a semi-algorithmic procedure of computing such corrections in section 3.3.5. Let us illustrate this concept on a concrete example. We consider a semi-simple non-planar

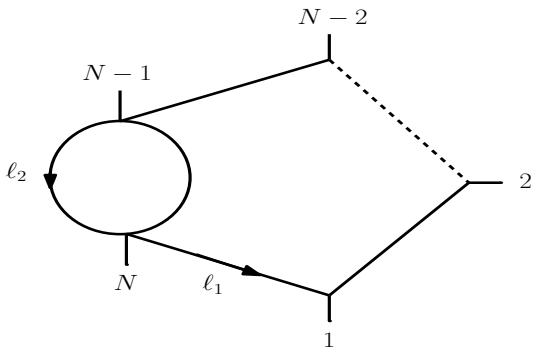

Figure 3.8: N-gon integral with a bubble-like sub-loop.

penta-box integral with $N = 5$, $p_6 = 0$ and $p_5^2 \neq 0$ (fig. 3.7). The ℓ_2 leading singularity is given by

$$\mathcal{R}_{box,np} = \frac{1}{(\ell_1 - p_4)^2(\ell_1 - p_5)^2 - \ell_1^2(\ell_1 - p_4 - p_5)^2} \xrightarrow{\text{cut}} \frac{1}{(\ell_1 - p_4)^2(\ell_1 - p_5)^2}. \tag{3.38}$$

The box leading singularity factorizes on the maximal cut. According to our strategy, we start with

$$\mathcal{N}_{np,pb}^{(1)} \sim (\ell_1 - p_4)^2, \quad \mathcal{N}_{np,pb}^{(2)} \sim (\ell_1 - p_5)^2. \tag{3.39}$$

After cutting the ℓ_2 sub-box and cancelling the numerators, we are left with one-loop four-point integrands spanned by $\{p_1, p_2, (p_3 + p_4), p_5\}$ and $\{p_1, p_2, (p_3 + p_5), p_4\}$, respectively. The *on-shell* pure candidates are now given by the insertions

$$\mathcal{N}_{np,pb}^{(1)} = s_{12}s_{15}(\ell_1 - p_4)^2, \quad \mathcal{N}_{np,pb}^{(2)} = s_{12}s_{14}(\ell_1 - p_5)^2. \tag{3.40}$$

As we will see in section 3.3.5, these integrals indeed require an off-shell correction term.
There is a third relevant family of integral topologies for which a pure insertion can be constructed in an algorithmic way. These are N-point planar integrals containing a bubble-like subloop, generally defined via

$$I_N^{(bubble)} = e^{2\gamma_E\epsilon} \int \frac{d^D\ell_1}{i\pi^{D/2}} \frac{d^D\ell_2}{i\pi^{D/2}} \frac{1}{\ell_2^2(\ell_1 - \ell_2 - p_N)^2} \frac{1}{\prod_{i=0}^{N-2}(\ell_1 + q_i)^2}, \tag{3.41}$$

with $q_i = \sum_{j=1}^{i} p_j$, $q_0 = 0$. The momentum routing can be extracted from fig. 3.8. Let us recall the well-known result [138] for the massless one-loop bubble integral with generic propagator powers and full ϵ-dependence.

$$\begin{aligned} I^{bubble}(p^2, \{n_1, n_2\}) &= e^{\epsilon\gamma_E} \int \frac{d^D\ell}{i\pi^{D/2}} \frac{1}{[\ell^2]^{n_1}\,[(\ell + p)^2]^{n_2}} \\ &= (-1)^{n_1+n_2} e^{\epsilon\gamma_E} \frac{\Gamma(2 - \epsilon - n_1)\Gamma(2 - \epsilon - n_2)\Gamma(n_1 + n_2 + \epsilon - 2)}{\Gamma(n_1)\Gamma(n_2)\Gamma(4 - 2\epsilon - n_1 - n_2)(-p^2)^{n_1+n_2+\epsilon-2}}. \end{aligned} \tag{3.42}$$

Let us concentrate on two important special cases where the result can be easily transformed into a function of uniform trancendental weight:

- $n_1 = n_2 = 1$

$$I^{bubble}(p^2, \{1, 1\}) = \frac{f(p^2, \epsilon)}{(1 - 2\epsilon)\epsilon}, \tag{3.43}$$

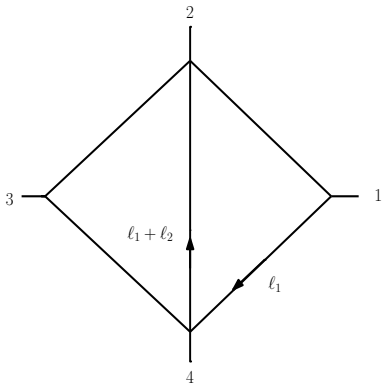

Figure 3.9: Massless slashed-box integral.

- $n_1 = 1,\ n_2 = 2$ or vice versa

$$I^{bubble}(p^2, \{1,2\}) = -\frac{f(p^2,\epsilon)}{p^2\epsilon}, \tag{3.44}$$

where $f(p^2,\epsilon)$ is a pure function of weight zero. This observation together with the propagator-like p^2-dependence of the bubble integral provide a general strategy for integrals from the I_N^{bubble} family. We start with either a *dotted* bubble sub-loop $I_N^{bubble}\left[\frac{1}{\epsilon\ell_2^2}\right]$ or a normalized undotted integral $I_N^{(bubble)}\left[\frac{(1-2\epsilon)}{\epsilon}\right]$ and integrate out the bubble part. In the first case, we are left with a N-point one-loop integral over ℓ_1 with external legs $\{p_1,\cdots,p_{N-1},p_N\}$ and, in the second case, we obtain a $(N-1)$-point one-loop integral with $\{p_1,\cdots,p_{N-2},(p_{N-1}+p_N)\}$.[4] To obtain a pure integral we only need to compensate for the maximal cut of the residual one-loop integral. It should be noticed that, although at one-loop level the dotted and the undotted bubble integrals are dependent, this is, in general, not true for the corresponding two-loop integrals since the external momenta of the sub-loop depend on the second loop momentum. Later, we will see examples where we indeed can construct two independent pure integrals with this approach.

3.3.3 Extended loop-by-loop approach

All pure integrals we discussed so far could be constructed by combining two one-loop maximal cuts. In principle, we just glued together two one-loop results to obtain a pure two-loop insertion. However, this is not possible in general. In the following, we want to discuss two concrete examples where the loop-by-loop approach requires a more delicate treatment of the intermediate residue which arises after cutting one of the sub-loops. First, we discuss a pedagogical example of the scalar massless slashed-box diagram (fig. 3.9). The corresponding integral is defined by

$$I_{sb} = e^{2\epsilon\gamma_E}\int\frac{d^D\ell_1}{i\pi^{D/2}}\frac{d^D\ell_2}{i\pi^{D/2}}\frac{1}{\ell_1^2(\ell_1-p_1)^2(\ell_2-p_1-p_2)^2(\ell_2-p_1-p_2-p_3)^2(\ell_1-\ell_2)^2}. \tag{3.45}$$

The kinematics is parametrized by $s=(p_1+p_2)^2$ and $t=(p_2+p_3)^2$. Let us briefly discuss the difference of this example to the previous cases. Since the diagram consists of two triangles, there are not enough propagators in both sub-loops to localize all internal degrees of freedom in four dimensions. However, this problem appears already for one-loop triangle integrals and was

[4] After computing the ℓ_2 integral we take the $\epsilon\to 0$ limit.

analyzed there. It was shown that an additional propagator can be cut. This statement becomes more precise if we consider a generalized definition of loop-integrals in a projective extension of loop-momentum space. One possible realization of this idea is the so-called *embedding space formalism* (ESF) (see e.g. [207, 208]). We point to [167] for a more detailed introduction to ESF and give an overview in appendix B. The embedding space extension of the slashed-box integral in $(D = 4)$-dimensions is given by

$$I_{sb}^{(D=4)} \sim \int \frac{\mathrm{d}Y_1\,\mathrm{d}Y_2}{(X_0Y_1)(X_1Y_1)(Y_1Y_2)(IY_1)(X_2Y_2)(X_3Y_2)(IY_2)}, \tag{3.46}$$

with the *infinitity point* I and the *initial point* X_0 as defined in appendix B.[5] Note that the two *infinitity propagators* (IY_1) and (IY_2) provide exactly the both missing factors which can be cut now. In the first step, we impose the maximal cut conditions $(X_0Y_1) = (X_1Y_1) = (Y_1Y_2) = (IY_1) = 0$ on the Y_1 sub-box. Since the inverse propagators are now linear in the embedding space variables Y_1, Y_2 the Jacobian associated with these cut conditions is given by

$$J = \frac{1}{\sqrt{G(X_0, X_1, Y_2, I)}}, \tag{3.47}$$

with $G(V_1, \cdots, V_n) := \det\{(V_iV_j)\}_{i,j=1}^n$. The Gram determinant is a perfect square and reads explicitly

$$G(X_0, X_1, Y_2, I) = ((X_0Y_2) - (X_1Y_2))^2. \tag{3.48}$$

Inserting this into (3.46), gives

$$I_{sb}^{(D=4)}{}_{Y_1-\mathrm{cut}} \sim \int \frac{\mathrm{d}Y_2}{((X_0Y_2) - (X_1Y_2))(X_2Y_2)(X_3Y_2)(IY_2)}. \tag{3.49}$$

Using the bilinearity of the embedding space scalar product we can interprete eq. (3.49) as a box integral with an auxiliary propagator $(\tilde{X}Y_2)$, where $\tilde{X} := X_0 - X_1$ and apply eq. (3.47) again to take the second residue. The maximal cut is given by

$$\mathcal{R}_{sb} \sim \frac{1}{\sqrt{G(\tilde{X}, X_2, X_3, I)}} = \frac{1}{s+t}. \tag{3.50}$$

This calculation explains the prefactor $(s + t)$ in eq. (2.106). Now we want to apply the ESF approach to a five-point massive integral which cannot be treated by the loop-by-loop method in momentum space. Our example is the scalar triangle-box diagram with the massive leg attached to the box-side (fig. 3.10). The integral is defined via

$$I_{tb} = e^{2\epsilon\gamma_E} \int \frac{d^D\ell_1}{i\pi^{D/2}} \frac{d^D\ell_2}{i\pi^{D/2}} \frac{1}{\ell_1^2(\ell_1 - p_1)^2(\ell_1 - p_1 - p_2)^2(\ell_2 + p_4 + p_5)^2(\ell_2 + p_5)^2(\ell_1 - \ell_2)^2}. \tag{3.51}$$

In the embedding space representation the integral becomes

$$I_{tb}^{(D=4)} \sim \int \frac{\mathrm{d}Y_1\,\mathrm{d}Y_2}{(X_0Y_1)(X_1Y_1)(X_2Y_1)(X_3Y_2)(X_4Y_2)(Y_1Y_2)(IY_2)}. \tag{3.52}$$

[5] The delta functions $\delta((Y_1Y_1))$ and $\delta((Y_2Y_2))$ which ensure the *lightcone* constraint are included in the integration measure.

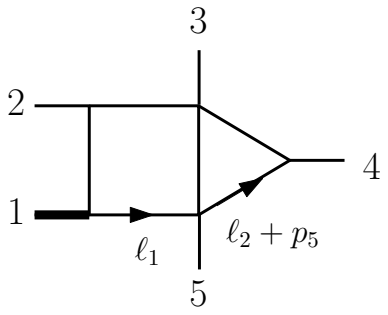

Figure 3.10: Five-point triangle-box integral with the massive leg at the box-side.

We cut the four box-side propagators $\{(X_0Y_1), (X_1Y_1), (X_2Y_1), (Y_1Y_2)\}$ and obtain the following Jacobian factor

$$J = \frac{1}{\sqrt{G(X_0, X_1, X_2, Y_2)}} = \frac{1}{(q^2(X_2Y_2) - s_{12}(X_1Y_2))^2}. \tag{3.53}$$

By introducing the auxiliary vector $\tilde{X} := q^2 X_2 - s_{12} X_1$, we can write the Y_2 sub-loop as a triangle integral

$$I_{tb}^{(D=4)}{}_{Y_1-\text{cut}} \sim \int \frac{\mathrm{d}Y_2}{(\tilde{X}Y_2)(X_3Y_2)(X_4Y_2)(IY_2)}. \tag{3.54}$$

The maximal cut is given by

$$\mathcal{R}_{tb} \sim \frac{1}{\sqrt{G(\tilde{X}, X_3, X_4, I)}} = \frac{1}{s_{12}(s_{15} - s_{23}) - q^2 s_{34}}, \tag{3.55}$$

where we used $(\tilde{X}X_3) = -s_{12}s_{23}$ and $(\tilde{X}X_4) = q^2 s_{34} - s_{12}s_{15}$. Due to the linear structure of the propagators in the ESF approach, we were able to express the residue of the Y_1-cut in terms of propagators and treat it as an ordinary one-loop integral.

3.3.4 Extra-dimensional insertions

While in section 3.3.2 and section 3.3.3 we discussed methods for constructing integrals with constant leading singularities based on residue calculations, here we want to employ a more indirect idea which is inspired by the fact that analytic properties of Feynman integrals can depend on their space-time dimension. In particular, it can happen that an integral is pure when calculated for a special value of the space-time dimension and is not in any other dimension. E.g. one-loop bubble diagrams are naturally UT-functions in $2 - 2\epsilon$ dimensions. From the explicit formula (3.42) for the massless bubble integral with full ϵ-dependence we can see that the dimension change $4 - 2\epsilon \to 2 - 2\epsilon$ can be implemented by dotting one of the two propagators. For a generalization see [209].
Since we are interested in five-point processes let us first discuss the one-loop pentagon integral with on-shell external momenta $p_i^2 = 0,\ i = 1, \cdots, 5$. The integral is defined by

$$I_{pt} = e^{\epsilon\gamma_E} \int \frac{d^D\ell}{i\pi^{D/2}} \frac{1}{\prod_{i=0}^{4}(\ell + q_i)^2}, \tag{3.56}$$

where $q_i = \sum_{j=1}^{i} p_j$ and $q_0 = 0$. In four dimensions there are more propagators than cuts can be taken. So any maximal cut of the pentagon will explicitly depend on the corresponding cut

choices. For example, if we cut the first four propagators the maximal cut will be $\frac{1}{J(l_*)(\ell_*-p_5)^2}$, where ℓ_* is a solution to the cut conditions $(\ell_*+q_i)^2=0,\ i=0,\cdots,3$ and J is the Jacobian. It is easy to see that we cannot generate a pentagon integral with all constant leading singularities being constant by starting with a scalar pentagon and using only loop-momentum independent numerators [136]. One possible solution to this problem are *chiral* numerators which explicitly encode the cut conditions. This approach is widely used e.g. in the framework of the generalized unitarity [210–212]. Here, we want to explore a different approach which is based on shifting the space-time dimension to $D=6-2\epsilon$. This idea was applied for some of the massless two-loop five-point integrals in [48]. The reason for this can most easily be seen in terms of the Baikov representation (see section 2.3.2) which makes the dimensional dependence of loop integrals manifest. In the Baikov variables ρ_i the pentagon integral is

$$I_{pt} \sim [G(p_1,\cdots,p_4)]^{(-D+5)/2} \int \prod_{i=1}^{5} \frac{\mathrm{d}\rho_i}{\rho_i} \, [G(\ell,p_1,\cdots,p_4)]^{(D-6)/2}\,, \tag{3.57}$$

where G is the Gram determinant. We omit all constant factors from eq. (2.46) since they are irrelevant for the residue calculation. Since the number of integrations now coincide with the number of propagators the maximal cut can be read off to be

$$\mathcal{R}_{pt} \sim \left.\frac{[G(\ell,p_1,\cdots,p_4)]^{(D-6)/2}}{[G(p_1,\cdots,p_4)]^{(D-5)/2}}\right|_{\rho_i=0}. \tag{3.58}$$

For $D=6$ the maximal cut is given by the inverse square-root of the five-point Gram determinant depending only on external kinematics

$$\mathcal{R}_{pt}^{(D=6)} \sim \frac{1}{\sqrt{G(p_1,\cdots,p_4)}}. \tag{3.59}$$

This calculation shows that the natural starting point for a pure pentagon integral is $I_{pt}^{(D=6)}\left[\sqrt{G(p_1,\cdots,p_4)}\right]$. We can use eq. (3.57) in order to relate the six-dimensional pentagon to the four-dimensional one.

$$I_{pt}^{(D=6)} \sim I_{pt}^{(D=4)}\left[\frac{G(\ell,p_1,\cdots,p_4)}{G(p_1,\cdots,p_4)}\right]. \tag{3.60}$$

Consequently, the pure insertion for the four-dimensional one-loop pentagon integral is given by

$$\mathcal{N}_{pt,1L} = \frac{G(\ell,p_1,\cdots,p_4)}{\sqrt{G(p_1,\cdots,p_4)}} \sim \mathrm{tr}_5\mu, \tag{3.61}$$

where we used eq. (3.15) and eq. (3.6) in order to write the pure insertion in terms of μ and tr_5.

Let us proceed with two-loop five-point integrals. First of all, we can use our insight about the one-loop pentagon to extend the loop-by-loop approach to pentagon-like residues. Let us, for instance, consider one of the three two-loop penta-box topologies with one external mass (fig. 3.11). After cutting the ℓ_2 sub-box we are left with a one-loop pentagon integral over ℓ_1. Due to our discussion in the previous part, we should attach $\mathrm{tr}_5\mu_{11}$ to the numerator in order to make this pentagon pure. Combining all parts, we conclude that

$$\mathcal{N}_{pb}^{(1)} = s_{45}\mathrm{tr}_5\mu_{11} \tag{3.62}$$

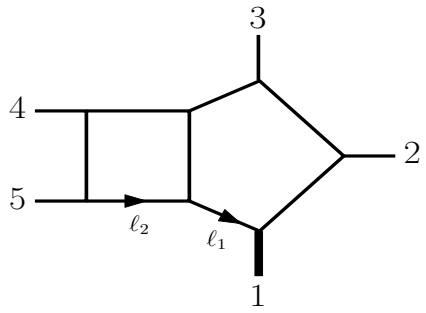

Figure 3.11: Massive penta-box diagram.

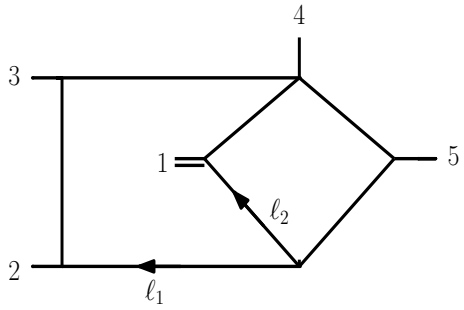

Figure 3.12: Non-planar penta-box integral with mass on the box side.

is a good candidate for a pure insertion.
Next, we try to cut the pentagon sub-loop first. The independent external momenta of the pentagon sub-loop are $\{\ell_2, p_1, p_2, p_3\}$. So both the Baikov and the Gram determinants of the pentagon sub-loop will depend on ℓ_2. Therefore, it seems natural to start with

$$\mathcal{N}_{pb}^{(2)} \sim \mathrm{tr}_5\mu_{12}. \tag{3.63}$$

Let us explicitly compute at least two of the leading singularities of $I_{pb}\left[\mathrm{tr}_5\mu_{12}\right]$ to show that it is indeed a good choice. We perform the cut computation in the Baikov representation but instead of using genuine two-loop Baikov coordinates we employ a loop-by-loop approach [49, 143].
The result is

$$\mathcal{R}_{pb}^{(2)} = \pm\frac{4}{s_{45}} \tag{3.64}$$

This calculation shows explicitly that

$$\mathcal{N}_{pb}^{(2)} = s_{45}\mathrm{tr}_5\mu_{12} \tag{3.65}$$

is indeed a good candidate. Since we have not checked all leading singularities we still need to verify the ϵ-factorization of the numerical differential equation. It is worth mentioning that in the concrete case of the planar penta-box the integrals $I_{pb}\left[s_{45}\mathrm{tr}_5\mu_{12}\right]$ and $I_{pb}\left[s_{45}\mathrm{tr}_5\mu_{11}\right]$ are not linearly independent, so they can not be both used simultaneously as master integrals. However, we will see later examples where both μ_{11}- and μ_{12}-insertions indeed lead to independent integrals.
Let us now extend this approach to a non-planar example. We consider the non-planar penta-box topology (fig. 3.12) with 6 master integrals. We denote this topology by $I_{pb}^{(np)}$. After cutting the ℓ_2-subbox we are left with three propagators $\left\{\frac{1}{\ell_1^2}, \frac{1}{(\ell_1+p_2)^2}, \frac{1}{(\ell_1+p_2+p_3)^2}\right\}$ depending only on ℓ_1 and the box Jacobian given by

$$\mathcal{R}_{np,subbox}\frac{1}{(\ell_1-p_1)^2(\ell_1-p_5)^2-\ell_1^2(\ell_1+p_2+p_3+p_4)^2}. \tag{3.66}$$

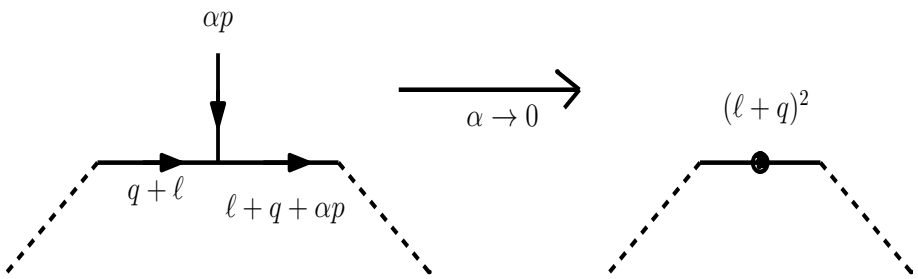

Figure 3.13: The soft limit of two propagators separated by an external leg. The dot denotes the double propagator.

On the maximal cut this Jacobian factorizes to $\frac{1}{(\ell_1-p_1)^2(\ell_1-p_5)^2}$. Together with the three ℓ_1-dependent propagators we obtain a one-loop pentagon integral. So we expect

$$\mathcal{N}^{(1)}_{np,pb} = \mathrm{tr}_5 \mu_{11} \tag{3.67}$$

to be a pure insertion. In analogy to the planar penta-box, we can ask whether

$$\mathcal{N}^{(2)}_{np,pb} = \mathrm{tr}_5 \mu_{12} \tag{3.68}$$

would also give rise to a pure integral. An explicit calculation shows that this is indeed the case. Furthermore, in the non-planar case both $\mathcal{N}^{(1)}_{np,pb}$ and $\mathcal{N}^{(2)}_{np,pb}$ give rise to independent Feynman integrals. There is an important subtlety in this calculation. Since the ℓ_2-subloop leading singularity only factorizes on-shell an off-shell correction may, in principle, be required. However, such a correction was not needed for a μ-like insertion in practice. It would be interesting, to understand better why this is the case.
By analyzing the loop-by-loop maximal cut of the *scalar* integral of the non-planar penta-box topology (fig. 3.12) we found a third parity-odd insertion that gives rise to an on-shell pure integral. Based on this observation, we searched for a third μ insertion. It was indeed found by combining a μ numerator insertion with doubling one of the central rung propagators. Concretely, the insertion is given by

$$\mathcal{N}^{(3)}_{np,db} = \frac{q^2}{\epsilon(\ell_2+p_1)^2}\mathrm{tr}_5\left[\mu_{12}+\mu_{11}\right]. \tag{3.69}$$

Heuristically, a double propagator can be compared to a pair of propagators separated by a *soft* external particle

$$\frac{1}{[(\ell+q)^2]^2} \sim \frac{1}{(\ell+q)^2}\frac{1}{(\ell+q+\alpha p)^2}, \tag{3.70}$$

with $\alpha \to 0$ (see fig. 3.13). By doubling one of the central rung propagators we turned the sub-box part of the diagram into a pentagon-like subdiagram.

A short summary of this discussion: try to find a suitable μ-insertion whenever you are faced with a pentagon sub-loop. If there is no such sub-loop, look for a suitable double propagator to "create" one.

3.3.5 Construction of off-shell correction terms

In section 3.3.2 it was already mentioned that the loop-by-loop approach sometimes requires construction of *correction terms* which vanish on-shell and, therefore, cannot be obtained by a maximal-cut computation. Here, we discuss how the remaining off-shell terms can be found. In the following, we will assume that the differential equation for the intermediate basis $\tilde{\mathbf{I}}$ takes the form

$$\mathrm{d}\tilde{\mathbf{I}} = [A_0(\mathbf{s}) + \epsilon A_1(\mathbf{s})]\,\tilde{\mathbf{I}}\,\mathrm{d}\mathbf{s}, \tag{3.71}$$

where the matrices A_0 and A_1 are ϵ-independent. For the integrals considered in this thesis it was sufficient to focus on differential equations consisting of constant and linear terms in ϵ. Since, in this section, we are only interested in off-shell corrections we can further assume that A_0 is a lower-triangular matrix with vanishing diagonal elements and so nilpotent.
Before dealing with the general multivariate problem, we should recall the univariate case

$$\mathrm{d}\tilde{\mathbf{I}} = [A_0(x) + \epsilon A_1(x)]\,\tilde{\mathbf{I}}\,\mathrm{d}x. \tag{3.72}$$

We perform the basis change

$$\tilde{\mathbf{I}} \to \mathbf{G} = \exp\left[-\int_0^x A_0(x')\,\mathrm{d}x'\right]\tilde{\mathbf{I}}. \tag{3.73}$$

By inserting (3.73) into (3.72), one can prove that the new integral basis fulfills the canonical differential equation[6]

$$\mathrm{d}\mathbf{G} = \epsilon \exp\left[-\int_0^x A_0(x')\,\mathrm{d}x'\right] A_1(x) \exp\left[\int_0^x A_0(x')\,\mathrm{d}x'\right]\mathrm{d}x\,\mathbf{G}. \tag{3.74}$$

This trick is usually referred to as *integrating out* $A_0(x)$. Since A_0 is nilpotent the matrix exponential $\exp\left[-\int_0^x A_0(x')\,\mathrm{d}x'\right]$ can be computed in a closed form. For all cases we were faced with in practice, we could even assume $A_0^2 = 0$. Then, the new integral basis is given by

$$\tilde{\mathbf{I}} \to \left[\mathbb{1} - \int_0^x A_0(x')\,\mathrm{d}x'\right]\tilde{\mathbf{I}}. \tag{3.75}$$

Let us return back to the multivariate problem. First, we apply the integrability conditions of eq. (2.71) to eq. (3.71) and obtain

$$\partial_i A_{0,j} - \partial_j A_{0,i} + [A_{0,i}, A_{j,0}] = 0, \quad i,j = 1,\ldots,6. \tag{3.76}$$

Due to the particular simple form of the $A_{0,i}$, we can assume that $[A_{0,i}, A_{0,j}] = 0$. So, there exists a matrix-valued *potential* $\Phi(\mathbf{s})$ with $\partial_i \Phi = A_{0,i},\ i = 1,\cdots,n$ which can be constructed from the partial derivatives $A_{0,i}$ by methods of standard vector calculus. The explicit formula of the basis change is then

$$\tilde{\mathbf{I}} \to [\mathbb{1} - \Phi(\mathbf{s})]\,\tilde{\mathbf{I}}. \tag{3.77}$$

Since in the case of five-point integrals with one external mass the pre-canonical differential equation is only known in numerical form, due to the absence of analytic IBP's, we cannot directly apply the method described above. However, in all relevant cases, we managed to obtain the analytic form of A_0 by a functional reconstruction procedure. Due to a rather simple form

[6] Here, we assume that $A_0(x)$ commutes with its integral $\int_0^x \mathrm{d}x'\,A_0(x')$. Otherwise, the matrix exponential in eq. (3.73) has to be replaced by the generic *Magnus series* (see e.g. [203,213]).

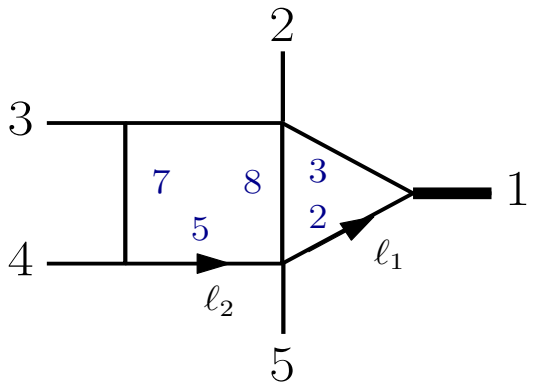

(a) Hard triangle-box topology.

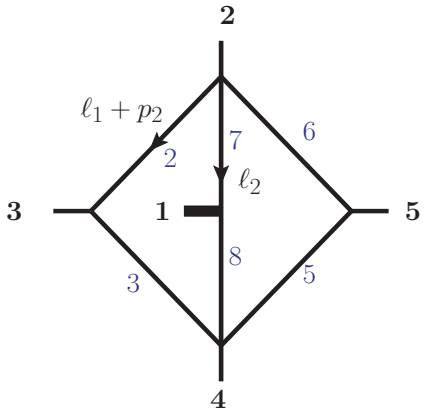

(b) Hard non-planar double-box topology.

Figure 3.14: Two topologies with most complicated pure bases. Blue numbers label the propagators.

of A_0, we, in all cases, managed to reconstruct it with $\mathcal{O}(30)$ numerical evaluations. Note that in all but one cases we only needed to compute the differential equations with six or more cut propagators. In all these cases we were able to compute the univariate differential equation which was used as a starting point of the reconstruction procedure. Furthermore, we employed the PSLQ algorithm [214] (implemented in the `Mathematica` function `FindIntegerNullVector[]`) to "guess" the analytic form of the dependence on the last two variables. So, the reconstruction task was effectively reduced to a two-variable problem which allowed us to keep the number of numerical evaluations rather small. We had to modify the standard rational reconstruction procedure due to presence of square-roots in the canonical basis. Since all these roots were known analytically before the reconstruction, only a minor change of the standard method was needed. Technical details of our reconstruction approach are discussed in appendix C.

3.3.6 The two most challenging topologies

After we discussed several general ideas we used to construct the pure bases for both planar and non-planar topologies we want to show how we combined these approaches for two most challenging topologies in the present integral families. These are the planar triangle-box topology with the massive leg attached to the triangle side (fig. 3.14a) denoted by I_{htb} with 6 master integrals and the non-planar double-box integral topology ($I_{np,hdb}$) with the mass attached to

the central rung with 4 master integrals (fig. 3.14b). Both topologies have in common that they have more master integrals than their massless counterparts, the massles triangle-box has 2 master integrals and the massless non-planar double-box only 1. By experience, these *additional* insertions are often hard to construct. This property is also shared by the non-planar penta-box integral of fig. 3.12 with 6 master integrals, whereas the corresponding massless integral has only 3 masters.
Let us begin with the planar triangle-box topology. The first pure integrand can be derived by the loop-by-loop approach of section 3.3.2. We obtain

$$\mathcal{N}^{(1)}_{htb} = s_{34}\sqrt{\lambda(s_{23}, s_{45}, q^2)}. \tag{3.78}$$

For the next two integrals we construct modified μ-like insertions given by

$$\begin{aligned} \mathcal{N}^{(2)}_{htb} &= \frac{1}{\epsilon}\mathrm{tr}_5\frac{\mu_{11}}{\rho_8}, \\ \mathcal{N}^{(3)}_{htb} &= \frac{1}{\epsilon}\mathrm{tr}_5\frac{\mu_{12}}{\rho_8}. \end{aligned} \tag{3.79}$$

These insertions can be understood as soft limit of pure non-planar penta-box integrals, as discussed at the end of 3.3.4. Note that this type of insertions was already used in the case of the massless five-point hexa-box topology in [48].
Further insertions can be found by analyzing the following one-loop IBP relation

$(q^2 s_{45})$ 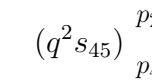

$+\frac{D-4}{2}(q^2 - s_{23} + s_{45})$ 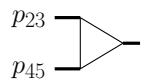

$= (D{-}3)\,\big($ 

$\big)\,,$ (3.80)

where $p_{ij} = p_i + p_j$. This relation shows that a particular combination of a dotted three-mass triangle integral with the corresponding scalar integral can be written as a sum of three pure bubble integrals. We combine this observation with the loop-by-loop approach and construct the following pure insertions

$$\begin{aligned} \mathcal{N}^{(4)}_{htb} &= s_{34}\left(\frac{q^2 s_{45}}{\rho_2} + \frac{D-4}{2}(q^2 - s_{23} + s_{45})\right), \\ \mathcal{N}^{(5)}_{htb} &= s_{34}\left(\frac{q^2 s_{23}}{\rho_3} + \frac{D-4}{2}(q^2 + s_{23} - s_{45})\right), \end{aligned} \tag{3.81}$$

where the second insertion is related to the first by $p_{23} \leftrightarrow p_{45}$. Note that these insertions give rise to independent two-loop integrals while the corresponding dotted one-loop triangles are linearly dependent. The reason is that the IBP relation (3.80) applied at the sub-loop level becomes loop-momentum dependent which leads to two independent two-loop integrals.
Finally, we obtained the last insertion

$$\mathcal{N}^{(6)}_{htb} = s_{34}\left(\frac{D-4}{2}(q^2 + s_{23} - s_{45}) - q^2\frac{(\ell_1 - p_4)^2}{\rho_2} - s_{15}\frac{\rho_7}{\rho_5}\right) \tag{3.82}$$

by combining the loop-by-loop approach with the method of section 3.3.5. We started with $s_{34}q^2\frac{(\ell_1-p_4)^2}{\rho_2}$ which is dictated by the loop-by-loop approach and obtained the two additional terms by integrating out the analytically reconsructed A_0-part of the differential equation.

Let us continue with the non-planar double-box integral topology (fig. 3.14b) which we refer to as *hard-double-box* in following. We begin with computing the maximal cut of the scalar integral. The crucial difference of this topology to the cases discussed in section 3.3.2 is the *generic* configuration of the external momenta. Since we have external momenta p_2 and p_4 attached to both triple vertices, the leading singularities of both the left and the right sub-boxes do not factorize in terms of propagator-like objects as in the *simple* and the *semi-simple* cases.[7] However, for the leading singularity of the easy-box integral (fig. 3.15) a factorization in terms of helicity spinors exists and can be found for instance in [215].[8]

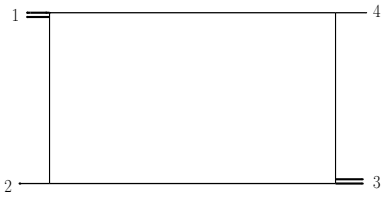

Figure 3.15: Easy-box integral.

The leading singularity of the easy-box integral can be factorized as follows

$$(p_1+p_2)^2(p_2+p_3)^2 - p_1^2 p_3^2 = [p_1\cdot q]\,[p_1\cdot \bar{q}]\,, \tag{3.83}$$

with $q^\mu = \langle 2|\gamma^\mu|4]$, $\bar{q}^\mu = \langle 4|\gamma^\mu|2]$. The notation we use here is explained in A. Since both the left and the right sub-boxes have three massive external legs the factorization formula (3.83) is not applicable to them. Instead, we cut the *external* sub-box, spanned by $\{-(\ell_2-p_2), p_3, (\ell_2+p_1+p_4), p_5\}$, which has two massless external legs, with inverse propagators $\mathcal{C}_1 = \{(\ell_1+p_2)^2, (\ell_1+p_2+p_3)^2, (\ell_1+\ell_2-p_5)^2, (\ell_1+\ell_2)^2\}$ and write the remaining four-dimensional integral as

$$I_{hdb,\mathcal{C}_1} \sim \int \frac{\mathrm{d}^4\ell_2}{i\pi^2} \frac{1}{[(\ell_2-p_2)\cdot Q]\left[(\ell_2-p_2)\cdot \bar{Q}\right]\ell_2^2(\ell_2+p_1)^2}, \tag{3.84}$$

with $Q^\mu = \langle 3|\gamma^\mu|5]$, $\bar{Q}^\mu = \langle 5|\gamma^\mu|3]$. We parametrize ℓ_2 by

$$\ell_2^\mu = p_2^\mu + \alpha_1 p_3^\mu + \alpha_2 p_5^\mu + \beta_1\langle 3|\gamma^\mu|5] + \beta_2\langle 5|\gamma^\mu|3], \quad \alpha_i,\beta_i\in\mathbb{C}, \tag{3.85}$$

so that

$$(\ell_2-p_2)\cdot Q = \beta_2 p_3\cdot p_5, \qquad (\ell_2-p_2)\cdot\bar{Q} = \beta_1 p_3\cdot p_5, \tag{3.86}$$

and change the integration variables to α_i,β_i. The Jacobian associated to this change of variables becomes

$$J = \epsilon^{\mu\nu\rho\sigma} p_{3,\mu} p_{5,\nu} Q_\rho \bar{Q}_\sigma \sim (p_3\cdot p_5)^2 \tag{3.87}$$

up to a numerical prefactor. So, the integral in eq. (3.84) becomes

$$I_{hdb,\mathcal{C}_1} \sim \int \frac{\mathrm{d}\alpha_1\,\mathrm{d}\alpha_2\,\mathrm{d}\beta_1\,\mathrm{d}\beta_2}{i\pi^2} \frac{1}{\beta_1\beta_2\ell_2^2(\alpha_i,\beta_i)(\ell_2(\alpha_i,\beta_i)+p_1)^2}. \tag{3.88}$$

[7] Here, the on-shell factorization is understood.

[8] We are deeply grateful to Michael Ruf for pointing to this paper and discussing the computation of the leading singularity.

The residue at $\beta_1 = 0,\ \beta_2 = 0$ can now be trivially taken. The result is

$$I_{hdb,\mathcal{C}_1,\beta_i} \sim \int \frac{\mathrm{d}\alpha_1\,\mathrm{d}\alpha_2}{i\pi^2} \frac{1}{p_1(\mathbf{s},\alpha_1,\alpha_2)p_2(\mathbf{s},\alpha_1,\alpha_2)}, \tag{3.89}$$

where

$$\begin{aligned} p_1 &= \frac{1}{2}\left(\alpha_2\left(q^2 + (\alpha_1 - 1)\,s_{12} - \alpha_1 s_{34} - \alpha_1 s_{45} - s_{15} + s_{34}\right) + \alpha_1 s_{23}\right), \\ p_2 &= \alpha_1 s_{45} + (\alpha_1 - 1)\,(\alpha_2 - 1)\,s_{12} + \alpha_2\left(-\alpha_1 s_{34} - \alpha_1 s_{45} + s_{34}\right). \end{aligned} \tag{3.90}$$

The zeros of the two factors fully fix the two remaining degrees of freedom and so the maximal cut is given by

$$\mathcal{R}_{hdb} = \frac{1}{\sqrt{\Sigma_5^{(2)}}}, \tag{3.91}$$

with

$$\begin{aligned} \Sigma_5^{(2)} = &\left(q^2\,(s_{45} - s_{12}) + s_{12}\,(s_{15} + s_{23}) - s_{23}s_{34} - s_{15}s_{45} + s_{34}s_{45}\right)^2 \\ &+ 4 s_{12} s_{23}\,(s_{12} - s_{34} - s_{45})\left(q^2 - s_{15}\right). \end{aligned} \tag{3.92}$$

An alternative derivation of this result, which uses ESF approach, is given in [56]. The obvious choice for the first insertion is

$$\mathcal{N}_{hdb}^{(1)} = \sqrt{\Sigma_5^{(2)}}. \tag{3.93}$$

The second pure insertion was constructed such that it cancels one of the chiral products $(\ell_2 - p_2)\cdot Q$ and $(\ell_2 - p_2)\cdot \bar{Q}$. We used a combination of $(\ell_2 - p_2)\cdot Q$ and $(\ell_2 - p_2)\cdot \bar{Q}$ and their Z_2 transforms $(\ell_2 + p_1 + p_4)\cdot Q$ and $(\ell_2 + p_1 + p_4)\cdot \bar{Q}$ such that the full insertion transforms as a singlet under the $Z_2 \times Z_2$-symmetry of the diagram. Using Dirac-trace algebra the result can be cast into the form

$$\mathcal{N}_{hdb}^{(3)} = \frac{1}{8}\left\{\mathrm{tr}\left[(\not{\ell}_2 - \not{p}_2)\not{p}_3\not{p}_1\not{p}_5\right] + \mathrm{tr}\left[(\not{\ell}_2 + \not{p}_1 + \not{p}_4)\not{p}_3\not{p}_1\not{p}_5\right] + 8\left[(\ell_2 + p_1)^2 - \ell_2^2\right](s_{12} - s_{34} - s_{45})\right\}. \tag{3.94}$$

The third integrand is constructed using μ-insertions and doubled propagators. Doubling the central rung propagators creates an artificial pentagon-like structure. Applying the symmetries of the diagram we obtain the following pure candidate

$$\mathcal{N}_{hdb}^{(3)} = \frac{1}{\epsilon}\mathrm{tr}_5\mu_{12}\left(\frac{1}{\rho_7} + \frac{1}{\rho_8}\right). \tag{3.95}$$

The last pure candidate comes from a loop-by-loop argument. We cancel the leading singularity of the outer box and then double one of the two central rung propagators to make the remaining bubble sub-integral pure. However, this only gives an integral which is pure on-shell. The full insertion requires an off-shell completion which can be constructed by using the approach of section 3.3.5. The result reads

$$\mathcal{N}_{hdb}^{(4)} = \frac{1}{\epsilon}\frac{q^2}{\rho_7}\left[(\ell_2 - p_2 - p_3)^2(\ell_2 + p_1 + p_3 + p_4)^2 - (\ell_2 - p_2)^2(\ell_2 + p_1 + p_4)^2\right] + R_{\mathrm{hdb}}^{(4)}. \tag{3.96}$$

The explicit form of the off-shell part $R_{\mathrm{hdb}}^{(4)}$ can be found in eq. (4.62).

3.4 Numerical differential equations

In this section, we describe the numerical approach to constructing the analytic form of canonical differential equations based on [48]. In the following, we will assume that we already have a pure integral basis

$$\mathrm{d}\mathbf{G} = \epsilon\, \mathrm{d}\mathbf{M}\mathbf{G}, \tag{3.97}$$

with

$$\mathrm{d}\mathbf{M} = \sum_{a=1}^{N} M_a \mathrm{d}\log(W_a), \tag{3.98}$$

where $\mathbb{A} = \{W_1, \cdots, W_N\}$ is the alphabet of the integral topology and $\{M_1, \cdots, M_N\}$ is a collection of constant matrices with rational entries.
Let us now assume that we not only have the pure basis $\mathbf{G}$ but also know the alphabet $\mathbb{A}$ in advance. In this case, the only unknown quantities in eq. (3.97) are the constant matrices M_a which can be determined by comparing the functional form of eq. (3.98) to a sufficiently large number of numerical samples for the connection $\mathrm{d}M$. Since we can not deal with a numerical differential form we instead work with derivatives taken along a random direction in the kinematic space. Let $\vec{c}$ be a randomly chosen vector in the kinematic space (or more precisely, in its dual space). We define the *directional derivative operator* by $\vec{c}\cdot\nabla_{\vec{s}}\mathbf{G}$. With this definition the canonical differential equation takes the form

$$\vec{c}\cdot\nabla_{\vec{s}}\mathbf{G} = \epsilon \sum_a M_a \vec{c}\cdot\nabla_{\vec{s}}\log(W_a)\mathbf{G} \equiv \mathbf{C}\mathbf{G}, \tag{3.99}$$

where $\mathbf{C}$ is the matrix-valued *directional connection*. Now, the DE is expressed in terms of ordinary matrices instead of differential forms. We use `FIRE6` [154] to compute the connection $\mathbf{C}$ on a set of rational points $\{\vec{s}_1, \cdots, \vec{s}_N\}$ for a rational value of the dimensional regulator $\epsilon = \epsilon_0$. Note that we can easily obtain any partial derivative back from the connection by simply setting $\vec{c} = \vec{e}_i$, with $\vec{e}_i$ being the i-th unit vector. We flatten the connections $\mathbf{C}(\vec{s}_i)$ into a $n^2 \times N$ matrix

$$\tilde{\mathbf{C}} = \begin{pmatrix} \mathbf{C_{11}}(\vec{s}_1) & \mathbf{C_{11}}(\vec{s}_2) & \cdots & \mathbf{C_{11}}(\vec{s}_N) \\ \mathbf{C_{12}}(\vec{s}_1) & \mathbf{C_{12}}(\vec{s}_2) & \cdots & \mathbf{C_{12}}(\vec{s}_N) \\ \cdots & \cdots & \cdots & \cdots \\ \mathbf{C_{nn}}(\vec{s}_1) & \mathbf{C_{nn}}(\vec{s}_2) & \cdots & \mathbf{C_{nn}}(\vec{s}_N) \end{pmatrix}, \tag{3.100}$$

where n is the dimension of $\mathbf{G}$. Next, we write the left-hand-side of eq. (3.99) in a similar manner. We define the matrix $\mathbf{L}$ by

$$L_{ij} \equiv \vec{c}\cdot\frac{1}{W_j}\frac{\partial W_j}{\partial \vec{s}}\bigg|_{\vec{s}=\vec{s}_i}, \quad i,j = 1,\cdots,N. \tag{3.101}$$

Using these definitions, we get

$$\tilde{\mathbf{C}} = \epsilon_0 \begin{pmatrix} \sum_{j=1}^N L_{1j}M_{11,j} & \sum_{j=1}^N L_{2j}M_{11,j} & \cdots & \sum_{j=1}^N L_{Nj}M_{11,j} \\ \sum_{j=1}^N L_{1j}M_{12,j} & \sum_{j=1}^N L_{2j}M_{12,j} & \cdots & \sum_{j=1}^N L_{Nj}M_{12,j} \\ \cdots & \cdots & \cdots & \cdots \\ \sum_{j=1}^N L_{1j}M_{nn,j} & \sum_{j=1}^N L_{2j}M_{nn,j} & \cdots & \sum_{j=1}^N L_{Nj}M_{nn,j} \end{pmatrix} \tag{3.102}$$

By comparing eq. (3.100) with (3.102), we obtain

$$\vec{M}_{ij} = \frac{1}{\epsilon_0} L^{-1}\tilde{\mathbf{C}}_{ij}, \tag{3.103}$$

where $\tilde{\mathbf{C}}_{ij}$ is the (i,j)-th row vector of $\tilde{\mathbf{C}}$ and $\vec{M}_{ij}$ contains the (i,j)-th entries of the connection matrices M_a. We implemented the described procedure in a `Mathematica` program and tested it for several known integral topologies including the massless five-point penta-box topology and the one-loop pentagon integral with one off-shell leg. In case of purely rational differential equations, all computations could be performed using exact arithmetics. The presence of non-rationalized square-roots, in the case of five-point integrals with an off-shell leg, requires a different approach due to high complexity of the involved algebraic expressions. We used high-precision ($150 - 200$ digits) floating point numbers in all intermediate steps and reconstructed the *manifestly rational* entries of M_a afterwards using the built-in `Mathematica` routine `Rationalize[]`. Crucial steps here are computing determinants and matrix inversions. Since the result has to be rational the success of this procedure provides a non-trivial check on the result. An alternative idea is to work in a *finite field* to parametrize the phase-space kinematics. Here, all finite field values have to be chosen in such a way that all relevant Gram determinants are perfect squares in the particular finite field. Since approximately half of all numbers in a given finite field are perfect squares this is a requirement that can be satisfied easily. A detailed discussion of this approach can be found in [55].
In the following, we want to discuss one further application of the numerical connection $\tilde{\mathbf{C}}$. As stated above, the task of reconstructing the analytic differential equation requires knowledge of both the pure basis and the symbol alphabet. However, for the computation of $\tilde{\mathbf{C}}$ the alphabet is not needed. Moreover, the connection itself can be used to extract some important information about the alphabet. First of all, the size N of the alphabet can be determined in this way. For that purpose, we compute $\tilde{\mathbf{C}}_{\mathbf{m}}$ for a fixed but arbitrary number of points $m < n^2$. Let us consider the rank of this matrix which is given by the number of independent columns. Since the entries of the matrix are linear combinations of the alphabet letters it is clear that the rank can be maximally as high as the size of the alphabet. In practice, we increase m up to some number m_{max} such that the rank of $\tilde{\mathbf{C}}_{\mathbf{m}}$ stabilizes. Also, here, the rank calculation is performed over high-precision floating point numbers with several choices of the direction vector $\vec{c}$.
The reconstruction procedure can be applied to the complete integral basis as well as to arbitrary parts of it separately. This allows to start at lower sectors of the basis where the alphabet is already known and add higher sectors until the reconstruction fails at some point. In this way, we can identify exactly at which places in the differential equation new alphabet letters appear. Concretely, we can extract the index pair (i,j) such that the unknown letter has to appear in the j-th coefficient of the i-th master integral. This information simplifies the search for new letters significantly.

3.5 Numerical integration of pure DE

3.5.1 Generalized power-series approach

After the differential equation is brought into the canonical form

$$\mathrm{d}\mathbf{G} = \epsilon\, \mathrm{d}M\mathbf{G}, \tag{3.104}$$

it can be, at least in principle, integrated order-by-order in ϵ in terms of Chen's iterated integrals (see section 2.4.1). However, it was discussed in section 2.4.3 that an explicit representation of iterated integrals in terms of well-known functions like harmonic or Goncharov polylogarithms can in general not always be achieved. We need to bring the differential equation to the Fuchsian form (2.86) such that it has only linear singularities. This requires i.a. a simultaneous rationalization

of all square-roots appearing in the symbol alphabet which is not possible in general. Even if one manages to remove this obstacle the number of special functions in the final result may grow very fast which could make the numerical evaluation slow. So, e.g. for the five-point massless integrals, some of the pentagon functions are represented by cleverly chosen one-fold integrals which can be evaluated via efficient numerical algorithms [51,52]. A further difficulty with analytic expressions for multi-loop multi-scale integrals is that the general problem of *analytic continuation* to an arbitrary region of the phase space still remains a very challenging task. Introducing new and often complicated variables which are needed for rationalizing the alphabet may cause an even more complicated behaviour of the analytic solution near both physical and spurious singularities. For these reasons, we decided to follow a fully numerical approach outlined in references [71, 72] in this work. The idea of this approach is to pull back the connection down on a univariate path through the phase space and then to expand this univariate connection in a series around some set of points along the path. The different expansions will then be connected to each other by continuity conditions on the boundaries of the expansion segments. The following presentation of this approach closely follows section 6 of ref. [55].
We consider a straight line

$$\vec{s}(t) = \vec{s}_b + (\vec{s}_e - \vec{s}_b)t, \quad t \in [0,1]\,, \tag{3.105}$$

where $\vec{s}_b$ and $\vec{s}_e$ are arbitrary beginning and end points. In the following, we will assume that $\mathbf{G}(\vec{s}_b)$ is known from the boundary conditions. The goal is now to compute $\mathbf{G}(\vec{s}_e)$. Combining the univariate differential equation

$$\begin{aligned} \frac{\mathrm{d}}{\mathrm{d}t}\mathbf{G} &= \epsilon \mathbf{A}(t)\mathbf{G}(t), \\ \mathbf{A} &= \frac{\mathrm{d}M(\vec{s}(t))}{\mathrm{d}t} \end{aligned} \tag{3.106}$$

and the Laurent expansion of $\mathbf{G}$

$$\mathbf{G} = \sum_{j=0}^{\infty} \epsilon^j \mathbf{G}^{(j)}, \tag{3.107}$$

we obtain a recursive relation for the integrals $\mathbf{G}^{(i)}$

$$\mathbf{G}^{(i)} = \int \mathbf{A}(t)\mathbf{G}^{(i-1)}(t)\mathrm{d}t + \mathbf{c}^{(i)}, \tag{3.108}$$

with $\mathbf{c}^{(i)}$ being the i-th order integration constants. In this discussion, we assume that the integral basis $\mathbf{G}$ is normalized in such a way that the expansion starts at weight 0 and, consequently, the $\mathbf{G}^{(i)}$ have weight i. The lowest-weight solution $\mathbf{G}^{(0)} = \mathbf{c}^{(0)}$ is constant and fully determined by the boundary condition of the differential equation.
Since we are going to solve eq. (3.108) by expanding the connection $\mathbf{A}(t)$ into a power-series we have to define a segmentation of the path (3.105) first because a series around a given point has in general a finite radius of convergence. We have to make sure that we use a series expansion only inside its range of convergence. A *segmentation* $S = \{S_k = [t_k - r_k, t_k + r_k) | k = 0, \cdots, N_e - 1\}$ of a path is a set of intervalls with empty intersection covering the $[0,1]$ intervall

$$[0,1] \subset \bigcup_{k=0}^{N_e-1} S_k, \tag{3.109}$$

where N_e is the number of segments. Here $t_k \in \mathbb{R}$ are the expansion points and $r_k \in (0, R_k)$ are the segments' radii which are bounded by the convergence radii R_k of the expansion around t_k.

Let us for now assume that the set of pairs $\{(t_k, r_k)\}$ is fixed and discuss the construction of local solutions $\mathbf{G}_k^{(i)}(t)$ which are valid on a single S_k. The local solution is defined in the following way

$$\mathbf{G}^{(i)}(t) = \sum_{k=0}^{N_e-1} \chi_k(t)\, \mathbf{G}_k^{(i)}(t)\,, \quad t \in [0,1]\,, \tag{3.110}$$

with

$$\chi_k(t) = \begin{cases} 1, & t \in [t_k - r_k, t_k + r_k) \\ 0, & \text{otherwise} \end{cases} . \tag{3.111}$$

Consider now the expansion of the univariate connection around a fixed t_k

$$\mathbf{A}(t) = \sum_{i=-2}^{\infty} \mathbf{A}_{i,k} (t - t_k)^{\frac{i}{2}}, \tag{3.112}$$

where the $\mathbf{A}_{i,k}$ are constant matrices. Since $\mathbf{G}$ is pure the connection can, at most, have logarithmic singularities such that the sum (3.112) starts at -2 and we have to account for half-integer powers because the connection can, in general, have square-root terms. Series of that form are called *generalized power-series*. Recursively inserting the series expansion into the relation (3.108) and performing the integration, gives

$$\begin{aligned} \mathbf{G}_k^{(i)}(t) &= \mathbf{c}_k^{(i)} + \sum_{j=-2}^{\infty} \mathbf{A}_{j,k} \int (t - t_k)^{\frac{j}{2}} \mathbf{G}_k^{(i-1)}(t) dt \\ &= \sum_{j_1=0}^{\infty} \sum_{j_2=0}^{N_{i,k}} \mathbf{c}_k^{(i,j_1,j_2)} (t - t_k)^{\frac{j_1}{2}} \log(t - t_k)^{j_2}, \end{aligned} \tag{3.113}$$

where the integration has been carried out fully algorithmic in terms of standard functions $(t-t_k)^{\frac{j_1}{2}}$ and $\log(t-t_k)^{j_2}$. We make use of following notation: $\mathbf{c}_k^{(i)} = \mathbf{c}_k^{(i,0,0)}$ are the integration constants and $\mathbf{c}_k^{(i,j_1,j_2)}$ are constant vectors determined iteratively from the matrices $\mathbf{A}_{j,k}$. $N_{i,k}$ is the maximal power of the logarithm in the local solution at weight i. The series solution (3.113) contains full information about the branch cut structure of $\mathbf{G}$ encoded in logarithmic and half-integer contributions. For a regular t_k we have $N_{i,k} = 0$ and $\mathbf{c}_k^{(i,j_1,0)} = 0$ for odd j_1. We will discuss our treatment of branch cuts in eq. (3.113) more closely in section 3.5.2. The boundary conditions $\mathbf{c}_k^{(i,0,0)}$ can be related to the known initial boundary conditions $\mathbf{G}^{(i)}(0)$ by the continuity of the full solution at the boundaries of each two neighbouring segments. We require

$$\mathbf{G}_0^{(i)}(0) = \mathbf{G}^{(i)}(0) \tag{3.114}$$

and

$$\mathbf{G}_k^{(i)}(t_k - r_k) = \mathbf{G}_{k-1}^{(i)}(t_{k-1} + r_{k-1})\,, \quad k = 1, \ldots, N_e - 1\,, \tag{3.115}$$

where the right-hand-side of eq. (3.115) is understood to be the left-sided limit of the $(k-1)$-th segment solution which exists by construction. The outlined procedure allows to compute our target values $\mathbf{G}^{(i)}(\vec{s}_e) = \mathbf{G}_{N_e-1}^{(i)}(1)$ if the integral values at the starting point $\mathbf{G}^{(i)}(\vec{s}_b) = \mathbf{G}_0^{(i)}(0)$ are known. The computation of the starting point $\mathbf{G}^{(i)}(0)$ will be discussed in section 3.5.3.
Let us now discuss the strategy of choosing the pairs $\{(t_k, r_k)\}$. It is a well-known fact that the convergence of a series on the complex plane is mainly governed by the singularities of the

expanded function. So, the singularities will clearly affect our choice of $\{(t_k, r_k)\}$. The convergence radius of a series around an arbitrary point is always given by the distance to the nearest singularity. However, one would in general not want to go too close to the radius of convergence since the rate of convergence would likely become worser near to the boundary. In practice, we decided to set $r_k = \frac{R_k}{2}$. Note that a singularity can still affect the expansion inside the unit intervall even if it is itself placed outside the unit intervall but, in some sense, *close enough* to it. In particular, we also have to take care of complex singularities even though all our expansion points are real. Since the connection is an at most algebraic function of the kinematic invariants it can have only a finite number of singularities which we split here in a real $R = \{\sigma_k\}_{k=1,\cdots,N_s}$ and a complex $C = \{\lambda_k\}_{k=1,\cdots,N_c}$ set. In order to avoid complex arithmetic, we can use the following set of real regular points $C_r = \{\text{Re}(\lambda_k) - \text{Im}(\lambda_k), \text{Re}(\lambda_k), \text{Re}(\lambda_k) + \text{Im}(\lambda_k)\}_{k=1,\cdots,N_c}$ instead of C. Given our constraint of using half of the radius of convergence, we need to use all $t_k \in R \cup C_r$ with $t_k \in (-2, 3)$ as expansion points since a singularity has to be placed maximally twice as far as the intervall length from the intervall boundaries in order to affect the expansion, and we set the corresponding r_k to be half the distance to the nearest point in $R \cup C_r \cup \{-2, 3\}$. In general, the singular points alone might not be enough to cover the complete unit intervall. In this case, we add regular points t_k placed in the middle of uncovered regions of $(-2, 3)$ with a non-empty overlap with $[0, 1]$ and set r_k to be the minimum of the following two quantities,

- half of the distance to the nearest element of $R \cup C_r \cup \{-2, 3\}$,
- the distance to the closest already determined segment.

3.5.2 Analytic continuation

The master equation eq. (3.113) contains logarithmic and square-root branch cuts associated to singularities and square-root branch points of $\mathbf{A}(t)$ which arise from either zeros or poles of some alphabet letters. In this section, we discuss how to analyticly continue eq. (3.113) across these branch cuts. First of all, we need to classify different types of singularities. On the one hand we have *physical* singularities corresponding to vanishing first-entry letters. In the planar case, these are exactly the cyclic Mandelstams and the external masses and, in the non-planar case, also non-cyclic kinematic invariants can appear. Values of t_k at which only non-first-entry letters have thresholds are referred to as *non-physical* singularities. However, it might happen that for some point t_k a first-entry and a non-first-entry letter vanish together. This is for example the case for $W_1 = q^2$ and $W_{33} = \frac{q^2+s_{45}-s_{23}+\sqrt{\Delta_3^{(1)}}}{q^2+s_{45}-s_{23}-\sqrt{\Delta_3^{(1)}}}$ since

$$W_{33} = \frac{q^2 + s_{45} - s_{23} + \sqrt{\Delta_3^{(1)}}}{q^2 + s_{45} - s_{23} - \sqrt{\Delta_3^{(1)}}} = q^2\, \widehat{W}_{33}\,, \quad \text{with} \quad \widehat{W}_{33} = \frac{4 s_{45}}{\left(q^2 + s_{45} - s_{23} - \sqrt{\Delta_3^{(1)}}\right)^2}\,, \tag{3.116}$$

and so, we have $W_{33} \to 0$ for $q^2 \to 0$ and $s_{45} < s_{23}$. The important observation here is that $\widehat{W}_{33}$ does not go to 0 in the limit $q^2 \to 0$ and so, the simultaneous vanishing of the two letters is just an artifact of having a factorizable letter. Geometrically that means that we have only one irreducible vanishing surface, namely that of $q^2 = 0$, although two different letters vanish. The situation would be different if also $\widehat{W}_{33}$ would vanish for $q^2 \to 0$. In this case, we would indeed find a so-called *overlapping singularity* where two independent irreducible vanishing surfaces intersect. A

practical way of checking which irreducible surfaces are attached to a given letter, is to investigate the poles of the letter's dlog form. E.g.

$$d\log(W_{33}) = \left[\frac{\sqrt{\Delta_3^{(1)}}\left(s_{13}+s_{12}+\sqrt{\Delta_3^{(1)}}\right)^2}{2s_{45}\,\Delta_3^{(1)}\,q^2}\right]\left[\frac{s_{13}+s_{12}}{2}\left(\frac{dq^2}{q^2}-\frac{ds_{45}}{s_{45}}\right)-ds_{23}\right]. \tag{3.117}$$

The independent vanishing surfaces are $q^2=0$, $s_{45}=0$ and $\Delta_3^{(1)}=0$. Let us now sharpen our classification of singularities. Given a singular point t_k we can first check whether one of the first-entries vanishes there. If so, we should check whether any other letter vanishes or diverges at t_k. If this either does not happen at all or only because of vanishing of the first-entry letter, like in the example of W_{33}, then t_k is a physical threshhold. If any non-first-entry letter vanishes independently we have found an overlapping singularity. If t_k finally does not belong to a first-entry letter, then it is a non-physical threshhold.
Let us now state how to analyticly continue through each of the singularity types and the square-root branch points:

Physical thresholds: Here we use the $i\varepsilon$ prescription inherited from the Feynman rules

$$s_i(t) \to s_i(t) + i\varepsilon = s_{b,i} + (s_{e,i}-s_{b,i})t + i\varepsilon, \quad \varepsilon > 0\,. \tag{3.118}$$

We mimic this behaviour by shifting t

$$t \to t + i\,\mathrm{sign}(s_{e,i}-s_{b,i})\,\varepsilon, \quad \varepsilon > 0. \tag{3.119}$$

Using this prescription, we can define the analytic continuation of the logarithm to be

$$\log(t-t_k) = \begin{cases} \log(t-t_k) & \text{for } t > t_k\,, \\ \log(t_k-t) + i\,\mathrm{sign}(s_{e,i}-s_{b,i})\pi & \text{for } t < t_k\,. \end{cases} \tag{3.120}$$

Non-physical thresholds: It is a well-known fact that non-physical thresholds cannot appear inside the Euclidean region. We only need to take care of them outside the Euclidean region. Since there is no established way to analyticly continue through a non-physical singularity we simply choose another starting point in order to avoid the singularity in case the path crosses such a point.

Square-root branch points: Square-root branch points are inherited from pure normalisations of some integrals. Therefore, we can choose an arbitrary prescription which will not affect the original Feynman integral. We define

$$(t-t_k)^{\frac{j_1}{2}} = \begin{cases} (t-t_k)^{\frac{j_1}{2}} & \text{for} \quad t > t_k\,, \\ i(t_k-t)^{\frac{j_1}{2}} & \text{for} \quad t < t_k\,. \end{cases} \tag{3.121}$$

Overlapping singularities: The last type of singularities we have to discuss are the overlapping singularities. Our procedure here is just the same as in the case of the non-physical thresholds: We choose another path and avoid such a singularity. It should be mentioned that we were never faced an overlapping singularity both for planar and hexa-box topologies.

3.5.3 Boundary conditions

After we discussed how to obtain numerical values for the integrals at any target point both in the Euclidean and physical regions starting at the known boundary conditions the only missing ingredient are the boundary conditions themselves. Their computation will be the topic of this section. As in section 3.5.1, we proceed order-by-order in ϵ. For a fixed i we assume that $\mathbf{G}^{(i-1)}(0)$ is already known. Let us first establish the general idea. Boundary conditions for a differential equation are a piece of external information about the master integrals which fixes the linear space of solutions to a single vector. The classical way of thinking about boundary conditions is as a known value of the solution at a single point or in a single limit. However, both computing such a limit and also a correct matching of the general solution to a particular limit might be highly non-trivial tasks. On the other hand we can use the known analyticity conditions on the Feynman integrals as a source for boundary values. A simple example of this approach was discussed in section 2.4.4 where we used that planar integrals can not have singularities on $u = 0$. Here we have a more general type of such constraints. As already mentioned in the previous section, Feynman integrals do not have non-physical singularities in the Euclidean region. This translates into a set of constraints that the right-hand-side of eq. (3.106) has to have vanishing residues at all spurious singularities. *Spurious* means here simply that none of the first-entry letters vanish at this point. To make this condition manifest we expand the univariate connection $\mathbf{A}(t)$ around a spurious singularity t_k up to the leading order

$$\mathbf{A}(t) = \frac{1}{t - t_k}\mathbf{A}_{-2,k} + \mathcal{O}[(t - t_k)^0] \tag{3.122}$$

and require

$$\mathbf{A}_{-2,k}\left[\mathbf{G}_k^{(i)}(t_k)\right] = 0\,, \quad \forall i, \tag{3.123}$$

to prevent the order $(i + 1)$ solution from having a spurious logarithmic singularity. By the continuity of the solution eq. (3.115) and the regularity of eq. (3.113) at t_k, we can relate $\mathbf{G}^{(i)}(t_k)$ to the starting point $\mathbf{G}^{(i)}(0)$ by a known *shift vector* $\mathbf{v}_k^{(i)}$

$$\mathbf{G}_k^{(i)}(t_k) = \mathbf{G}^{(i)}(0) + \mathbf{v}_k^{(i)}. \tag{3.124}$$

The shift vectors can be computed as differences of two segment solutions

$$\mathbf{v}_k^{(i)} = \mathbf{G}_k^{(i)}(t_k) - \mathbf{G}_0^{(i)}(0), \tag{3.125}$$

since the differences do not depend on the boundary constants.
Applying $\mathbf{A}_{-2,k}$ to both sides of eq. (3.124) gives an explicit constraint for $\mathbf{G}^{(i)}(0)$

$$\mathbf{A}_{-2,k}\left[\mathbf{G}^{(i)}(0)\right] = -\mathbf{A}_{-2,k}\left[\mathbf{v}_k^{(i)}\right]. \tag{3.126}$$

For $i = 0$ we have $\mathbf{v}_k^{(0)} = 0$ since the weight 0 integral solution is constant and eq. (3.126) simplifies to

$$\mathbf{A}_{-2,k}\left[\mathbf{G}^{(0)}(0)\right] = 0. \tag{3.127}$$

This result was already obtained in 2.4.3 (see eq.(2.100)) where we discussed the symbol-level solution of the differential equation. There is, however, a subtle difference between the two statements: The argument of 2.4.3 was developed at the level of the full DE while here we work with a univariate slice which is, in general, blind to some of the non-physical singularities. Despite

that for all topologies we computed in this thesis the common kernel $\mathcal{K} := \bigcap_k \ker(A_{-2,k})$ of all $\mathbf{A}_{-2,k}$, with t_k being a non-physical singularity, is indeed one-dimensional which we will prove in 4.1.4 and 4.2.4 this might be in general not true for the univariate-slice version of the DE. Let us for now assume that we can collect enough singular points such that $\mathbf{G}^{(0)}(0)$ can be determined from eq. (3.127) up to an overall constant which can easily be fixed from the weight 0 part of a simple single-scaled integral. Since we assumed that $\dim\mathcal{K} = 1$ any element of $\mathcal{K}$ has to be proportional to the weight 0 solution. So, then the weight i constraint eq. (3.126) leads to

$$\mathbf{G}^{(i)}(0) = f^{(i)}\mathbf{G}^{(0)}(0) + \mathbf{G}_p^{(i)}(0), \tag{3.128}$$

where $\mathbf{G}_p^{(i)}(0)$ is a *particular solution* of eq. (3.126) and the weight i constant $f^{(i)}$ can again be fixed from a single-scale integral. $\mathbf{G}_p^{(i)}(0)$ can be obtained by numerical solving eq. (3.126).
Let us briefly discuss the practical implementation of this strategy both for planar and hexa-box integrals. We start with a point $\vec{s}_0$ in the Euclidean region and follow an arbitrary chosen sequence of straight paths until we have crossed enough singular points to constrain $\mathbf{G}^{(i)}(\vec{s}_0)$ up to an overall constant. Once we have the boundary conditions at one point, we can transport the solution to any kinematic region by the analytic continuation procedure from 3.5.2 and compute new boundary points in each region. Let us make clear that we do not always need to go the complete path from our starting point $\vec{s}_0$ for which the boundary conditions are known to the point $\vec{s}$ at which we want to compute $\mathbf{G}^{(i)}(\vec{s})$. We can take any point $\vec{s}_1$ at which the solution $\mathbf{G}(\vec{s}_1)$ is already known and use it as the new starting point. Once the number of points at which the integrals are already known becomes big enough, we can always expect to have a known value at a point in the neighborhood of the point where we need to compute the integrals. In section 4.1.5 we study this behaviour for the planar topologies.
Finally, it should be mentioned that for some of the hexa-box topologies we used additional information besides the first-entry condition, like explicit results for multiple single-scale integrals and symmetries which connect integrals from different topologies, to obtain some of the boundary conditions. We explain this in more detail in 4.2.5.

3.5.4 Numerical precision

After we explained our approach of numerical integration of the canonical DE, let us discuss how to control the numerical precision of this calculation which we quantify as the number p of valid digits after the decimal point. The reason for a finite numerical precision is, in the first place, that our algorithm is only applicable if we truncate the series expansion (3.113) at some finite order n_k. Let us emphasize that we assume all calculational operations to be done with a much higher precision than p so that we can ignore the purely calculational effects and concentrate on the precision of the series truncation. In general, both the integration procedure and also the boundary conditions are affected by truncation errors. Let us for now assume that the latter are known with a much higher precision than p and discuss the transporting precision first. In the first step, we fix the truncation order n_k for the expansion around t_k by comparing the truncated expansion of the connection $\mathbf{A}_{[k]}(t)$ defined via

$$\mathbf{A}_{[k]}(t) = \sum_{i=-2}^{n_k} \mathbf{A}_{i,k}(t-t_k)^{\frac{i}{2}} \tag{3.129}$$

with the full connection $\mathbf{A}(t)$. We require n_k to be high enough to ensure

$$\max_{i,j} \left|A_{[k],ij}(t) - A_{ij}(t)\right| < 10^{-(p+\delta)}, \quad t \in [t_k - r_k, t_k + r_k)\,, \tag{3.130}$$

where δ is a positive integer chosen such that the final precision of the integrals is still bigger than p. So, loosely speaking, δ is a security offset which compensates possible loosing of precision during the calculation. We decided to choose δ to be

$$\delta = \lceil \log_{10}(n_s) \rceil + 1, \tag{3.131}$$

where n_s is the number of segments if we start at the initial point $\vec{s}_0$ and

$$\delta = \lceil \log_{10}(\bar{n}_s n_{ps}) \rceil + 1, \tag{3.132}$$

where $\bar{n}_s$ is the average number of segments per point and n_{ps} is the number of points in the considered chain if we use a previously computed point $\vec{s}_1$ as boundary conditions instead of $\vec{s}_0$. To motivate this particular choice of δ we use the Cauchy convergence criterion to estimate the real upper bound on the truncation error and computed

$$\Delta_k = \max_{i,a} \left| \sum_{j_1=n_k-m}^{n_k} \sum_{j_2=0}^{N_{i,k}} c_{k,a}^{(i,j_1,j_2)} (r_k)^{\frac{j_1}{2}} (\log r_k)^{j_2} \right| , \tag{3.133}$$

where a labels the master integrals and $m \ll n_k$ is some integer value (in practice, we use $m = \lceil \frac{n_k}{50} \rceil$). We can numerically verify that the theoretical expectation $\Delta_k \sim 10^{-(p+\delta)}$ is indeed fulfilled for all k and so the full error along the path can be approximately estimated with $n_s 10^{-(p+\delta)}$.
We finish this section with an estimation of the precision of the boundary conditions $\mathbf{G}^{(i)}(\vec{s}_0)$. On the one hand we have here the same truncation error coming from transporting the solution along the chosen set of paths, as described in 3.5.3. This error can be estimated in the same way as explained before for the integration step. On the other hand we might have a significant error from numerical solving eq. (3.126). To have a qualitative estimation for this kind of error we use the fact that Feynman integrals in the Euclidean region are either purely real or purely imaginary functions depending on their prefactors in the canonical basis. However, this condition is broken by the finite precision of eq. (3.126). We decided to use the magnitudes of the spurious real or imaginary parts as an estimation for the numerical error of the boundary conditions.

Chapter 4

Discussion of results

In this chapter we present the main results of the thesis: section 4.1 discusses the planar integral topologies, the hexa-box topologies are presented in 4.2 while the last section 4.3 contains first results on double-pentagon topologies.

4.1 Planar topologies

4.1.1 Definition of planar topologies

In this section we define the planar five-point integrals with one off-shell leg. There are four independent integral families which we denote with $I^{[f]}$ with $f \in \{\text{mzz}, \text{zmz}, \text{zzz}, \text{one-loop}^2\}$ where the first three correspond to genuine two-loop integrals of penta-box type and the last one is the product of a one-loop pentagon integral with a one-loop bubble integral. The letters m and z indicate, respectively, massive and massless legs on the pentagon side of the penta-box topologies. The topologies are depicted in fig. 4.13. Note that all external momenta are incoming. Let us define the propagator structure associated to the four topologies. For the genuine two-loop integrals we have

$$I^{[f]}[\vec{\nu}] = e^{2\epsilon\gamma_E} \int \frac{d^D\ell_1}{i\pi^{D/2}} \frac{d^D\ell_2}{i\pi^{D/2}} \frac{\rho_{9,f}^{-\nu_9}\ \rho_{10,f}^{-\nu_{10}}\ \rho_{11,f}^{-\nu_{11}}}{\rho_{1,f}^{\nu_1}\ \rho_{2,f}^{\nu_2}\ \rho_{3,f}^{\nu_3}\ \rho_{4,f}^{\nu_4}\ \rho_{5,f}^{\nu_5}\ \rho_{6,f}^{\nu_6}\ \rho_{7,f}^{\nu_7}\ \rho_{8,f}^{\nu_8}}\,, \tag{4.1}$$

where $D = 4 - 2\epsilon$ and $\vec{\nu} \in \mathbb{Z}^{11}$ denotes the list of indices. We have $\nu_i \leq 0$ for $i = 9, 10, 11$. The inverse propagators and ISP's are given explicitly by

$$\begin{aligned}
\vec{\rho}_{\text{mzz}} &= \big\{\ell_1^2, (\ell_1+p_1)^2, (\ell_1+p_1+p_2)^2, (\ell_1+p_1+p_2+p_3)^2, (\ell_2-p_4-p_5)^2, \ell_2^2, (\ell_2-p_5)^2,\\
&\quad (\ell_1-\ell_2)^2, (\ell_1-p_5)^2, (\ell_2+p_1)^2, (\ell_2+p_1+p_2)^2\big\}\,,\\
\vec{\rho}_{\text{zmz}} &= \big\{\ell_1^2, (\ell_1+p_5)^2, (\ell_1+p_5+p_1)^2, (\ell_1+p_5+p_1+p_2)^2, (\ell_2-p_3-p_4)^2, \ell_2^2, (\ell_2-p_4)^2,\\
&\quad (\ell_1-\ell_2)^2, (\ell_2+p_5)^2, (\ell_2+p_1+p_5)^2, (\ell_1-p_4)^2\big\}\,,\\
\vec{\rho}_{\text{zzz}} &= \big\{\ell_1^2, (\ell_1+p_2)^2, (\ell_1+p_2+p_3)^2, (\ell_1+p_2+p_3+p_4)^2, (\ell_2-p_1-p_5)^2, \ell_2^2, (\ell_2-p_1)^2,\\
&\quad (\ell_1-\ell_2)^2, (\ell_1-p_1)^2, (\ell_2+p_2)^2, (\ell_2+p_2+p_3)^2\big\}\,.
\end{aligned} \tag{4.2}$$

The last three entries of each list are ISP's which we choose in such a way that the propagator set becomes maximally symmetric under the exchange of ℓ_1 and ℓ_2.
Since all integrals in $I^{[\text{one-loop}^2]}$ are products of two one-loop integrals it is sufficient to consider the one-loop pentagon topology $I^{[\text{one-loop}]}$ with one off-shell leg. In following, we will restrict ourselves

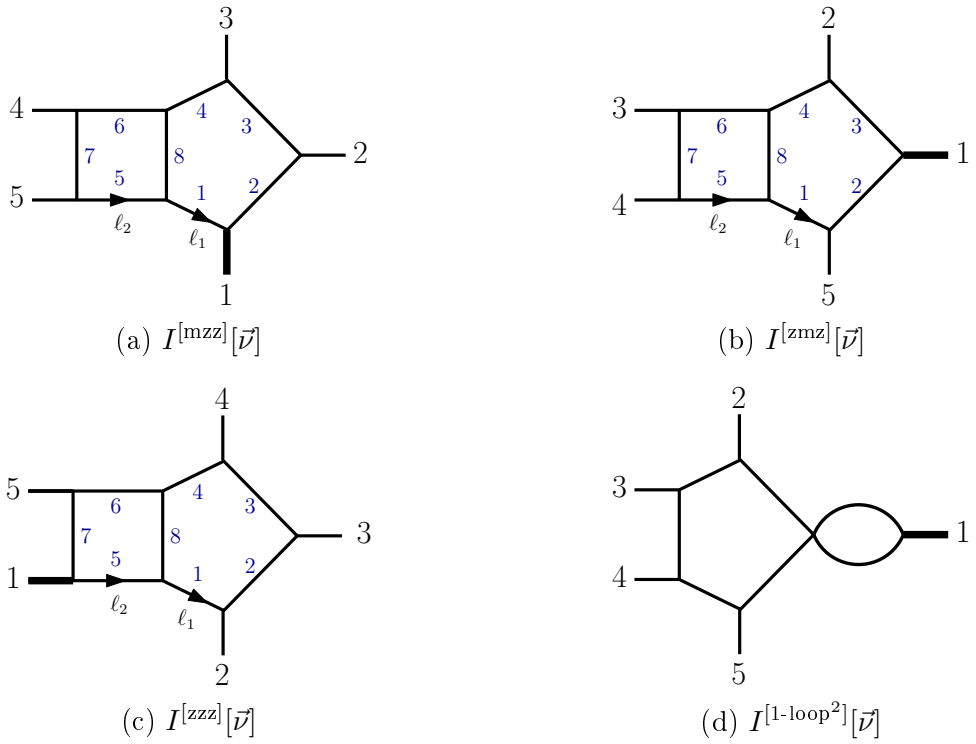

(a) $I^{[\text{mzz}]}[\vec{\nu}]$ (b) $I^{[\text{zmz}]}[\vec{\nu}]$

(c) $I^{[\text{zzz}]}[\vec{\nu}]$ (d) $I^{[\text{1-loop}^2]}[\vec{\nu}]$

Figure 4.1: Two-loop five-point one-mass topologies. The thick external line with label 1 denotes the massive external leg.

to non-factorizable two-loop topologies and the one-loop pentagon topology.
The latter is defined via

$$I^{[\text{one-loop}]}[\vec{\nu}] = e^{\epsilon\gamma_E} \int \frac{d^D\ell}{i\pi^{D/2}} \frac{1}{\rho_1^{\nu_1}\ \rho_2^{\nu_2}\ \rho_3^{\nu_3}\ \rho_4^{\nu_4}\ \rho_5^{\nu_5}}. \tag{4.3}$$

The inverse propagators are given explicitly by

$$\begin{aligned}\vec{\rho}_{\text{one-loop}} = \big\{&\ell^2, (\ell+p_1)^2, (\ell+p_1+p_2)^2, (\ell+p_1+p_2+p_3)^2, \\ &(\ell+p_1+p_2+p_3+p_4)^2\big\}.\end{aligned} \tag{4.4}$$

As mentioned in 2.3.3, all Feynman integrals corresponding to a specific topology span a linear space. Let us denote these spaces by $V^{[f]}$. The dimension of $V^{[f]}$ is given by the number of master integrals which can be, for example, determined by a numerical reduction of the integral space using one of the standard IBP reduction tools (e. g. `FIRE` [154] or `KIRA` [156]. We get the following results

$$\begin{aligned}&\dim(V^{[\text{mzz}]}) = 74, \quad \dim(V^{[\text{zmz}]}) = 75, \quad \dim(V^{[\text{zzz}]}) = 86, \\ &\dim(V^{[\text{one-loop}]}) = 13.\end{aligned} \tag{4.5}$$

Some master integrals are shared among several topologies so the actual number of independent master integrals is smaller than the sum of the individual dimensions. Fig. 4.2 gives an overview of independent five-point (sub)-topologies together with the corresponding numbers of master integrals per topology. In total, there are 35 new integrals in the two-loop sectors and 1 new integral in the one-loop sector to determine. Note that the one-loop pentagon is needed up to $\mathcal{O}(\epsilon^4)$ so that standard one-loop results are not sufficient.

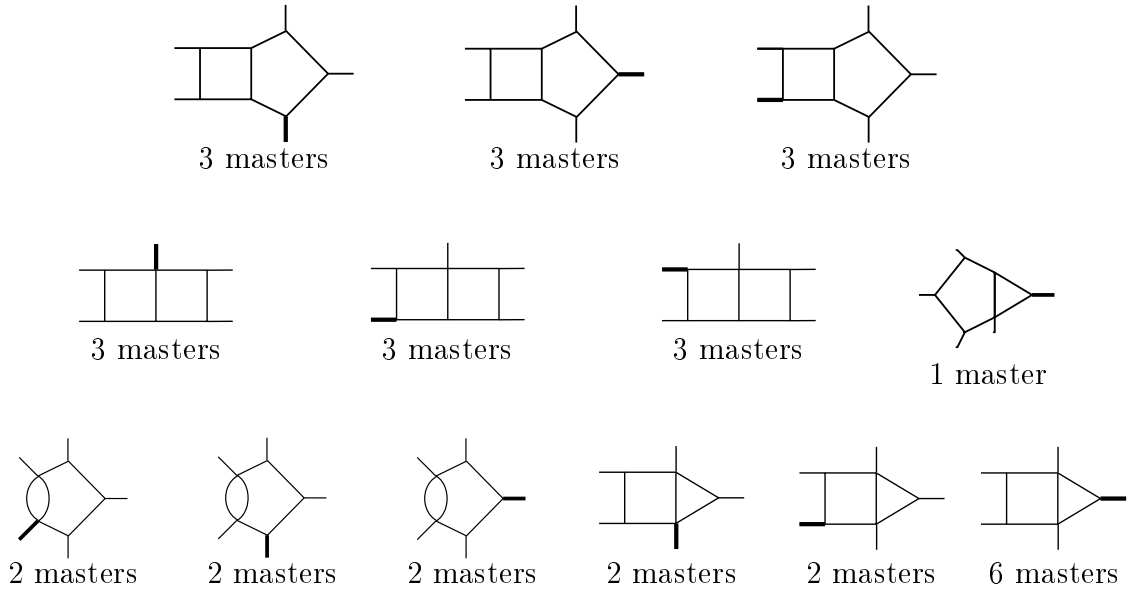

Figure 4.2: Propagator structures of two-loop five-point master integrals.

4.1.2 Pure basis

In this section we present the pure basis for planar five-point master integrals with one off-shell leg. In the following, pure master integrals will be denoted by $\mathbf{G}^{[f]}$ in contrast to the initial basis $\mathbf{I}^{[f]}$ with $f \in \{\text{mzz}, \text{zmz}, \text{zzz}, \text{one-loop}\}$. The construction of pure basis was discussed in detail in 3.3 with application to both planar and non-planar integrals so here we will not repeat this but just give the explicit form of the pure integrands for the genuine five-point topologies. The pure integrals with four and fewer external legs have already been known and could be taken from the literature [48, 216, 217]. Some of the pure integrals in the lower sectors (with 3 and 4 propagators) can differ from the integrals in the literature since we favoured integrands with the smallest possible number of doubled propagators. The full integral basis can be found in the ancillary files attached to our publication [55].

Let us briefly introduce our notation: Each five-point topology is represented by a diagram and a set of pure numerator insertions $\mathcal{N}^{(i)}_{top,f}$ where the upper index labels the master integrands of the given topology and the lower indices decode the *name* of the topology and the *name* of the integral family (top-level topology) this topology belongs to. So, for example, $\mathcal{N}^{(2)}_{\text{pb,zmz}}$ represents the second pure numerator insertion of the penta-box topology in the zmz integral family. The routing of the loop momenta and the ordering of external legs can be read off the diagrams. Graph edges corresponding to propagators which appear explicitly in the insertions are labeled with the propagator's numbers. Note that we normalized the integral bases with ϵ^2 for the one-loop pentagon topology and ϵ^4 for the two-loop topologies such that all Laurent-series expansions start at $\mathcal{O}(\epsilon^0)$.

Here is our choice for five-point planar integrals:

Penta-boxes

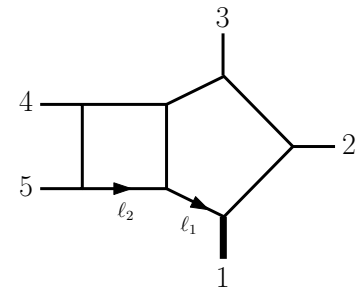

$$\begin{aligned}
\mathcal{N}^{(1)}_{\text{pb,mzz}} &= \epsilon^4 s_{45}\text{tr}_5\mu_{12},\\
\mathcal{N}^{(2)}_{\text{pb,mzz}} &= \epsilon^4\frac{1-2\epsilon}{1+2\epsilon}\text{tr}_5(\mu_{11}\mu_{22}-\mu_{12}^2),\\
\mathcal{N}^{(3)}_{\text{pb,mzz}} &= \epsilon^4 s_{45}s_{12}s_{23}(\ell_1-p_5)^2\,.
\end{aligned} \tag{4.6}$$

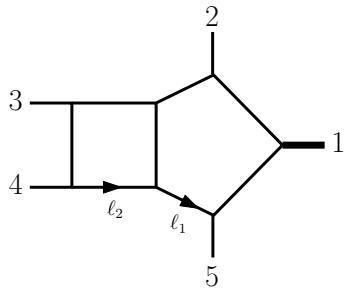

$$\begin{aligned}
\mathcal{N}^{(1)}_{\text{pb,zmz}} &= \epsilon^4 s_{34}\text{tr}_5\mu_{12},\\
\mathcal{N}^{(2)}_{\text{pb,zmz}} &= \epsilon^4\frac{1-2\epsilon}{1+2\epsilon}\text{tr}_5(\mu_{11}\mu_{22}-\mu_{12}^2),\\
\mathcal{N}^{(3)}_{\text{pb,zmz}} &= \epsilon^4 s_{34}(s_{15}s_{12}-q^2s_{34})(\ell_1-p_4)^2\,.
\end{aligned} \tag{4.7}$$

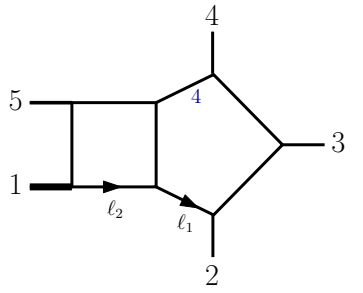

$$\begin{aligned}
\mathcal{N}^{(1)}_{\text{pb,zzz}} &= \epsilon^4 s_{15}\text{tr}_5\mu_{12},\\
\mathcal{N}^{(2)}_{\text{pb,zzz}} &= \epsilon^4\frac{1-2\epsilon}{1+2\epsilon}\,\text{tr}_5\,(\mu_{11}\mu_{22}-\mu_{12}^2),\\
\mathcal{N}^{(3)}_{\text{pb,zzz}} &= \epsilon^4 s_{23}s_{34}(s_{15}(\ell_1-p_1)^2-q^2\rho_4).
\end{aligned} \tag{4.8}$$

Penta-triangle

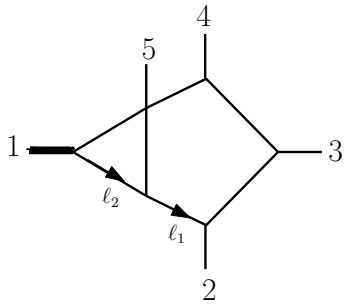

$$\mathcal{N}^{(1)}_{\text{pt,zzz}} = \epsilon^4\,\text{tr}_5\,\mu_{11}\,. \tag{4.9}$$

Double-boxes

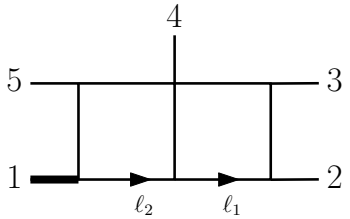

$$\begin{aligned}
\mathcal{N}^{(1)}_{\text{db,zzz}} &= \epsilon^4 s_{23}(s_{12}s_{15}-s_{34}q^2),\\
\mathcal{N}^{(2)}_{\text{db,zzz}} &= \epsilon^4 s_{23}(s_{15}-q^2)(\ell_2+p_2)^2,\\
\mathcal{N}^{(3)}_{\text{db,zzz}} &= \epsilon^4\,\text{tr}_5\,\mu_{12}\,.
\end{aligned} \tag{4.10}$$

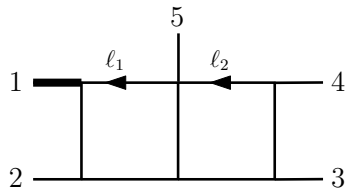

$$\begin{aligned}\mathcal{N}^{(1)}_{\text{db,zmz}} &= \epsilon^4 s_{34}s_{23}s_{12},\\ \mathcal{N}^{(2)}_{\text{db,zmz}} &= \epsilon^4 s_{34}(s_{12}-q^2)(\ell_1-p_4)^2,\\ \mathcal{N}^{(3)}_{\text{db,zmz}} &= \epsilon^4 \,\text{tr}_5\,\mu_{12}\,.\end{aligned} \tag{4.11}$$

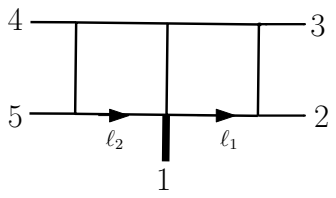

$$\begin{aligned}\mathcal{N}^{(1)}_{\text{db,mzz}} &= \epsilon^4 s_{23}s_{45}s_{34},\\ \mathcal{N}^{(2)}_{\text{db,mzz}} &= \epsilon^4 s_{23}s_{45}(\ell_2+p_2)^2,\\ \mathcal{N}^{(3)}_{\text{db,mzz}} &= \epsilon^4 \,\text{tr}_5\,\mu_{12}\,.\end{aligned} \tag{4.12}$$

Triangle-boxes

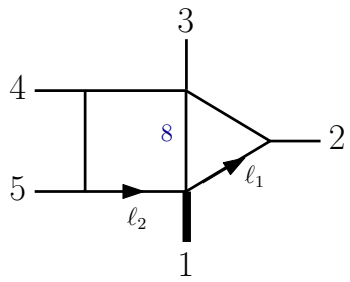

$$\begin{aligned}\mathcal{N}^{(1)}_{\text{tb,mzz}} &= \epsilon^4 s_{45}(s_{34}-s_{15}),\\ \mathcal{N}^{(2)}_{\text{tb,mzz}} &= \epsilon^3 \,\text{tr}_5\,\mu_{22}\frac{1}{\rho_8}\,.\end{aligned} \tag{4.13}$$

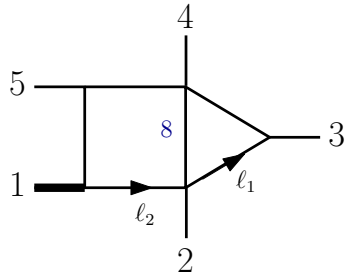

$$\begin{aligned}\mathcal{N}^{(1)}_{\text{tb,zzz}} &= \epsilon^4 s_{15}(s_{12}-s_{45}) - q^2 s_{34},\\ \mathcal{N}^{(2)}_{\text{tb,zzz}} &= \epsilon^3 \,\text{tr}_5\,\mu_{22}\frac{1}{\rho_8}\,.\end{aligned} \tag{4.14}$$

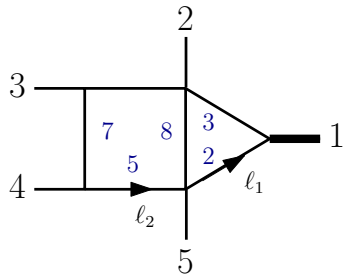

$$
\begin{aligned}
\mathcal{N}^{(1)}_{\text{tb,zmz}} &= \epsilon^4 s_{34}\sqrt{\Delta_3},\\
\mathcal{N}^{(2)}_{\text{tb,zmz}} &= \epsilon^3 \,\text{tr}_5\,\mu_{22}\frac{1}{\rho_8},\\
\mathcal{N}^{(3)}_{\text{tb,zmz}} &= \epsilon^4 \left(s_{34}(q^2-s_{23}+s_{45}) - \frac{1}{\epsilon}\frac{q^2 s_{34}s_{45}}{\rho_2}\right),\\
\mathcal{N}^{(4)}_{\text{tb,zmz}} &= \epsilon^4 \left(s_{34}(q^2+s_{23}-s_{45}) - \frac{1}{\epsilon}\frac{q^2 s_{23}s_{34}}{\rho_3}\right),\\
\mathcal{N}^{(5)}_{\text{tb,zmz}} &= \epsilon^4 \left(s_{34}(q^2+s_{23}-s_{45}) + \frac{1}{\epsilon}s_{15}s_{34}\frac{\rho_7}{\rho_5}\right.\\
&\qquad \left. + \frac{1}{\epsilon}q^2 s_{34}\frac{(\ell_1-p_4)^2}{\rho_2}\right),\\
\mathcal{N}^{(6)}_{\text{tb,zmz}} &= \epsilon^3 \,\text{tr}_5\,\mu_{12}\frac{1}{\rho_8}\,.
\end{aligned}
\tag{4.15}
$$

Bubble-pentagons

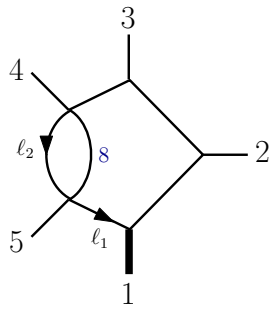

$$
\begin{aligned}
\mathcal{N}^{(1)}_{\text{bp,mzz}} &= \epsilon^3(1-2\epsilon)s_{12}s_{23},\\
\mathcal{N}^{(2)}_{\text{bp,mzz}} &= \epsilon^3 \,\text{tr}_5\,\mu_{11}\frac{1}{\rho_8}.
\end{aligned}
\tag{4.16}
$$

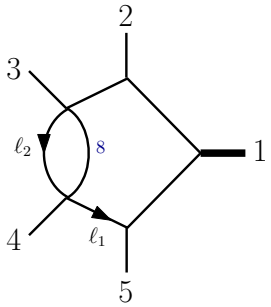

$$
\begin{aligned}
\mathcal{N}^{(1)}_{\text{bp,zmz}} &= \epsilon^3(1-2\epsilon)(s_{12}s_{15}-s_{34}q^2),\\
\mathcal{N}^{(2)}_{\text{bp,zmz}} &= \epsilon^3 \,\text{tr}_5\,\mu_{11}\frac{1}{\rho_8}\,.
\end{aligned}
\tag{4.17}
$$

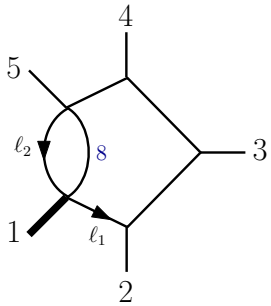

$$
\begin{aligned}
\mathcal{N}^{(1)}_{\text{bp,zzz}} &= \epsilon^3(1-2\epsilon)s_{23}s_{34},\\
\mathcal{N}^{(2)}_{\text{bp,zzz}} &= \epsilon^3 \,\text{tr}_5\,\mu_{11}\frac{1}{\rho_8}\,.
\end{aligned}
\tag{4.18}
$$

One-loop pentagon

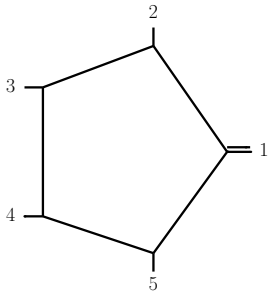

$$\mathcal{N}^{(1)}_{\text{pt,one-loop}} = \epsilon^2 \text{tr}_5 \mu. \tag{4.19}$$

4.1.3 Planar alphabet

As explained in section 3.4, we need both the pure basis and the symbol alphabet in order to apply the procedure of numerical reconstruction of the differential equation. In 4.1.2 we declared our choice of pure basis so now we have to deal with the alphabet. The first information we need is the size of the alphabet for each of the topologies. In 3.4 we explained how to obtain this information by computing the rank of $\tilde{\mathbf{C}}^{[\mathbf{f}]}$. We obtain the following results

$$\begin{aligned} &\dim\left(\mathcal{A}^{\text{mzz}}\right) = 38, \quad \dim\left(\mathcal{A}^{\text{zmz}}\right) = 48, \quad \dim\left(\mathcal{A}^{\text{zzz}}\right) = 49, \\ &\dim\left(\mathcal{A}^{\text{1-loop}}\right) = 30. \end{aligned} \tag{4.20}$$

The four alphabets may have common elements so we should also compute the total number of letters which we can get by putting all numerical connections together. The resulting matrix has rank 55.

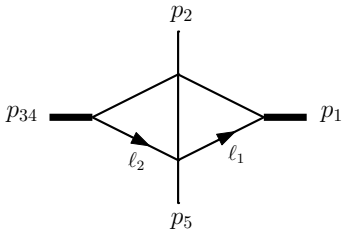

Figure 4.3: Slashed box integral with two opposite massive legs.

Let us discuss the explicit construction of the letters. From eq.(4.20) we see that 30 out of 55 letters are already present in the one-loop pentagon topology. These letters can be read off the one-loop canonical differential equation which can be computed analytically. The second natural source of letters are the kinematic prefactors of pure insertions which cancel the corresponding leading singularities. For example, the square-root expression $\sqrt{\Delta_3^{(3)}}$ appears as the leading singularity of the scalar slashed-box integral with two opposite massive legs (see fig. 4.3). Let us focus on the remaining letters. While the alphabet is still not complete we can use the reconstruction algorithm of 3.4 to determine in which part of the differential equation we have to search for missing letters. Let (i, j) be a fixed index pair such that the list of entries $\mathbf{M}_{ij}$ can not be reconstructed yet. Then, the coefficient of $\mathbf{G}_j$ in the right-hand-side of the equation for $\text{d}\mathbf{G}_i$ has to contain a new letter. We found out that all remaining letters appear in integral sectors with 7 and 6 propagators. This fact allows us to extract all letters from *on-shell* and

next-to-on-shell differential equations which at least in the planar case can still be computed by `KIRA` with full kinematic dependence with comparably small effort, in contrast to the *off-shell* reduction problem. We, indeed, checked that all 55 letters could in principle be computed in this way.

Although we are now ready to compute the analytic differential equation we want to take one step back and look more closely at the alphabet letters. There is no unique representation of the alphabet so one might ask whether a specific letter choice is more suited than others. In this work we followed the strategy of choosing letters in a way that makes algebraic properties of the alphabet manifest, as far as this was possible. Before we move on with discussing our criteria for choosing a particular letter representation let us briefly clarify what we exactly mean by independent letters. Although letters themselves are in general algebraic functions of the kinematics, the way they appear in the connection is through their logarithms. So, in principle, the actual set of functions we should consider to be independent is $\{\log(|W_1|, \cdots, \log(|W_{55}|)\}$ rather than $\{W_1, \cdots, W_{55}\}$. Note that we take the absolute value of the letters in order to get rid off any global phase information. Since the log-function maps multiplicative structures to additive ones we have to look for multiplicatively independent objects. So for example $\sqrt{\Delta_3^{(1)}}$ and $\Delta_3^{(1)}$ are not independent and cannot be both used as letters. For a given algebraic function of Mandelstam invariants $\Omega(\mathbf{s})$ we can easily decide whether its logarithm $\log(|\Omega|)$ belongs to the linear space spanned by the letters. For that purpose, we can evaluate $\{\log(|\Omega|), \log(|W_1|), \cdots, \log(|W_{55}|)\}$ on 56 different phase-space points and compute the rank of the corresponding matrix. If the rank is still 55 then Ω is part of the functional space spanned by the planar alphabet and can be in principle used instead of one of the previous letters.

An obvious criterion for choosing a *simpler* letter representation is the minimizing of the letter's mass dimension. We managed to find an alphabet representation with the maximal mass dimension being equal to four. Since we have with $\left\{\mathrm{tr}_5, \sqrt{\Delta_3^{(1)}}, \sqrt{\Delta_3^{(3)}}\right\}$ three square-roots in the planar alphabet we have to deal with a quite large set of genuinely algebraic letters. In general, there are three types of such letters: the square-roots themselves, letters involving one square-root and a polynomial part and letters involving two different square-roots and a polynomial part. Inspired by the fact that tr_5 is odd under parity transformation we decided to construct an alphabet representation where for each letter W we have a definite behaviour of $\log(|W|)$ under mapping each of the three square-roots to its negative

$$\mathrm{tr}_5 \to -\mathrm{tr}_5, \quad \sqrt{\Delta_3^{(1)}} \to -\sqrt{\Delta_3^{(1)}}, \quad \sqrt{\Delta_3^{(3)}} \to -\sqrt{\Delta_3^{(3)}}. \tag{4.21}$$

The reason for looking at transformations (4.21) is that the pure integrals $\mathbf{G}$ have a definite behaviour under these transformations which is inherited from pure prefactors containing the square-roots since the initial Feynman integrals are invariant under these sign flips. It is easy to see that both polynomial letters and the square-roots themselves are even under all transformations [1].

For the mixed letters with both a square-root and a polynomial part we have chosen the following representation $W_{\text{mixed}} = \frac{a+\sqrt{b}}{a-\sqrt{b}}$, where a and b are some polynomials in the Mandelstam invariants. Let us compute the action of sign-flipping in front of the square-root $\frac{a+\sqrt{b}}{a-\sqrt{b}} \to \frac{a-\sqrt{b}}{a+\sqrt{b}} = \left(\frac{a+\sqrt{b}}{a-\sqrt{b}}\right)^{-1}$. So, followingly, $\log(|W_{\text{mixed}}|)$ is odd under flipping the square-root sign.

Finally, we close the alphabet under the $(2 \leftrightarrow 5, 3 \leftrightarrow 4)$ permutations of the external legs to upgrade the alphabet to the planar amplitude level. This increases the number of letters by

[1] Note that we are looking at the behaviour of $\log(|W|)$.

3 such that the full alphabet has now 58 letters. The alphabet given in terms of Mandelstam invariants can be found in `anc/alphabet.m` in the ancillary files atttached to [55].
Let us discuss different parts of the alphabet in more detail. First, the alphabet contains the six first-entry Mandelstam invariants

$$\{W_1,\dots,W_6\} = \{q^2,\, s_{34},\, s_{12},\, s_{15},\, s_{23},\, s_{45}\}\,. \tag{4.22}$$

The next two sets contain scalar products of two external momenta or differences of two Mandelstam invariants written in terms of scalar products

$$\begin{aligned}\{W_7,\dots,W_{13}\} = \{&2\,p_2\cdot p_5,\, 2\,p_1\cdot p_2,\, 2\,p_1\cdot p_5,\, 2\,p_1\cdot p_3,\, 2\,p_1\cdot p_4,\\ &2\,p_2\cdot p_4,\, 2\,p_3\cdot p_5\}\,,\\ \{W_{14},\dots,W_{21}\} = \{&2\,p_2\cdot(p_3+p_4),\, 2\,p_5\cdot(p_3+p_4),\, 2\,p_2\cdot(p_4+p_5),\, 2\,p_5\cdot(p_2+p_3),\\ &2\,p_3\cdot(p_1+p_2),\, 2\,p_4\cdot(p_1+p_5),\, 2\,p_3\cdot(p_1+p_5),\, 2\,p_4\cdot(p_1+p_2)\}.\end{aligned} \tag{4.23}$$

Next, we list polynomial expressions with mass dimension four. The first set contains letters with four-point kinematics and the second consists of genuine five-point letters

$$\begin{aligned}\{W_{22},\dots,W_{30}\} = \{&\mathrm{tr}_+(1\,2\,1\,5),\, \mathrm{tr}_+(1\,2\,1\,3),\, \mathrm{tr}_+(1\,5\,1\,4),\, \mathrm{tr}_+(1\,2\,1\,4),\, \mathrm{tr}_+(1\,5\,1\,3),\\ &\mathrm{tr}_+(1\,2\,1\,[4+5]),\, \mathrm{tr}_+(1\,5\,1\,[2+3]),\\ &\mathrm{tr}_+([2+3]\,4\,[2+3]\,1),\, \mathrm{tr}_+([4+5]\,3\,[4+5]\,1)\}\,,\\ \{W_{31},W_{32}\} = \{&\mathrm{tr}_+(1\,2\,3\,4)-\mathrm{tr}_+(1\,2\,4\,5),\, \mathrm{tr}_+(1\,5\,4\,3)-\mathrm{tr}_+(1\,5\,3\,2)\}\,.\end{aligned} \tag{4.24}$$

We used the chiral Dirac trace

$$\mathrm{tr}_\pm(i\,j\,k\,l) = 2\left((p_i\cdot p_j)(p_k\cdot p_l)-(p_i\cdot p_k)(p_j\cdot p_l)+(p_i\cdot p_l)(p_j\cdot p_k)\pm i\varepsilon^{\mu\nu\rho\sigma}p_i^\mu p_j^\nu p_k^\rho p_l^\sigma\right). \tag{4.25}$$

We remind that the Levi-Civita symbol can be trivially traded for tr_5 since we have $\mathrm{tr}_5 = 4i\epsilon_{\mu\nu\rho\sigma}p_1^\mu p_2^\nu p_3^\rho p_4^\sigma$. Furthermore, note that despite including the chiral trace all letters in these two sets are manifestly parity-invariant since they either contain two equal indices or the chiral parts cancel out in the differences. Let us move on to the odd letters. The three following sets contain odd letters involving $\sqrt{\Delta_3^{(1)}}$ and $\sqrt{\Delta_3^{(3)}}$

$$\begin{aligned}\{W_{33},\dots,W_{36}\} = \Bigg\{&\frac{s_{12}+s_{13}+\sqrt{\Delta_3^{(1)}}}{s_{12}+s_{13}-\sqrt{\Delta_3^{(1)}}},\, \frac{s_{14}+s_{15}+\sqrt{\Delta_3^{(1)}}}{s_{14}+s_{15}-\sqrt{\Delta_3^{(1)}}},\\ &\frac{s_{12}+s_{15}+\sqrt{\Delta_3^{(3)}}}{s_{12}+s_{15}-\sqrt{\Delta_3^{(3)}}},\, \frac{s_{14}+s_{13}+\sqrt{\Delta_3^{(3)}}}{s_{14}+s_{13}-\sqrt{\Delta_3^{(3)}}}\Bigg\},\end{aligned} \tag{4.26}$$

$$\{W_{37},W_{38},W_{39}\} = \left\{\frac{s_{12}-s_{13}+\sqrt{\Delta_3^{(1)}}}{s_{12}-s_{13}-\sqrt{\Delta_3^{(1)}}},\, \frac{s_{15}-s_{14}+\sqrt{\Delta_3^{(1)}}}{s_{15}-s_{14}-\sqrt{\Delta_3^{(1)}}},\, \frac{s_{12}-s_{15}+\sqrt{\Delta_3^{(3)}}}{s_{12}-s_{15}-\sqrt{\Delta_3^{(3)}}}\right\}$$

and tr_5

$$\begin{aligned}\{W_{40},\dots,W_{46}\} = \Bigg\{&\frac{\mathrm{tr}_+(2\,3\,4\,5)}{\mathrm{tr}_-(2\,3\,4\,5)},\, \frac{\mathrm{tr}_+(1\,2\,3\,4)}{\mathrm{tr}_-(1\,2\,3\,4)},\, \frac{\mathrm{tr}_+(1\,5\,4\,3)}{\mathrm{tr}_-(1\,5\,4\,3)},\, \frac{\mathrm{tr}_+(4\,5\,1\,2)}{\mathrm{tr}_-(4\,5\,1\,2)},\\ &\frac{\mathrm{tr}_+(3\,2\,1\,5)}{\mathrm{tr}_-(3\,2\,1\,5)},\, \frac{\mathrm{tr}_+(1\,2\,4\,3)}{\mathrm{tr}_-(1\,2\,4\,3)},\, \frac{\mathrm{tr}_+(1\,5\,3\,4)}{\mathrm{tr}_-(1\,5\,3\,4)}\Bigg\}.\end{aligned} \tag{4.27}$$

Finally, we have the three square-roots themselves

$$\{W_{48}, W_{49}, W_{50}\} = \{\sqrt{\Delta_3^{(1)}}, \mathrm{tr}_5, \sqrt{\Delta_3^{(3)}}\} \tag{4.28}$$

and two letters involving two different square-roots simultaneously

$$\begin{aligned} W_{47} &= \frac{\Omega^{--}\,\Omega^{++}}{\Omega^{+-}\,\Omega^{-+}}, \quad \text{where} \quad \Omega^{\pm\pm} = s_{12}s_{15} - s_{12}s_{23} - s_{15}s_{45} \pm s_{34}\sqrt{\Delta_3^{(1)}} \pm \mathrm{tr}_5, \\ W_{58} &= \frac{\tilde{\Omega}^{--}\,\tilde{\Omega}^{++}}{\tilde{\Omega}^{+-}\,\tilde{\Omega}^{-+}}, \quad \text{where} \quad \tilde{\Omega}^{\pm\pm} = s_{12}s_{13} - s_{12}s_{25} - s_{13}s_{34} \pm s_{45}\sqrt{\Delta_3^{(3)}} \pm \mathrm{tr}_5. \end{aligned} \tag{4.29}$$

Note that the last two letters are invariant under the sign flip operators.
Let us finally make some comments on the letters. First of all, not all letters appear in all topologies. This information is summarized in table 4.1 in section 4.1.4 where the analytic DE for the planar topologies is discussed more closely. Next, the letters $\{W_{30}, W_{53}, W_{55}\}$ are obtained by permuting the external legs and appear only at the amplitude level. Third observation is that the following 9 letters $\{W_{50}, \ldots, W_{58}\}$ do not appear in the symbols up to weight four and are so irrelevant for any physical application on the two-loop level. Finally, we note that all *relevant* letters could, in principle, be determined from maximal-cut differential equations of appropriate sub-topologies.
The planar alphabet we presented in this section will be the starting point for constructing the non-planar alphabet extension which will be needed in section 4.2.3.

4.1.4 Construction of canonical DE's and symbol-level soltions

In this section we discuss the computation of the analytical canonical DE

$$\mathrm{d}\mathbf{G}^{[f]} = \epsilon \sum_{a=1}^{N} M_{a,f}\, \mathrm{dlog}(W_a)\mathbf{G}^{[f]}, \tag{4.30}$$

where $M_{a,f}$ are constant matrices with rational entries, W_a are alphabet letters and N denotes the number of letters in the planar alphabet. Since we now have both the pure bases $\mathbf{G}^{[f]}$ and the planar alphabet we can apply the reconstruction procedure from 3.4. First of all, we need a sufficiently large number of numerical samples for the canonical DE for each of the topologies. For the three genuinely non-planar integral families mzz, zmz and zzz we computed the pure connection on 105 rational phase-space points. Since the kinematic invariants are constructed from momenta with randomly chosen but rational entries also tr_5 becomes automatically rationalized on each of these points (see appendix A for details). The computation was done in parallel on 105 working nodes on the `NEMO` cluster using `FIRE6` [154] public code for performing the numerical IBP reduction. The IBP reduction took on average about $3-4\,\mathrm{h}$ per phase-space point.
In the following table 4.1 we show which alphabet letters are relevant for each of the topologies. *Relevant* means here simply that the corresponding $M_{a,f}$ from eq.(4.30) is non-zero.

topology	relevant letters	# of relevant letters
mzz	$W_1, \cdots, W_9, W_{11}, \cdots, W_{19}, W_{17}, \cdots, W_{19}, W_{21}, \cdots, W_{25}, W_{27}, W_{31}, W_{33}, W_{34}, W_{37}, W_{38}, W_{40}, W_{41}, W_{43}, \cdots, W_{49}$	38
zmz	$W_1, \cdots, W_{15}, W_{18}, \cdots, W_{26}, W_{31}, \cdots, W_{51}, W_{54}, W_{57}, W_{58}$	48
zzz	$W_1, \cdots, W_{15}, W_{17}, \cdots, W_{20}, W_{22}, \cdots, W_{24}, W_{26}, W_{28}, W_{29}, W_{32}, \cdots, W_{40}, W_{42}, \cdots, W_{52}, W_{54}, W_{56}, \cdots, W_{58}$	49
one-loop	$W_1, \cdots, W_9, W_{12}, \cdots, W_{15}, W_{18}, W_{19}, W_{22}, \cdots, W_{24}, W_{33}, W_{34}, W_{37}, W_{38}, W_{40}, W_{43}, \cdots, W_{49}$	30

Table 4.1: Appearance of symbol letters in different planar topologies.

With these data we are able to compute the connection matrices $M_{a,f}$ for all four topologies. Due to presence of two different non-rationalized square-roots $\left(\sqrt{\Delta_3^{(1)}} \text{ and } \sqrt{\Delta_3^{(3)}}\right)$ we have to apply the floating point version of the reconstruction approach as discussed in 3.4. The explicit connections are given in the ancillary files `anc/f/diffEq-f.m` attached to [55].
Before we move on with integrating the DE we want to look more closely at some analytic properties of the DE. A suitable framework for this discussion is provided by the notion of *symbols* which was introduced in 2.4.3. Once we obtained the canonical differential equation we can easily compute the symbol level solution of the Feynman integrals for any weight n using the defining equation (2.99)

$$S(\mathbf{G}^{(n)}) = \sum_{i_1,\ldots,i_n} c_{i_1,\ldots,i_n} W_{i_1} \otimes \ldots \otimes W_{i_n}, \tag{4.31}$$

with the rational multi-coefficients $c_{i_1,\cdots,i_n}$. The constant weight zero solution which we need as starting point for both computing the symbols and integrating the DE can also be extracted from the differential equation by applying the first-entry condition (see 3.5.2 for more details). The only letters which can appear on first-entry level in planar topologies are the cyclic Mandelstam invariants $s_{12}, s_{23}, s_{34}, s_{45}, s_{15}$ and the external momentum squared q^2. That means that the weight 0 solution $\mathbf{G}_f^{(0)}$ has to be in the kernel of all connection matrices except from the first six ones. So we have

$$M_{a,f}\mathbf{G}_f^{(0)} = 0, \quad a = 7, \cdots, 58. \tag{4.32}$$

This provides enough conditions to determine all but one entries of $\mathbf{G}^{(0)}$ for all four topologies. The last condition is just an overall normalization which can be fixed from a single one-scale integral. We use the factorized double-bubble integrals $G_{73}^{(\text{mzz})}, G_{75}^{(\text{zmz})}, G_{86}^{(\text{zzz})}$ and the one-loop bubble $G_{13}^{(\text{1-loop})}$ in order to fix the normalization. The pure bubble integral normalized accordingly to eq.(2.28) is explicitly given by

$$G_{13}^{(\text{1-loop})} = \frac{e^{\gamma\epsilon}(1-2\epsilon)\epsilon(-s_{15}-i\varepsilon)^{-\epsilon}\Gamma(1-\epsilon)^2\Gamma(\epsilon)}{\Gamma(2-2\epsilon)}. \tag{4.33}$$

The results are

$$\begin{aligned}
\mathbf{G}^{(0)}_{\text{mzz}} &= \Big\{0,0,\frac{3}{2},0,0,0,\frac{9}{4},\frac{3}{2},0,1,0,\frac{1}{4},0,\frac{1}{2},1,0,0,0,0,0,0,0,0,0,0,0,0,0,0,0,0,0,0,-\frac{1}{2},0,-\frac{1}{2},0,\\
&-\frac{1}{2},0,0,-1,0,0,0,1,1,0,0,-\frac{1}{4},1,1,0,0,\frac{1}{2},\frac{1}{2},\frac{1}{2},\frac{1}{2},\frac{1}{2},1,0,1,0,1,0,\frac{1}{2},-\frac{1}{2},-\frac{1}{2},-\frac{1}{2},-\frac{1}{2},-\frac{1}{2},\\
&-\frac{1}{2},1,1,1,1,1,0\Big\},\\
\mathbf{G}^{(0)}_{\text{zmz}} &= \Big\{0,0,0,\frac{3}{4},0,0,\frac{3}{4},0,0,1,0,1,0,0,0,0,0,0,0,0,0,0,0,0,0,0,\frac{3}{2},\frac{3}{2},-\frac{3}{2},0,0,0,0,0,0,0,\\
&-\frac{1}{2},0,-\frac{1}{2},0,0,0,-1,0,-1,0,0,1,1,0,0,0,0,0,0,0,1,\frac{1}{2},\frac{1}{2},\frac{1}{2},\frac{1}{2},\frac{1}{2},\frac{1}{2},\frac{1}{2},\frac{1}{2},\frac{1}{2},-\frac{1}{2},-\frac{1}{2},-\frac{1}{2},\\
&-\frac{1}{2},-\frac{1}{2},0,1,1,1,1\Big\},\\
\mathbf{G}^{(0)}_{\text{zzz}} &= \Big\{0,0,\frac{1}{2},0,2,0,0,0,0,\frac{3}{4},0,0,0,0,\frac{1}{4},0,0,0,0,0,0,0,\frac{3}{2},\frac{3}{2},-\frac{3}{2},0,0,0,0,0,0,0,0,0,0,\\
&0,0,0,0,-1,0,0,-\frac{1}{2},0,-\frac{1}{2},0,-\frac{1}{2},0,0,0,0,0,1,1,1,0,0,0,0,1,1,0,1,0,\frac{1}{2},\frac{1}{2},\frac{1}{2},\frac{1}{2},\frac{1}{2},\frac{1}{2},\frac{1}{2},\\
&\frac{1}{2},-\frac{1}{2},-\frac{1}{2},-\frac{1}{2},-\frac{1}{2},-\frac{1}{2},-\frac{1}{2},2,2,1,1,1,1,1,1\Big\},\\
\mathbf{G}^{(0)}_{\text{one-loop}} &= \{0,2,2,1,0,1,0,1,1,1,1,1,1\}.
\end{aligned} \tag{4.34}$$

We computed the symbols up to weight four and provided an automated code for this computation in the ancillary file `anc/usageExample.m` of reference [55].

Let us highlight some features of the integrals which can already be read off the differential equation. The first noticable observation is that at weight two all symbols which are required for the planar five-point amplitude with one off-shell leg correspond only to one-loop box and triangle integrals. This was already known in the massless case [51]. Note that this is not trivial and goes beyond simply imposing the integrability constraints on the symbol [68]. Letters $\{W_{20}, W_{21}, W_{35}, W_{39}\}$ are not forbidden by the integrability condition but still do not appear at weight two.

We also checked that the *Steinmann relations* [218–222] are fulfilled that means in our case that the letters $W_3 = s_{12}$ and $W_4 = s_{15}$ never appear together in the first two entries of any symbol and therefore there is no double discontinuity associated with two overlapping channels (see fig. 4.4). Indeed, even the stronger *extended Steinmann relation* [223] holds. That means that W_3 and W_4 do not appear as the n-th and the $(n+1)$-th symbol entries at any weight n. We proved this statement by explicitly checking that

$$M_{3,f} M_{4,f} = M_{4,f} M_{3,f} = 0 \tag{4.35}$$

for all four topologies. Finally, we searched for more similar relations like

$$M_i M_j = M_j M_i = 0 \tag{4.36}$$

and found several of them. If we restrict ourselves to cases where one of the letters is a first-entry letter and demand that the relation is closed under permuting of the external legs ($2 \leftrightarrow 5, 3 \leftrightarrow 4$)

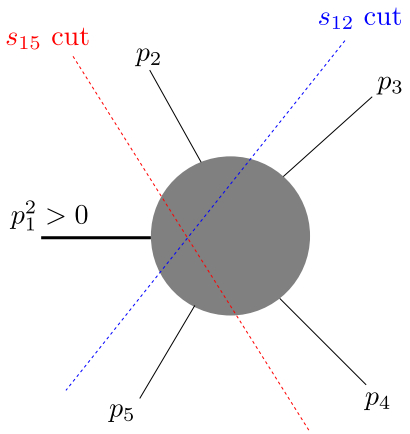

Figure 4.4: Illustration of Steinmann relations: the cuts in the s_{12} and s_{15} channels overlap and are therefore incompatible.

so that the relation becomes an amplitude level statement there are four further pairs besides (W_3, W_4). These are

$$\begin{aligned}
&(W_3, W_{19}) = \big(s_{12},\, 2\,p_4\cdot(p_1+p_5)\big)\,, \quad (W_4, W_{18}) = \big(s_{15},\, 2\,p_3\cdot(p_1+p_2)\big)\,,\\
&(W_3, W_{34}) = \left(s_{12},\, \frac{s_{14}+s_{15}+\sqrt{\Delta_3}}{s_{14}+s_{15}-\sqrt{\Delta_3}}\right)\,, \quad (W_4, W_{33}) = \left(s_{15},\, \frac{s_{13}+s_{12}+\sqrt{\Delta_3}}{s_{13}+s_{12}-\sqrt{\Delta_3}}\right)\,.
\end{aligned} \tag{4.37}$$

It would be interesting to investigate this in future.

4.1.5 Numerical integration, validation and discussion of results

In this section we discuss the details of the numerical integration using the methods of section 3.5. We give high-precision sample values for seven phase-space points and also present over 20k lower-precision evaluations over the physical region. All integrals have been computed up to weight four. Finally, we discuss the validation of the results.

High-precision evaluations

First of all, we obtained high-precision boundary conditions in the Euclidean region. Following the strategy described in 3.5.3 we computed the solution along the path $\vec{s}_{\text{eu-1}} \to \vec{s}_{\text{eu-2}} \to \vec{s}_{\text{eu-3}} \to \vec{s}_{\text{eu-4}} \to \vec{s}_{\text{eu-5}}$, with

$$\begin{aligned}
\vec{s}_{\text{eu-1}} &= \Big(-11,\quad -1,\quad -\frac{5}{2},\quad -\frac{7}{2},\quad -3,\quad -\frac{153}{14}\Big),\\
\vec{s}_{\text{eu-2}} &= \Big(-11,\quad -10,\quad -\frac{5}{2},\quad -\frac{7}{2},\quad -4,\quad -12\Big),\\
\vec{s}_{\text{eu-3}} &= \Big(-11,\quad -10,\quad -\frac{5}{2},\quad -\frac{7}{2},\quad -30,\quad -12\Big),\\
\vec{s}_{\text{eu-4}} &= \Big(-11,\quad -12,\quad -\frac{5}{2},\quad -32,\quad -50,\quad -12\Big),\\
\vec{s}_{\text{eu-5}} &= \Big(-11,\quad -12,\quad -80,\quad -32,\quad -50,\quad -42\Big),
\end{aligned} \tag{4.38}$$

where $\vec{s} = (q^2, s_{12}, s_{23}, s_{34}, s_{45}, s_{15})$. This path crosses enough singularities to fully constrain $\mathbf{G}^{(i)}(\vec{s}_{\text{eu-1}})$.

$G_3^{(4)}$	zzz	Re	+11.908529680841593329567378444341231494621544817813763
		Im	−143.838382350973365135537289916582866482644144160477 63
$G_3^{(4)}$	zmz	Re	+44.162165744735300867233118554182853322209473851043647
		Im	−46.218746133850339969944403077556678434364686840750803
$G_3^{(4)}$	mzz	Re	+29.802763651793108812023893217593351307350121722845006
		Im	+273.866278462665151139132952255724164190163163896399 92
$G_1^{(4)}$	1-loop	Re	−12.997557921493867410660219778141561158754063252253784
		Im	−34.691238289230523215562386582080833547255858602481034

Table 4.2: Sample numerical values of four integrals at weight four evaluated at the physical point $\vec{s}_{\text{ph-1}}$ defined in eq. (4.39). For $\texttt{f} \in \{\text{mzz}, \text{zmz}, \text{zzz}\}$, G_3 denotes the penta-box integral with the insertions $\mathcal{N}^{(3)}_{\text{pb},\texttt{f}}$ given in eqs. (4.6), (4.7) and (4.8), respectively (the other two insertions for each penta-box are only non-zero starting at weight five). For the one-loop topology, we quote the result for the one-loop pentagon with the insertion given in eq. (4.19). The results are truncated to fit the confines of the table. Results with at least 128 digits of precision can be found in the ancillary files `anc/f/numIntegrals-f.m`. This table is adapted from the publication [55].

In the next step we evaluated the integrals at one point in each of the six physical regions (see table 3.1 for the definition of the phase-space regions) with at least 128 digits precision.
The six physical points are

$$\begin{aligned}
\vec{s}_{\text{ph-1}} &= \left(\frac{137}{50}, -\frac{22}{5}, \frac{241}{25}, -\frac{377}{100}, \frac{13}{50}, \frac{249}{50}\right),\\
\vec{s}_{\text{ph-2}} &= \left(\frac{137}{50}, -\frac{22}{5}, -\frac{91}{100}, -\frac{377}{100}, -\frac{9}{10}, \frac{249}{50}\right),\\
\vec{s}_{\text{ph-3}} &= \left(\frac{137}{50}, -\frac{22}{5}, -\frac{91}{100}, \frac{13}{50}, -\frac{9}{10}, -\frac{9}{4}\right),\\
\vec{s}_{\text{ph-4}} &= \left(\frac{137}{50}, \frac{357}{50}, -\frac{91}{100}, \frac{241}{25}, -\frac{9}{10}, \frac{249}{50}\right),\\
\vec{s}_{\text{ph-5}} &= \left(\frac{137}{50}, \frac{357}{50}, -\frac{91}{100}, -\frac{161}{100}, -\frac{9}{10}, -\frac{9}{4}\right),\\
\vec{s}_{\text{ph-6}} &= \left(\frac{137}{50}, \frac{357}{50}, \frac{13}{50}, -\frac{161}{100}, \frac{241}{25}, -\frac{9}{4}\right).
\end{aligned} \tag{4.39}$$

The numerical results for these six physical points and the Euclidean boundary point are attached to our publication [55] and can be used as both benchmarks and boundaries in future studies. In table 4.2, we present the numerical result for the weight four part of three penta-box integrals and the one-loop pentagon integral, with the first 51 digits after the decimal point explicitly shown, evaluated at $\vec{s}_{\text{ph-1}}$. To illustrate the integration procedure we plotted both real and imaginary parts of the four integrals in table 4.2 as function of $t \in [0, 1]$ (fig. 4.5 and fig. 4.6) on the path between $\vec{s}_{\text{eu-1}}$ and $\vec{s}_{\text{ph-1}}$. As one can see, all functions have non-smooth behaviour (either divergencies or kinks) on four points (approximately at $t \sim 0.21$, $t \sim 0.69$, $t \sim 0.82$ and $t \sim 0.92$) where the four Mandelstam invariants s_{23}, s_{45}, q^2 and s_{45} change sign.
Before we proceed with a further investigation of the integrals in the physical region let us shortly discuss two technical subtleties. First, note that all genuine two-loop five-point integrals with a purely six-dimensional insertion (μ-like insertions without doubled propagators) vanish at all computed orders up to 128 digits. This is expected since the μ-insertions vanish identically in exactly four dimensions. This means that the lowest non-zero contribution in the Laurent series of

such integrals has to be of weight five and is so beyond the scope of our calculation. For the same reason the pure one-loop pentagon starts at weight three. Integrals which have both a doubled propagator and a μ-like factor in the pure insertion start already at weight three. They do not vanish in four dimensions since doubling one of the propagators affects the numerator insertion via IBP relations.
The second item regards the one-loop topology. In order to restore the two-loop factorizable penta-bubble integral (fig. 4.1d) from the one-loop level result we have to multiply the pentagon integral with the q^2-bubble integral and expand the result to the required order. All other factorizable integrals appear explicitly in one of the three penta-box topologies and do not have to be computed separately.

Integral evaluation over the physical space

Here we want to show the applicability of the univariate series-expansion approach to phenomenological applications where evaluations at a very large number of points across the physical phase space are required.
Let us first describe our setup for a many-point calculation where we tried to decrease the average computation time per point. As already said in 3.5.3, in practice, we choose some of previously computed points as boundary conditions and transport the solution to the new point. Since the computation time depends linearly on the number of segments per path we want to select the starting point such that the number of segments is kept minimal. Since the whole set of points can be very large we only want to check a small subset of k nearest points and choose the point with the minimal number of segments. Note that simply taking the nearest point might not be optimal since the distribution of singular points is in general not uniform. We found that $k = 10$ is a good choice. In particular, the average computation time per point for this choice is circa 40% better than for the case where we simply take the nearest point.
In order to study the features of a phenomenological application we evaluated the four integral families on 20000 sample phase-space points corresponding to vector-boson production at the LHC with the phase-space cuts of reference [224] with p_2 and p_3 being the initial-state momenta. We used the `Sherpa` Monte-Carlo program [225] to generate the physical points. The high-precision evaluations of section 4.1.5 were taken as the initial points for our study. Figure 4.7 shows the average evaluation time per point and integral as function of the number of evaluation points for every of the four integral topologies. The computation was performed on a single CPU thread with 32 digits precision. As we expected the time decreases with increasing number of points and stabilizes at around 2 s per integral after around 10000 points. More precise analysis of asymptotic evaluation time for each topology is given in table 4.3. To investigate the effect of the numerical precision on the computation time we repeated the timing study with 16 digits precision. The result is also summarized in table 4.3. Doubling the precision nearly doubles both the computation time per integral and the truncation order, as expected. It might look surprisingly that the one-loop integral topology requires the highest time-per-integral value but this is easy explained by the very small number of master integrals (13) compared to the two-loop topologies. zmz seems to be the most time-intensive case among the three two-loop topologies, concerning the computation per integral. During the timing study we also observed that the average number of segments per point (denoted by $\bar{n}_s$ from 3.5.4) stabilizes at around two.
Finally, we point the reader to reference [75] for a time comparison against evaluating analytic expressions in terms of GPL's.

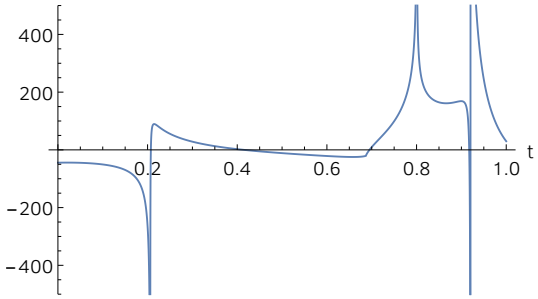

(a) $\mathrm{Re}(G_3^{(4)})$ of family mzz.

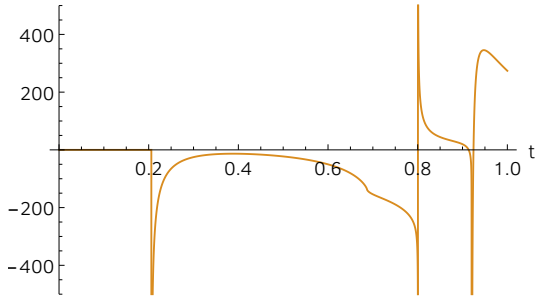

(b) $\mathrm{Im}(G_3^{(4)})$ of family mzz.

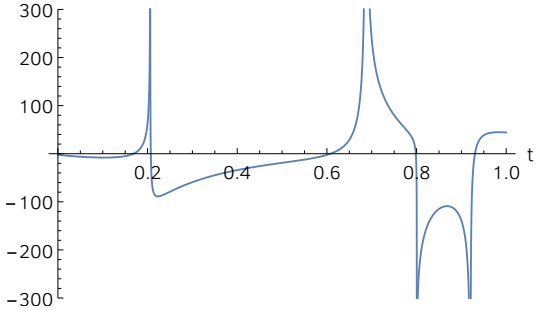

(c) $\mathrm{Re}(G_3^{(4)})$ of family zmz.

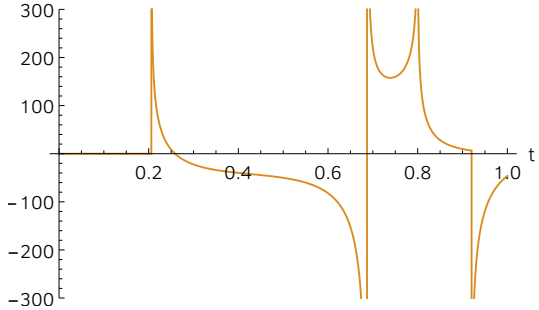

(d) $\mathrm{Im}(G_3^{(4)})$ of family zmz.

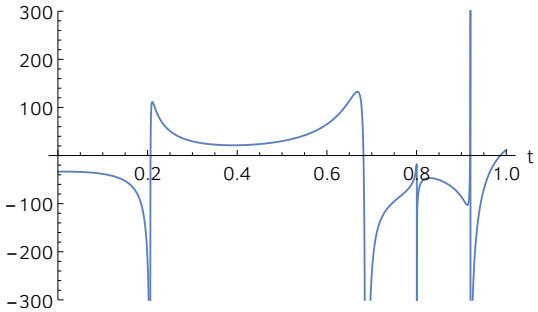

(e) $\mathrm{Re}(G_3^{(4)})$ of family zzz.

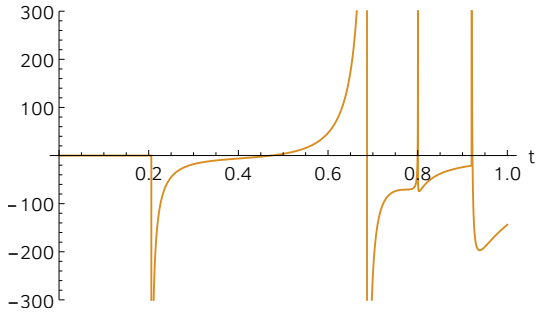

(f) $\mathrm{Im}(G_3^{(4)})$ of family zzz.

Figure 4.5: Integrals evaluated at weight four over a path from $\vec{s}_{\text{eu-1}}$ to $\vec{s}_{\text{ph-1}}$. Real and imaginary parts of the integrals are displayed separately. The visible singularities and discontinuities are associated to the physical thresholds for which analytic continuation is required. Figure adapted from [55].

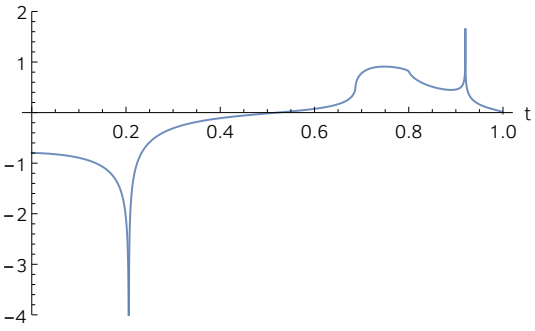

(a) $\mathrm{Re}(G_1^{(4)})$ of one-loop family.

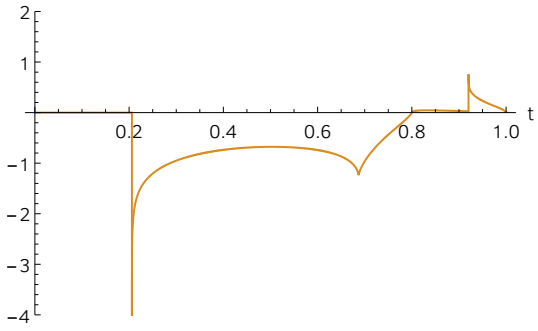

(b) $\mathrm{Im}(G_1^{(4)})$ of one-loop family.

Figure 4.6: One-loop pentagon at weight four, evaluated over a path from $\vec{s}_{\text{eu-1}}$ to $\vec{s}_{\text{ph-1}}$. Real and imaginary parts of the integrals are displayed individually. The visible kinks, singularities and discontinuities are associated with the physical thresholds for which analytic continuation is required. Figure adapted from [55].

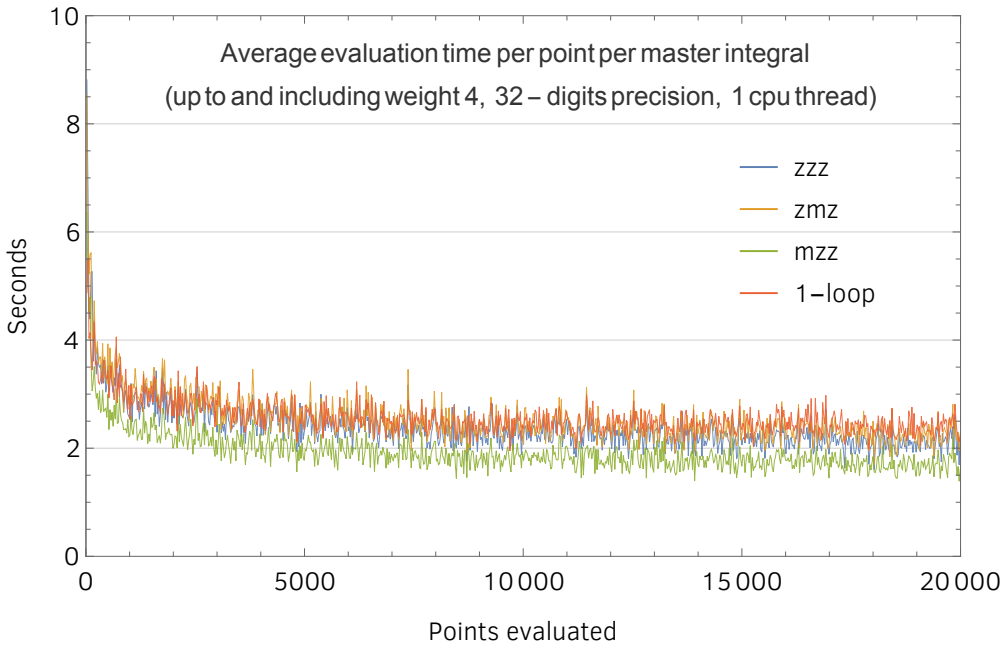

Figure 4.7: Timing study over a set of 20000 Monte-Carlo phase-space points in a physical scattering region. The average evaluation time per master integral is given by the total evaluation time divided by the number of master integrals of each topology (see also table 4.3). Each point of the plot is obtained by averaging the timing of 25 phase-space points. Plot adapted from [55].

Plots over physical phase space

In this paragraph we present plots for highest non-vanishing integrals for all families (i.e. integrals in table 4.2) over a two-dimensional sub-region of the phase-space part corresponding to $W + 2$-jets production at the LHC with initial-state momenta being p_2 and p_3. We fix four out of the

	Family	MI's	time per MI (s)	total time (s)	truncation order
32 digits	zzz	86	2.08	179	$70 < n_k < 140$
	zmz	75	2.24	168	
	mzz	74	1.69	125	
	1-loop	13	2.38	31	
16 digits	zzz	86	1.10	94	$40 < n_k < 80$
	zmz	75	1.15	86	
	mzz	74	0.88	65	
	1-loop	13	1.69	22	

Table 4.3: Characteristics of master-integral evaluation over 20000 phase-space points on a single CPU thread. The timing (in seconds) is given for 32-digit precision and 16-digit precision evaluations. The evaluation times in the fourth column correspond to the asymptotic timings, computed by averaging over the last 2000 phase-space points. We also give the truncation order of the series expansions (see section 3.5.4). Table adapted from [55].

six Mandelstam variables to be [2]

$$\begin{aligned} &q^2 = 1\,, \qquad s_{12} = -\frac{154120668029}{42334495831} = -3.64055\ldots\,, \\ &s_{15} = \frac{1619721713191}{211672479155} = 7.65202\,, \qquad s_{45} = \frac{761855318631}{42334495831} = 17.9961\ldots\,. \end{aligned} \tag{4.40}$$

and require $s_{23} > 0$ and $s_{34} < 0$. As shown in reference [226], we also need to ensure that the Gram matrix $G(p_1, p_2, p_3, p_4)$ has exactly three negative eigenvalues in this region. Obviously, this implies $\det G(p_1, p_2, p_3, p_4) < 0$. These constraints together with the requirement that all boundaries of the considered phase-space region have to be real fully specify the region to be

$$R = \left\{ (s_{23}, s_{34}) \;|\; s_{23}^{(2)} < s_{23} < \infty,\; s_{34}^{(-)} < s_{34} < s_{34}^{(+)} \right\}, \tag{4.41}$$

where

$$s_{34}^{(\pm)} = \frac{\mathcal{N} \pm \sqrt{\Delta}}{\mathcal{D}}\,, \tag{4.42}$$

with

$$\Delta = s_{23}s_{45}\left(s_{15}s_{45} + s_{12}\left(s_{12} + s_{23} - s_{45}\right) - q^2\left(s_{12} - s_{45}\right)\right)\left(\left(s_{15} - s_{23}\right)\left(s_{15} - q^2\right)\right), \tag{4.43}$$

$$\begin{aligned} \mathcal{N} = 2\Big(&s_{15}s_{45}^2 - s_{45}\left(s_{15}\left(q^2 + s_{12}\right) + s_{23}\left(s_{12} + s_{15} - 2q^2\right)\right) + s_{12}\left(s_{15} - s_{23}\right)\left(q^2 - s_{23}\right)\Big)\,, \\ \mathcal{D} = 2\Big(&q^4 + \left(s_{23} - s_{45}\right)^2 - 2q^2\left(s_{23} + s_{45}\right)\Big)\,, \end{aligned} \tag{4.44}$$

and

$$s_{23}^{(2)} = \frac{s_{15}\left(s_{15} + s_{45} - q^2\right)}{s_{15} - q^2}\,. \tag{4.45}$$

The phase-space region R corresponds to the Region 1 of fig. 4.8.

[2] These values correspond to a rationalization of one of the physical points obtained from SHERPA that were used in the previous paragraph. Mandelstam variables are normalized such that q^2, the vector-boson mass, is set to 1.

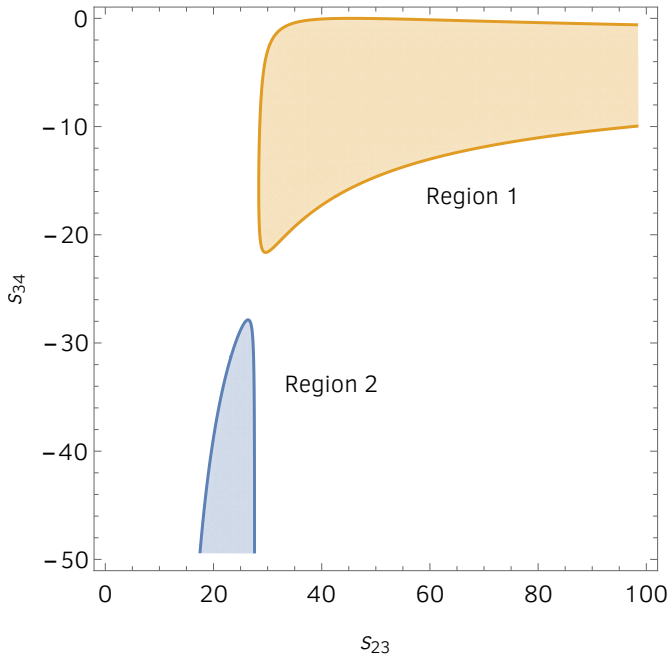

Figure 4.8: Regions where det $G(p_1, p_2, p_3, p_4) < 0$ in the $s_{23} > 0$ and $s_{34} < 0$ quadrant and under the assumption of eq. (4.40). Region 1 is unbounded as $s_{23} \to \infty$, and Region 2 as $s_{34} \to -\infty$. Figure adapted from [55].

Region 2 satisfies the weaker constraint of det$G(p_1, p_2, p_3, p_4) < 0$ but not the stronger constraint of the Gram matrix having three negative eigenvalues and is therefore excluded. For a more detailed discussion on determing the phase-space region R see [55]. Region 1 contains two physical branch points which are $s_{34} \to 0$ and $s_{23} \to \infty$. These limits correspond to (projective) points

$$P_1 = \left\{ s_{23} = \frac{s_{15}(s_{12} - s_{45})}{s_{12}}, s_{34} = 0 \right\} \quad \text{and} \quad P_2 = \{ s_{23} = \infty, s_{34} = s_{12} \} \,. \tag{4.46}$$

Since we are interested in phenomenological applications at the LHC we introduce a cut-off for the maximally available center-of-mass energy at $s_{23} = (13 \text{ TeV}/80 \text{ GeV})^2$, which corresponds to the LHC center-of-mass energy divided by the mass scale similar to the W-boson mass.
To have better control over the $s_{23} \to \infty$ limit we map R to a finite region $\bar{R}$ via the following coordinate map

$$s_{23}(x) = \frac{s_{23}^{(2)}}{(1-x)}, \quad s_{34}(x, y) = y\, s_{34}^{(+)}(x) + (1-y)\, s_{34}^{(-)}(x), \quad 0 < x < 1,\ 0 < y < 1, \tag{4.47}$$

where we highlight that $s_{34}^{(\pm)}$ are functions of x, following from their dependence on s_{23}. Both singular points eq. (4.46) are now mapped to

$$P_1 = \{ x = 0.376542\ldots,\ y = 1 \} \quad \text{and} \quad P_2 = \{ x = 1,\ 0 \le y \le 1 \} \tag{4.48}$$

and the s_{23} cut-off becomes $x = 0.998926\ldots$. In the new x, y coordinates the restricted region $\bar{R}$ is given by

$$\bar{R} = \{ (x, y) \mid 0 < x < 0.998926\ldots,\ 0 < y < 1 \} \,. \tag{4.49}$$

Note that although the $x = 1$ threshhold is beyond the LHC cut-off we still come very close to it and might so expect interesting behaviour of the integrals near to this boundary.
For the rest of this paragraph we discuss the plots in figs. 4.9-4.11. The plots were generated by evaluating the four selected integrals at $2 \cdot 10^5$ points with $0 < y < 0.9$ and further $2 \cdot 10^5$ points in the intervall $0.9 \leq y < 1$ where a larger variation was observed. Figure 4.9 presents both the real and imaginary parts of the three non-vanishing penta-box integrals at weight four with insertions $\mathcal{N}^{(3)}_{\text{pb},\mathtt{f}}$, given in eq. (4.6) , eq. (4.7) and eq. (4.8) for $f \in \{\text{mzz}, \text{zmz}, \text{zzz}\}$ (here we remind that two other penta-boxes first arise at weight five). The plots indeed show expected non-trivial behaviour near the both branch points. So fig. 4.9a and 4.9b show logarithmic divergencies for both threshhold points P_1 and P_2 where both real and imaginary parts go to $+\infty$. The zmz integral (fig. 4.9c and 4.9d) has a divergency to $-\infty$ at P_2. At P_1 the imaginary part also goes to $-\infty$. The real part does this as well but the dip is localized on a much smaller area. The smaller region around this dip is shown in figure 4.10. The behaviour of the zzz integral is very similar (see fig. 4.9e and fig. 4.9f) with the difference that the real part goes to $+\infty$ at P_1. Finally, we discuss the behaviour of the weight four contribution to the one-loop pentagon integral in fig. 4.11 (Note that at one loop the highest pole is -2 and so μ-like insertions can already appear at weight three). In contrast to the two-loop integrals, the pure pentagon is parity-odd and, therefore, it has to vanish at three of the four boundaries of $\bar{R}$ since we have $\text{tr}_5 = 0$ there which we indeed observe in fig. 4.11. Fig. 4.12 shows more closely the small peak of the imaginary part around P_1 and confirms the vanishing of the integral at the region boundary.

Validation of the result

The results of our computation were validated in several ways. The three main checks are:

- Both reconstruction of the differential equation and its numerical integration were performed with two independent implementations.
- The high-precision evaluations were compared to values obtained by `pySecDec` [172]. Here, two-loop integrals were checked at the Euclidean point and one-loop integrals both in Euclidean and physical regions. We found agreement within the statistical error estimate of `pySecDec`.
- Integrals in the mzz topology were validated against the results of [50]. We tested at least one integral per sector in all six physical regions. We found agreement within 128 digits. Later, D. Canko, C. Papadopoulos and N. Syrrakos found agreement within 32 digits between the analytic result [75] and our numerical results for all integrals and all physical points.

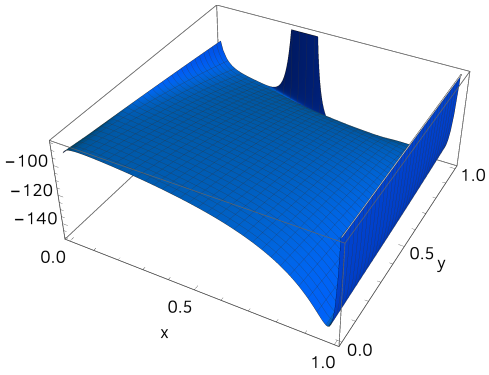

(a) $\mathrm{Re}(G_3^{(4)})$ of mzz topology.

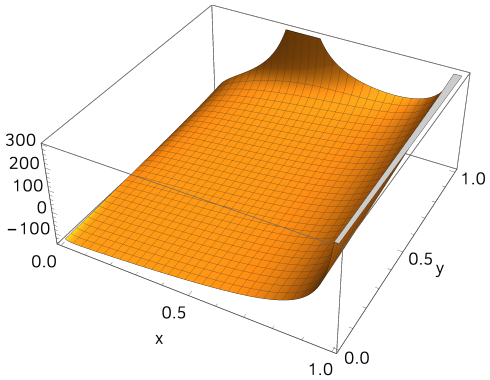

(b) $\mathrm{Im}(G_3^{(4)})$ of mzz topology.

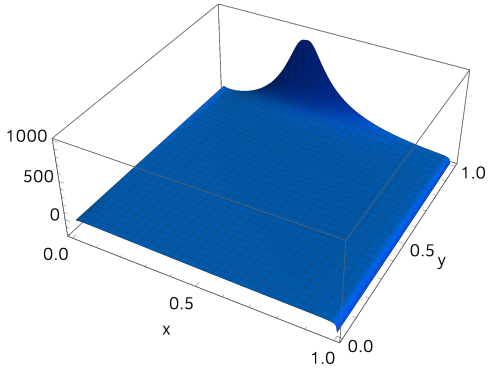

(c) $\mathrm{Re}(G_3^{(4)})$ of zmz topology.

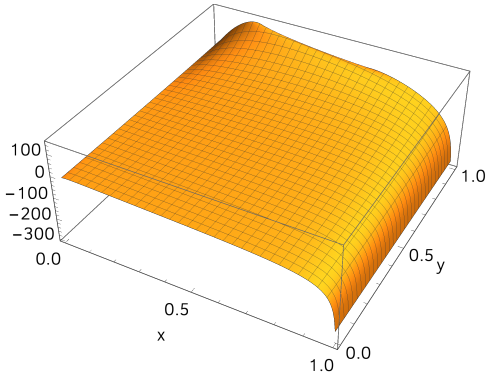

(d) $\mathrm{Im}(G_3^{(4)})$ of zmz topology.

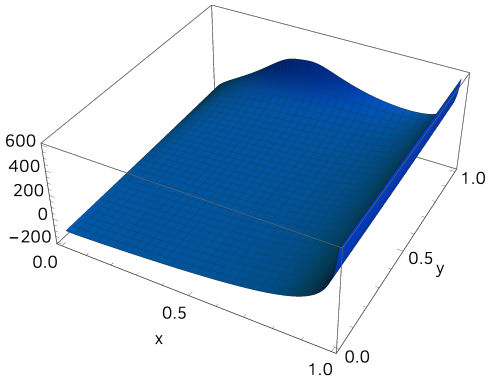

(e) $\mathrm{Re}(G_3^{(4)})$ of zzz topology.

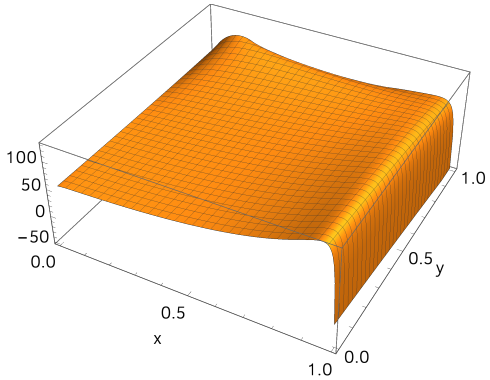

(f) $\mathrm{Im}(G_3^{(4)})$ of zzz topology.

Figure 4.9: Integrals plotted over $\bar{R}$, a two-dimensional sub-region of the physical region defined in eq. (4.49). The integrals are singular at the point P_1 of eq. (4.48) on the top edge ($y = 1$) of the unit square, and on the right edge ($x \to 1$) of the unit square, corresponding to the threshold at the point P_2 of eq. (4.48). Figures adapted from [55].

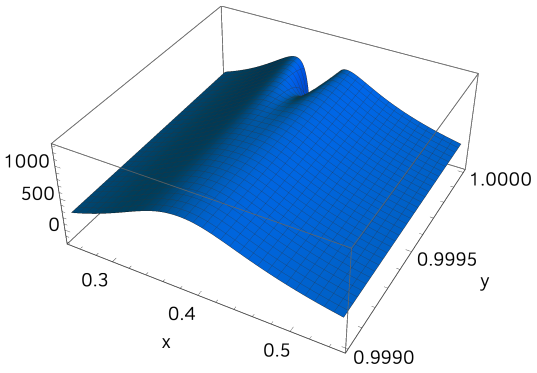

(a) $\mathrm{Re}(G_3^{(4)})$ of zmz topology.

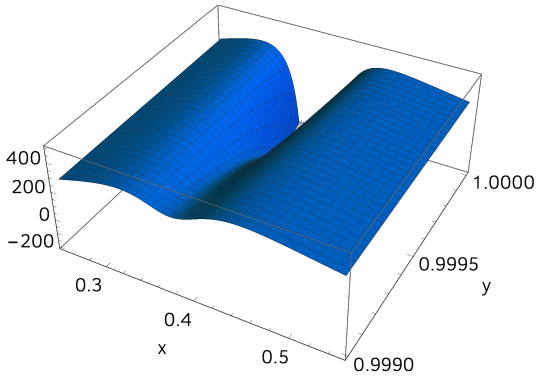

(b) $\mathrm{Re}(G_3^{(4)})$ of zzz topology.

Figure 4.10: Enlarged view of the integrals in figs. 4.9c and 4.9e near the threshold $s_{34} = 0$.

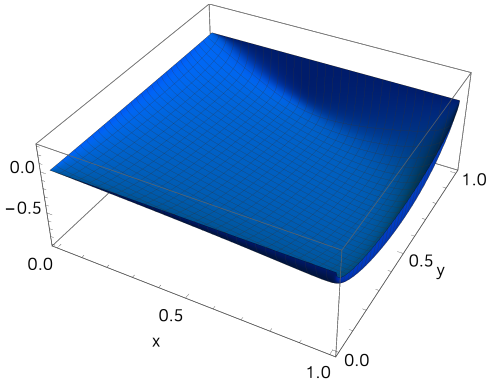

(a) $\mathrm{Re}(G_1^{(4)})$ of one-loop topology.

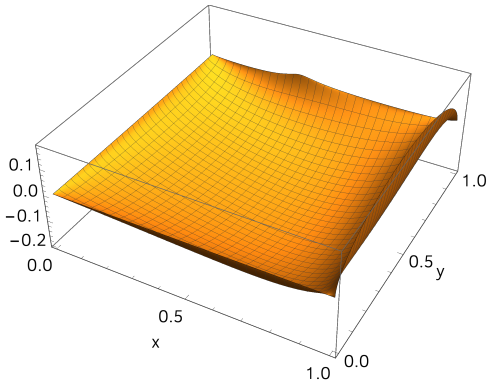

(b) $\mathrm{Im}(G_1^{(4)})$ of one-loop topology.

Figure 4.11: Weight-four contribution to the pure one-loop pentagon plotted over the region $\bar{R}$ defined in eq. (4.49). Due to its normalization, the function should vanish at $\det G(p_1, p_2, p_3, p_4) = 0$, corresponding to the edges of the unit square. Because of the cut-off at $x = 0.998926\ldots$, the function does not vanish on the $x = 1$ edge. Figures adapted from [55].

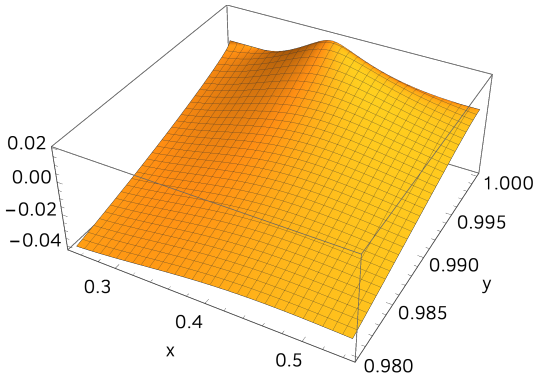

$\mathrm{Im}(G_1^{(4)})$ of one-loop topology.

Figure 4.12: Enlarged view of the integral in 4.11b near the threshold $s_{34} = 0$.

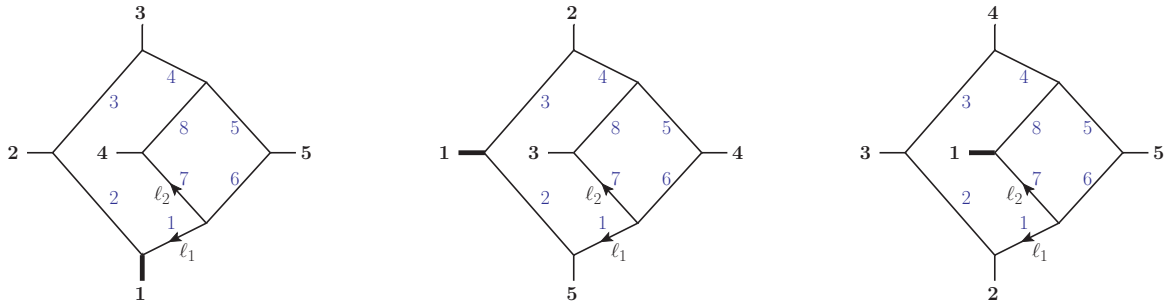

(a) $I_{hb}^{[\mathrm{mzz}]}[\vec{\nu}]$ (b) $I_{hb}^{[\mathrm{zmz}]}[\vec{\nu}]$ (c) $I_{hb}^{[\mathrm{zzz}]}[\vec{\nu}]$

Figure 4.13: Two-loop five-point non-planar hexa-box topologies with one off-shell leg. The thick external line with label 1 denotes the massive leg.

4.2 Hexa-box topologies

4.2.1 Definition of the hexa-box topologies

In this section we define hexa-box topologies with one external massive leg which are shown in fig. 4.13. There are three independent top-level integral topologies which are, similar to the planar case, denoted by $I_{hb}^{[f]}$, with $f \in \{\mathrm{mzz}, \mathrm{zmz}, \mathrm{zzz}\}$, where the letters label the external legs at the hexagon side. The zzz topology is part of the leading color contribution to the Higgs-and Z-boson production associated with two jets while the other two topologies first appear in sub-leading color contributions to the production of a massive boson associated with two massless jets. The three hexa-box integral families are defined by

$$I_{hb}^{[f]}[\vec{\nu}] = e^{2\epsilon\gamma_E} \int \frac{d^D\ell_1}{i\pi^{D/2}} \frac{d^D\ell_2}{i\pi^{D/2}} \frac{\rho_{9,f}^{-\nu_9}\ \rho_{10,f}^{-\nu_{10}}\ \rho_{11,f}^{-\nu_{11}}}{\rho_{1,f}^{\nu_1}\ \rho_{2,f}^{\nu_2}\ \rho_{3,f}^{\nu_3}\ \rho_{4,f}^{\nu_4}\ \rho_{5,f}^{\nu_5}\ \rho_{6,f}^{\nu_6}\ \rho_{7,f}^{\nu_7}\ \rho_{8,f}^{\nu_8}}\,, \tag{4.50}$$

where $D = 4 - 2\epsilon$ and $\vec{\nu}$ denotes the list of indices. Here, we have $\nu_i \leq 0,$ for $i \geq 9$. The inverse propagators and ISP's are given explicitly by

$$\begin{aligned}
\vec{\rho}_{\mathrm{mzz}} &= \big\{\ell_1^2, (\ell_1+p_1)^2, (\ell_1+p_1+p_2)^2, (\ell_1+p_1+p_2+p_3)^2, (\ell_1+\ell_2-p_5)^2, (\ell_1+\ell_2)^2, \ell_2^2, (\ell_2+p_4)^2,\\
&\quad (\ell_2+p_1)^2, (\ell_1+p_4)^2, (\ell_2+p_1+p_2)^2\big\}\,,\\
\vec{\rho}_{\mathrm{zmz}} &= \big\{\ell_1^2, (\ell_1+p_5)^2, (\ell_1+p_5+p_1)^2, (\ell_1+p_5+p_1+p_2)^2, (\ell_1+\ell_2-p_4)^2, (\ell_1+\ell_2)^2, \ell_2^2, (\ell_2+p_3)^2,\\
&\quad (\ell_2+p_5)^2, (\ell_1+p_3)^2, (\ell_2+p_5+p_1)^2\big\}\,,\\
\vec{\rho}_{\mathrm{zzz}} &= \big\{\ell_1^2, (\ell_1+p_2)^2, (\ell_1+p_2+p_3)^2, (\ell_1+p_2+p_3+p_4)^2, (\ell_1+\ell_2-p_5)^2, (\ell_1+\ell_2)^2, \ell_2^2, (\ell_2+p_1)^2,\\
&\quad (\ell_2+p_2)^2, (\ell_1+p_1)^2, (\ell_2+p_2+p_3)^2\big\}\,.
\end{aligned} \tag{4.51}$$

The first eight entries in every list are inverse propagators while the last three are ISP's chosen such that the list becomes maximally symmetric under the exchange of ℓ_1 and ℓ_2. The routing of the loop momenta can be read off fig. 4.13 and all external momenta are considered to be incoming. The master integral count for the three topologies is

$$\dim(V_{hb}^{[\mathrm{mzz}]}) = 86, \quad \dim(V_{hb}^{[\mathrm{zmz}]}) = 86, \quad \dim(V_{hb}^{[\mathrm{zzz}]}) = 135. \tag{4.52}$$

In fig. 4.14 we show all five-point non-planar integral topologies together with the corresponding number of master integrals per topology which have to be computed. In total, we have 9 topologies with 29 integrals.

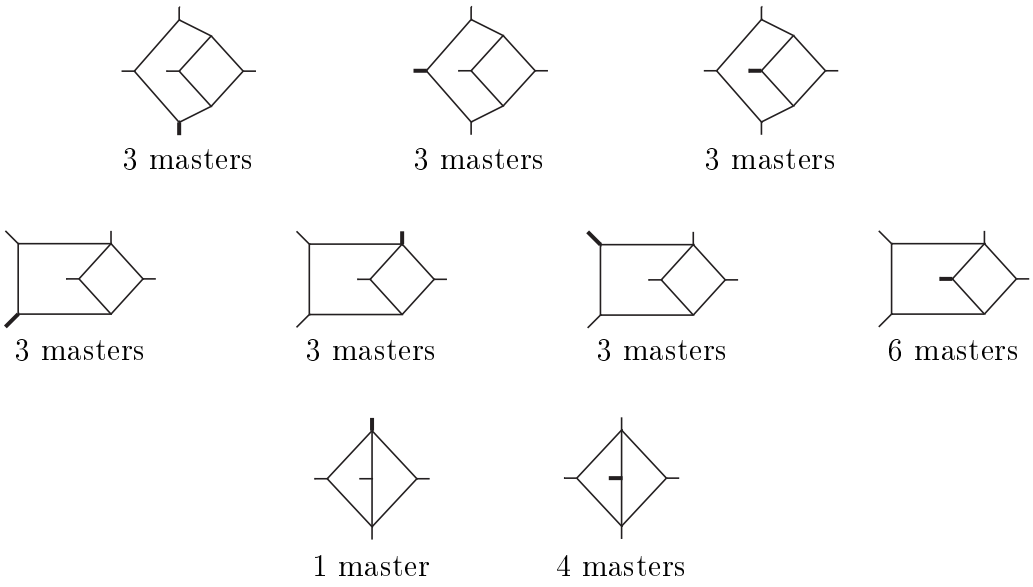

Figure 4.14: Propagator structures of two-loop five-point non-planar master integrals in the hexa-box topologies.

4.2.2 Pure basis

Here, we present our choice of pure insertions for non-planar five-point topologies with one off-shell leg which are shown in fig. 4.14. All other topologies that appear in the three hexa-box integral families are either planar five-point integrals (see 4.1.2) or have less than five external legs and so are available in the literature [48, 216, 227]. We multiply the pure bases with ϵ^4 such that the integral expansion starts at $\mathcal{O}(\epsilon^0)$. For a detailed discussion of constructing the pure non-planar five-point integrals we refer to section 3.3.
Here is our list of pure hexa-box integrals:

Hexa-boxes

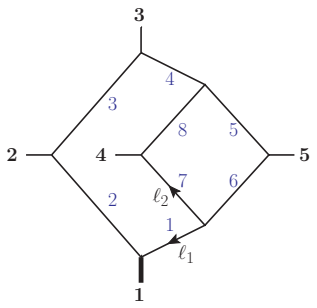

$$\begin{aligned}
\mathcal{N}^{(1)}_{\text{hb,mzz}} =& \epsilon^4 (\ell_1 - p_4)^2 \text{tr}_5\, \mu_{11}, \\
\mathcal{N}^{(2)}_{\text{hb,mzz}} =& \epsilon^4 (\ell_1 - p_5)^2 \text{tr}_5\, \mu_{11}, \\
\mathcal{N}^{(3)}_{\text{hb,mzz}} =& \epsilon^4 s_{12} s_{23} \left[(\ell_1 - 1 p_4)^2 (\ell_1 - p_5)^2 - \rho_1 \rho_4 \right] .
\end{aligned} \tag{4.53}$$

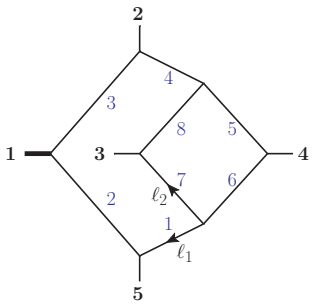

$$\begin{aligned}
\mathcal{N}^{(1)}_{\text{hb,zmz}} =&\epsilon^4(\ell_1-p_3)^2\text{tr}_5\,\mu_{11},\\
\mathcal{N}^{(2)}_{\text{hb,zmz}} =&\epsilon^4(\ell_1-p_4)^2\text{tr}_5\,\mu_{11},\\
\mathcal{N}^{(3)}_{\text{hb,zmz}} =&\epsilon^4\left[s_{12}s_{15}-q^2s_{34}\right]\left[(\ell_1-p_3)^2(\ell_1-p_4)^2-\rho_1\rho_4\right].
\end{aligned} \tag{4.54}$$

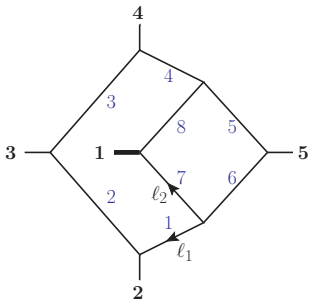

$$\begin{aligned}
\mathcal{N}^{(1)}_{\text{hb,zzz}} =&\epsilon^4(\ell_1-p_1)^2\text{tr}_5\,\mu_{11},\\
\mathcal{N}^{(2)}_{\text{hb,zzz}} =&\epsilon^4(\ell_1-p_5)^2\text{tr}_5\,\mu_{11},\\
\mathcal{N}^{(3)}_{\text{hb,zzz}} =&\epsilon^4 s_{23}s_{34}\left[(\ell_1-p_1)^2(\ell_1-p_5)^2-\rho_1\rho_4\right].
\end{aligned} \tag{4.55}$$

non-planar Penta-boxes

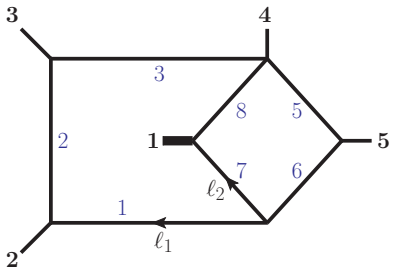

$$\begin{aligned}
\mathcal{N}^{(1)}_{\text{npb,zzz}} =&\epsilon^4\left[s_{23}(s_{34}-s_{12}-s_{15}+q^2)(\ell_1-p_1)^2+C^{(1)}_{\text{npb,zzz}}\rho_1\right],\\
\mathcal{N}^{(2)}_{\text{npb,zzz}} =&\epsilon^4\left[s_{23}s_{12}(\ell_1-p_5)^2+C^{(2)}_{\text{npb,zzz}}\rho_1\right],\\
\mathcal{N}^{(3)}_{\text{npb,zzz}} =&\epsilon^4 s_{23}\left[(\ell_1-p_1)^2(\ell_1-p_5)^2-\rho_1(\ell_1+p_2+p_3+p_4)^2\right],\\
\mathcal{N}^{(4)}_{\text{npb,zzz}} =&\epsilon^3q^2\text{tr}_5\frac{\mu_{12}+\mu_{11}}{\rho_8},\\
\mathcal{N}^{(5)}_{\text{npb,zzz}} =&\epsilon^4\text{tr}_5\mu_{12},\\
\mathcal{N}^{(6)}_{\text{npb,zzz}} =&\epsilon^4\text{tr}_5\mu_{11}.
\end{aligned} \tag{4.56}$$

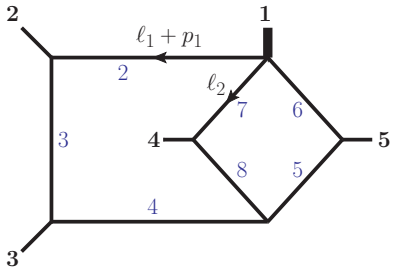

$$\begin{aligned}
\mathcal{N}^{(1)}_{\text{npb,mzz-2}} =&\epsilon^4\left[s_{23}s_{34}(\ell_1-p_4)^2+C^{(1)}_{\text{npb,mzz-2}}\rho_4\right],\\
\mathcal{N}^{(2)}_{\text{npb,mzz-2}} =&\epsilon^4\text{tr}_5\mu_{11},\\
\mathcal{N}^{(3)}_{\text{npb,mzz-2}} =&\epsilon^4 s_{23}\left[(\ell_1-p_4)^2(\ell_1-p_5)^2-\ell_1^2\rho_4\right].
\end{aligned} \tag{4.57}$$

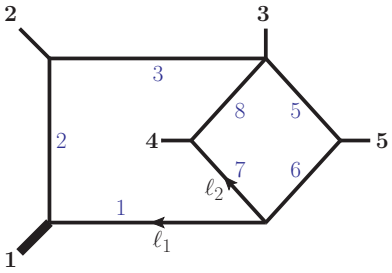

$$
\begin{aligned}
\mathcal{N}^{(1)}_{\text{npb,mzz}-1} =&\epsilon^4\left[(s_{12}s_{15}-s_{34}q^2)(\ell_1-p_4)^2+C^{(1)}_{\text{npb,mzz}-1}\rho_1\right],\\
\mathcal{N}^{(2)}_{\text{npb,mzz}-1} =&\epsilon^4\text{tr}_5\mu_{11},\\
\mathcal{N}^{(3)}_{\text{npb,mzz}-1} =&\epsilon^4(s_{12}-q^2)\left[(\ell_1-p_4)^2(\ell_1+p_5)^2\right.\\
&\left.-\rho_1(\ell_1+p_1+p_2+p_3)^2\right].
\end{aligned}
\tag{4.58}
$$

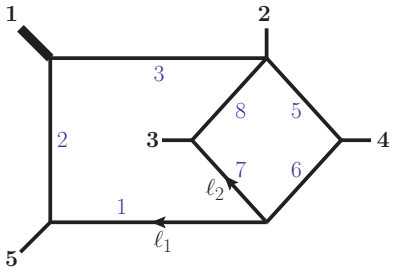

$$
\begin{aligned}
\mathcal{N}^{(1)}_{\text{npb,zmz}} =&\epsilon^4\left[s_{12}s_{45}(\ell_1-p_3)^2+C^{(1)}_{\text{npb,zmz}}\rho_1\right],\\
\mathcal{N}^{(2)}_{\text{npb,zmz}} =&\epsilon^4\text{tr}_5\mu_{11},\\
\mathcal{N}^{(3)}_{\text{npb,zmz}} =&\epsilon^4(s_{15}-q^2)\left[(\ell_1-p_3)^2(\ell_1-p_4)^2\right.\\
&\left.-\rho_1(\ell_1-p_3-p_4)^2\right].
\end{aligned}
\tag{4.59}
$$

non-planar Double-boxes

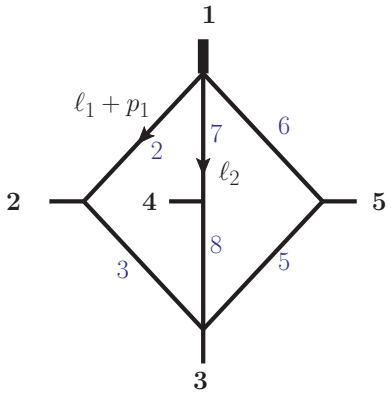

$$
\mathcal{N}^{(1)}_{\text{ndb,mzz}} = \epsilon^4\text{tr}_5. \tag{4.60}
$$

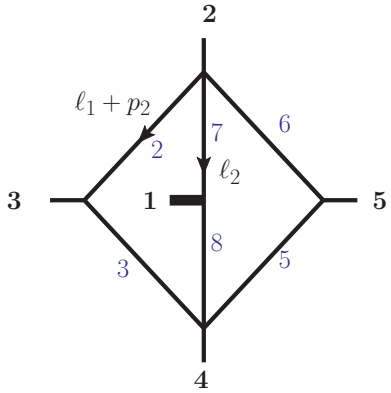

$$
\begin{aligned}
\mathcal{N}^{(1)}_{\text{ndb,zzz}} =&\epsilon^4\sqrt{\Sigma^{(2)}_5},\\
\mathcal{N}^{(2)}_{\text{ndb,zzz}} =&\epsilon^4\frac{1}{8}\left(\text{tr}\left[(\not{\ell}_2-\not{p}_2)\not{p}_3\not{p}_1\not{p}_5\right]+\text{tr}\left[(\not{\ell}_2+\not{p}_1+\not{p}_4)\not{p}_3\not{p}_1\not{p}_5\right]\right.\\
&\left.+8\left[(\ell_2+p_1)^2-\ell_2^2\right](s_{12}-s_{34}-s_{45})\right),\\
\mathcal{N}^{(3)}_{\text{ndb,zzz}} =&\epsilon^3\text{tr}_5\mu_{12}\left[\frac{1}{\rho_7}+\frac{1}{\rho_8}\right],\\
\mathcal{N}^{(4)}_{\text{ndb,zzz}} =&\epsilon^3\left[\frac{q^2}{\rho_7}\left[(\ell_2-p_2-p_3)^2(\ell_2+p_1+p_3+p_4)^2\right.\right.\\
&\left.\left.-(\ell_2-p_2)^2(\ell_2+p_1+p_4)^2\right]+C^{(4)}_{\text{ndb,zzz}}\right].
\end{aligned}
\tag{4.61}
$$

Here, we give explicit expressions for off-shell corrections terms in eqs. (4.53)-(4.61).

$$
\begin{aligned}
C^{(1)}_{\text{npb,zzz}} &= \frac{1}{2}\left(s_{12}(s_{23}-s_{15}) - s_{23}s_{34} + q^2(s_{12}-s_{45}) + s_{15}s_{45} - s_{34}s_{45}\right), \\
C^{(2)}_{\text{npb,zzz}} &= -s_{23} - s_{34} - C^{(1)}_{\text{npb,zzz}}, \\
C^{(1)}_{\text{npb,mzz}-2} &= \frac{1}{2}\left(-q^2 s_{34} + s_{12}\left(s_{15}-s_{23}\right) - s_{23}s_{34} - s_{15}s_{45} + s_{34}s_{45}\right), \\
C^{(1)}_{\text{npb,mzz}-1} &= \frac{1}{2}\left(q^2 s_{34} - s_{12}\left(s_{15}+s_{23}\right) + s_{23}s_{34} + s_{15}s_{45} - s_{34}s_{45}\right), \\
C^{(1)}_{\text{npb,zmz}} &= \frac{1}{2}\left(s_{12}\left(s_{23}-s_{15}\right) - s_{23}s_{34} + \left(s_{34}-s_{15}\right)s_{45}\right), \\
C^{(4)}_{\text{db,zzz}} &= (s_{23}-s_{45}-q^2)\frac{\rho_2\rho_5}{\rho_3} - (s_{12}+s_{15})\frac{\rho_3\rho_6}{\rho_2} + \frac{1}{\epsilon}(1-2\epsilon)(1-3\epsilon)\frac{q^2}{s_{12}-q^2}\rho_3\rho_5 \\
&\quad + \frac{1}{\epsilon^2}(1-2\epsilon)(2-3\epsilon)(1-3\epsilon)\frac{q^2}{(s_{12}-q^2)s_{12}}\rho_3\rho_5\rho_7.
\end{aligned}
\tag{4.62}
$$

4.2.3 Symbol alphabet

Let us now discuss the extension of the planar alphabet needed for the hexa-box topologies. By computing the rank of the numerical matrix $\tilde{\mathbf{C}}^{[f]}$ (see section 3.4), we obtain

$$
\dim\left(\mathbb{A}^{\text{mzz}}\right) = 39, \quad \dim\left(\mathbb{A}^{\text{zmz}}\right) = 56, \quad \dim\left(\mathbb{A}^{\text{zzz}}\right) = 63. \tag{4.63}
$$

Most of the letters could be obtained directly from the planar alphabet by permuting all external massless legs and then removing dependent letters. Applying this procedure to the 58 letters of the planar alphabet from section 4.1.3 gives 156 independent letters. This is already sufficient for the mzz topology but not for the two others. Up to permutations, there are four new letters which can not be obtained from the planar alphabet. One of them appears in the diagonal entry of a particular scalar integral in a non-planar four-point subtopology in the zzz-DE and is therefore given by the pure prefactor (inverse leading singularity) of this integral. Since this letter corresponds to a four-point integral it can also be taken from the literature [227]. The letter is polynomial in the Mandelstam invariants. The three remaining letter types appear only in the both permutations of the non-planar five-point double-box subtopology with the mass attached to the central rung (*hard non-planar double-box*, discussed in section 3.3.6) (fig. 4.2.3). This was expected since a new type of square-root $\sqrt{\Sigma_5}$ appears in this subtopology. Indeed, one of the three new letters can be identified as the square-root itself. In analogy to other algebraic letters, we assume that one the two remaining letters has the form

$$
\frac{p(\vec{s}) + \sqrt{\Sigma_5^{(1)}}}{p(\vec{s}) - \sqrt{\Sigma_5^{(1)}}}, \tag{4.64}
$$

where p is a multi-variate polynomial of mass dimension four. Since the new square-root appears in solutions of a particular quadratic equation (see 3.3.6) it can be written in the form

$$
\Sigma_5^{(1)} = b^2 - 4ac \tag{4.65}
$$

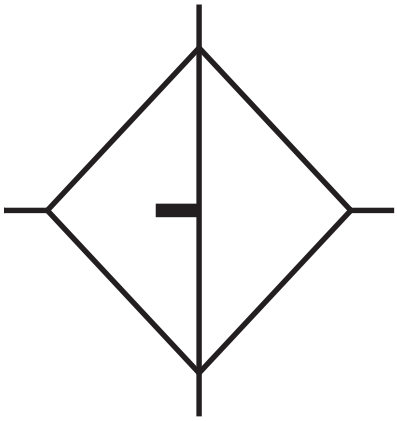

Figure 4.15: Hard non-planar double-box topology with 4 master integrals.

for some polynomials a, b, c. Assuming that p is also related to the polynomials a, b, c we could construct an independent letter which is given by

$$\frac{b - 2a + \sqrt{\Sigma_5^{(1)}}}{b - 2a - \sqrt{\Sigma_5^{(1)}}}, \tag{4.66}$$

with

$$\begin{aligned} b &= -s_{12}s_{15} + s_{12}s_{23} + 2s_{15}s_{34} - s_{23}s_{34} + s_{15}s_{45} + s_{34}s_{45}, \\ a &= s_{34}(s_{15} - s_{23} + s_{45}), \\ c &= s_{15}(-s_{12} + s_{34} + s_{45}). \end{aligned} \tag{4.67}$$

From the position of the last letter in the DE we concluded that it has to depend on both $\sqrt{\Sigma_5^{(1)}}$ and tr_5. We made the ansatz

$$\frac{\tilde{\Omega}^{--}\tilde{\Omega}^{++}}{\tilde{\Omega}^{-+}\tilde{\Omega}^{+-}}, \tag{4.68}$$

with $\tilde{\Omega}^{\pm\pm} = \tilde{p}(\vec{s}) \pm \sqrt{\Sigma_5^{(1)}} \pm \mathrm{tr}_5$. The polynomial $\tilde{p}$ was obtained by investigating a univariate cut DE of the corresponding subtopology which could be computed analytically. We found $\tilde{p} = q^2 s_{34}$. Finally, we completed the alphabet by all permutations of these four new letters and obtained the full planar- and hexa-box alphabet with 204 letters.
We organize the symbol alphabet in the following form. The letters are grouped into permutation orbits generated by a single element. Since letters may be invariant under some of the permutations of the massless momenta operators $\tilde{\sigma}$ which generate these orbits are actually not permutations themselves but equivalence classes of permutations modulo some sub-group G of S_4, so we have $\tilde{\sigma} \in S_4/G$. The sub-group G is the permutation group of a subset of the massless external legs. So e.g. $S_3[3, 4, 5]$ contains all permutations of p_3, p_4 and p_5 among each other. A second organizing principle is the behaviour of a letter under flipping the sign of each of the three square-root types $\sqrt{\Sigma_5}, \sqrt{\Delta_3}$ or tr_5 which we refer to as the action of the *Galois group*. In total, there are 127 Galois-invariant letters and 77 letters which transform in a nontrivial way under the Galois group.

In the following, we present the complete set of permutation orbits organized first by the Galois property and then by the mass dimension. To achieve a compact representation we again use the tr_+ symbol as defined in eq. (4.25).
We start with the Galois invariant letters

$$\begin{aligned}
W_1 &= q^2, \\
\{W_2,\dots,W_5\} &= \{\sigma\left(s_{12}\right) : \sigma \in S_4/S_3[3,4,5]\}, \\
\{W_6,\dots,W_{11}\} &= \{\sigma\left(s_{23}\right) : \sigma \in S_4/(S_2[2,3]\times S_2[4,5])\}, \\
\{W_{12},\dots,W_{15}\} &= \{\sigma\left(2\,p_1\cdot p_2\right) : \sigma \in S_4/S_3[3,4,5]\}, \\
\{W_{16},\dots,W_{27}\} &= \{\sigma\big(2\,p_2\cdot(p_3+p_4)\big) : \sigma \in S_4/S_2[3,4]\}, \\
\{W_{28},\dots,W_{33}\} &= \{\sigma\big(\mathrm{tr}_+(1\,2\,1\,5)\big) : \sigma \in S_4/(S_2[2,5]\times S_2[3,4])\}, \\
\{W_{34},\dots,W_{45}\} &= \{\sigma\big(\mathrm{tr}_+(1\,2\,1\,[4+5])\big) : \sigma \in S_4/S_2[4,5]\}, \\
\{W_{46},\dots,W_{57}\} &= \{\sigma\big(\mathrm{tr}_+(1\,[2+3]\,4\,[2+3])\big) : \sigma \in S_4/S_2[2,3]\}, \\
\{W_{58},\dots,W_{69}\} &= \{\sigma\big(\mathrm{tr}_+(1\,2\,[4+5]\,[2+3])\big) : \sigma \in S_4/S_2[4,5]\}, \\
\{W_{70},\dots,W_{93}\} &= \{\sigma\big(\mathrm{tr}_+(1\,2\,3\,4)-\mathrm{tr}_+(1\,2\,4\,5)\big) : \sigma \in S_4\}, \\
\{W_{94},\dots,W_{117}\} &= \{\sigma\big(\mathrm{tr}_+(1\,2\,1\,[1+5]\,4\,[1+5])\big) : \sigma \in S_4\}.
\end{aligned} \tag{4.69}$$

Note that although a particular letter can be written in terms of tr_+ it still can be Galois-invariant. The non-trivial letters under the Galois group are

$$\begin{aligned}
\{W_{118},\dots,W_{123}\} &= \left\{\sigma\left(\frac{s_{12}+s_{13}+\sqrt{\Delta_3^{(1)}}}{s_{12}+s_{13}-\sqrt{\Delta_3^{(1)}}}\right) : \sigma \in S_4/(S_2[2,3]\times S_2[4,5])\right\}, \\
\{W_{124},\dots,W_{129}\} &= \left\{\sigma\left(\frac{s_{12}-s_{13}+\sqrt{\Delta_3^{(1)}}}{s_{12}-s_{13}-\sqrt{\Delta_3^{(1)}}}\right) : \sigma \in S_4/(S_2[2,3]\times S_2[4,5])\right\}, \\
\{W_{130},\dots,W_{137}\} &= \left\{\sigma\left(\frac{\mathrm{tr}_+(1\,2\,3\,4)}{\mathrm{tr}_-(1\,2\,3\,4)}\right) : \sigma \in \mathcal{S}\right\}, \\
\{W_{138},\dots,W_{161}\} &= \left\{\sigma\left(\frac{\mathrm{tr}_+(1\,5\,3\,[1+2])}{\mathrm{tr}_-(1\,5\,3\,[1+2])}\right) : \sigma \in S_4\right\}, \\
\{W_{162},\dots,W_{185}\} &= \left\{\sigma\left(\frac{s_{12}s_{23}+s_{23}s_{34}-s_{34}s_{45}+s_{45}s_{15}-s_{12}s_{15}+\sqrt{\Sigma_5^{(1)}}}{s_{12}s_{23}+s_{23}s_{34}-s_{34}s_{45}+s_{45}s_{15}-s_{12}s_{15}-\sqrt{\Sigma_5^{(1)}}}\right) : \sigma \in S_4\right\}, \\
\{W_{186},\dots,W_{188}\} &= \left\{\sigma\left(\frac{\Omega^{--}\Omega^{++}}{\Omega^{-+}\Omega^{+-}}\right) : \sigma \in S_4/(S_2[2,3]\times S_2[4,5]\times S_2[s_{23},s_{45}])\right\}, \\
\{W_{189},\dots,W_{194}\} &= \left\{\sigma\left(\frac{\tilde\Omega^{--}\tilde\Omega^{++}}{\tilde\Omega^{-+}\tilde\Omega^{+-}}\right) : \sigma \in S_4/(S_2[3,4]\times S_2[2,5])\right\},
\end{aligned} \tag{4.70}$$

where

$$\begin{aligned}\Omega^{\pm\pm} &= s_{12}s_{15} - s_{12}s_{23} - s_{15}s_{45} \pm s_{34}\sqrt{\Delta_3^{(1)}} \pm \sqrt{\Delta_5},\\ \tilde{\Omega}^{\pm\pm} &= q^2 s_{34} \pm \mathrm{tr}_5 \pm \sqrt{\Sigma_5^{(1)}},\end{aligned} \tag{4.71}$$

and the set of permutations $\mathcal{S}$ is given by

$$\begin{aligned}\mathcal{S} = \big\{&\{1,2,3,4,5\},\{1,2,3,5,4\},\{1,2,4,3,5\},\{1,2,4,5,3\},\\ &\{1,2,5,3,4\},\{1,3,2,4,5\},\{1,3,2,5,4\},\{1,4,2,5,3\}\big\}.\end{aligned} \tag{4.72}$$

Finally, the square-roots are letters themselves

$$\begin{aligned}\{W_{195},\ldots,W_{197}\} &= \left\{\sigma\left(\sqrt{\Delta_3^{(1)}}\right) : \sigma \in S_4/(S_2[2,3]\times S_2[4,5]\times S_2[s_{23},s_{45}])\right\},\\ W_{198} &= \mathrm{tr}_5,\\ \{W_{199},\ldots,W_{204}\} &= \left\{\sigma\left(\sqrt{\Sigma_5^{(1)}}\right) : \sigma \in S_4/(S_2[3,4]\times S_2[2,5])\right\}.\end{aligned} \tag{4.73}$$

The letters in the orbits of W_{58}, W_{162}, W_{189} and W_{199} cannot be obtained from the closure of the planar alphabet. The complete alphabet expressed in terms of Mandelstam invariants is given in the ancillary file `anc/alphabet.m` attached to [56].

4.2.4 Construction of the canonical DE

With the pure basis and the extended alphabet we can proceed with reconstruction of the canonical differential equation

$$\mathrm{d}\mathbf{G}^{[f]} = \epsilon \sum_{a=1}^{N} M_{a,f}\,\mathrm{dlog}(W_a)\mathbf{G}^{[f]}, \tag{4.74}$$

where N is the size of the alphabet. Similar to the planar case, the number of actually contributing letters with nonzero $M_{a,f}$ is much smaller than the total number of letters. Contributing letters are given in table 4.4.

topology	relevant letters	# of relevant letters
mzz	$W_1, W_2, W_4, \cdots, W_{12}, W_{14}, \cdots, W_{17}, W_{21}, W_{22}, W_{24}, W_{25},$ $W_{27}, \cdots, W_{30}, W_{33}, W_{70}, W_{71}, W_{118}, W_{123}, W_{124}, W_{129}, \cdots, W_{134},$ $W_{137}, W_{186}, W_{195}, W_{198}$	39
zmz	$W_1, W_2, W_5, \cdots, W_{16}, W_{19}, W_{21}, W_{22}, W_{24}, W_{27}, \cdots, W_{33}, W_{70},$ $W_{72}, W_{91}, W_{93}, W_{118}, W_{119}, W_{122}, \cdots, W_{125}, W_{128}, \cdots, W_{137},$ $W_{162}, W_{164}, W_{183}, W_{185}, \cdots, W_{187}, W_{189}, W_{195}, W_{196}, W_{198}, W_{199}$	56
zzz	$W_1, W_2, W_4, \cdots, W_{16}, W_{20}, \cdots, W_{22}, W_{25}, W_{27}, W_{28}, W_{30}, \cdots, W_{33},$ $W_{46}, W_{52}, W_{67}, W_{69}, W_{94}, W_{108}, W_{112}, W_{117}, W_{118}, W_{120}, W_{121}, W_{123},$ $W_{124}, W_{126}, W_{127}, W_{129}, W_{131}, \cdots, W_{138}, W_{152}, W_{156}, W_{161}, W_{163},$ $W_{166}, W_{177}, W_{179}, W_{186}, W_{188}, W_{190}, W_{195}, W_{197}, W_{198}, W_{200}$	63

Table 4.4: Relevant letters for the hexa-box topologies.

The input data for the reconstruction are numerical differential equations computed at 105 points for both mzz and zmz topologies and at 125 points for the zzz topology. The numerical IBP reduction was performed using `FIRE6` [154] reduction code on the `NEMO` cluster. All kinematic invariants were computed from randomly chosen rational external momenta and are so not only rational by themselves but also automatically rationalize tr_5 (see appendix A for details on constructing external momenta). The IBP reduction took $8 - 11\,\mathrm{h}$ per point. We chose $\epsilon_0 := \frac{4-D_0}{2} = \frac{13}{8}$ for all three topologies. Due to presence of multiple square-roots inside the numerical connections, the computation of the M_a matrices was performed using 150 digits floating point numbers followed by reconstructing the rational entries via the `Mathematica Rationalize[]` routine.
Like in the planar case, the first-entry condition is sufficient to compute the weight zero part of the integrals. Note that for non-planar integrals adjacent legs do not have to be cyclicly ordered. So is e.g. $s_{14} = -s_{15} + s_{23} - s_{45} + q^2$ a first-entry letter for the mzz topology. The first-entry letters per topology are summarized in table 4.5.

topology	first-entry letters
mzz	$W_1, W_2, W_4, \cdots, W_6, W_9, \cdots, W_{11}$
zmz	$W_1, W_2, W_5 \cdots, W_7, W_9, \cdots, W_{11}$
zzz	$W_1, W_2, W_4 \cdots, W_6, W_8, W_9, W_{11}$

Table 4.5: First-entry letters of the hexa-box topologies.

The weight zero solution has to be a constant vector fulfilling

$$M_{a,f}\mathbf{G}_f^{(0)} = 0, \quad a \in \{1, \cdots, N\} \setminus \mathcal{I}^{[f]}_{\text{1-entry}}, \tag{4.75}$$

where $\mathcal{I}^{[f]}_{\text{1-entry}}$ denotes the set of indices corresponding to first-entry letters. In all three cases, this gives enough constraints to determine the weight zero solution up to an overall constant which can be extracted from a single-scale integral. The results are

$$\begin{aligned}
\mathbf{G}^{(0)}_{\text{mzz}} = \Big\{ & 0, 0, 8, -\frac{1}{2}, 1, -2, -2, 0, \frac{9}{2}, 0, 8, 0, 0, 0, 0, 0, 4, 2, 0, 2, 0, 2, 0, 0, 0, 0, 0, 0, -4, 0, -4, 0, 0, 0, 0, 0, 0, 0, 0, \\
& 0, 0, 0, 0, 0, 0, 0, 0, 2, 0, 2, 0, 2, 0, 2, 0, 4, 0, 4, 0, 0, 0, 0, 1, 0, 1, -4, -4, -4, 0, 0, 0, 4, 4, 4, 4, 4, 4, 4, 4, 0, 4, \\
& 0, 4, 4, 4, 4, 4, 4, 4, 4, 4 \Big\}, \\
\mathbf{G}^{(0)}_{\text{zmz}} = \{ & 0, 0, 0, -1, -1, -1, -1, 2, 0, 0, 2, 0, 0, 0, 0, 0, 0, 8, 4, 2, 0, 2, 0, 0, 0, 0, 0, 0, 0, 0, 0, 0, 0, 0, 0, 0, 0, 0, 0, 0, 0, \\
& 0, 0, 0, 0, 0, 4, 0, 4, 0, 4, 0, 4, 0, 4, 0, 4, 0, 4, 0, 4, 0, 0, 0, 0, 0, 0, 0, 0, 0, 0, 0, 0, 4, 4, 4, 4, 4, 4, 4, 4, 4, 0, 4, 0, 4, \\
& 4, 4, 4, 4, 4, 4, 4, 4 \}, \\
\mathbf{G}^{(0)}_{\text{zzz}} = \{ & 0, 0, 4, 6, 4, 4, 0, 0, 0, 6, 4, 4, 0, 0, 0, 0, 4, 4, 0, 0, 0, 0, 0, 0, 8, 0, 0, 0, 0, 0, 0, 0, 0, 4, 0, 4, 0, 0, -4, 0, \\
& -4, 0, 0, 0, 0, 0, 0, 0, 0, 6, 6, 6, 0, 0, 0, 6, 6, 6, 0, 0, 0, 0, 0, 0, 0, -4, 0, 0, 0, 0, 0, 4, 0, 4, 0, 4, 0, 4, 0, 4, 0, 4, \\
& 0, 4, 0, 4, 0, 0, 0, 0, 0, 0, 0, 0, 0, 0, 0, 0, 0, -4, -4, -4, -4, -4, -4, 0, 0, 0, 0, 4, 4, 4, 4, 4, 4, 4, 4, 4, 0, 4, \\
& 0, 4, 0, 4, 0, 4, 4, 4, 4, 4, 4, 4, 4, 4, 4, 4 \}.
\end{aligned} \tag{4.76}$$

Beginning with the weight zero solution, the integral symbols can be computed straight-forwardly. We provided a `Mathematica` code for automated symbol computation in the ancillary files of [56].

As in the planar case, we checked that the Steinmann relations for the hexa-box topologies are fulfilled. The number of forbidden pairs differs here from topology to topology. So, the overlapping channels of mzz and zzz are $\{s_{12}, s_{14}, s_{15}\}$, corresponding to the letters $\{W_2, W_4, W_5\}$. The only forbidden pair of zmz is $\{s_{12}, s_{15}\}$, corresponding to the letters $\{W_2, W_5\}$. In the planar case, also so-called *extended* Steinmann relations (see 4.1.4) hold while here the situation ia again topology-dependent. We found

- **mzz**: The extended Steinmann relations are satisfied. Indeed, we found that

$$M_2\, M_4 = M_4\, M_2 = M_2\, M_5 = M_5\, M_2 = M_4\, M_5 = M_5\, M_4 = 0\,. \tag{4.77}$$

- **zmz**: The extended Steinmann relations are not satisfied. Through weight six, the master integrals whose symbols involve the sequence $[\ldots, W_2, W_5, \ldots]$ are at positions $\{1, 2, 3, 8, 9, 10\}$ and the integrals whose symbols involve the sequence $[\ldots, W_5, W_2, \ldots]$ are at positions $\{1, 2, 3, 11, 12, 13\}$.

- **zzz**: The extended Steinmann relations are satisfied for some pairs of channels, but not all. We found that

$$M_2\, M_5 = M_5\, M_2 = M_4\, M_5 = M_5\, M_4 = 0\,, \tag{4.78}$$

  which implies that letters W_2 and W_4 never appear next to W_5. On the other hand, through weight six, the master integrals whose symbols involve the sequence $[\ldots, W_2, W_4, \ldots]$ are at positions $\{1, 2, 3, 10, 11, 12, 13, 14, 15\}$ and the integrals whose symbols involve the sequence W_4, W_2 are at positions $\{1, 2, 3, 4, 5, 6, 7, 8, 9\}$.

It would be interesting to investigate further which integrals satisfy the extended Steinmann relations and which not.

4.2.5 Numerical integration and validation

The topic of this section is the numerical integration of the canonical DE obtained in 4.2.4 which is performed by methods of section 3.5. We discuss the computation of boundary conditions and present high-precision target values in all physical regions. Finally, we discuss the validation of our result.

Numerical results

First, we computed the initial values for the three topologies in their specific Euclidean regions. In contrast to the planar case where a common Euclidean region for all topologies exists and is given by $s_{ij} < 0, q^2 < 0$ for all cyclic Mandelstam invariants, here each topology has its own Euclidean region since additional constraints on non-cyclic invariants are needed. The three Euclidean regions are

$$\begin{aligned}
\mathcal{E}_{\text{mzz}} &= \{\vec{s} \in \mathbb{R}^6 \,|\, q^2 < 0, s_{12} < 0, s_{23} < 0, s_{34} < 0, s_{45} < 0, s_{15} < 0, s_{35} < 0, s_{14} < 0\}\,, \\
\mathcal{E}_{\text{zmz}} &= \{\vec{s} \in \mathbb{R}^6 \,|\, q^2 < 0, s_{12} < 0, s_{23} < 0, s_{34} < 0, s_{45} < 0, s_{15} < 0, s_{35} < 0, s_{24} < 0\}\,, \\
\mathcal{E}_{\text{zzz}} &= \{\vec{s} \in \mathbb{R}^6 \,|\, q^2 < 0, s_{12} < 0, s_{23} < 0, s_{34} < 0, s_{45} < 0, s_{15} < 0, s_{25} < 0, s_{14} < 0\}\,.
\end{aligned} \tag{4.79}$$

Note that all three hexa-box Euclidean regions are subsets of the planar Euclidean region. Next, we give the initial points $\vec{s}_{\mathcal{E}_f,0}$ and the paths we used to collect enough constraints in order to

determine $\mathbf{G}^{[f]}(\vec{s}_{\mathcal{E}_f,0})$ for each of the three topologies (see 3.5.3 for details).
For mzz we choose

$$\vec{s}_{\mathcal{E}_{\text{mzz}},0} = (-13,-7,-21,-2,-4,-10)\,. \tag{4.80}$$

Then, we transport the solution from this point to the three points

$$\begin{aligned}
\vec{s}_{\mathcal{E}_{\text{mzz}},1} &= \left(-\frac{6829}{10},-\frac{14777}{20},-\frac{903}{10},-\frac{14677}{20},-\frac{27}{20},-\frac{3389}{5}\right)\,,\\
\vec{s}_{\mathcal{E}_{\text{mzz}},2} &= \left(-\frac{4874}{5},-\frac{3913}{4},-\frac{2079}{20},-\frac{9407}{10},-\frac{65}{4},-\frac{19426957}{18640}\right)\,,\\
\vec{s}_{\mathcal{E}_{\text{mzz}},3} &= \left(-\frac{193817}{20},-\frac{192017}{20},-\frac{147}{2},-\frac{191917}{20},-\frac{11}{20},-\frac{38743}{4}\right)\,,
\end{aligned} \tag{4.81}$$

and obtain 82 independent conditions. The four still undetermined initial conditions all correspond to known single-scale integrals.
For the zzz topology, we choose

$$\vec{s}_{\mathcal{E}_{\text{zzz}},0} = (-13,-7,-31,-22,-4,-17) \tag{4.82}$$

as the initial point.
If we consider the paths from $\vec{s}_{\mathcal{E}_{\text{zzz}},0}$ to the three points

$$\begin{aligned}
\vec{s}_{\mathcal{E}_{\text{zzz}},1} &= \left(-\frac{117}{55},-\frac{8}{21},-\frac{68}{139},-\frac{6}{127},-\frac{83}{173},-\frac{61}{82}\right)\,,\\
\vec{s}_{\mathcal{E}_{\text{zzz}},2} &= \left(-\frac{446}{137},-\frac{31}{119},-\frac{40}{53},-\frac{15}{137},-\frac{32}{27},-\frac{149}{96}\right)\,,\\
\vec{s}_{\mathcal{E}_{\text{zzz}},3} &= \left(-\frac{104}{61},-\frac{39}{55},-\frac{59}{115},-\frac{21}{184},-\frac{1}{2},-\frac{88}{145}\right)\,,
\end{aligned} \tag{4.83}$$

we obtain 134 independent conditions. This is the maximal number we could have expected given that there are 135 master integrals in this topology, and we can fix the remaining normalisation by the explicit computation of the pure q^2-sunrise integral which, in our conventions, is given by

$$\mathbf{G}^{[\text{zzz}]}_{135} = 4(-q^2)^{-2\epsilon}\frac{\Gamma(1-\epsilon)^3\Gamma(1+2\epsilon)}{\Gamma(1-3\epsilon)}. \tag{4.84}$$

Finally, for the zmz topology we determined the initial condition at

$$\vec{s}_{\mathcal{E}_{\text{zmz}},0} = (-13,-7,-21,-2,-4,-30)\,. \tag{4.85}$$

We consider the paths to

$$\begin{aligned}
\vec{s}_{\mathcal{E}_{\text{zmz}},1} &= \left(-\frac{155}{128},-\frac{103}{83},-\frac{51}{109},-\frac{17}{82},-\frac{69}{197},-\frac{101}{85}\right)\,,\\
\vec{s}_{\mathcal{E}_{\text{zmz}},2} &= \left(-\frac{69}{43},-\frac{148}{137},-\frac{12}{77},-\frac{57}{89},-\frac{23}{97},-\frac{77}{73}\right)\,,\\
\vec{s}_{\mathcal{E}_{\text{zmz}},3} &= \left(-\frac{181}{105},-\frac{79}{88},-\frac{21}{74},-\frac{38}{67},-\frac{33}{103},-\frac{89}{93}\right)\,,
\end{aligned} \tag{4.86}$$

and collect 62 constraints along the way. The undetermined integrals are either simple integrals that can be computed to arbitrary order in ϵ, or integrals that appear in the mzz or zzz hexa-box

topologies (sometimes with different order of the massless momenta) and can thus be computed using differential equations and boundary conditions determined for these two topologies.
These computations were done independently using the public code `DiffExp` [72] and an own implementation. With the latter we get results with 100 digits precision. We validated this result by the code of [72] up to 25 digits. Unfortunately, we were not able to obtain higher precision from the latter.
Using these boundary points we computed all integrals in all six physical regions (see table 3.1) at the same set of points we used in the planar case (eq.(4.87)) with the publicly available code [72]. The physical points are

$$\begin{aligned}
\vec{s}_{\text{ph-1}} &= \left(\frac{137}{50}, -\frac{22}{5}, \frac{241}{25}, -\frac{377}{100}, \frac{13}{50}, \frac{249}{50}\right),\\
\vec{s}_{\text{ph-2}} &= \left(\frac{137}{50}, -\frac{22}{5}, -\frac{91}{100}, -\frac{377}{100}, -\frac{9}{10}, \frac{249}{50}\right),\\
\vec{s}_{\text{ph-3}} &= \left(\frac{137}{50}, -\frac{22}{5}, -\frac{91}{100}, \frac{13}{50}, -\frac{9}{10}, -\frac{9}{4}\right),\\
\vec{s}_{\text{ph-4}} &= \left(\frac{137}{50}, \frac{357}{50}, -\frac{91}{100}, \frac{241}{25}, -\frac{9}{10}, \frac{249}{50}\right),\\
\vec{s}_{\text{ph-5}} &= \left(\frac{137}{50}, \frac{357}{50}, -\frac{91}{100}, -\frac{161}{100}, -\frac{9}{10}, -\frac{9}{4}\right),\\
\vec{s}_{\text{ph-6}} &= \left(\frac{137}{50}, \frac{357}{50}, \frac{13}{50}, -\frac{161}{100}, \frac{241}{25}, -\frac{9}{4}\right).
\end{aligned} \tag{4.87}$$

The computation was done with a precision of 100 digits. Note that for some of the physical points we took an indirect path consisting of two straight line segments in order to avoid crossing of a non-physical singularity.

Validation of results

In order to validate our results we performed several checks:

- Boundary value computations were done with two independent in-house implementations of the algorithm described in 3.5 and additionally with the public code `DiffExp` [72] at lower precision.
- Boundary values for the integrals in the mzz topology and some selected integrals in two other topologies were reproduced by the authors of reference [53].
- We verified the absence of non-physical branch cuts in the Euclidean region at weight five which gives a non-trivial check of the weight four result.
- As consistency check of the evaluations in the physical regions, we checked that we get the same results at each point independently of which point we took as boundary point.
- We compared results in the physical regions obtained with code [53] with one of our two in-house implementations at lower precision.

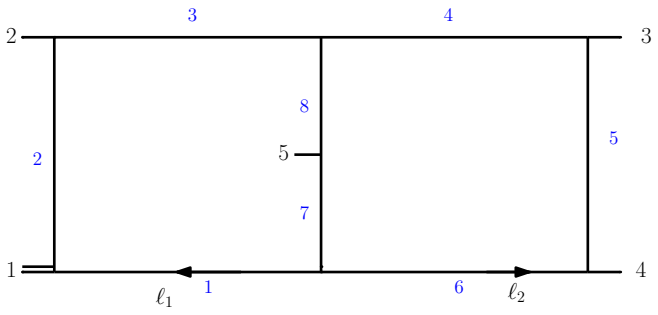

(a) $I^{[\mathrm{zm}]}[\vec{\nu}]$

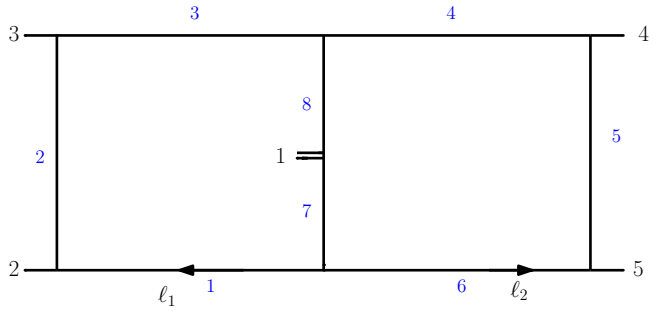

(b) $I^{[\mathrm{zz}]}[\vec{\nu}]$

Figure 4.16: Two-loop five-point non-planar double-pentagon topologies with one off-shell leg. The double external line with label 1 denotes the massive leg.

4.3 First look at the double-pentagon sector

In this section, we give first results on the pure bases for the both double-pentagon topologies which complete the set of the two-loop five-point integral topologies with one massive leg. The current status of the work we want to present here is the complete pure basis for the topology 4.16a in 4.16 and an *on-shell* pure basis for the more complicated topology 4.16b in 4.16 where the off-shell completion of the numerator insertion for one top-level integral is still missing.

4.3.1 Definition of topologies

Let us first define the double-pentagon integral topologies depicted in 4.16. In analogy to the cases already considered, they are denoted by $\mathbf{I}^{[f]}_{dp}$ with $f \in \{\mathrm{zm}, \mathrm{zz}\}$ where the letters label the legs attached to the left rung of the graphs. We define the integral families as

$$I^{[f]}_{dp}[\vec{\nu}] = e^{2\epsilon\gamma_E} \int \frac{d^D\ell_1}{i\pi^{D/2}} \frac{d^D\ell_2}{i\pi^{D/2}} \frac{\rho_{9,f}^{-\nu_9}\ \rho_{10,f}^{-\nu_{10}}\ \rho_{11,f}^{-\nu_{11}}}{\rho_{1,f}^{\nu_1}\ \rho_{2,f}^{\nu_2}\ \rho_{3,f}^{\nu_3}\ \rho_{4,f}^{\nu_4}\ \rho_{5,f}^{\nu_5}\ \rho_{6,f}^{\nu_6}\ \rho_{7,f}^{\nu_7}\ \rho_{8,f}^{\nu_8}}\,, \tag{4.88}$$

where $D = 4 - 2\epsilon$ as usual. The lists of inverse propagators and ISP's are given by

$$\begin{aligned}
\vec{\rho}_{\mathrm{zm}} = \big\{&\ell_1^2, (\ell_1+p_1)^2, (\ell_1+p_1+p_2)^2, (\ell_2+p_3+p_4)^2, (\ell_2+p_4)^2, \ell_2^2, (\ell_1+\ell_2)^2, (\ell_1+\ell_2-p_5)^2 \\
&(\ell_1+p_4)^2, (\ell_2+p_1)^2, (\ell_2+p_1+p_2)^2\big\}\,, \\
\vec{\rho}_{\mathrm{zz}} = \big\{&\ell_1^2, (\ell_1+p_2)^2, (\ell_1+p_2+p_3)^2, (\ell_2+p_4+p_5)^2, (\ell_2+p_5)^2, \ell_2^2, (\ell_1+\ell_2)^2, (\ell_1+\ell_2-p_1)^2, \\
&(\ell_1+p_5)^2, (\ell_2+p_3)^2, (\ell_2+p_2+p_3)^2\big\}\,.
\end{aligned} \tag{4.89}$$

We have $\nu_i \leq 0$ for $i \geq 9$ and the loop-momentum routing can be read off the diagram 4.16. All external momenta are considered to be incoming. The master integral count for the both topologies is

$$\dim(V_{dp}^{[\mathrm{zm}]}) = 142, \quad \dim(V_{dp}^{[\mathrm{zz}]}) = 179. \tag{4.90}$$

Except for the double-pentagons themselves with 9 master integrals each, there are no new five-point subtopologies. All integrals which appear only in the double-pentagon topologies belong to known three- and four-point topologies.

4.3.2 Pure basis

We discuss the pure basis construction for the double-pentagon topologies here separately since it has some new aspects compared to the treatment of 3.3. The master integrals are divided into the parity-even and the parity-odd groups with 3 and 6 integrals respectively for each of the both topologies. The numerators for the parity-odd integrals are constructed out of two types of insertions. There are μ-insertions on one hand and derivatives of the Baikov polynomial with respect to inverse propagators on the other hand. Both types of insertions have already been used for the massless double-pentagon integral [47, 49]. Let us begin with the zz-topology. Since we have two pentagon-type sub-loops one natural insertion to start with is

$$\mathcal{N}^{(1)}_{\mathrm{dp,zz}} \sim \mathrm{tr}_5 \mu_{12}. \tag{4.91}$$

From dimensional analysis we conclude that we still need a kinematic prefactor of mass-dimension two. We fixed it by a functional reconstruction of the $\mathcal{O}(\epsilon^0)$-part of the connection using the momentum-twistor parametrization of appendix appendix: Parameter and integrating it out, similar to the procedure of section 3.3.5 . The result reads

$$\mathcal{N}^{(1)}_{\mathrm{dp,zz}} = \sqrt{\Delta_3^{(1)}}\mathrm{tr}_5 \mu_{12}. \tag{4.92}$$

Following a similar argument, we construct

$$\begin{aligned} \mathcal{N}^{(2)}_{\mathrm{dp,zz}} &= \mathrm{tr}_5 \left[-s_{23}\mu_{22} + \frac{1}{2}(q^2 - s_{23} - s_{45})\mu_{12} \right], \\ \mathcal{N}^{(3)}_{\mathrm{dp,zz}} &= \mathrm{tr}_5 \left[-s_{45}\mu_{11} + \frac{1}{2}(q^2 - s_{23} - s_{45})\mu_{12} \right]. \end{aligned} \tag{4.93}$$

For the three remaining parity-odd insertions we use the observation from [49] that the six-dimensional massless double-pentagon with a doubled propagator is pure up to a kinematic prefactor. In the massive case, adding a single double propagator was not always sufficient but we managed to find a pure linear combination of insertions with double propagators. Let us make a technical remark. Using IBP relations in the Baikov space, we can trade a double propagator for a derivative of the numerator insertion with respect to the corresponding inverse propagator. So we can replace a six-dimensional double-pentagon integral with the i-th propagator being doubled by a four-dimensional double-pentagon integral with a nontrivial numerator insertion

$$I_{dp}^{(D=6-2\epsilon)} \left[\frac{1}{\rho_i} \right] \sim I_{dp}^{(D=4-2\epsilon)} \left[\frac{1}{G} \frac{\partial P}{\partial \rho_i} \right]. \tag{4.94}$$

We use the right-hand-side representation of the integrand since it is more suitable for working with cut differential equations. In the following, we use the short notation $P_i := \frac{\partial P}{\partial \rho_i}$. We used the

same approach for both topologies. For one of the purity-odd zm integrals an additional *off-shell* correction was needed (see eq.(4.95)).
Finally, we have to find the parity-even insertions. Two of the three insertions per topology can be taken from reference [212] where a *prescriptive integrand basis* for non-planar massless six-particle scattering was given. These integrands are constructed to have support on a single maximal cut and normalized in order to have unit leading singularities. So they naturally give rise to pure integrals. The insertions are given in the literature in terms of chiral traces $\mathrm{tr}_+[...]$. In order to extract the parity-even part, we simply replaced $\mathrm{tr}_+[...]$ by the standard Dirac trace $\mathrm{tr}[...]$. For practical use, all traces were expressed in terms of inverse propagators, ISP's and kinematic invariants using `FeynCalc` [228, 229]. To obtain the last integrand we took one of the parity-even insertions of the massless double-pentagon of reference [49] which is also given in terms of Dirac traces and replaced the massless leg by the massive one. In case of the zm-topology, this was already sufficient to obtain a pure integral while for the zz-topology we had to add contributions proportional to the two other parity-even integrands and to fix the overall kinematic prefactor. However, for this integral we still need to determine the off-shell correction.

zm topology

$$
\begin{aligned}
\mathcal{N}^{(1)}_{\mathrm{dp},zm} =&\epsilon^4 \mathrm{tr}_5 \left(s_{12}-s_{34}\right)\mu_{12},\\
\mathcal{N}^{(2)}_{\mathrm{dp},zm} =&\epsilon^4 \mathrm{tr}_5 s_{12}(\mu_{22}+\mu_{12}),\\
\mathcal{N}^{(3)}_{\mathrm{dp},zm} =&\epsilon^4 \mathrm{tr}_5 (s_{34}\mu_{11}+s_{12}\mu_{12}),\\
\mathcal{N}^{(4)}_{\mathrm{dp},zm} =&\epsilon^4 \frac{1}{\mathrm{tr}_5}\left[(s_{12}-q^2)P_3-\frac{q^2 s_{34}}{s_{12}}P_4-\frac{1}{2}\frac{q^2}{s_{12}}(s_{12}-s_{34})\mathrm{tr}_5^2\mu_{12}+\frac{3}{4}q^2\mathrm{tr}_5^2(\mu_{22}+\mu_{12})\right.\\
&\left.+\frac{1}{4}\frac{q^2}{s_{12}}(s_{34}\mu_{11}+s_{12}\mu_{12})\mathrm{tr}_5^2+R^{(5)}_{\mathrm{dp,zm}}\right],\\
\mathcal{N}^{(5)}_{\mathrm{dp},zm} =&\epsilon^4 \frac{s_{34}}{\mathrm{tr}_5}P_4,\\
\mathcal{N}^{(6)}_{\mathrm{dp},zm} =&\epsilon^4 \frac{s_{12}-s_{34}}{\mathrm{tr}_5}P_8,\\
\mathcal{N}^{(7)}_{\mathrm{dp},zm} =&\epsilon^4 \mathrm{Tr}\left[\not{p}_2(\not{\ell}_1+\not{p}_1)\not{\ell}_1(\not{\ell}_1+\not{\ell}_2)(\not{\ell}_1+\not{\ell}_2-\not{p}_5)(\not{\ell}_2+\not{p}_3+\not{p}_4)(\not{\ell}_2+\not{p}_4)\not{p}_4\right],\\
\mathcal{N}^{(8)}_{\mathrm{dp},zm} =&\epsilon^4 \frac{1}{2}\left(\mathrm{Tr}\left[\not{p}_2(\not{\ell}_1+\not{\ell}_2)\not{\ell}_1\not{\ell}_2(\not{\ell}_2+\not{p}_4)\not{p}_3(\not{\ell}_1+\not{\ell}_2-\not{p}_5)(\not{\ell}_1+\not{\ell}_2)\right]\right.\\
&\left.-\mathrm{Tr}\left[\not{p}_3(\not{\ell}_2+\not{p}_4)\not{\ell}_2\not{\ell}_1(\not{\ell}_1+\not{p}_1)\not{p}_2(\not{\ell}_1+\not{\ell}_2-\not{p}_5)(\not{\ell}_1+\not{\ell}_2)\right]\right),\\
\mathcal{N}^{(9)}_{\mathrm{dp},zm} =&\epsilon^4\left(\mathrm{Tr}\left[\not{p}_5\not{p}_1\not{p}_2\not{p}_3(\not{\ell}_2+\not{p}_4)(\not{\ell}_1+\not{\ell}_2)\not{\ell}_1(\not{p}_3+\not{p}_4)\right]-\rho_1\rho_4\mathrm{Tr}\left[\not{p}_5\not{p}_1\not{p}_2\not{p}_3\right]\right).
\end{aligned}
\tag{4.95}
$$

The off-shell correction term $R^{(4)}_{\mathrm{dp,zm}}$ is given by

$$
\begin{aligned}
R^{(4)}_{\mathrm{dp,zm}} =& \frac{1}{4}\frac{q^2}{s_{12}}\mathrm{tr}_5^2\left[(\mu_{11}\rho_6+\mu_{12}(\rho_8-\rho_7)+\left(-2\mu_{12}-2\mu_{22}+\frac{q^2}{2\epsilon}\frac{\mu_{12}+\mu_{22}}{\rho_2}\right)\rho_3\right.\\
&\left.-\frac{1}{4\epsilon}\left(-\mu_{22}\frac{\rho_1\rho_8}{\rho_7}+\mu_{22}\frac{\rho_1\rho_3}{\rho_2}+\mu_{11}\frac{\rho_6\rho_8}{\rho_7}+\mu_{11}\frac{\rho_4\rho_7}{\rho_8}-\mu_{11}\frac{\rho_4\rho_6}{\rho_5}+2\mu_{12}\frac{\rho_3\rho_6}{\rho_8}\right)\right].
\end{aligned}
\tag{4.96}
$$

zz topology

$$
\begin{aligned}
\mathcal{N}^{(1)}_{\text{dp,zz}} =&\epsilon^4 \text{tr}_5 \sqrt{\Delta_3^{(1)}}\mu_{12},\\
\mathcal{N}^{(2)}_{\text{dp,zz}} =&\epsilon^4 \text{tr}_5 \left[-s_{23}\mu_{22} + \frac{1}{2}(q^2 - s_{23} - s_{45})\mu_{12}\right],\\
\mathcal{N}^{(3)}_{\text{dp,zz}} =&\epsilon^4 \text{tr}_5 \left[-s_{45}\mu_{11} + \frac{1}{2}(q^2 - s_{23} - s_{45})\mu_{12}\right],\\
\mathcal{N}^{(4)}_{\text{dp,zz}} =&\epsilon^4 \frac{1}{\text{tr}_5}\left[(s_{23}P_3 - \frac{1}{2}(q^2 + s_{23} - s_{45})P_7 - \frac{1}{2}(q^2 + s_{23} - s_{45})\text{tr}_5^2\mu_{12}\right],\\
\mathcal{N}^{(5)}_{\text{dp,zz}} =&\epsilon^4 \frac{1}{\text{tr}_5}\left[(s_{45}P_4 - \frac{1}{2}(q^2 - s_{23} + s_{45})P_7 - \frac{1}{2}(q^2 - s_{23} + s_{45})\text{tr}_5^2\mu_{12}\right],\\
\mathcal{N}^{(6)}_{\text{dp,zz}} =&\epsilon^4 \frac{\sqrt{\Delta_3^{(1)}}}{\text{tr}_5}P_8,\\
\mathcal{N}^{(7)}_{\text{dp,zz}} =&\epsilon^4 \text{Tr}\left[\not{p}_2(\not{\ell}_1 + \not{p}_2)(\not{\ell}_1 + \not{p}_2 + \not{p}_3)(\not{\ell}_1 + \not{\ell}_2 - \not{p}_1)(\not{\ell}_1 + \not{\ell}_2)\not{\ell}_2(\not{\ell}_2 + \not{p}_5)\not{p}_4\right],\\
\mathcal{N}^{(8)}_{\text{dp,zz}} =&\epsilon^4 \text{Tr}\left[\not{p}_3(\not{\ell}_1 + \not{p}_2)\not{\ell}_1(\not{\ell}_1 + \not{\ell}_2)(\not{\ell}_1 + \not{\ell}_2 - \not{p}_1)(\not{\ell}_2 + \not{p}_4 + \not{p}_5)(\not{\ell}_2 + \not{p}_5)\not{p}_5\right],\\
\mathcal{N}^{(9)}_{\text{dp,zz}} =&\epsilon^4 \frac{\sqrt{\Delta_3^{(1)}}}{q^2 - s_{23} + s_{45}}\left(\text{Tr}\left[\not{p}_1\not{p}_2\not{p}_3\not{p}_4(\not{\ell}_2 + \not{p}_5)(\not{\ell}_1 + \not{\ell}_2)\not{\ell}_1(\not{p}_4 + \not{p}_5)\right]\right.\\
&\left. -\rho_1\rho_4 \text{Tr}\left[\not{p}_1\not{p}_2\not{p}_3\not{p}_4\right] - \frac{1}{2\epsilon^4}\mathcal{N}^{(7)}_{\text{dp,zz}} + \frac{3}{2\epsilon^4}\mathcal{N}^{(8)}_{\text{dp,zz}}\right).
\end{aligned}
\tag{4.97}
$$

The last insertion $\mathcal{N}^{(9)}_{\text{dp,zz}}$ in eq. (4.97) is only pure on-shell.

Chapter 5

Conclusion and outlook

In the last decade we have witnessed remarkable progress with NNLO predictions for multi-particle processes (two and more final states) in QCD. This progress is due to the development of new methods for computing both amplitudes and master integrals. By now, a large number of NNLO calculations for $2 \to 2$ processes are available and first results for $2 \to 3$ scattering of massless particles start to appear. With the public code `Caravel` [230] first steps towards an automated calculation of multi-leg amplitudes at two-loop were done. Recently, NNLO cross sections for $pp \to \gamma\gamma\gamma$, $pp \to \gamma\gamma j$ and $pp \to jjj$ were obtained [231–234] as first two-loop phenomenological results in five-point scattering.

In this work, we contributed to the exploration of the two-loop five-point frontier by computing five-point integrals with one off-shell leg in all planar families and three non-planar hexa-box integral families. We constructed canonical differential equations for all integral topologies and integrated them numerically with the generalized power-series approach. To avoid dealing with highly complex analytic IBP reduction we performed multiple numerical reductions and reconstructed the canonical differential equation following the procedure of reference [48].

A crucial ingredient of this approach is the pure integral basis which gives rise to the canonical differential equation. We found such bases for all mentioned topologies as well as for one of the two double-pentagon topologies, and constructed an *on-shell* pure basis for the second double-pentagon. We used a combination of heuristic and (semi)-algorithmic ideas based on several principles like loop-by-loop residue computations, dimension shifts and integrating out the $\mathcal{O}(\epsilon)$-part of the pre-canonical DE. The strategy of working with numerical DE's caused an additional difficulty for constructing pure bases since we could, at least mostly, work only at the integrand level but were not able to directly manipulate the DE. We could, at least partially, circumvent this obstacle by working with *cut* DE's and using functional reconstruction methods. However, the most crucial results have been obtained by a purely integrand-based case-by-case analysis. Although we could not provide an algorithmic way to construct pure bases for generic integral topologies, we still gained useful insights about the structure of five-point pure integrals. Explicit use of extra-dimensional μ-type objects allowed to express many pure integrands in remarkably compact form which can be found by "educated guessing". A deeper understanding of leading singularities beyond the four-dimensional limit would surely provide a better explanation of extra-dimensional pure integrands found in the present work.

A further notable result is the symbol alphabet of the planar and the hexa-box topologies which had to be constructed independently in order to use the reconstruction procedure of reference [48]. The planar alphabet has been found by combining known one-loop and four-point contributions with computing analytic cut differential equations in canonical form. In the non-planar case, four additional types of letters have been found by analyzing the structure of non-planar leading sin-

gularities. The full alphabet contains of 204 letters which can be generated by permuting 21 basic letter types including three different classes of square-root expressions and is significantly more complicated than the five-point massless alphabet which has 31 letters and only one square-root. Notably, a new type of intrinsically non-planar five-point square root appeared for the first time in two hexa-box topologies.
A further interesting observation concerns the extended Steinmann conjecture on double discontinuities of Feynman integrals. In the planar case, we confirmed it to all orders in ϵ while for two of the three hexa-box topologies the extended Steinmann relations are not satisfied.
Furthermore, we showed that numerical integration method based on expanding the differential equation into a generalized power series is highly competative with the traditional analytic integration in both precision and computation time and can be therefore used not only for providing benchmarks but also for actual phenomenological studies. We also demonstrated how this approach can be used for computing boundary conditions for the differential equation and extending the result to an arbitrary kinematic region. Of course, obtaining analytic expressions for the integrals is still a very important task which was, in the case of the planar integrals, already successfully solved in terms of polylogarithms [75] and special *pentagon functions* [76].
Integrals computed in this thesis have already enabled a couple of amplitude calculations [77–79]. Here, the result [79] is particularly impressive since it provides the full analytic leading-color amplitude for processes including four partons and a W-boson in QCD.
In summary, it can be said that the numerically-based differential equation approach has proven itself to be a useful tool in computing Feynman integrals at the current two-loop five-point frontier and will, probably, find further applications.
Finally, let us give a brief overview of the possible extensions of this work. The most obvious next step is the completion of five-point master integrals with one off-shell leg by computing the both double-pentagon topologies. We are optimistic that this goal can be achieved with comparably small improvements of the approach presented in this thesis, mainly concerning better handling of intermediate expressions which, even numerically, become very large for these topologies. A possible way to improve this could be a more systematic usage of finite field techniques and functional-reconstruction methods which are already well established in amplitude calculations.
A further goal could be the planar massless six-point master integrals since all their sub-topologies are included in the planar five-point master integrals with one off-shell leg. Important results on six-point integrands were obtained in reference [212]. Other possible directions could be five-point integrals with two or more massive external legs or massive internal propagators or three-loop four-point integrals with one or more massive external legs.
We are convinced that the newly obtained methodology and results will lead to a broad availability of five-point NNLO QCD predictions for the LHC in the near future.

Appendix A

Useful parametrizations of the five-point phase space

For most of the time the five-point one-mass phase space is parametrized by the cyclic Mandelstam invariants $\vec{s}$ defined in eq. (3.1). Eq. (3.2) gives the five remaining non-cyclic variables in terms of the cyclic ones. However, sometimes alternative representations might be more convenient. In our implementation of the numerical DE described in section 3.2 we have the possibility to switch between either directly choosing numerical values for the Mandelstam invariants or for the external momentum components p_i^μ. Due to the special form of tr_5

$$\mathrm{tr}_5 = 4i\epsilon_{\mu\nu\rho\sigma} p_1^\mu p_2^\nu p_3^\rho p_4^\sigma \tag{A.1}$$

Δ_5 becomes automatically a perfect square if all momentum components are rational.
In this section, we want to discuss some special parametrizations of the five-point massive kinematics. In section A.1 we briefly review the *spinor-helicity formalism*(see e.g. [236, 237]). Then, in section A.2 we introduce *momentum twistors* [238] and discuss their application in the presence of a massive external leg. Finally, we give a concrete set of momentum-twistor variables which rationalizes tr_5 and $\sqrt{\Delta_3^{(1)}}$ simultaneously.

A.1 Helicity spinors

Here, our presentation closely follows [237]. Each four-vector p^μ can uniquely be mapped onto a complex 2×2-matrix $P^{\dot{a}b}$ via

$$P^{\dot{a}b} = p^\mu \bar{\sigma}_\mu^{\dot{a}b}, \tag{A.2}$$

where

$$\bar{\sigma}_\mu^{\dot{a}b} = (\mathbb{1}^{\dot{a}b}, \vec{\sigma}^{\dot{a}b}), \tag{A.3}$$

with $\vec{\sigma} = (\sigma_1, \sigma_2, \sigma_3)$ being the *Pauli matrices*

$$\sigma_1 = \begin{pmatrix} 0 & 1 \\ 1 & 0 \end{pmatrix}, \quad \sigma_2 = \begin{pmatrix} 0 & -i \\ i & 0 \end{pmatrix}, \quad \sigma_3 = \begin{pmatrix} 1 & 0 \\ 0 & -1 \end{pmatrix}. \tag{A.4}$$

Explicitly, the matrix $P^{\dot{a}b}$ can be written as

$$P^{\dot{a}b} = \begin{pmatrix} p^0 + p^3 & p^1 - ip^2 \\ p^1 + ip^2 & p^0 - p^3 \end{pmatrix}. \tag{A.5}$$

The mass square p^2 is now encoded in the determinant of $P^{\dot{a}b}$

$$\det(P^{\dot{a}b}) = p^2. \tag{A.6}$$

If p^μ is massless then $P^{\dot{a}b}$ can be expressed as a product of two *Weyl spinors* $\lambda, \tilde{\lambda}$

$$P^{\dot{a}b} = \tilde{\lambda}^{\dot{a}}\lambda^b, \tag{A.7}$$

which transform with the $(0, 1/2)$- and $(1/2, 0)$-representations of the Lorentz group, respectively. The spinor indices $a, \dot{a}$ are raised and lowered by a two-dimensional totally antisymmetric tensor

$$\lambda_a = \epsilon_{ab}\lambda^b, \quad \tilde{\lambda}_{\dot{a}} = \epsilon_{\dot{a},\dot{b}}\tilde{\lambda}^{\dot{b}}, \tag{A.8}$$

where

$$\epsilon_{ab} = \epsilon^{ab} = \epsilon^{\dot{a}\dot{b}} = \epsilon_{\dot{a}\dot{b}} = \begin{pmatrix} 0 & 1 \\ -1 & 0 \end{pmatrix}, \quad \epsilon_{ba} = -\epsilon_{ab}. \tag{A.9}$$

Often a *bracket* notation is used

$$\begin{aligned} \langle\lambda| &\equiv \lambda^a, \quad |\lambda\rangle \equiv \lambda_a, \\ [\tilde{\lambda}| &\equiv \tilde{\lambda}_{\dot{a}}, \quad |\tilde{\lambda}] \equiv \tilde{\lambda}^{\dot{a}}. \end{aligned} \tag{A.10}$$

We define two bilinear antisymmetric products $\langle\cdot,\cdot\rangle$ and $[\cdot,\cdot]$ via

$$\begin{aligned} \langle\lambda\mu\rangle &\equiv \lambda^a\mu_a = \epsilon_{ab}\lambda^a\mu^b = -\langle\mu\lambda\rangle, \\ [\tilde{\lambda}\tilde{\mu}] &\equiv \tilde{\lambda}_{\dot{a}}\tilde{\mu}^{\dot{a}} = \epsilon_{\dot{a}\dot{b}}\tilde{\lambda}^{\dot{b}}\tilde{\mu}^{\dot{a}} = -\epsilon_{\dot{a}\dot{b}}\tilde{\lambda}^{\dot{a}}\tilde{\mu}^{\dot{b}} = -[\tilde{\mu}\tilde{\lambda}]. \end{aligned} \tag{A.11}$$

A massless four-momentum p_i^μ can be obtained from the corresponding spinors $\lambda_i, \tilde{\lambda}_i$ via

$$p_i^\mu = \frac{1}{2}\lambda_i^a\sigma^\mu_{a\dot{b}}\tilde{\lambda}_i^{\dot{b}} = \frac{1}{2}\langle i|\sigma^\mu|i], \tag{A.12}$$

where we used the short notation $\langle i| \equiv \langle\lambda_i|$ and $|i] \equiv |\tilde{\lambda}_i]$. Alternatively, we can use Dirac-algebra and cast eq. (A.12) into the form

$$p^\mu = \frac{1}{2}\langle p|\gamma^\mu|p], \tag{A.13}$$

where

$$[p| \equiv \bar{u}_+(p) = \bar{v}_-(p), \quad \langle p| \equiv \bar{u}_-(p) = \bar{v}_+(p). \tag{A.14}$$

Mandelstam invariants for massless momenta can be expressed in terms of spinor products

$$s_{ij} = (p_i + p_j)^2 = \langle ij\rangle[ji]. \tag{A.15}$$

We can use eq. (A.12) to generate a set of four independent massless four-momenta p_i^μ with rational entries by choosing randomly four pairs of rational spinors $\lambda_i, \tilde{\lambda}_i$. The massive momentum p_1^μ can be as well included in this scheme by introducing two auxiliary massless momenta q_1^μ, q_2^μ, with $p_1^\mu = q_1^\mu + q_2^\mu$ and $q_1^2 = q_2^2 = 0$. However, the five momenta we have to generate are not independent but fulfill the momentum conservation $\sum_{i=1}^5 p_i^\mu = 0$. This constraint is implemented by using momentum-twistor variables which are introduced in section A.2 where we follow the presentation of reference [239].

A.2 Momentum-twistor variables

To catch up momentum conservation we switch to so-called *dual variables* $y_i,\ i = 1, \ldots, n$, defined by

$$p_i = y_i - y_{i-1}, \tag{A.16}$$

with $y_0 = 0$. The indices are cyclic modulo n. The inverse map is

$$y_i = \sum_{j=1}^{i} p_j, \quad y_0 = 0. \tag{A.17}$$

It is easy to see that now momentum conservation is guaranteed since

$$\sum_{i=1}^{n} p_i = \sum_{i=1}^{n} (y_i - y_{i-1}) = y_n - y_0 = 0. \tag{A.18}$$

We define a new set of spinors $[\tilde{\mu}_i|$ via

$$[\tilde{\mu}_i| = \langle p_i | \not{y}_i = \langle p_i | (\not{y}_{i-1} + \not{p}_i) = \langle p_i | \not{y}_{i-1}, \tag{A.19}$$

where we used the Dirac equation $\langle p_i | \not{p}_i = 0$. With a bit of algebra (see [239] for details) we can express $[\tilde{\lambda}_i|$ in terms of $\langle \lambda_j|$'s and $[\tilde{\mu}_j|$'s

$$[\tilde{\lambda}_i| = -\frac{\langle i, i+1\rangle [\tilde{\mu}_{i-1}| + \langle i+1, i-1\rangle [\tilde{\mu}_i| + \langle i-1, i\rangle [\tilde{\mu}_{i+1}|}{\langle i, i+1\rangle \langle i-1, i\rangle}. \tag{A.20}$$

We choose randomly the λ_i's and $\tilde{\mu}_i$'s and derive from them the external momenta using eq. A.20 and eq. (A.12). Four-momenta constructed in this way sum to zero automatically.
Often one combines the λ_i's and $\tilde{\mu}_i$'s to a four-component twistor Z_i defined as

$$Z_i \equiv \begin{pmatrix} |\lambda_i\rangle \\ |\tilde{\mu}_i] \end{pmatrix}. \tag{A.21}$$

Geometrically, a dual point y_i is associated to a line in the twistor space connecting Z_{i-1} and Z_i. See [239] for details on the geometric structure of momentum-twistor space. The set of spinors $Z_1, \ldots, Z_n$ is usually combined to a $4 \times n$ *twistor matrix*

$$\mathcal{Z}_n = (Z_1, \ldots, Z_n). \tag{A.22}$$

Due to the $U(1)$ rescaling symmetry of each of the Z_i's and the global Poincare-group symmetry $\mathcal{Z}_n$ can be parametrized by $3n - 10$ independent variables.
As already mentioned, every rational choice of the helicity spinors automatically rationalizes tr_5. However, for some applications it might be helpful to have a phase-space parametrization in which one further square-root becomes rational. We decided to rationalize $\sqrt{\Delta_3^{(1)}}$ since it appears already at the one-loop level as well as in the top-level on-shell differential equation for the zz-double-pentagon topology, due to our basis choice (see section 4.3.2). A manifestly rational parametrization of both tr_5 and $\sqrt{\Delta_3^{(1)}}$ would speed up the numerical computation of the on-shell differential equation significantly. Since the massive leg is implemented as a sum of two massless

momenta it is convenient to begin with a generic six-point configuration which is parametrized by eight free parameters. Inspired by reference [240], we chose the 6×4 twistor matrix $\mathcal{Z}_6$ to be

$$\mathcal{Z}_6 = \begin{pmatrix} \frac{1}{x_1} & \frac{1}{x_2}+\frac{1}{x_1} & 1 & 0 & -\frac{x_6x_7-x_5x_8}{x_3}+\frac{1}{x_1}+\frac{1}{x_1x_2}+\frac{1}{x_1x_2x_3} & \frac{1}{x_2x_1}+\frac{1}{x_2x_3x_1}+\frac{1}{x_1} \\ 1 & 1 & 0 & 1 & 1 & 1 \\ 1 & 0 & 0 & 0 & x_7 & x_5 \\ 0 & 1 & 0 & 0 & x_8 & x_6 \end{pmatrix}. \tag{A.23}$$

Using eq. (A.20) and eq. (A.15) we compute the cyclic six-point Mandelstam invariants

$$\begin{aligned}
\tilde{s}_{12} &= \frac{x_1x_2x_3\left(x_5+x_6-1\right)}{x_3+1}, \quad \tilde{s}_{23} = x_2, \quad \tilde{s}_{34} = \frac{x_1x_2x_3x_7}{x_2x_3+x_3-x_1x_2x_6x_7+x_1x_2x_5x_8+1}, \\
\tilde{s}_{45} &= x_3, \\
\tilde{s}_{56} &= -\frac{x_1x_2x_3\left(x_1x_2x_7x_6^2+\left(x_3\left(x_2\left(x_7-1\right)-1\right)-x_1x_2x_5x_8-1\right)x_6+x_3\left(-x_5x_2+x_2+1\right)x_8+x_8\right)}{\left(x_3+1\right)\left(x_2x_3+x_3-x_1x_2x_6x_7+x_1x_2x_5x_8+1\right)}, \\
\tilde{s}_{16} &= -\frac{-x_1x_2x_8x_5^2-\left(-x_1x_8x_3+x_3-x_1x_2\left(x_6x_7-x_6x_8+x_8\right)+1\right)x_5}{x_1\left(x_6x_7-x_5x_8\right)} \\
&\quad -\frac{x_1x_2x_6^2x_7+x_3x_7+x_7-x_6\left(x_1\left(x_7-1\right)x_3+x_3+x_1x_2x_7+1\right)-x_1x_3x_8+x_3x_8+x_8}{x_1\left(x_6x_7-x_5x_8\right)},
\end{aligned} \tag{A.24}$$

which we denote here with $\tilde{s}_{ij}$ in order to distinguish them from the *true five-point* Mandelstam variables s_{ij}. We complete the set of independent six-point invariants by

$$\tilde{s}_{123} = \frac{x_1x_2x_3x_6}{x_3+1}, \quad \tilde{s}_{234} = -\frac{x_2\left(x_1x_2\left(x_6x_7-x_5x_8\right)+x_3\left(x_1x_8+x_2\left(x_7+x_8-1\right)-1\right)-1\right)}{x_2x_3+x_3-x_1x_2x_6x_7+x_1x_2x_5x_8+1}. \tag{A.25}$$

We define

$$\vec{\tilde{s}} = \left\{\tilde{s}_{12}, \tilde{s}_{23}, \tilde{s}_{34}, \tilde{s}_{45}, \tilde{s}_{56}, \tilde{s}_{16}, \tilde{s}_{123}, \tilde{s}_{234}\right\}. \tag{A.26}$$

The advantage of this parametrization is that two invariants $\tilde{s}_{23}$ and $\tilde{s}_{45}$ are given by single twistor variables. We rescale $\vec{\tilde{s}}$ by $\frac{1}{\tilde{s}_{16}}$ and define new variables

$$\tilde{x}_2 := \frac{x_2}{\tilde{s}_{16}}, \quad \tilde{x}_3 := \frac{x_3}{\tilde{s}_{16}}. \tag{A.27}$$

Up to this point, we worked with a generic six-point momentum configuration. In order to extract the special case of the five-point massive kinematics we have to fix two degrees of freedom. We choose

$$x_1 = 0, \quad x_5 = 1 \tag{A.28}$$

in order to simplify the functional form of the Mandelstam invariants.
Now we can identify the six remaining variables with the standard five-point Mandelstam invariants via

$$q^2 = \tilde{s}_{23}, s_{12} = \tilde{s}_{234}, s_{23} = \tilde{s}_{45}, s_{34} = \tilde{s}_{56}, s_{45} = \tilde{s}_{16}, s_{15} = \tilde{s}_{123}. \tag{A.29}$$

The rescaled three-point Gram determinant $\tilde{\Delta}_3^{(1)}$ in terms of momentum-twistor variables becomes

$$\tilde{\Delta}_3^{(1)}(\tilde{x}_2, \tilde{x}_3) = \tilde{x}_2^2 + \tilde{x}_3^2 + 1 - 2\tilde{x}_2\tilde{x}_3 - 2\tilde{x}_2 - 2\tilde{x}_3. \tag{A.30}$$

Since $\Delta_3^{(1)}$ is form-invariant under the variable transformation (A.24) it can be turned into a perfect square independently from tr_5. A particular change of variables which turns the Källén function into a pefect square is well-known in the literature. The variable transformation

$$\tilde{x}_2 = \omega_1\omega_2, \qquad \tilde{x}_3 = (\omega_1 - 1)(\omega_2 - 1) \tag{A.31}$$

provides a possible solution. Now we have

$$\tilde{\Delta}_3^{(1)}(\omega_1, \omega_2) = (\omega_1 - \omega_2)^2. \tag{A.32}$$

The backward transformation is given by

$$\omega_{1,2}(\tilde{x}_2, \tilde{x}_3) = \frac{\tilde{x}_2 - \tilde{x}_3 + 1 \pm \sqrt{\Delta_3^{(1)}}}{2}. \tag{A.33}$$

Finally, we restore the mass dimension of the kinematic variables by multiplying each of them by a common scale S. We obtain

$$\begin{aligned}
&q^2 = Sw_1w_2, \quad s_{12} = -Sw_1w_2\left(x_7 + x_8 - 1\right), \quad s_{23} = S\left(w_1 - 1\right)\left(w_2 - 1\right), \\
&s_{34} = -\frac{S\left(w_1 - 1\right)w_1\left(w_2 - 1\right)w_2x_6\left(x_7 - 1\right)\left(x_6 - x_7 - x_8 + 1\right)}{w_1w_2x_7x_6^2 - x_6\left(w_1\left(-x_7\right) + w_2w_1\left(x_7 + x_8 - 1\right) - w_2x_7 + w_1 + w_2 - 1\right) - x_8}, \\
&s_{45} = S, \quad s_{15} = \frac{S\left(w_1 - 1\right)w_1\left(w_2 - 1\right)w_2x_6\left(x_6 - x_7 - x_8 + 1\right)}{\left(w_1 - 1\right)\left(w_2 - 1\right)\left(x_6 - x_6x_7\right) + \left(x_6x_7 - x_8\right)\left(w_1w_2x_6 + 1\right)}.
\end{aligned} \tag{A.34}$$

The three-point Gram becomes

$$\Delta_3^{(1)}(S, \omega_1, \omega_2) = S^2(\omega_1 - \omega_2)^2. \tag{A.35}$$

To provide a concrete example of a phase-space point with both tr_5 and $\sqrt{\Delta_3^{(1)}}$ being rational we choose randomly a point in the twistor-parameter space to be

$$\{S = 2, \omega_1 = 2, \omega_2 = 3, x_7 = 7, x_6 = 5, x_8 = 11\}, \tag{A.36}$$

which corresponds to

$$\vec{s} = \left\{12, -204, 4, \frac{240}{19}, 2, -\frac{40}{19}\right\}. \tag{A.37}$$

Appendix B

Embedding-space formalism

In this section, we give a brief overview of the *embedding-space formalism* (ESF). Here, we adopt the notation from [56]. For a more detailed discussion see e.g. [167]. The basic idea is to embed the D-dimensional kinematic space into a higher dimensional projective space such that possible singularities at *infinity* become manifest. This enables us to take residues at these singularities. In section 3.3.3 we show explicitly how to use ESF to compute leading singularities of some two-loop integrals. In [56] we give a further interesting example.
In the following, we embed the kinematic space into the complex *projective space* $\mathbb{CP}^{D+1}$ with elements V parametrized by tuples of homogenous coordinates

$$V = \left(v^\mu, V^+, V^-\right), \tag{B.1}$$

equipped with the equivalence relation $V \sim \alpha V$ for any $\alpha \in \mathbb{C}$ with $\alpha \neq 0$. We define a bilinear form on $\mathbb{CP}^{D+1}$ by

$$(VW) := -2v_\mu w^\mu - V^+W^- - V^-W^+. \tag{B.2}$$

Next, we define the projective version of a planar one-loop n-point Feynman integral. In the following, we focus on the special cases of $n = 3$ and $n = 4$. Let $p_1, \ldots, p_n$ denote the external momenta and ℓ the loop-momentum. The n propagators are given by

$$D_i = \left(\ell + \sum_{j=0}^{i} p_j\right)^2, \quad 0 \leq i \leq n-1. \tag{B.3}$$

We map the external momenta on a set of projective points $X_0, \ldots, X_{n-1}$ via

$$p_i \mapsto X_i = \left[-\sum_{j=1}^{i} p_j, -\left[\sum_{j=1}^{i} p_j\right]^2, 1\right], \quad 1 \leq i \leq n-1. \tag{B.4}$$

The *reference point* X_0 is given by $X_0 := [0, 0, 1]$. With this definition we have

$$(X_iX_j) = (p_{i-j+1} + \cdots + p_i)^2, \quad \text{for} \quad i > j \quad \text{and} \quad (X_iX_i) = 0. \tag{B.5}$$

Up to numerical prefactors, the projective one-loop integral is now given by [167]

$$I_n^D \sim \int \frac{\mathrm{d}^{D+2}Y\, \delta((YY))}{\mathrm{vol}(GL(1))} \frac{[(IY)]^{n-D}}{\prod_{i=0}^{n-1}(YX_i)}. \tag{B.6}$$

Here, I is the *infinitity point* which we set to

$$I := [0, -1, 0], \tag{B.7}$$

such that $(X_i I) = 1$ for all i. The integration domain in eq. (B.6) is restricted by $\delta((YY))$ to a real D-dimensional quadric defined by $(YY) = 0$. In practice, we implement this condition by parametrizing Y as

$$Y = \left(\ell, -\ell^2, 1\right). \tag{B.8}$$

With this choice we have

$$(X_i Y) = \frac{1}{D_i}, \tag{B.9}$$

which reproduces the standard Feynman propagators. The numerator factor $[(IY)]^{n-D}$ which ensures the homogeneity of the integrand is called the *infinitity propagator*. For $n = 3$ and $\epsilon \to 0$ it appears explicitly in the denominator. To compute the leading singularity we need to cut it together with other propagators. In this way, singularities at infinitity become manifest in this representation. A triangle integral, for instance, is represented by *four* propagators in the ESF, namely three actual propagators and the infinitity propagator. In that sense, a triangle integral can be treated as a box integral with one edge put to infinitity.
Moreover, computing cuts in the embedding space has the advantage of working with propagators which are *linear* in the loop-momentum Y instead of the usual quadratic dependence. The Jacobian factor J which needs to be added in order to compute the quartic cut in four dimensions, defined by

$$\begin{aligned} (X_0 Y) = (X_1 Y) = (X_2 Y) = (X_3 Y) = 0, \quad \text{for } n = 4, \\ (X_0 Y) = (X_1 Y) = (X_2 Y) = (IY) = 0, \quad \text{for } n = 3, \end{aligned} \tag{B.10}$$

is, therefore, given by

$$J = \begin{cases} \frac{1}{\sqrt{G(X_0, X_1, X_2, X_3)}}, & n = 4, \\ \frac{1}{\sqrt{G(X_0, X_1, X_2, I)}}, & n = 3. \end{cases} \tag{B.11}$$

The embedding space Gram determinant G is defined by

$$G(X_1, \ldots, X_n) = \det\left\{(X_i X_j)\right\}_{i,j=1}^{n}. \tag{B.12}$$

For planar two-loop integrals eq. (B.6) can be applied loop-by-loop. We demonstrate this on two examples in 3.3.3.

Appendix C

Functional reconstruction

In the section 3.3.5 we showed how to integrate out $\mathcal{O}(\epsilon^0)$-part of the connection matrix. We did a similar computation in 4.3.2 to compute the kinematic prefactors of the parity-odd insertions. However, the analytic form of the $A^{(0)}$ matrix is not known in the first place since we work with purely numerical differential equations. In this section, we want to discuss our reconstruction procedure for $\mathcal{O}(\epsilon^0)$ part of the matrix. Let us assume that we managed to bring the differential equation into the form

$$\frac{\partial \mathbf{I}}{\partial s_i} = \left[A_i^{(0)}(\vec{s}) + \epsilon A_i^{(1)}(\vec{s})\right] \mathbf{I}. \tag{C.1}$$

For simplicity, we work here with a single component of the differential equation. Then, we simply repeat the calculation for the next variable. Since solving IBP relations generates only rational expressions, the only non-rational terms in the connection can come from square-roots in the definition of the pre-canonical basis $\mathbf{I}$ which are known analytically. Let us first assume that the constant part of the connection $A_i^{(0)}(\vec{s})$ is rational and so standard functional reconstruction can be applied. To extract the constant part from the pre-canonical connection we use eq. (3.25) and obtain

$$A_i^{(0)}(\vec{s}_j) = \frac{\epsilon_1\epsilon_2}{\epsilon_2 - \epsilon_1}\Delta A_i(\vec{s}_j), \quad j = 1, \ldots, N_r, \tag{C.2}$$

where N_r is the number of sample points.
Let us briefly review the functional reconstruction process in the univariate case. A generic rational function $f \in K(\mathbb{R})$ is given by the ratio of two polynomials. In the univariate case we have

$$f(x) = \frac{\sum_{i=0}^{R_n} a_i x^i}{\sum_{j=0}^{R_d} \beta_j x^j}, \tag{C.3}$$

where $\alpha_0, \ldots, \alpha_{R_n}, \beta_0, \ldots, \beta_{R_d} \in \mathbb{R}, R_d, R_n \in \mathbb{N}$. We use the *Thiele's continued-fraction formula* [241] to represent f as a continued-fraction

$$f(x) = a_0 + \cfrac{x - y_0}{a_1 + \cfrac{x - y_1}{a_2 + \cfrac{x - y_2}{\ldots + \cfrac{x - y_{R-1}}{a_R}}}}. \tag{C.4}$$

Here, $y_0, \ldots, y_{R-1}$ are the interpolation points and $a_0, \ldots, a_R$ are the unknown coefficients. The advantage of the Thiele's representation is that $f(y_i)$ does not depend on a_j's with $j > i$. This

allows for a recursive computation of the coefficients. The algorithm stops when the reconstructed function starts to reproduce the black-box evaluations. Finally, the reconstructed function can easily be brought into the standard form (C.3).
The most general multivariate case is more complicated. We refer to Peraro's paper [125] for a generic reconstruction algorithm for multivariate dense rational functions. Since all functions we needed to reconstruct in our work are rather simple and have maximally degree four in any of the variables both in the numerator and the denominator it was sufficient to apply the univariate algorithm recursively variable by variable. To reduce the number of numerical evaluations we reconstructed the analytical dependence in only three or maximally four out of six kinematic variables. To determine the remaining analytic structure we applied the PSLQ-algorithm [214]. Let us explain this on a simple example. Assume that we have a rational function in three variables

$$f(x_1, x_2, x_3) = \frac{x_1^2 x_2 + x_1 x_2 x_3 + x_3^2 x_2}{x_1 - x_2 + x_3}, \tag{C.5}$$

which has to be reconstructed. We set $x_2 = 7, x_3 = 11$ and apply the Thiele's formula with respect to x_1. The result is

$$\tilde{f}(x_1) = \frac{7x_1^2 + 77x_1 + 847}{x_1 + 4}. \tag{C.6}$$

By dimensional analysis we conclude that the coefficient of the quadratic term in the numerator has to be a linear polynomial in x_2 and x_3 while the second coefficient is a quadratic polynomial and the constant part has to be given by a cubic polynomial. Now we can make an ansatz and apply the PSLQ-algorithm to determine the coefficients of this ansatz. So, for instance, we have

$$847 = \alpha_1 7^3 + \alpha_2 11^3 + \alpha_3 11^2 \cdot 7 + \alpha_4 7^2 \cdot 11. \tag{C.7}$$

This equation is fulfilled for $\alpha_1 = 0, \alpha_2 = 0, \alpha_3 = 1, \alpha_4 = 0$. The same procedure can be applied to all coefficients. By using PSLQ we could keep the number of needed numerical IBP evaluations at $\mathcal{O}(30)$ per topology.
Finally, we briefly discuss the treatment of square roots which can appear in $A_i^{(0)}(\vec{s})$. In this case, we can assume that the potential Φ[1] (see 3.3.5 for the definition of Φ) has the general form

$$\Phi(\vec{s}) = \frac{f(\vec{s})}{\sqrt{Q(\vec{s})}}, \tag{C.8}$$

where f is a rational function and Q is one of the Gram determinants which appear in the symbol alphabet. At this stage we can assume that all Gram determinants are known analytically. By a simple calculation we show that

$$A_i^{(0)}(\vec{s}) = \frac{\partial \Phi(\vec{s})}{\partial s_i} = \frac{(\partial_i f)Q - \frac{1}{2}(\partial_i Q)f}{Q^{3/2}} \equiv \frac{F}{Q^{3/2}}, \tag{C.9}$$

where F is again a rational function. Using eq. (C.9) we can extract the *purely rational* part F of $A_i^{(0)}(\vec{s})$ and reconsruct it first. Then, we simply divide the result by $Q^{3/2}$.

[1]For simplicity, we work here with a scalar potential Φ which should in general be understood as an entry of the matrix-valued potential.

Bibliography

[1] G. Aad *et al.*, "Observation of a new particle in the search for the Standard Model Higgs boson with the ATLAS detector at the LHC," *Phys. Lett. B*, vol. 716, pp. 1–29, 2012.

[2] S. Chatrchyan *et al.*, "Observation of a New Boson at a Mass of 125 GeV with the CMS Experiment at the LHC," *Phys. Lett. B*, vol. 716, pp. 30–61, 2012.

[3] G. P. Korchemsky and A. V. Radyushkin, "Infrared factorization, Wilson lines and the heavy quark limit," *Phys. Lett. B*, vol. 279, pp. 359–366, 1992.

[4] S. J. Parke and T. R. Taylor, "Amplitude for n-gluon scattering," *Phys. Rev. Lett.*, vol. 56, pp. 2459–2460, Jun 1986.

[5] F. Berends and W. Giele, "Recursive calculations for processes with n gluons," *Nuclear Physics B*, vol. 306, no. 4, pp. 759–808, 1988.

[6] R. Britto, F. Cachazo, B. Feng, and E. Witten, "Direct proof of tree-level recursion relation in Yang-Mills theory," *Phys. Rev. Lett.*, vol. 94, p. 181602, 2005.

[7] R. Eden, P. Landshoff, D. Olive, and J. Polkinghorne, *The Analytic S-Matrix*. Cambridge University Press, 1966.

[8] Z. Bern, L. J. Dixon, D. C. Dunbar, and D. A. Kosower, "One loop n point gauge theory amplitudes, unitarity and collinear limits," *Nucl. Phys. B*, vol. 425, pp. 217–260, 1994.

[9] Z. Bern, L. J. Dixon, and D. A. Kosower, "One loop corrections to five gluon amplitudes," *Phys. Rev. Lett.*, vol. 70, pp. 2677–2680, 1993.

[10] Z. Bern and D. A. Kosower, "The computation of loop amplitudes in gauge theories," *Nuclear Physics B*, vol. 379, no. 3, pp. 451–561, 1992.

[11] R. Britto, F. Cachazo, and B. Feng, "Generalized unitarity and one-loop amplitudes in N=4 super-Yang-Mills," *Nucl. Phys. B*, vol. 725, pp. 275–305, 2005.

[12] G. 't Hooft and M. Veltman, "Scalar one-loop integrals," *Nuclear Physics B*, vol. 153, pp. 365–401, 1979.

[13] A. Denner and S. Dittmaier, "Scalar one-loop 4-point integrals," *Nucl. Phys. B*, vol. 844, pp. 199–242, 2011.

[14] Z. Bern, L. J. Dixon, F. Febres Cordero, S. Höche, H. Ita, D. A. Kosower, D. Maître, and K. J. Ozeren, "The BlackHat Library for One-Loop Amplitudes," *J. Phys. Conf. Ser.*, vol. 523, p. 012051, 2014.

[15] G. Cullen, N. Greiner, G. Heinrich, G. Luisoni, P. Mastrolia, G. Ossola, T. Reiter, and F. Tramontano, "Automated One-Loop Calculations with GoSam," *Eur. Phys. J. C*, vol. 72, p. 1889, 2012.

[16] M. Aaboud *et al.*, "Precision measurement and interpretation of inclusive W^+ , W^- and Z/γ^* production cross sections with the ATLAS detector," *Eur. Phys. J. C*, vol. 77, no. 6, p. 367, 2017.

[17] G. Aad *et al.*, "Measurement of the inclusive cross-section for the production of jets in association with a Z boson in proton-proton collisions at 8 TeV using the ATLAS detector," *Eur. Phys. J. C*, vol. 79, no. 10, p. 847, 2019.

[18] S. Chatrchyan *et al.*, "Measurement of W^+W^- and ZZ Production Cross Sections in pp Collisions at $\sqrt{s} = 8TeV$," *Phys. Lett. B*, vol. 721, pp. 190–211, 2013.

[19] P. Jaiswal and T. Okui, "An explanation of the ww excess at the lhc by jet-veto resummation," *Physical Review D*, vol. 90, 07 2014.

[20] T. Gehrmann, M. Grazzini, S. Kallweit, P. Maierhöfer, A. von Manteuffel, S. Pozzorini, D. Rathlev, and L. Tancredi, "W^+W^- Production at Hadron Colliders in Next to Next to Leading Order QCD," *Phys. Rev. Lett.*, vol. 113, no. 21, p. 212001, 2014.

[21] M. Grazzini, S. Kallweit, and D. Rathlev, "Zz production at the lhc: Fiducial cross sections and distributions in nnlo qcd," *Physics Letters B*, vol. 750, pp. 407–410, 2015.

[22] H. Ita, "Two-loop integrand decomposition into master integrals and surface terms," *Physical Review D*, vol. 94, p. 116015, 2016.

[23] S. Abreu, F. Febres Cordero, H. Ita, M. Jaquier, and B. Page, "Subleading Poles in the Numerical Unitarity Method at Two Loops," *Phys. Rev. D*, vol. 95, no. 9, p. 096011, 2017.

[24] S. Abreu, F. F. Cordero, H. Ita, M. Jaquier, B. Page, and M. Zeng, "Two-loop four-gluon amplitudes from numerical unitarity," *Phys. Rev. Lett.*, vol. 119, p. 142001, Oct 2017.

[25] S. Abreu, F. Febres Cordero, H. Ita, B. Page, and M. Zeng, "Planar Two-Loop Five-Gluon Amplitudes from Numerical Unitarity," *Phys. Rev. D*, vol. 97, no. 11, p. 116014, 2018.

[26] Y. Zhang, "Integrand-level reduction of loop amplitudes by computational algebraic geometry methods," *Journal of High Energy Physics*, vol. 2012, pp. 1–24, 2012.

[27] P. Mastrolia, E. Mirabella, G. Ossola, and T. Peraro, "Scattering amplitudes from multivariate polynomial division," *Physics Letters B*, vol. 718, pp. 173–177, 2012.

[28] P. Mastrolia and G. Ossola, "On the integrand-reduction method for two-loop scattering amplitudes," *Journal of High Energy Physics*, vol. 2011, pp. 1–29, 2011.

[29] S. Badger, H. Frellesvig, and Y. Zhang, "Hepta-cuts of two-loop scattering amplitudes," *Journal of High Energy Physics*, vol. 2012, 02 2012.

[30] A. Kotikov, "Differential equations method. new technique for massive feynman diagram calculation," *Physics Letters B*, vol. 254, no. 1, pp. 158–164, 1991.

[31] A. Kotikov, "Differential equation method. the calculation of n-point feynman diagrams," *Physics Letters B*, vol. 267, no. 1, pp. 123–127, 1991.

[32] Z. Bern, L. J. Dixon, and D. A. Kosower, "Dimensionally regulated pentagon integrals," *Nucl. Phys. B*, vol. 412, pp. 751–816, 1994.

[33] E. Remiddi, "Differential equations for Feynman graph amplitudes," *Nuovo Cim. A*, vol. 110, pp. 1435–1452, 1997.

[34] T. Gehrmann and E. Remiddi, "Differential equations for two loop four point functions," *Nucl. Phys. B*, vol. 580, pp. 485–518, 2000.

[35] J. M. Henn, "Multiloop integrals in dimensional regularization made simple," *Phys. Rev. Lett.*, vol. 110, p. 251601, Jun 2013.

[36] T. Gehrmann, J. M. Henn, and N. A. Lo Presti, "Analytic form of the two-loop planar five-gluon all-plus-helicity amplitude in QCD," *Phys. Rev. Lett.*, vol. 116, no. 6, p. 062001, 2016. [Erratum: Phys.Rev.Lett. 116, 189903 (2016)].

[37] S. Badger, C. Brønnum-Hansen, H. B. Hartanto, and T. Peraro, "First look at two-loop five-gluon scattering in QCD," *Phys. Rev. Lett.*, vol. 120, no. 9, p. 092001, 2018.

[38] S. Badger, C. Brønnum-Hansen, T. Gehrmann, H. B. Hartanto, J. Henn, N. A. Lo Presti, and T. Peraro, "Applications of integrand reduction to two-loop five-point scattering amplitudes in QCD," *PoS*, vol. LL2018, p. 006, 2018.

[39] S. Abreu, J. Dormans, F. Febres Cordero, H. Ita, and B. Page, "Analytic Form of Planar Two-Loop Five-Gluon Scattering Amplitudes in QCD," *Phys. Rev. Lett.*, vol. 122, no. 8, p. 082002, 2019.

[40] S. Badger, C. Brønnum-Hansen, H. B. Hartanto, and T. Peraro, "Analytic helicity amplitudes for two-loop five-gluon scattering: the single-minus case," *JHEP*, vol. 01, p. 186, 2019.

[41] D. Chicherin, T. Gehrmann, J. M. Henn, P. Wasser, Y. Zhang, and S. Zoia, "Analytic result for a two-loop five-particle amplitude," *Phys. Rev. Lett.*, vol. 122, no. 12, p. 121602, 2019.

[42] S. Abreu, F. Febres Cordero, H. Ita, B. Page, and V. Sotnikov, "Planar Two-Loop Five-Parton Amplitudes from Numerical Unitarity," *JHEP*, vol. 11, p. 116, 2018.

[43] S. Abreu, L. J. Dixon, E. Herrmann, B. Page, and M. Zeng, "The two-loop five-point amplitude in $\mathcal{N} = 4$ super-Yang-Mills theory," *Phys. Rev. Lett.*, vol. 122, no. 12, p. 121603, 2019.

[44] D. Chicherin, T. Gehrmann, J. M. Henn, P. Wasser, Y. Zhang, and S. Zoia, "The two-loop five-particle amplitude in $\mathcal{N} = 8$ supergravity," *JHEP*, vol. 03, p. 115, 2019.

[45] S. Abreu, J. Dormans, F. Febres Cordero, H. Ita, B. Page, and V. Sotnikov, "Analytic Form of the Planar Two-Loop Five-Parton Scattering Amplitudes in QCD," *JHEP*, vol. 05, p. 084, 2019.

[46] S. Badger, D. Chicherin, T. Gehrmann, G. Heinrich, J. M. Henn, T. Peraro, P. Wasser, Y. Zhang, and S. Zoia, "Analytic form of the full two-loop five-gluon all-plus helicity amplitude," *Phys. Rev. Lett.*, vol. 123, no. 7, p. 071601, 2019.

[47] D. Chicherin, T. Gehrmann, J. M. Henn, P. Wasser, Y. Zhang, and S. Zoia, "All Master Integrals for Three-Jet Production at Next-to-Next-to-Leading Order," *Phys. Rev. Lett.*, vol. 123, no. 4, p. 041603, 2019.

[48] S. Abreu, B. Page, and M. Zeng, "Differential equations from unitarity cuts: nonplanar hexa-box integrals," *JHEP*, vol. 01, p. 006, 2019.

[49] S. Abreu, L. J. Dixon, E. Herrmann, B. Page, and M. Zeng, "The two-loop five-point amplitude in $\mathcal{N} = 8$ supergravity," *JHEP*, vol. 03, p. 123, 2019.

[50] C. G. Papadopoulos, D. Tommasini, and C. Wever, "The Pentabox Master Integrals with the Simplified Differential Equations approach," *JHEP*, vol. 04, p. 078, 2016.

[51] T. Gehrmann, J. M. Henn, and N. A. Lo Presti, "Pentagon functions for massless planar scattering amplitudes," *JHEP*, vol. 10, p. 103, 2018.

[52] D. Chicherin and V. Sotnikov, "Pentagon Functions for Scattering of Five Massless Particles," *JHEP*, vol. 12, p. 167, 2020.

[53] C. G. Papadopoulos and C. Wever, "Internal Reduction method for computing Feynman Integrals," *JHEP*, vol. 02, p. 112, 2020.

[54] H. B. Hartanto, S. Badger, C. Brønnum-Hansen, and T. Peraro, "A numerical evaluation of planar two-loop helicity amplitudes for a W-boson plus four partons," *JHEP*, vol. 09, p. 119, 2019.

[55] S. Abreu, H. Ita, F. Moriello, B. Page, W. Tschernow, and M. Zeng, "Two-Loop Integrals for Planar Five-Point One-Mass Processes," *JHEP*, vol. 11, p. 117, 2020.

[56] S. Abreu, H. Ita, B. Page, and W. Tschernow, "Two-loop hexa-box integrals for non-planar five-point one-mass processes," *JHEP*, vol. 03, p. 182, 2022.

[57] G. Aad *et al.*, "Measurements of the W production cross sections in association with jets with the ATLAS detector," *Eur. Phys. J. C*, vol. 75, no. 2, p. 82, 2015.

[58] A. M. Sirunyan *et al.*, "Measurement of the differential cross sections for the associated production of a W boson and jets in proton-proton collisions at $\sqrt{s} = 13$ TeV," *Phys. Rev. D*, vol. 96, no. 7, p. 072005, 2017.

[59] J. Campbell, R. K. Ellis, and D. Rainwater, "Next-to-leading order qcd predictions for $w+2$ jet and $z+2$ jet production at the cern lhc," *Phys. Rev. D*, vol. 68, p. 094021, Nov 2003.

[60] C. F. Berger, Z. Bern, L. J. Dixon, F. F. Cordero, D. Forde, T. Gleisberg, H. Ita, D. A. Kosower, and D. Maître, "Next-to-leading order qcd predictions for $w+3$-jet distributions at hadron colliders," *Phys. Rev. D*, vol. 80, p. 074036, Oct 2009.

[61] F. R. Anger, F. Febres Cordero, S. Höche, and D. Maître, "Weak vector boson production with many jets at the lhc $\sqrt{s} = 13$ TeV," *Phys. Rev. D*, vol. 97, p. 096010, May 2018.

[62] S. Kallweit, J. M. Lindert, P. Maierhofer, S. Pozzorini, and M. Schönherr, "NLO QCD+EW predictions for V + jets including off-shell vector-boson decays and multijet merging," *JHEP*, vol. 04, p. 021, 2016.

[63] P. Azzurri, M. Schönherr, and A. Tricoli, "Vector Bosons and Jets in Proton Collisions," *Rev. Mod. Phys.*, vol. 93, no. 2, p. 025007, 2021.

[64] L. Di Giustino, S. J. Brodsky, S.-Q. Wang, and X.-G. Wu, "Infinite-order scale-setting using the principle of maximum conformality: A remarkably efficient method for eliminating renormalization scale ambiguities for perturbative QCD," *Phys. Rev. D*, vol. 102, no. 1, p. 014015, 2020.

[65] M. Bonvini, "Probabilistic definition of the perturbative theoretical uncertainty from missing higher orders," *Eur. Phys. J. C*, vol. 80, no. 10, p. 989, 2020.

[66] C. Duhr, A. Huss, A. Mazeliauskas, and R. Szafron, "An analysis of Bayesian estimates for missing higher orders in perturbative calculations," *JHEP*, vol. 09, p. 122, 2021.

[67] N. Deutschmann, C. Duhr, F. Maltoni, and E. Vryonidou, "Gluon-fusion Higgs production in the Standard Model Effective Field Theory," *JHEP*, vol. 12, p. 063, 2017. [Erratum: JHEP 02, 159 (2018)].

[68] A. B. Goncharov, M. Spradlin, C. Vergu, and A. Volovich, "Classical Polylogarithms for Amplitudes and Wilson Loops," *Phys. Rev. Lett.*, vol. 105, p. 151605, 2010.

[69] C. Duhr, H. Gangl, and J. R. Rhodes, "From polygons and symbols to polylogarithmic functions," *JHEP*, vol. 10, p. 075, 2012.

[70] C. Duhr, "Hopf algebras, coproducts and symbols: an application to Higgs boson amplitudes," *JHEP*, vol. 08, p. 043, 2012.

[71] F. Moriello, "Generalised power series expansions for the elliptic planar families of Higgs + jet production at two loops," *JHEP*, vol. 01, p. 150, 2020.

[72] M. Hidding, "DiffExp, a Mathematica package for computing Feynman integrals in terms of one-dimensional series expansions," *Comput. Phys. Commun.*, vol. 269, p. 108125, 2021.

[73] R. Bonciani, V. Del Duca, H. Frellesvig, J. M. Henn, M. Hidding, L. Maestri, F. Moriello, G. Salvatori, and V. A. Smirnov, "Evaluating a family of two-loop non-planar master integrals for Higgs + jet production with full heavy-quark mass dependence," *JHEP*, vol. 01, p. 132, 2020.

[74] H. Frellesvig, M. Hidding, L. Maestri, F. Moriello, and G. Salvatori, "The complete set of two-loop master integrals for Higgs + jet production in QCD," *JHEP*, vol. 06, p. 093, 2020.

[75] D. D. Canko, C. G. Papadopoulos, and N. Syrrakos, "Analytic representation of all planar two-loop five-point Master Integrals with one off-shell leg," *JHEP*, vol. 01, p. 199, 2021.

[76] D. Chicherin, V. Sotnikov, and S. Zoia, "Pentagon Functions for One-Mass Planar Scattering Amplitudes," 10 2021.

[77] S. Badger, H. B. Hartanto, and S. Zoia, "Two-Loop QCD Corrections to $Wb\bar{b}$ Production at Hadron Colliders," *Phys. Rev. Lett.*, vol. 127, no. 1, p. 012001, 2021.

[78] S. Badger, H. B. Hartanto, J. Kryś, and S. Zoia, "Two-loop leading-colour QCD helicity amplitudes for Higgs boson production in association with a bottom-quark pair at the LHC," *JHEP*, vol. 11, p. 012, 2021.

[79] S. Abreu, F. F. Cordero, H. Ita, M. Klinkert, B. Page, and V. Sotnikov, "Leading-Color Two-Loop Amplitudes for Four Partons and a W Boson in QCD," 10 2021.

[80] Y. Guo, L. Wang, and G. Yang, "Bootstrapping a Two-Loop Four-Point Form Factor," *Phys. Rev. Lett.*, vol. 127, no. 15, p. 151602, 2021.

[81] S. L. Glashow, "The renormalizability of vector meson interactions," *Nuclear Physics*, vol. 10, pp. 107–117, 1959.

[82] S. L. Glashow, "Partial-symmetries of weak interactions," *Nuclear Physics*, vol. 22, no. 4, pp. 579–588, 1961.

[83] A. Salam and J. C. Ward, "Weak and electromagnetic interactions," *Nuovo Cim.*, vol. 11, pp. 568–577, 1959.

[84] A. Salam, "Weak and Electromagnetic Interactions," *Conf. Proc. C*, vol. 680519, pp. 367–377, 1968.

[85] S. Weinberg, "A Model of Leptons," *Phys. Rev. Lett.*, vol. 19, pp. 1264–1266, 1967.

[86] P. W. Higgs, "Broken symmetries, massless particles and gauge fields," *Phys. Lett.*, vol. 12, pp. 132–133, 1964.

[87] F. Englert and R. Brout, "Broken symmetry and the mass of gauge vector mesons," *Phys. Rev. Lett.*, vol. 13, pp. 321–323, Aug 1964.

[88] G. S. Guralnik, C. R. Hagen, and T. W. B. Kibble, "Global Conservation Laws and Massless Particles," *Phys. Rev. Lett.*, vol. 13, pp. 585–587, 1964.

[89] H. Georgi and S. L. Glashow, "Unity of all elementary-particle forces," *Phys. Rev. Lett.*, vol. 32, pp. 438–441, Feb 1974.

[90] J. C. Pati and A. Salam, "Lepton Number as the Fourth Color," *Phys. Rev. D*, vol. 10, pp. 275–289, 1974. [Erratum: Phys.Rev.D 11, 703–703 (1975)].

[91] A. Buras, J. Ellis, M. Gaillard, and D. Nanopoulos, "Aspects of the grand unification of strong, weak and electromagnetic interactions," *Nuclear Physics B*, vol. 135, no. 1, pp. 66–92, 1978.

[92] S. Laporta and E. Remiddi, "The analytical value of the electron (g ? 2) at order ?3 in qed," *Physics Letters B*, vol. 379, no. 1, pp. 283–291, 1996.

[93] T. Aoyama, M. Hayakawa, T. Kinoshita, and M. Nio, "Tenth-order qed contribution to the electron $g-2$ and an improved value of the fine structure constant," *Phys. Rev. Lett.*, vol. 109, p. 111807, Sep 2012.

[94] T. Aoyama, M. Hayakawa, T. Kinoshita, and M. Nio, "Tenth-order electron anomalous magnetic moment: Contribution of diagrams without closed lepton loops," *Phys. Rev. D*, vol. 91, p. 033006, Feb 2015.

[95] D. Hanneke, S. Fogwell Hoogerheide, and G. Gabrielse, "Cavity control of a single-electron quantum cyclotron: Measuring the electron magnetic moment," *Phys. Rev. A*, vol. 83, p. 052122, May 2011.

[96] P. Cladé, E. de Mirandes, M. Cadoret, S. Guellati-Khélifa, C. Schwob, F. m. c. Nez, L. Julien, and F. m. c. Biraben, "Determination of the fine structure constant based on bloch oscillations of ultracold atoms in a vertical optical lattice," *Phys. Rev. Lett.*, vol. 96, p. 033001, Jan 2006.

[97] R. Davis, Jr., D. S. Harmer, and K. C. Hoffman, "Search for neutrinos from the sun," *Phys. Rev. Lett.*, vol. 20, pp. 1205–1209, 1968.

[98] Q. R. Ahmad *et al.*, "Measurement of the rate of $\nu_e + d \rightarrow p + p + e^-$ interactions produced by ^{8}B solar neutrinos at the Sudbury Neutrino Observatory," *Phys. Rev. Lett.*, vol. 87, p. 071301, 2001.

[99] Y. Fukuda *et al.*, "Evidence for oscillation of atmospheric neutrinos," *Phys. Rev. Lett.*, vol. 81, pp. 1562–1567, 1998.

[100] Y. Abe *et al.*, "Indication of Reactor $\bar{\nu}_e$ Disappearance in the Double Chooz Experiment," *Phys. Rev. Lett.*, vol. 108, p. 131801, 2012.

[101] K. Abe *et al.*, "Evidence of Electron Neutrino Appearance in a Muon Neutrino Beam," *Phys. Rev. D*, vol. 88, no. 3, p. 032002, 2013.

[102] B. Pontecorvo, "Mesonium and anti-mesonium," *Sov. Phys. JETP*, vol. 6, p. 429, 1957.

[103] B. Pontecorvo, "Neutrino Experiments and the Problem of Conservation of Leptonic Charge," *Zh. Eksp. Teor. Fiz.*, vol. 53, pp. 1717–1725, 1967.

[104] T. Yanagida, "Horizontal Symmetry and Masses of Neutrinos," *Prog. Theor. Phys.*, vol. 64, p. 1103, 1980.

[105] N. Cabibbo, "Unitary Symmetry and Leptonic Decays," *Phys. Rev. Lett.*, vol. 10, pp. 531–533, 1963.

[106] M. Kobayashi and T. Maskawa, "Cp violation in the renormalizable theory of weak interaction," *Progress of Theoretical Physics*, vol. 49, pp. 652–657, 1973.

[107] M. E. Peskin and D. V. Schroeder, *An introduction to quantum field theory*. Boulder, CO: Westview, 1995. Includes exercises.

[108] F. J. Dyson, "Divergence of perturbation theory in quantum electrodynamics," *Phys. Rev.*, vol. 85, pp. 631–632, 1952.

[109] R. P. Feynman, "The theory of positrons," *Phys. Rev.*, vol. 76, pp. 749–759, Sep 1949.

[110] R. P. Feynman, "Space-time approach to quantum electrodynamics," *Phys. Rev.*, vol. 76, pp. 769–789, Sep 1949.

[111] R. P. Feynman, "Mathematical formulation of the quantum theory of electromagnetic interaction," *Phys. Rev.*, vol. 80, pp. 440–457, Nov 1950.

[112] Z. Koba, T. Tati, and S. i. Tomonaga, "On a Relativistically Invariant Formulation of the Quantum Theory of Wave Fields. II: Case of Interacting Electromagnetic and Electron Fields," *Prog. Theor. Phys.*, vol. 2, no. 3, pp. 101–116, 1947.

[113] J. Schwinger, "On quantum-electrodynamics and the magnetic moment of the electron," *Phys. Rev.*, vol. 73, pp. 416–417, Feb 1948.

[114] J. Schwinger, "Quantum electrodynamics. i. a covariant formulation," *Phys. Rev.*, vol. 74, pp. 1439–1461, Nov 1948.

[115] F. J. Dyson, "The radiation theories of tomonaga, schwinger, and feynman," *Phys. Rev.*, vol. 75, pp. 486–502, Feb 1949.

[116] F. J. Dyson, "The s matrix in quantum electrodynamics," *Phys. Rev.*, vol. 75, pp. 1736–1755, Jun 1949.

[117] T. Kinoshita, "Mass singularities of feynman amplitudes," *Journal of Mathematical Physics*, vol. 3, 1 1962.

[118] T. D. Lee and M. Nauenberg, "Degenerate systems and mass singularities," *Phys. Rev.*, vol. 133, pp. B1549–B1562, Mar 1964.

[119] Z. Bern, L. J. Dixon, D. C. Dunbar, and D. A. Kosower, "Fusing gauge theory tree amplitudes into loop amplitudes," *Nucl. Phys. B*, vol. 435, pp. 59–101, 1995.

[120] Z. Bern, L. J. Dixon, and D. A. Kosower, "One loop amplitudes for e+ e- to four partons," *Nucl. Phys. B*, vol. 513, pp. 3–86, 1998.

[121] D. Forde, "Direct extraction of one-loop integral coefficients," *Phys. Rev. D*, vol. 75, p. 125019, 2007.

[122] R. K. Ellis, W. T. Giele, and Z. Kunszt, "A Numerical Unitarity Formalism for Evaluating One-Loop Amplitudes," *JHEP*, vol. 03, p. 003, 2008.

[123] G. Ossola, C. G. Papadopoulos, and R. Pittau, "Reducing full one-loop amplitudes to scalar integrals at the integrand level," *Nucl. Phys. B*, vol. 763, pp. 147–169, 2007.

[124] A. von Manteuffel and R. M. Schabinger, "A novel approach to integration by parts reduction," *Phys. Lett. B*, vol. 744, pp. 101–104, 2015.

[125] T. Peraro, "Scattering amplitudes over finite fields and multivariate functional reconstruction," *JHEP*, vol. 12, p. 030, 2016.

[126] G. 't Hooft and M. Veltman, "Regularization and renormalization of gauge fields," *Nuclear Physics B*, vol. 44, no. 1, pp. 189–213, 1972.

[127] G. Hooft, "Renormalizable lagrangians for massive yang-mills fields," *Nuclear Physics B*, vol. 35, no. 1, pp. 167–188, 1971.

[128] P. Mastrolia and S. Mizera, "Feynman Integrals and Intersection Theory," *JHEP*, vol. 02, p. 139, 2019.

[129] F. Brown, "Invariant differential forms on complexes of graphs and Feynman integrals," in *Algebraic Structures in Perturbative Quantum Field Theory: A Conference in Honor of Dirk Kreimer´s 60th Birthday*, 1 2021.

[130] M. Marcolli, "Feynman integrals and motives," *arXiv e-prints*, p. arXiv:0907.0321, July 2009.

[131] S. Abreu, R. Britto, C. Duhr, and E. Gardi, "Algebraic Structure of Cut Feynman Integrals and the Diagrammatic Coaction," *Phys. Rev. Lett.*, vol. 119, no. 5, p. 051601, 2017.

[132] J. Broedel, C. Duhr, F. Dulat, B. Penante, and L. Tancredi, "From modular forms to differential equations for Feynman integrals," in *KMPB Conference: Elliptic Integrals, Elliptic Functions and Modular Forms in Quantum Field Theory*, pp. 107–131, 2019.

[133] E. Panzer, *Feynman integrals and hyperlogarithms.* PhD thesis, Humboldt U., 2015.

[134] N. Nakanishi, *Graph theory and Feynman integrals.* Mathematics and its applications ; vol.11, New York ; London: Gordon and Breach, 1971.

[135] S. Catani, "The Singular behavior of QCD amplitudes at two loop order," *Phys. Lett. B*, vol. 427, pp. 161–171, 1998.

[136] J. M. Henn, "Lectures on differential equations for Feynman integrals," *J. Phys. A*, vol. 48, p. 153001, 2015.

[137] C. Bogner and S. Weinzierl, "Feynman graph polynomials," *Int. J. Mod. Phys. A*, vol. 25, pp. 2585–2618, 2010.

[138] V. Smirnov, *Analytic Tools for Feynman Integrals*, vol. 250. 01 2012.

[139] R. E. Cutkosky, "Singularities and Discontinuities of Feynman Amplitudes," *Journal of Mathematical Physics*, vol. 1, pp. 429–433, Sept. 1960.

[140] P. A. Baikov, "Explicit solutions of the multiloop integral recurrence relations and its application," *Nucl. Instrum. Meth. A*, vol. 389, pp. 347–349, 1997.

[141] R. N. Lee, "Calculating multiloop integrals using dimensional recurrence relation and D-analyticity," *Nucl. Phys. B Proc. Suppl.*, vol. 205-206, pp. 135–140, 2010.

[142] A. G. Grozin, "Integration by parts: An Introduction," *Int. J. Mod. Phys. A*, vol. 26, pp. 2807–2854, 2011.

[143] H. Frellesvig and C. G. Papadopoulos, "Cuts of Feynman Integrals in Baikov representation," *JHEP*, vol. 04, p. 083, 2017.

[144] A. V. Smirnov and A. V. Petukhov, "The Number of Master Integrals is Finite," *Lett. Math. Phys.*, vol. 97, pp. 37–44, 2011.

[145] F. Tkachov, "A theorem on analytical calculability of 4-loop renormalization group functions," *Physics Letters B*, vol. 100, no. 1, pp. 65–68, 1981.

[146] K. Chetyrkin and F. V. Tkachov, "Integration by parts: The algorithm to calculate β-functions in 4 loops," *Nuclear Physics*, vol. 192, pp. 159–204, 1981.

[147] T. Bitoun, C. Bogner, R. P. Klausen, and E. Panzer, "The number of master integrals as Euler characteristic," *PoS*, vol. LL2018, p. 065, 2018.

[148] R. N. Lee, "Modern techniques of multiloop calculations," in *49th Rencontres de Moriond on QCD and High Energy Interactions*, pp. 297–300, 2014.

[149] S. Laporta, "High precision calculation of multiloop Feynman integrals by difference equations," *Int. J. Mod. Phys. A*, vol. 15, pp. 5087–5159, 2000.

[150] C. Anastasiou and A. Lazopoulos, "Automatic integral reduction for higher order perturbative calculations," *JHEP*, vol. 07, p. 046, 2004.

[151] A. von Manteuffel and C. Studerus, "Reduze 2 - Distributed Feynman Integral Reduction," 1 2012.

[152] C. Studerus, "Reduze-Feynman Integral Reduction in C++," *Comput. Phys. Commun.*, vol. 181, pp. 1293–1300, 2010.

[153] A. V. Smirnov, "FIRE5: a C++ implementation of Feynman Integral REduction," *Comput. Phys. Commun.*, vol. 189, pp. 182–191, 2015.

[154] A. V. Smirnov and F. S. Chuharev, "FIRE6: Feynman Integral REduction with Modular Arithmetic," *Comput. Phys. Commun.*, vol. 247, p. 106877, 2020.

[155] A. V. Smirnov, "Algorithm FIRE – Feynman Integral REduction," *JHEP*, vol. 10, p. 107, 2008.

[156] P. Maierhöfer, J. Usovitsch, and P. Uwer, "Kira—A Feynman integral reduction program," *Comput. Phys. Commun.*, vol. 230, pp. 99–112, 2018.

[157] J. Klappert, F. Lange, P. Maierhöfer, and J. Usovitsch, "Integral reduction with Kira 2.0 and finite field methods," *Comput. Phys. Commun.*, vol. 266, p. 108024, 2021.

[158] R. N. Lee, "Group structure of the integration-by-part identities and its application to the reduction of multiloop integrals," *JHEP*, vol. 07, p. 031, 2008.

[159] L. D. Landau, "On analytic properties of vertex parts in quantum field theory," *Nuclear Physics*, vol. 13, pp. 181–192, 1959.

[160] M. Veltman, *Diagrammatica: The Path to Feynman Diagrams*. Cambridge Lecture Notes in Physics, Cambridge University Press, 1994.

[161] S. Mandelstam, "Analytic properties of transition amplitudes in perturbation theory," *Phys. Rev.*, vol. 115, pp. 1741–1751, Sep 1959.

[162] P. Ball, V. M. Braun, and H. G. Dosch, "Form factors of semileptonic d decays from qcd sum rules," *Phys. Rev. D*, vol. 44, pp. 3567–3581, Dec 1991.

[163] D. A. Kosower and K. J. Larsen, "Maximal Unitarity at Two Loops," *Phys. Rev. D*, vol. 85, p. 045017, 2012.

[164] F. Cachazo, "Sharpening The Leading Singularity," 3 2008.

[165] N. Arkani-Hamed, F. Cachazo, and J. Kaplan, "What is the Simplest Quantum Field Theory?," *JHEP*, vol. 09, p. 016, 2010.

[166] J. Leray, "Le calcul différentiel et intégral sur une variété analytique complexe. (problème de cauchy. iii.)," *Bulletin de la Société Mathématique de France*, vol. 87, pp. 81–180, 1959.

[167] S. Abreu, R. Britto, C. Duhr, and E. Gardi, "Cuts from residues: the one-loop case," *JHEP*, vol. 06, p. 114, 2017.

[168] S. Caron-Huot and K. J. Larsen, "Uniqueness of two-loop master contours," *JHEP*, vol. 10, p. 026, 2012.

[169] E. Panzer, "Algorithms for the symbolic integration of hyperlogarithms with applications to Feynman integrals," *Comput. Phys. Commun.*, vol. 188, pp. 148–166, 2015.

[170] V. A. Smirnov, "Evaluating multiloop Feynman integrals by Mellin-Barnes representation," *Nucl. Phys. B Proc. Suppl.*, vol. 135, pp. 252–256, 2004.

[171] A. V. Smirnov and M. N. Tentyukov, "Feynman Integral Evaluation by a Sector decomposiTion Approach (FIESTA)," *Comput. Phys. Commun.*, vol. 180, pp. 735–746, 2009.

[172] S. Borowka, G. Heinrich, S. Jahn, S. P. Jones, M. Kerner, J. Schlenk, and T. Zirke, "pySecDec: a toolbox for the numerical evaluation of multi-scale integrals," *Comput. Phys. Commun.*, vol. 222, pp. 313–326, 2018.

[173] O. V. Tarasov, "Connection between Feynman integrals having different values of the space-time dimension," *Phys. Rev. D*, vol. 54, pp. 6479–6490, 1996.

[174] R. N. Lee, "Space-time dimensionality D as complex variable: Calculating loop integrals using dimensional recurrence relation and analytical properties with respect to D," *Nucl. Phys. B*, vol. 830, pp. 474–492, 2010.

[175] V. A. Smirnov and M. Steinhauser, "Solving recurrence relations for multiloop Feynman integrals," *Nucl. Phys. B*, vol. 672, pp. 199–221, 2003.

[176] N. Kamran, "Exterior differential systems," *Handbook of Global Analysis*, 12 2008.

[177] K.-T. Chen, "Iterated path integrals," *Bulletin of the American Mathematical Society*, vol. 83, no. 5, pp. 831 – 879, 1977.

[178] F. C. S. Brown, "Multiple zeta values and periods of moduli spaces $\mathfrak{M}_{0,n}$," *arXiv Mathematics e-prints*, p. math/0606419, June 2006.

[179] A. B. Goncharov, "A simple construction of Grassmannian polylogarithms," *arXiv e-prints*, p. arXiv:0908.2238, Aug. 2009.

[180] M. Kontsevich and D. Zagier, *Periods*, pp. 771–808. Berlin, Heidelberg: Springer Berlin Heidelberg, 2001.

[181] N. Arkani-Hamed, J. L. Bourjaily, F. Cachazo, and J. Trnka, "Local Integrals for Planar Scattering Amplitudes," *JHEP*, vol. 06, p. 125, 2012.

[182] J. Henn, B. Mistlberger, V. A. Smirnov, and P. Wasser, "Constructing d-log integrands and computing master integrals for three-loop four-particle scattering," *JHEP*, vol. 04, p. 167, 2020.

[183] P. Wasser, "Analytic properties of feynman integrals for scattering amplitudes," 2018.

[184] T. Gehrmann, J. M. Henn, and T. Huber, "The three-loop form factor in N=4 super Yang-Mills," *JHEP*, vol. 03, p. 101, 2012.

[185] J. Drummond, C. Duhr, B. Eden, P. Heslop, J. Pennington, and V. A. Smirnov, "Leading singularities and off-shell conformal integrals," *JHEP*, vol. 08, p. 133, 2013.

[186] J. Moser, "The order of a singularity in fuchs' theory.," *Mathematische Zeitschrift*, vol. 72, pp. 379–398, 1959/60.

[187] M. Tenenbaum and H. Pollard, *Ordinary Differential Equations*. Dover Books on Mathematics Series, Dover Publications, Incorporated, 2012.

[188] A. B. Goncharov, "Multiple zeta-values, Galois groups, and geometry of modular varieties," *arXiv Mathematics e-prints*, p. math/0005069, May 2000.

[189] E. Remiddi and J. A. M. Vermaseren, "Harmonic polylogarithms," *Int. J. Mod. Phys. A*, vol. 15, pp. 725–754, 2000.

[190] R. Hain, "Classical Polylogarithms," *arXiv e-prints*, pp. alg–geom/9202022, Feb. 1992.

[191] D. Gaiotto, J. Maldacena, A. Sever, and P. Vieira, "Pulling the straps of polygons," *JHEP*, vol. 12, p. 011, 2011.

[192] J. Broedel, C. Duhr, F. Dulat, B. Penante, and L. Tancredi, "Elliptic Feynman integrals and pure functions," *JHEP*, vol. 01, p. 023, 2019.

[193] F. C. S. Brown and A. Levin, "Multiple Elliptic Polylogarithms," *arXiv e-prints*, p. arXiv:1110.6917, Oct. 2011.

[194] H. Frellesvig, "On Epsilon Factorized Differential Equations for Elliptic Feynman Integrals," 10 2021.

[195] G. Källén and E. Merzbacher, "Elementary particle physics," *Physics Today*, vol. 18, pp. 56–58, 1964.

[196] R. N. Lee, "Reducing differential equations for multiloop master integrals," *JHEP*, vol. 04, p. 108, 2015.

[197] M. Prausa, "epsilon: A tool to find a canonical basis of master integrals," *Comput. Phys. Commun.*, vol. 219, pp. 361–376, 2017.

[198] O. Gituliar and V. Magerya, "Fuchsia: a tool for reducing differential equations for Feynman master integrals to epsilon form," *Comput. Phys. Commun.*, vol. 219, pp. 329–338, 2017.

[199] C. Meyer, "Algorithmic transformation of multi-loop master integrals to a canonical basis with canonica," *Computer Physics Communications*, vol. 222, pp. 295–312, 2018.

[200] P. Wasser, "Analytic properties of feynman integrals for scattering amplitudes," 2018.

[201] C. Dlapa, J. Henn, and K. Yan, "Deriving canonical differential equations for Feynman integrals from a single uniform weight integral," *JHEP*, vol. 05, p. 025, 2020.

[202] Z. Bern, J. Parra-Martinez, R. Roiban, M. S. Ruf, C.-H. Shen, M. P. Solon, and M. Zeng, "Scattering Amplitudes and Conservative Binary Dynamics at $\mathcal{O}(G^4)$," *Phys. Rev. Lett.*, vol. 126, no. 17, p. 171601, 2021.

[203] M. Argeri, S. Di Vita, P. Mastrolia, E. Mirabella, J. Schlenk, U. Schubert, and L. Tancredi, "Magnus and Dyson Series for Master Integrals," *JHEP*, vol. 03, p. 082, 2014.

[204] N. Arkani-Hamed, J. L. Bourjaily, F. Cachazo, and J. Trnka, "Singularity Structure of Maximally Supersymmetric Scattering Amplitudes," *Phys. Rev. Lett.*, vol. 113, no. 26, p. 261603, 2014.

[205] N. Arkani-Hamed, J. L. Bourjaily, F. Cachazo, A. B. Goncharov, A. Postnikov, and J. Trnka, *Grassmannian Geometry of Scattering Amplitudes*. Cambridge University Press, 4 2016.

[206] R. K. Ellis and G. Zanderighi, "Scalar one-loop integrals for QCD," *JHEP*, vol. 02, p. 002, 2008.

[207] D. Simmons-Duffin, "Projectors, Shadows, and Conformal Blocks," *JHEP*, vol. 04, p. 146, 2014.

[208] S. Caron-Huot and J. M. Henn, "Iterative structure of finite loop integrals," *JHEP*, vol. 06, p. 114, 2014.

[209] O. V. Tarasov, "Generalized recurrence relations for two loop propagator integrals with arbitrary masses," *Nucl. Phys. B*, vol. 502, pp. 455–482, 1997.

[210] Z. Bern, E. Herrmann, S. Litsey, J. Stankowicz, and J. Trnka, "Evidence for a Nonplanar Amplituhedron," *JHEP*, vol. 06, p. 098, 2016.

[211] J. L. Bourjaily, E. Herrmann, and J. Trnka, "Prescriptive Unitarity," *JHEP*, vol. 06, p. 059, 2017.

[212] J. L. Bourjaily, E. Herrmann, C. Langer, A. J. McLeod, and J. Trnka, "Prescriptive Unitarity for Non-Planar Six-Particle Amplitudes at Two Loops," *JHEP*, vol. 12, p. 073, 2019.

[213] W. Magnus, "On the exponential solution of differential equations for a linear operator," *Communications on Pure and Applied Mathematics*, vol. 7, pp. 649–673, 1954.

[214] J. Hastad, B. Just, J. C. Lagarias, and C.-P. Schnorr, "Polynomial Time Algorithms for Finding Integer Relations among Real Numbers," *SIAM J. Comput.*, vol. 18, pp. 859–881, 1989.

[215] Z. Bern, E. Herrmann, S. Litsey, J. Stankowicz, and J. Trnka, "Logarithmic Singularities and Maximally Supersymmetric Amplitudes," *JHEP*, vol. 06, p. 202, 2015.

[216] J. M. Henn, K. Melnikov, and V. A. Smirnov, "Two-loop planar master integrals for the production of off-shell vector bosons in hadron collisions," *JHEP*, vol. 05, p. 090, 2014.

[217] T. Gehrmann, A. von Manteuffel, and L. Tancredi, "The two-loop helicity amplitudes for $q\overline{q}' \to V_1 V_2 \to 4$ leptons," *JHEP*, vol. 09, p. 128, 2015.

[218] S. Caron-Huot, L. J. Dixon, A. McLeod, and M. von Hippel, "Bootstrapping a Five-Loop Amplitude Using Steinmann Relations," *Phys. Rev. Lett.*, vol. 117, no. 24, p. 241601, 2016.

[219] O. Steinmann, *Über den Zusammenhang zwischen den Wightmanfunktionen und den retardierten Kommutatoren.* PhD thesis, ETH Zurich, 1960.

[220] O. Steinmann, "Wightman-funktionen und retardierten kommutatoren. ii," 1960.

[221] K. E. Cahill and H. P. Stapp, "Optical theorems and steinmann relations," *Ann. Phys. (N.Y.), v. 90, no. 2, pp. 438-514.*

[222] L. J. Dixon, J. Drummond, T. Harrington, A. J. McLeod, G. Papathanasiou, and M. Spradlin, "Heptagons from the Steinmann Cluster Bootstrap," *JHEP*, vol. 02, p. 137, 2017.

[223] S. Caron-Huot, L. J. Dixon, F. Dulat, M. Von Hippel, A. J. McLeod, and G. Papathanasiou, "The Cosmic Galois Group and Extended Steinmann Relations for Planar $\mathcal{N} = 4$ SYM Amplitudes," *JHEP*, vol. 09, p. 061, 2019.

[224] Z. Bern, L. Dixon, F. F. Cordero, S. Höche, H. Ita, D. Kosower, and D. Maitre, "Ntuples for nlo events at hadron colliders.," *Computer physics communications.*, vol. 185, pp. 1443–1460, May 2014.

[225] T. Gleisberg, S. Hoeche, F. Krauss, M. Schonherr, S. Schumann, F. Siegert, and J. Winter, "Event generation with SHERPA 1.1," *JHEP*, vol. 02, p. 007, 2009.

[226] N. BYERS and C. N. YANG, "Physical regions in invariant variables for n particles and the phase-space volume element," *Rev. Mod. Phys.*, vol. 36, pp. 595–609, Apr 1964.

[227] F. Caola, J. M. Henn, K. Melnikov, and V. A. Smirnov, "Non-planar master integrals for the production of two off-shell vector bosons in collisions of massless partons," *JHEP*, vol. 09, p. 043, 2014.

[228] R. Mertig, M. Böhm, and A. Denner, "Feyn calc - computer-algebraic calculation of feynman amplitudes," *Computer Physics Communications*, vol. 64, pp. 345–359, 06 1991.

[229] V. Shtabovenko, R. Mertig, and F. Orellana, "New Developments in FeynCalc 9.0," *Comput. Phys. Commun.*, vol. 207, pp. 432–444, 2016.

[230] S. Abreu, J. Dormans, F. Febres Cordero, H. Ita, M. Kraus, B. Page, E. Pascual, M. S. Ruf, and V. Sotnikov, "Caravel: A C++ framework for the computation of multi-loop amplitudes with numerical unitarity," *Comput. Phys. Commun.*, vol. 267, p. 108069, 2021.

[231] S. Kallweit, V. Sotnikov, and M. Wiesemann, "Triphoton production at hadron colliders in NNLO QCD," *Phys. Lett. B*, vol. 812, p. 136013, 2021.

[232] H. A. Chawdhry, M. L. Czakon, A. Mitov, and R. Poncelet, "NNLO QCD corrections to three-photon production at the LHC," *JHEP*, vol. 02, p. 057, 2020.

[233] H. A. Chawdhry, M. Czakon, A. Mitov, and R. Poncelet, "NNLO QCD corrections to diphoton production with an additional jet at the LHC," *JHEP*, vol. 09, p. 093, 2021.

[234] M. Czakon, A. Mitov, and R. Poncelet, "Next-to-Next-to-Leading Order Study of Three-Jet Production at the LHC," *Phys. Rev. Lett.*, vol. 127, no. 15, p. 152001, 2021.

[235] T. Peraro, "FiniteFlow: multivariate functional reconstruction using finite fields and dataflow graphs," *JHEP*, vol. 07, p. 031, 2019.

[236] L. J. Dixon, "A brief introduction to modern amplitude methods," in *Theoretical Advanced Study Institute in Elementary Particle Physics: Particle Physics: The Higgs Boson and Beyond*, pp. 31–67, 2014.

[237] J. Henn and J. Plefka, *Scattering Amplitudes in Gauge Theories*, vol. 883. 11 2013.

[238] A. Hodges, "Eliminating spurious poles from gauge-theoretic amplitudes," *JHEP*, vol. 05, p. 135, 2013.

[239] S. Weinzierl, "Tales of 1001 Gluons," *Phys. Rept.*, vol. 676, pp. 1–101, 2017.

[240] S. Badger, H. Frellesvig, and Y. Zhang, "A Two-Loop Five-Gluon Helicity Amplitude in QCD," *JHEP*, vol. 12, p. 045, 2013.

[241] M. Abramowitz and I. A. Stegun, *Handbook of Mathematical Functions with Formulas, Graphs, and Mathematical Tables*, vol. 55. New York: Dover, ninth dover printing, tenth gpo printing ed., 1964.

Acknowledgment

First of all, I thank my supervisor Harald Ita for all his guidance and support tha he gave me during the last five years and, of course, giving me the opportunity to work on this project. He always had time to answer my questions and gave me very important insights but also I appreciate a lot having discussions not only about physics. I greatly appreciate his patience in all these conversations, especially the non-physical ones. I learned a lot for what I am deeply grateful. Last but not least, I would like to thank Harald for the time he invested in reading this manuscript and providing very concrete comments on it.
I also want to thank my second supervisor Stefan Dittmaier for very fruitful conversations both in formal meetings and during the lunch time.
I thank Fernando Febres Cordero for fruitful discussions and, of course, for letting me participate on his grant at the beginning of this project.
I am greatly indebted to all my collaborators: Samuel Abreu, Francesco Moriello, Ben Page and Mao Zeng for giving me the opportunity to work with them and teaching me a lot about physics. I am especially thankful to Samuel from whom I really learned a lot. It was a great pleasure to work with him.
I thank Michael Ruf for his help on computing multi-dimensional residues and Maximilian Klinkert for reading parts of this manuscript.
I would like to thank all my fellow Ph.D. students: Vasily Sotnikov, Jerry Dormans, Michael Ruf, Evgenij Pascual and Maximilian Klinkert for great working atmosphere and very helpful conversations.
I thank Philipp Maierhöfer for helping me with `KIRA`.
Finally, I want to thank the "Graduiertenkolleg 2044" for supporting my work and also organizing all these helpful and interesting events during the last years which contributed a lot to the stimulating working atmosphere.
I want to thank my friends Georg Schalaschov, Alexander Hermann, Andriy Achkasov, Svetlana Yaudosin and Jerome Müeller-Anders for their support and encouragement during this time.
Last but not least, I want to express my great gratitude to my mother who has constantly supported and strengthened me in all what I did, despite having much trouble in these five years herself. Mom, I thank you so much.